PROTEIN-LIPID INTERACTIONS

BIOPHYSICAL STUDIES OF THE IMPACT OF PROTEIN-LIPID INTERACTIONS ON STRUCTURE, FUNCTION AND ENERGETICS

SØREN BANG

PhD THESIS · MARCH 2010

FACULTY OF AGRICULTURAL SCIENCES
AARHUS UNIVERSITY

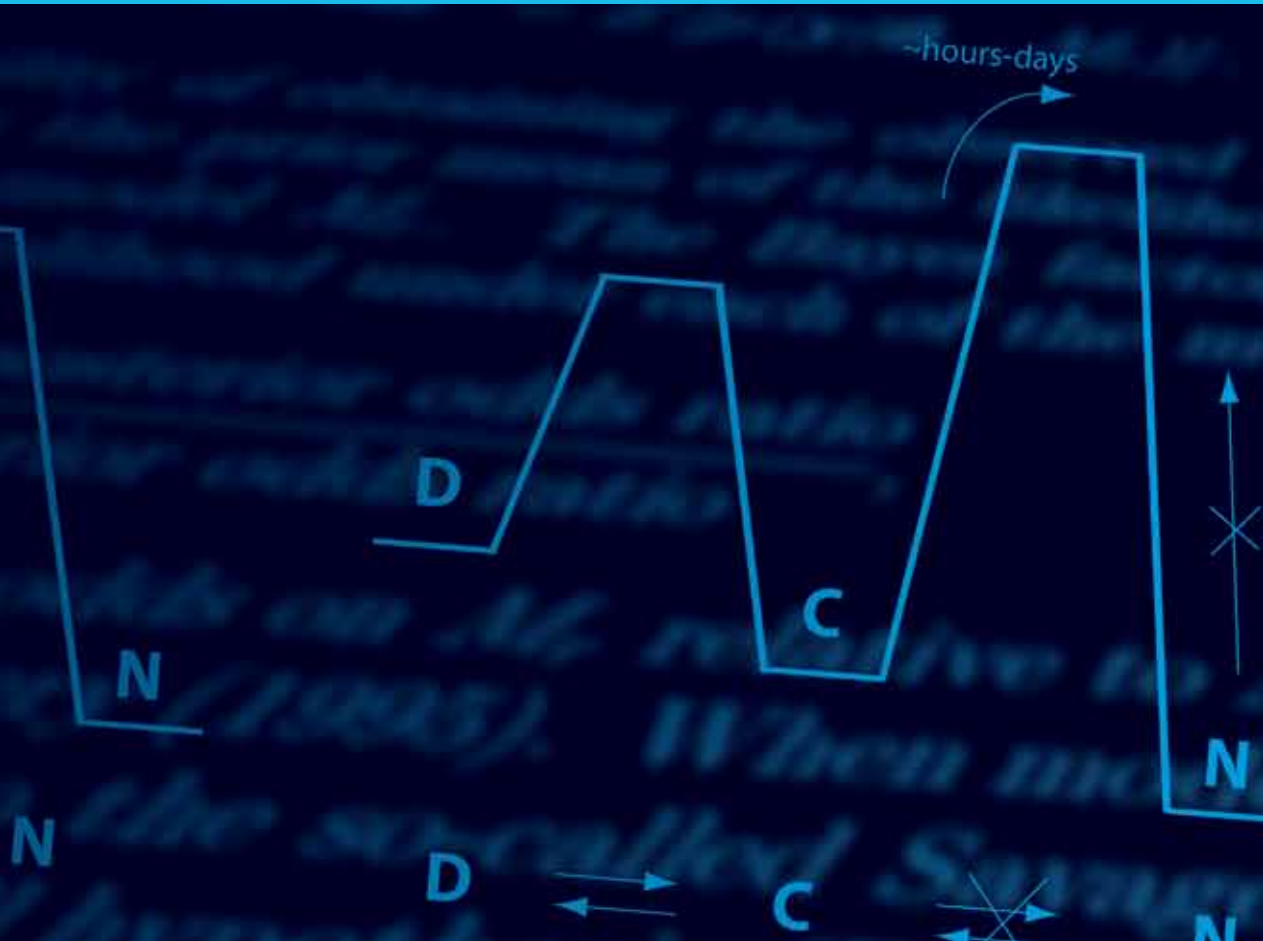

FACULTY OF AGRICULTURAL SCIENCES

DEPARTMENT OF FOOD SCIENCE

PROTEIN-LIPID INTERACTIONS

BIOPHYSICAL STUDIES OF THE IMPACT OF PROTEIN-LIPID INTERACTIONS ON STRUCTURE, FUNCTION AND ENERGETICS

SØREN BANG

PHD THESIS NO 002 · DEPARTMENT OF FOOD SCIENCE ,
AARHUS UNIVERSITY · MARCH 2010

FACULTY OF AGRICULTURAL SCIENCES
AARHUS UNIVERSITY

Department of Food science
Faculty of Agricultural Sciences
Aarhus University
P.O. Box 50
DK-8830 Tjele

Tryk: www.digisource.dk
ISBN: 87-91949-55-6

Title of PhD. Thesis:

Protein-lipid interactions

- Biophysical studies of the impact of protein-lipid interactions on structure, function and energetics

Author:

Søren Bang Nielsen
(+45) 51 94 30 63
Soeren.b.nielsen@gmail.com
University of Aarhus
Interdisciplinary Nanoscience Center (iNANO)
Department of Molecular Biology
Protein Biophysics group
Gustav Wieds Vej 10C
DK-8000 Aarhus

and

University of Aarhus
Faculty of Agricultural Sciences
Department of Food Science
Blichers Allé, P.O. 50
DK-8830 Tjele

Supervisors:

Professor Daniel Erik Otzen
(+45) 20 72 52 38
dao@inano.dk
University of Aarhus
Interdisciplinary Nanoscience Center (iNANO)
Department of Molecular Biology
Protein Biophysics group
Gustav Wieds Vej 10C
DK-8000 Aarhus

Research manager Jacob Holm Nielsen
(+45) 22 74 11 63
JacobH.Nielsen@agrsci.dk
University of Aarhus
Faculty of Agricultural Sciences
Department of Food Science
Blichers Allé, P.O. 50
DK-8830 Tjele

Thesis period:

September 1st 2006 to Jan 4th 2010

PhD. School:

The Graduate School of Agriculture, Food and Environment (SAFE)
Faculty of Agricultural Sciences
Aarhus University

Issues printed:

50

List of papers

This thesis is based on the following papers which will be referred to by the designated number throughout the thesis:

I Brian Vad, Line Aagot Thomsen, Kresten Bertelsen, Magnus Franzmann, Jan Mondrup Pedersen, **Søren B. Nielsen**, Thomas Vosegaard, Zuzana Valnickova, Troels Skrydstrup, Jan J. Enghild, Reinhard Wimmer, Niels Chr. Nielsen and Daniel E. Otzen. "*Divorcing Folding from Function: How acylation affects the Membrane-Perturbing Properties of an Anti-microbial Peptide?",* Biochim Biophys Acta Biomembranes Proteins and Proteomics ***In press***

II **Søren B. Nielsen**, Daniel Otzen. "*Impact of the antimicrobial peptide Novicidin on membrane structure and integrity", Manuscript submitted 05/11/09*

III Claudia U. Hjørringgard, Brian S. Vad, **Søren B. Nielsen**, Niels Chr. Nielsen, Daniel E. Otzen and Troels Skrydstrup, "*Effective Membrane Channel Forming Properties of Alamethicin:Cyclodextrin Conjugates*", *Manuscript submitted 30/11/09*

IV **Søren B. Nielsen**, Kristina Wilhelm, Brian Vad, Ludmilla Morozova-Roche and Daniel Otzen. "*The interaction of equine lysozyme:oleic acid complexes with lipid membranes suggests a cargo off-loading mechanism*", *Manuscript Submitted 27/12/09*

V **Søren B. Nielsen**, Magnus Franzmann, Rajiv V. Basaiawmoit, Reinhard Wimmer, Jens D. Mikkelsen and Daniel E. Otzen, "*β-sheet aggregation of kisspeptin is stimulated by heparin but inhibited by amphiphiles*"
Manuscript submitted 07/11/09

VI Pankaj Sehgal, **Søren Bang Nielsen**, Shona Pedersen, Reinhard Wimmer, Daniel E. Otzen. "*Modulation of cutinase stability and structure by phospholipid detergents*". Biochim Biophys Acta (2007) 1774, 1544-1554

Abbreviations

Aib	Aminoisobutyric acid
Alm	Alamethicin
AOT	Dioctanoyl succinate
AMP	Antimicrobial peptide
ANS	1-anilinonaphtalene-8-sulfonate
APD	Antimicrobial peptide database
Arg (R)	Arginine
bLA	Bovine α-lactalbumin
C6PC	1,2-dihexanoyl-*sn*-glycerol-3-phosphatidylcholine
C7PC	1,2-diheptanoyl-*sn*-glycerol-3-phosphatidylcholine
C8PC	1,2-dioctanoyl-*sn*-glycerol-3-phosphatidylcholine
C9PC	1,2-dinonanoyl-*sn*-glycerol-3-phosphatidylcholine
CD	Circular dichroism
DOPC	1,2-dioleoyl-sn-glycero-3-phosphocholine
DOPG	1,2-dioleoyl-sn-glycero-3-phosphocholine
CMC	Critical micelle concentration
DPC	Dodecylphosphatidylcholine
DPI	Dual polarization interferometry
DSC	Differential scanning calorimetry
CSLM	Cofocal scanning laser microscopy
EL	Equine lysozyme
ELOA	Equine lysozyme multimeric complexes with oleic acid
F. pisi	Fusarium solani pisi
FTIR	Fourier transform infrared spectroscopy
MG	Molten globule
HAMLET	Human α-lactalbumin made lethal to tumor cells
hLA	Human α-lactalbumin
LA	α-lactalbumin
LPS	Lipopolysaccharide
LTA	Lipoteichoic acid
Lys (K)	Lysine
mKp-10	Murine Kisspeptin-10
OCD	Oriented circular dichroism
NBD-X	(6-(N-(7-nitrobenz-2-oxa-1,3-diazol-4-yl)amino)hexanoic acid)
Nc	Novicidin
NMR	Nuclear magnetic resoncance

Phe (F)	Phenylalanine
PBS	Phosphate buffered saline
PC	Phosphatidylcholine
PG	Phosphatidylglycerol
PS	Phosphatidylserine
PI	Phosphatidylinositol
PE	Phosphatidylethanolamine
QCM-D	Quartz crystal microbalance with dissipation monitoring
SDS	Sodium dodecyl sulfate
TDOC	Taurodeoxycholate
Trp (W)	Tryptophan
Tyr (Y)	Tyrosine

Preface

The general theme of this thesis is the interaction of proteins and peptides with lipids in the form of phospholipid membranes and detergents and their mutual influence on structural conformations and functions. This has been done through investigations of the interactions of α-helix antimicrobial peptides novicidin and a synthetic pore construct based on alamethicin with phospholipid membranes, membrane interaction and structural characterizations of multimeric equine lysozyme complexes with oleic acid (ELOA), effect of detergents on the structure, stability and activity of *Fusarium solani pisi* cutinase and the effect of detergents on the aggregation of murine kisspeptin-10 (mKp-10).

The thesis has been submitted to the graduate School of Agriculture, Food and Environment (SAFE) at the Faculty of Agricultural Sciences at Aarhus University, Denmark, as part of the requirements for obtaining the PhD degree. It has been divided into five parts in which (I) antimicrobial peptides, bacterial and model membranes are introduced leading to a discussion of work regarding novicidin and synthetic alamethicin pores, (II) an introduction to protein folding and the impact of amphiphatic molecules on the structure and function of equine lysozyme in ELOA, *Fusarium solani pisi* cutinase and mKp-10. Part III comprises an introduction to biophysical methods employed in the study of proteins and membranes of this study. Part IV comprises coauthor agreements on scientific papers of this thesis which are included in part V, all of which are in submitted or published forms.

The present thesis has involved collaborations with several research groups and in no particular order, I would like to acknowledge these people: I would like to thank Søren Vrønning Hoffmann and Nykola Jones for their gracious access, assistance and troubleshooting with respect to measurements conducted at the SRCD facility at the Institute for Storage Ring Facilities at Aarhus University. I would like to thank Ludmilla Morozova-Roche and Kristina Wilhelm from Umeå University for giving me the opportunity to work the ELOA complex and its interaction with membranes. I also use this opportunity to thank Brian Vad and Vijay Shankar from the Protein Biophysics group for fruitful discussions regarding work on antimicrobial peptides and the remainder of the Protein Biophysics group for a great atmosphere in the laboratory, for sharing their individual expertises within different techniques and fields and for scientific discussions.

The bulk of the work presented in this PhD thesis has been carried out in the lab of Professor Dr. Daniel E. Otzen and I thank him for his excellent guidance and inspiring supervision. I further thank both Professor Dr. Daniel E. Otzen and Research director Jacob Holm Nielsen for granting me the opportunity to do the research leading to this thesis.

Finally, I would like to thank my family and not least my girlfriend Laila Kjær for their support and understanding during these years.

Summary

The main theme of this thesis is the interaction of proteins and peptides with lipids in the form of phospholipid membranes and detergents and the impact on membrane integrity and protein structure, activity and function.

The first part of this thesis describes the interaction and membrane-perturbing properties of the antimicrobial peptides novicidin (Nc) and alamethicin (Alm). Our studies of Nc described in **paper I** and **II** show that Nc selectively lyses anionic membranes mimicking bacterial surfaces even in coexistence with neutral membranes. Electrostatic attraction to anionic lipids guide the peptide to α-helical conformations of the peptide inserted in a surface bound state interchelate between phospholipid headgroups where it leads to membrane disorder and ultimately membrane disintegration by a detergent-like mechanism. Induction of α-helical structure was shown not to be a prerequisite for membrane disruption since a more effective disruption of purely zwitterionic membranes in which Nc exists in random coil conformations compared to partially anionic was observed. In **paper III**, the synthesis of Alm conjugates with cyclodextrins to constitute a synthetic pore construct was successfully demonstrated. Biophysical studies revealed that the activity of the pore constructs resemble those of the native peptide while displaying a more efficient release of vesicular content although at a lower rate. The higher efficiency of the synthetic pore constructs was assigned to a more restricted degree of conformational freedom based on the determination of more persistent secondary structures of the synthetic pore.

In the second part of this thesis, the influence of lipids on the structure, function and energetics of water soluble proteins and peptides whose natural targets are not lipid membranes. **Paper IV** demonstrates the interaction between phospholipid membranes and multimeric equine lysozyme complexes with oleic acid (ELOA) in which equine lysozyme is trapped in partially unfolded state through the interaction with oleic acid. Contrary to the related HAMLET complex, did not cause membrane disruption or internalization into liposomes. Instead, a cargo off-loading mechanism of ELOA in which OA is delivered to membranes was proposed based on the transition toward more native like conformations and partial recovery of enzymatic activity and increased stability toward proteolytic digestion on interaction with membranes. **Paper IV** thus suggest that protein complexes with oleic acid may exert their via extracellular targets and not solely through interaction with intracellular targets. **Paper V** demonstrates the aggregation of murine kisspeptin-10 (mKp-10) into amyloidal aggregates stimulated by heparin. While heparin stimulates aggregation, sub-micellar concentrations of SDS and DPC were shown to inhibit the aggregation through displacement of ensemble mKp-10 states toward a less aggregation prone state suggesting that mKp-10 aggregation may be regulated by natural amphiphiles *in vivo.* In **paper VI***, F. solani pisi* cutinase was shown to be destabilized by short-chain zwitterionic phospholipids (C6PC-C9PC) while retaining enzymatic activity. Refolding experiments in the presence of detergents together with activity measurements suggest that binding of detergent inactivate cutinase. Together with the profound stability of cutinase in the native state toward detergents, this suggests that cutinase exist in a kinetically trapped state surrounded by large energy barriers which is of great importance for industrial applications.

Dansk resume

Temaet for denne PhD afhandling her interaktionen af proteiner og peptider med lipider i form af phospholipid membraner og detergenter og disses indflydelse på membrane integritet samt protein structur, funktion og aktivitet.

Første del af afhandlingen beskriver indflydelsen af de antimikrobielle peptider novicidin (Nc) og alamethicin (Alm) på membran integritet og struktur. Vores undersøgelser af Nc er beskrevet i **artikel I** og **II** der viser at Nc selektivt interagerer og lyserer negativt ladede membraner der efterligner den bakterielle overflade – og det også i en blanding af negative ladede og med neutrale membraner. Peptidet tiltrækkes elektrostatisk til negativt ladede membraner der inducerer α-helix struktur og indsættes parallelt med membranoverfladen mellem phospholipid hovedgrupperne. Her forårsager Nc uorden i pakningen af lipider og ved højere koncentrationer opbrydning af membranen via en detergent-lignende mekanisme. Undersøgelser med neutrale membraner viste at α-helix struktur ikke er en nødvendighed for en effektiv påvirkning af membran integriteten da Nc viste sig at være mere effektiv i permeabilisringen af neutrale membraner der ikke forårsager α-helix struktur af Nc.

Artikel III demonstrerer syntesen af syntetiske porer baseret på Alm konjugater med cyklodekstriner. Biofysiske studier påviste at aktiviteten af de syntetiske porer ligner native Alm porer men udviser en mere effektiv, dog langsommere permeabilisering af lipid membraner. Den højere effektivitet af de syntetiske porer tilskrives en mere fastlåst struktur af de syntetiske porer.

I anden halvdel af afhandlingen drejes fokus mod effekten af lipider på strukturen og funktionen af vandopløselige proteiner hvis naturlige funktion ikke afhænger af lipid membraner. **Artikel IV** omhandler interaktionen mellem phospholipid membraner og et delvist udfoldet stadie af hestelysozym stabiliseret af oleinsyre (ELOA). I modsætning til det beslægtede HAMLET kompleks penetrerer ELOA ikke membraner. Baserer på overgangen mod mere native proteinkonformationer, forøgelse af lysozym aktivitet og øget stabilitet mod proteasefordøjelse foreslår vi i stedet en mekanisme hvor ELOA gennem binding til membranen afleverer oleinsyrer og derved tillades at folde mod mere native strukturer.

Artikel V beskriver en stimuleret aggregeringen af kisspeptin-10 fra mus (mKp-10) til amyloider med heparin. Mens heparin stimulerer aggregering inhiberer SDS og DPC koncentrationer under den kritiske micelle koncentration (CMC) aggregering gennem omdannelse af aggregerings-tilbøjelige stadier til stadier med mindre tilbøjelighed for aggregering.

Artikel VI omhandler opretholdelse af enzymatisk aktivitet på trods af en destabiliserende effekt af kortkædede amfolytter på cutinase fra *F. solani pisi*. Foldningen af cutinase i tilstedeværelse af detergenter leder til et inaktivt stadie. Tilsammen indikerer dette at nativt foldet cutinase er fanget i et fastlåst stadie omgivet af høje energibarrierer der ikke tillader proteinet at undersøge alternative protein strukturer.

Part I : Antimicrobial peptides and their interaction with membranes

This first part of the thesis describes the interaction of antimicrobial peptides (AMPs) with lipid membranes and is important for understanding the effect of AMPs on bacterial membranes. It consists of an introduction to the constituents of lipid membranes and their properties with an emphasis on properties governing the specificity of AMPs. This includes fundamental differences between bacterial and mammalian interfaces which are important for AMP selectivity toward the former. Model systems set to mimic and simplify the otherwise complex compositions of natural membranes are introduced and lead to a description of the impact of antimicrobial peptides on the integrity of such membranes and the influence of different membrane compositions on the structure and membrane disruptive capabilities of AMPs. Finally, this part includes a description and discussion of results obtained using the antimicrobial peptides novicidin and alamethicin covered by this work including suggestions for future work.

1. Lipid membranes

Lipid membranes constitute the semi-permeable barrier which defines the boundaries of a cell by separation and shielding of the interior of the cell from the surrounding environment (Figure 1). Compared to the dimensions of a cell (~1-100µm), lipid membranes are only two lipid molecules thick which correspond to 4-6nm depending on lipid constituents and lipid properties. Since lipid membranes have a hydrophobic core, they restrict the movements of polar molecules in and out of the cell. The transport is instead regulated by specific membrane proteins that facilitate the transport across the membrane and in this way take up nutrients or maintain chemical gradients essential for cell viability. The maintenance of such gradients would not be possible in the absence of a lipid membrane.

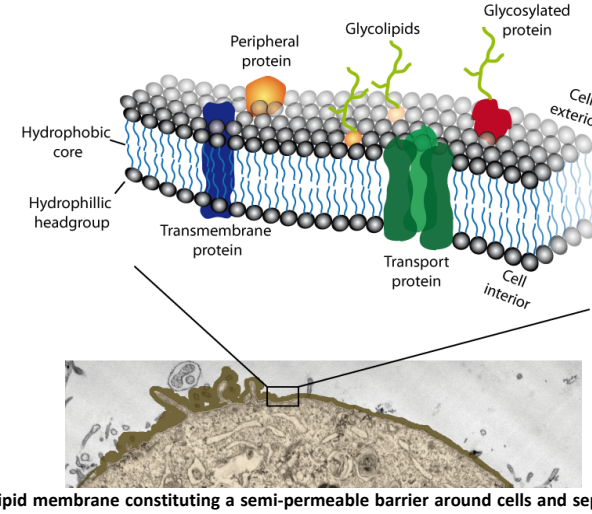

Figure 1 Mosaic of the lipid membrane constituting a semi-permeable barrier around cells and separate the extracellular space and cytoplasm. Different macromolecules are embedded in the membrane such as integral or transmembrane proteins, transport proteins which take up nutrients or maintain essential gradients across the membrane, peripheral proteins, glycoproteins and glycolipids. Illustration based on the fluid mosaic model by Singer and Nicolson (1972)[1]

1.1. Lipid properties

The major lipid components of cell membranes are phospholipids, glycolipids and sterols which share a common molecular structure composed by both a hydrophobic and hydrophilic part (Figure 2). The hydrophobic "tails" of phospholipids consist of two fatty acid acyl chains of 14-22 carbon atoms each linked to a glycerol backbone of which the tail linked to *sn*-1 carbon is typically saturated and the tail linked to *sn*-2 is usually unsaturated (contains carbon-carbon double bonds) and in the *cis* configuration which makes them fluid at room temperature. When a phosphate group is linked to the *sn*-3 position of glycerol backbone and to fatty acid acyl chains at the *sn*-1 and *sn*-2 positions, it comprises the simplest form of phospholipids called phosphatidic acid (PA) which serves as a precursor in the synthesis of many other lipids that they may modulate membrane curvature (see later sections) and act in cell signaling.

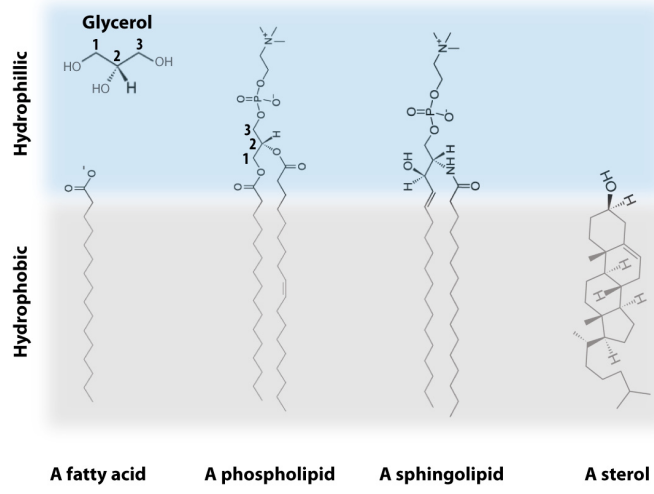

Figure 2 Examples of common constituents and building block of natural membranes including (left to right) the building blocks glycerol and fatty acids, 1-palmitoyl-2-oleoyl-*sn*-glycero-3-phosphocholine (POPC), N-palmitoyl-D-*erythro*-spingosylphosporylcholine (Sphingomyelin, SM) and cholesterol. The grey shaded area represents the hydrophobic part of the amphiphatic structures whereas the blue shaded region describes the water-soluble hydrophilic part of the molecule. Numbers 1,2 denotes the position of acyl chains and 3 denotes the position of the phosphate group on the glycerol backbone carbon atoms, respectively. The dotted square contains the sphingosine unit common for ceramides, thus including sphingomyelin.

PA phospholipids are essentially absent in biological membranes and additional groups such as choline, ethanolamine, glycerol, serine and inositol are esterified to the hydroxyl groups of the phosphate moiety to form phosphatidylcholine (PC), phosphatidylethanolamine (PE), phosphatidylglycerol (PG), phosphatidylserine (PS) and phosphatidylinositol (PI) headgroups. Figure 3 illustrates the net negative charge presented by phosphate groups in PA, PG, PS and PI phospholipids at neutral pH. The phosphate group becomes neutral only under very acidic conditions and is thus responsible for the negative charge of the otherwise neutral PI and PG headgroups (Refer to Table 1 for pKa values). Serine carries both a negative

and positive charge under physiological conditions which causes the PS headgroup to be anionic. The tetramethyl ammonium moiety of the PC headgroup is positively charged almost independent of the pH in solution (pKa 13) which makes PC headgroups zwitterionic under physiologically relevant conditions [2]. In PE, the tetramethyl moieties of the choline moiety are replaced with three hydrogen atoms which make the ethanolamine moiety more pH dependent (pKa~10-11). PE headgroups are thus zwitterionic at neutral and acidic conditions and become negatively charged only under basic environments[2, 3].

Phospholipids thus present a substantial range of hydrophilic headgroup variability in size and charge which together with the huge variability of the acyl chains makes the potential number of phospholipid species found in a single cell incredibly large.

Table 1 Dissociation constants of ionisable groups in phospholipid headgroups. The sign in brackets gives the net charge of the headgroup at the end of the titration step starting from pH 7.0. X denotes the hydrogen atoms of the amine group in serine and ethanolamine headgroups and the methyl groups of choline headgroups, respectively. Data adapted from [3]

Headgroup	pK ($PO4^-$)	pK ($PO4^{2-}$)	pK (COO^-)	pK (NX_3^+)	Charge at pH 7
Phosphatidic acid (PA)	3.5 (0)	9.5 (-2)			-1
Phosphatidylcholine (PC)	≤1 (+)			13[a]	+/-
Phosphatidylethanolamine (PE)	0.3 (+)			11.25(-2)	+/-
Phosphatidylserine (PS)	≤1 (+)		5.5 (+/-)	11.5 (-2)	-1
Phosphatidylinositol (PI)	2.7 (0)				-1
Phosphatidylglycerol (PG)	2.9 (0)				-1

[a] from ref. [2]

The second lipid group described here are sphingolipids as exemplified by sphingomyelin (SM) in Figure 2. The simplest sphingolipid is ceramide which consists of a hydrophobic fatty acid tail linked via an amide bond to sphingosine. The 1-hydroxy group of ceramides may further be substituted with phosphorylcholine or phosphorylethanolamine headgroups which are commonly termed sphingomyelins. SMs are common constituents of mammalian cells and are zwitterionic at neutral pH similar to their zwitterionic phosphocholine counterparts. An unusual feature of SMs is that the acyl chains are often unsaturated and comprises up to 24 carbon atoms [2]. Ceramides may also be substituted with sugar moieties such as glucose and galactose or even oligosaccharide structures to yield glycolipids of neutral charge.

Lastly, sterols are present in the cell membranes of plants (mainly sitosterol), fungi (mainly ergosterol) and mammals (mainly cholesterol) in which they may contribute as much as 20-50% of the total lipid composition [4, 5]. Whereas phospholipids and sphingolipids may possess a relatively large hydrophilic headgroup, only a hydroxyl group constitutes the hydrophilic part of cholesterol which is placed in the headgroup area whereas the remainder of the molecule is buried in hydrophobic region of the lipid bilayer

(Figure 2). The rigid steroid ring-structure of cholesterol restricts the motion of phospholipid acyl chains and thereby stabilizes the structure of cell membranes and thereby not only suppresses the permeability of ions, but also makes is less prone to disruption by antimicrobial peptides [6]. Thereby, the presence of cholesterol in mammalian cells, and not bacteria, is important for the selectivity and activity of antimicrobial peptides.

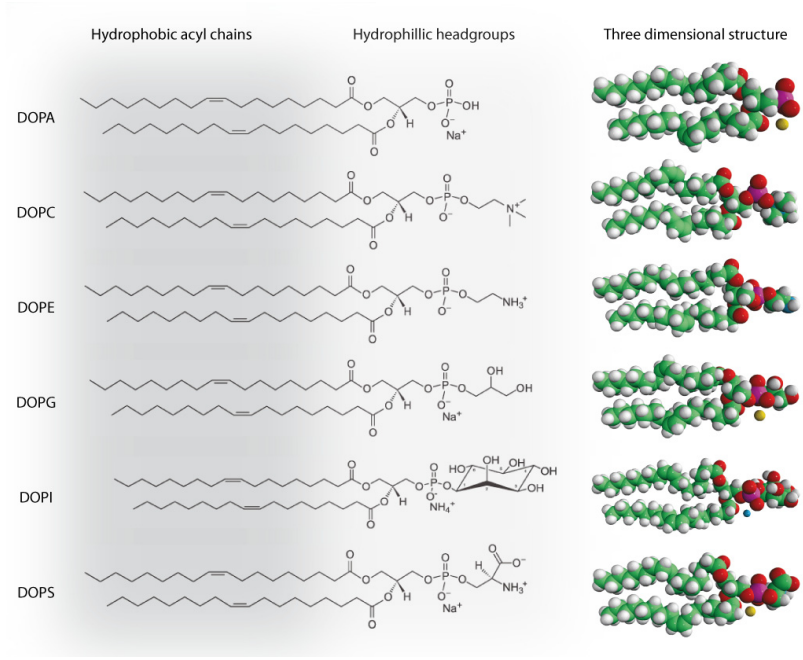

Figure 3 Illustration of the hydrophobic acyl chains (dark grey area) and hydrophilic headgroups (light grey area) of selected phospholipids and the corresponding three-dimensional structure. Carbon atoms are denoted in green, hydrogens in white, oxygen in red, phosphate in purple and sodium ions are represented in yellow. All phospholipids are shown with the oleoyl acyl chains for ease of presentation.

Lipid organization

In contrast to protein, DNA and other naturally occurring polymers important for life, lipid membranes lack the covalent linkages between adjacent lipids units. What causes lipids to self-assemble spontaneously into defined structures when they are added to water? The answer is to be found in the amphiphatic structure of lipids since the exposure of the hydrophobic acyl chains in the aqueous phase is highly unfavorable from a thermodynamic perspective. Lipids prevents conflicting propensity of the “heads” and “tails” to interact with water through clustering of the hydrophobic tails such that contact with water is minimized through exclusion of water. This is called the hydrophobic effect. Such clustering may lead to different aggregate structures such as the lipid bilayer, which is characteristic for biological membranes (Figure 1) but also micelles and inverted structures depending on the molecular geometry of the lipid. The most biological

relevant morphology of lipids is, however, that of the bilayer structure and is therefore the main focus of this work. However, *non-bilayer* lipids such as PE lipids from isolated natural sources have been suggested to be essential in the accommodation and activity of membrane proteins, membrane fusion and to maintain a constant curvature instability [7, 8].

A common feature of these aggregate structures is that they allow exposure of hydrophilic headgroups to water while the need for a hydrophobic environment is accommodated through packing of acyl chains in a hydrophilic environment. The aggregate structures are stabilized by cohesive forces by means of electrostatic and hydrogen bonding between headgroups and water, van der Waals attraction between acyl chains and the hydrophobic effect which excludes water from the hydrocarbon core.

The aggregate structure depends largely on the molecular geometry of lipids which is defined by several factors including the size of the headgroup, the length of the acyl chains and the degree of unsaturation. It is important to stress that the molecular structure represents the *average* geometry of the lipid since lipids are highly dynamic molecules and are not rigid structures as discussed in following sections.

PC, SM, PS, PI, PG and PA (with Ca^{2+}) lipids previously described are *bilayer forming* lipids and their geometry may be described to a good approximation by a cylindrical shape since the headgroup and hydrophobic domains have a similar diameter[9]. However, the naturally abundant PE headgroup (0.52-0.58$Å^2$ [10]) is smaller than PC (~0.62-0.65$Å^2$ [10]) and thus has a small headgroup. Further, PE headgroups often contain polyunsaturated acyl chains although chains are more saturated in bacteria such as *Escherischia coli* [11]. PE may thus be described by a cone shape which favors *inverted non-lamellar* structures in which the hydrophilic headgroups are clustered inward toward an internal aqueous core with the hydrophobic tails point out. However, PE lipids may exist in a bilayer arrangement when stabilized by bilayer forming lipids such as PC and PS at molar fractions of 20-30% and above [11]. The phenomenon that lipids may form phases different from the lamellar bilayer structure is known as lipid polymorphism. In general, the packing ratio of a lipid bilayer is approximately one leading to the lamellar structure observed in Figure 4, whereas packing ratios below one may result in micelle formation and a packing ratio above 1 to inverted non-lamellar structure.

The propensity of lipids to form bilayer structures are further affected by the length and degree of acyl chain unsaturation. A cylindrical lipid with long saturated acyl chains which allow tight packing of adjacent tails with maximum exclusion of water from hydrophobic core may readily form bilayers. In this arrangement, a linear array of the acyl chain and headgroup exist. However, if double bonds are introduced in one or both of the acyl chains, they will depart from the cylindrical shape since the carbon-carbon double bond introduces a kink which prevent it from packing with higher order compared to saturated acyl chain of the same length and decreases the overall length of the molecule. PE lipids with more saturated acyl chains are thus more prone to be stabilized in bilayer structures than those with more unsaturated lipids.

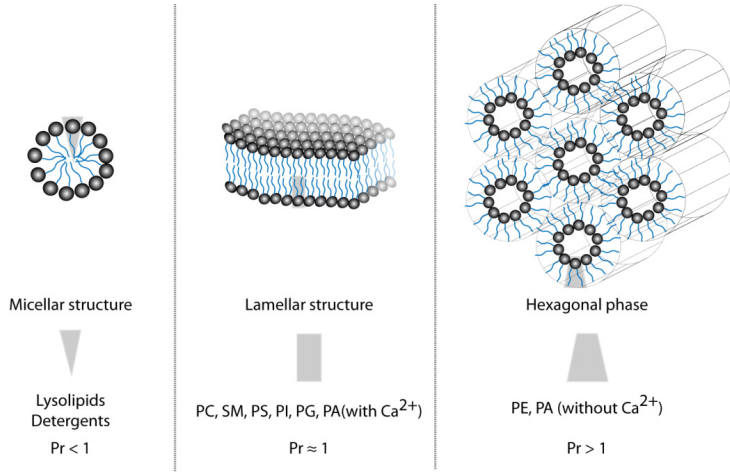

Figure 4 Polymorphic phases and the corresponding molecular shape of lipids. The packing ratio defined by Pr = v/(Al) defines the packing of lipids where v is the volume occupied by the hydrocarbon chains, A is the optimal surface area occupied by the lipid and l is the maximum length of the hydrocarbon chain. For lipids with a Pr < 1, the volume occupied by the acyl chains is small relative to the headgroup area leading to formation of micellar structures by e.g. detergents and lysolipids. Cylindrical lipids such as PC of Pr ≈ 1, the size of the acyl chains and headgroup domains match well and lead to lamellar structures. Truncated cones represent lipids such as PE and PA in the absence of calcium whose Pr > 1 result in formation of the hexagonal phase since the acyl chains are large relative to the headgroup. Illustration modified from [11] and [28].

Membrane dynamics

Phase transitions

Phospholipids can form a variety of different phase structures as a function of the headgroup and acyl chain composition, temperature, pressure and hydration [12]. This section limits itself to the phases relevant to the lamellar phases since these are most common for biological membranes.

Phase transitions may conveniently be observed by the amount of heat required to increase the temperature of a sample by the differential scanning calorimetry technique[13] as illustrated for the gel- to liquid disordered phase in Figure 4. First, the lipid bilayers may exist in the gel phase at temperatures below the transition temperature defined by the lipid headgroup and acyl chains of the lipids. The gel phase is characterized by a tight crystalline packing of stretched acyl chains. Consequently, the mobility within the bilayer and very slow diffusion rates are apparent.

When the temperature is raised above the transition temperature, the bilayer undergoes a phase transition into liquid disordered state, also denoted as the fluid phase. As indicated by the name, the acyl chains are more disordered in the liquid disordered phase and the increased thermal fluctuations result in an increased fluidity of the membrane. Owing to the thermally driven increase in entropy, the diffusion rates of lipids and embedded biomolecules are thus much faster in the fluid phase compared to the gel phase.

The increased rate of the dynamics of membranes in the fluid phase further makes it thicker than the same lipid membrane in the gel phase. The third phase described in Figure 4 is the liquid crystalline phase which may be described as an intermediate of the latter. When cholesterol is embedded to lipid bilayers, the rigid structure of the hydrophobic ring structure leads to an increase in the order of adjacent acyl chains and straightening of the acyl tails. While cholesterol increases the acyl chain order in the bilayer, it also prevents crystallization into the gel phase and the overall stabilization of the bilayer, making it less deformable and decreases the membrane permeability. The straightening of the acyl chains further leads to an increase in the bilayer thickness. The membrane thickness thus depends on chain length, degree of acyl chain unsaturation, temperature and modulating constituents such as cholesterol.

The phase at which a particular lipid exists depends largely on the degree of unsaturation and acyl chain length of the phospholipids at a given temperature. For instance, a 1,2-distearoyl-*sn*-glycero-3-phosphocholine (DSPC) which contain two identical saturated chains of 18 carbon atoms (C18:0) displays a phase transition from the crystalline gel to the liquid disordered state (Figure 4) at a temperature of 55°C. When a double bond is introduced in *one* of the acyl chains (C18:1, oleoyl) decreases the transition temperature to 6°C and when both acyl chains contain double bonds (1,2-dioleoyl-sn-glycero-3-phosphocholine, DOPC), the transition temperature is lowered to -20°C. Curiously, introduction of a double bond in the acyl chain at the *sn*-2 position of the glycerol backbone has a larger effect on the transition temperature than when the same double bond is placed at the *sn*-1 position. In regard to the headgroups, the variability of transition temperature is less profound ranging from -20 to 11°C in the order PC<PG<PE<PS for lipids with two oleoyl acyl chains.

The section above treats lipids of similar chain length which may be expected to give rise to ideal mixing. However, if acyl chains differ in chain length by more than ~2 carbon atoms it may lead to the development of co-existing fluid and gel phases. Phase separation may arise due to a difference in transition temperatures, especially if the lipids with longer acyl chains are also unsaturated. An example is the mixing of 1,2-dipalmitoyl-sn-glycero-3-phosphocholine (DPPC, C16:0 chains) with 1,2-dioleoyl-sn-glycero-3-phosphocholine (DOPC, C18:1 chains) which display heterogeneous in which the components separate into different domains corresponding to the pure components[14]. The DOPC domain is fluid at room temperature whereas the DPPC lipid exists in the gel phase. In the laboratory, this phase separation also emphasizes the need to prepare lipid mixtures at temperatures above the phase temperature of the constituent with the highest thermal transition to ensure proper mixing of lipid constituents. Addition of cholesterol to such a lipid system may lead to the formation of a uniform phase although such systems display complex phase behaviors depending on temperature and molar fraction of the constituents[14, 15].

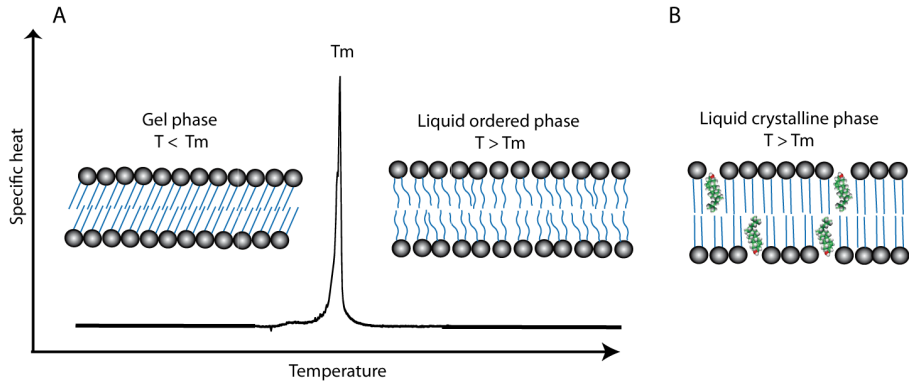

Figure 5 Schematics of the phase behavior of pure lipids and the effect of cholesterol on acyl chain order. (A) When a membrane in the gel phase is heated above the transition temperature (Tm) it changes to the liquid disordered (fluid state) in which the membrane area is expanded and thickness increases relative to the gel phase. The mobility of acyl chains is increased dramatically. (B) Addition of cholesterol to the fluid state decreases the mobility of acyl chains, straightens them and thereby increases order and bilayer thickness.

Dynamic properties of lipid membranes

Lipid membranes are highly dynamic structures in which several modes of motion occur on time scales ranging from picoseconds to hours or even days. The rates of such motions are largely influenced by the phase of the membrane and the events described below refer to those occurring in the liquid disordered state since organisms regulate their lipid compositions to be able to grow within a window between the gel phase and reversed-lamellar phases, i.e. in the lamellar bilayer state [16].

Lipid flip-flop across the bilayer (Figure 5) is a slow process which occurs with a rate ranging from minutes to hours or even days [5, 17]. The process is highly unfavorable since it requires the hydrophilic headgroup to traverse the hydrophobic core of the membrane. The flip flop transfer increases in the order PE > PA > PG > PC where the flip flop rates of PE lipids have been observed to be at least 10 times larger than PC[18]. In natural membranes, an asymmetric headgroup distribution between bilayer leaflets is mediated by flippases which move specific lipids toward or away from the cytosolic leaflet at the expense of energy or abolished by scramblases [19].

Figure 5 further shows that individual lipid molecules undergo axial diffusion (rotation) around its own axis and move laterally within the membrane on timescales in the order of nanoseconds. The latter allows Individual lipid molecules to explore the entire bilayer of a cell within reasonable time. Lipid protrusions from the bilayer plane (not shown) and changes in the acyl chain conformation around carbon-carbon bonds by trans/gauche isomerisation and acyl chain stretching are fast processes which occur at the picoseconds scale. Acyl chains are preferentially in the trans-conformation below the phase transition temperature but the higher energy gauche conformations may be adopted above the Tm. Wobbling is the process in which acyl chains change their direction within the bilayer occurs at a time scale of the order of milliseconds as illustrated in Figure 5[5].

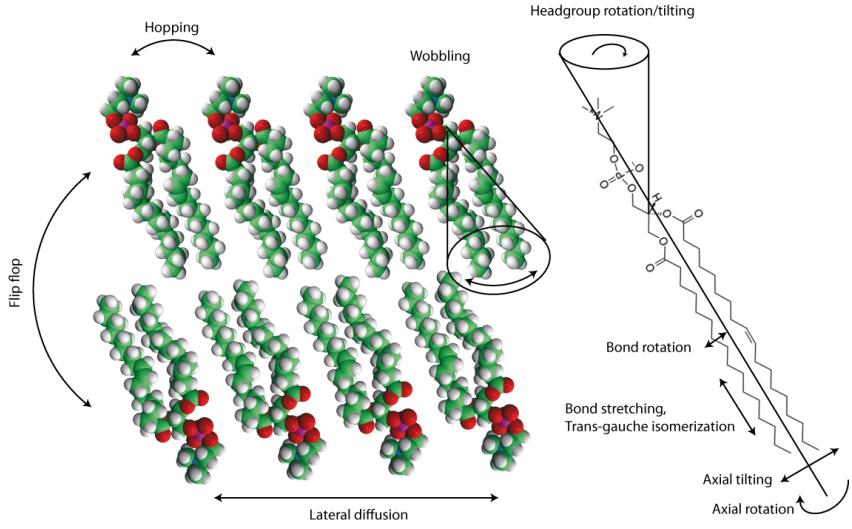

Figure 6 Modes of lipid movement within lipid bilayers (left) and with single lipid molecules. Lipids may exchange position with the adjacent molecules, transfer to the opposite leaflet by "flip flopping", undergo lateral diffusion within on leaflet and change the direction of their acyl chains within the bilayer by wobbling. Individual lipids undergo axial rotation and tilting, acyl chain stretching and trans-gauche isomerization, bond rotation and headgroup rotation/tilting. Lipid structures were obtained from Avanti Polar Lipids.

1.2. Natural lipid membrane compositions

The cell surface of mammalian and bacterial cells display several fundamental differences which are important for the selectivity of antimicrobial peptides toward bacteria. The central structural elements of cell membranes are phospholipids which will thus be the primary focus of following sections. Cell membranes further contain additional components such as proteins, carbohydrates and complex polymers which may constitute up to half of the total weight of isolated cell walls. Several of these constituents may pose significant barriers which antimicrobial peptides must face in order to exert their membrane disruptive activities in bacterial cell membranes.

Mammalian membranes

The lipid composition in the membranes of mammalian cells are highly variable in individual cell compartments and thousands of different lipid species may be found within any cell arising from the multitude of possible variations in headgroup and fatty acid acyl chains[4, 20]. The plasma membrane is, however, the first barrier exposed to exogenous AMPs and the lipid headgroups are involved in a potential interaction. The major lipid headgroups of these are PC, PE, PI, PS and SM[4]. The lipid constituents of mammalian cells are asymmetrically distributed between the two leaflets of the plasma membrane with anionic PS, PE and PI preferentially located in the inner leaflet of the plasma membrane facing the cytoplasm and zwitterionic SM and PC facing the extracellular space. The asymmetric distribution of

headgroups arises from translocation machineries which flip lipids to against a concentration gradient with the cost of energy from ATP [4, 21, 22]. Cell injuries or apoptosis can induce the loss of lipid asymmetry in membranes and leads to exposure of anionic PS which may at least in part explain why certain AMPs such as cecropin A and B may target tumor cells[23, 24]. In addition to the above phospholipids, mammalian cells on average contain 20-30% cholesterol but may constitute as much as 50% of lipids depending on the tissue type [4, 5].

Bacterial membranes

Bacteria have been divided into two subgroups depending on their ability to retain *crystal violet* in their cell wall. Gram positive bacteria bind the dye *crystal violet* in the cell wall due to a thick layer of peptidoglycan on the exterior side of the plasma membrane as illustrated in Figure 6. Gram positive bacteria include several genera such as S*treptococcus*, S*taphylococcus, Lactobacillus* and *Bacillus* and constitute both beneficial and pathogenic bacteria. Peptidoglycan is a complex matrix consisting of polysaccharide chains which are cross-linked by short peptides to constitute a meshwork which strengthens the bacterial cell wall. The cell wall of gram positive bacteria further consists of long chain polymers of ribitol phosphate and glycerol phosphate called teichoic acids. Teichoic acids (TA) can be found either covalently linked to the peptidoglycan layer or linked via lipids to the underlying cell membrane[25, 26]. Since TA contains phosphate groups, the polymer present an anionic character which may act as a scavenger for cationic antimicrobial peptides. Turning to the bacterial membrane which is the principal target of most antimicrobial peptides, the determining factor for initial association of cationic AMPs is the electrostatic attraction to negatively charged lipids. The major part of lipid headgroup species in gram positive bacteria is constituted by the anionic PG and cardiolipin (CL) which in essence is two PG moieties connected by a glycerol backbone and also referred to as diphosphatidylglycerol (DPG) [27]. These lipids are accompanied by PE and PI lipids as well as O-aminoacyl derivates of PG[28].

Bacteria which do not bind crystal violet to a large extent due to a much thinner peptidoglycan layer are termed Gram negative and differences in cell wall architecture compared to gram positive bacteria are illustrated in Figure 6. Gram negative bacteria include medically relevant bacteria such as *Salmonella typhimurium*, *Escherischia coli* and P*seudomonas aeruginosa*. They do not contain TA, but contain an additional outer membrane (OM). The outer membrane is stabilized by lipopolysaccharides (LPS) which are anchored to the membrane by multiple fatty acids via Lipid A and contribute to the negative charge of the bacterial surface due to the presence of negatively charged phosphate groups in the core and lipid A backbone[29]. The OM contains variable amounts of PC, PE, CL and PG phospholipids[27]. The OM lipid composition of these bacteria consists of three major parts including PE (70-80%), PG (20-25%) and CL (0-5%)[27, 28]. The plasma membrane of *Salmonella typimurium* has been shown to consist of approximately 60% PE, 33% PC and 7% CL whereas the ratio of these lipids in *Escherichia coli* plasma membranes has been described by 75-82% PE, 6-11% PG and 12-14% CL [28, 30]. The large proportion of PE lipids in these membranes is remarkable owing to the propensity of PE lipids to form non-lamellar structures. However,

studies have shown that PE lipids are important in regulation of membrane compositions to maintain an approximately constant spontaneous curvature and to modulate membrane curvature in budding, fusion and fission events [16, 31-33]. Altogether, the net anionic character of the bacterial interface suggests that a strong electrostatic interaction with cationic peptides is the primary driving force of the selectivity of AMPs.

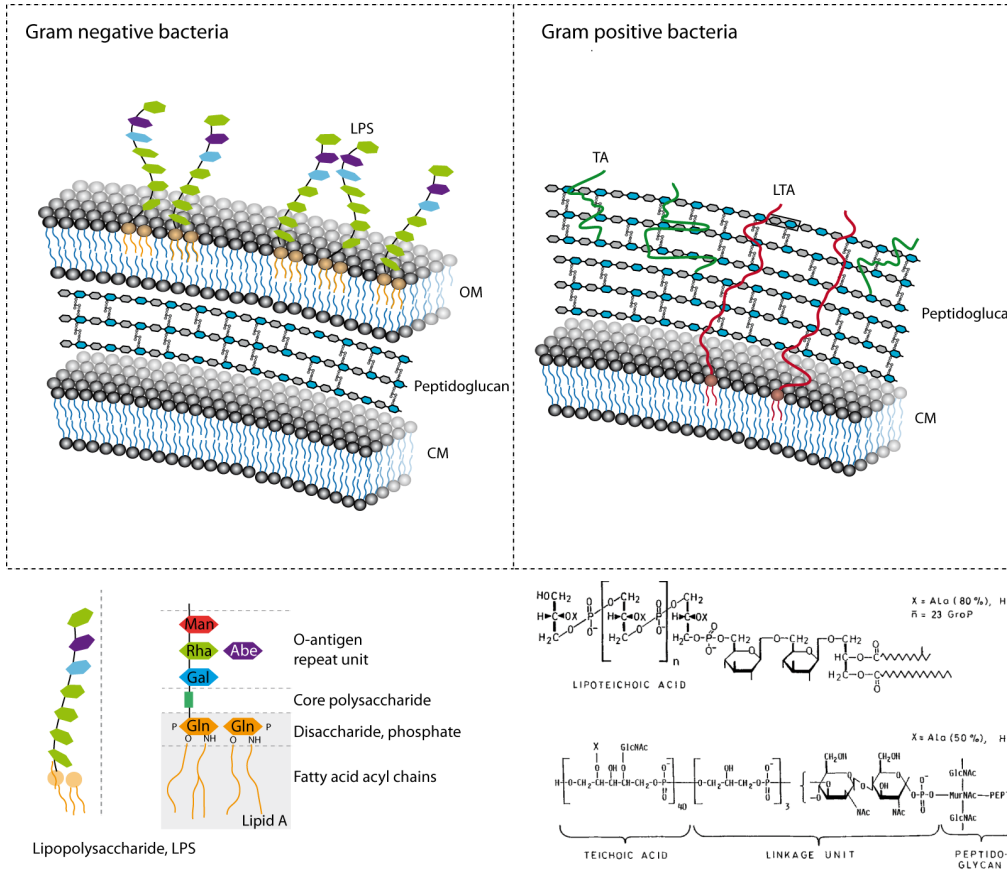

Figure 7 Illustration of important differences in the cell surface architecture of gram positive and gram negative bacteria. Outside the cytoplasma membrane of Gram negative bacteria, a thin peptidoglycan layer together with the periplasmic space (not illustrated) separate the outer (OM) and inner cytoplasma membrane (CM). Lipopolysacchrides (LPS) are anchored to the outer membrane via Lipid A. The cell wall of gram positive bacteria lack the OM but contains a thick layer of peptidoglycan to which polyol phosphate polymers of teichoic acids (TA) are associated. Lipoteichoic acids (LTA) are amphiphatic glycophosphates associated to the CM via a lipidic linker. Protein constituents were omitted and only a single lipid species is shown for clarity of illustration. The importance of lipid constituents is explained in the text. Illustration of teichoic and lipoteichoic acids from gram positive *Staphylococcus aureus* is reprinted from [26] with permission.

1.3. Model membranes

The previous sections describe the huge complexity of biological membranes not only within species variation but also inside individual compartments of a single cell. *In vitro*, it is rarely attempted to achieve close replica of the lipid compositions in such membranes since this can be very difficult. Further adding to the complexity is the diversity of non-phospholipid moieties such as membrane proteins and extracellular polymers. It is, however, generally accepted that the physical interaction of AMPs with membranes is the principal factor leading to cell death and assign the interaction with additional targets to accessory roles occurring once the membrane integrity is breached [34-38]. Monitoring the key parameters of membranes *in vivo* is difficult to achieve and the use of model membranes *in vitro* is therefore an important in defining specific interactions between antimicrobial peptides and membrane.

Cell membranes are in essence lamellar structures composed by two leaflets of varying composition. However, the lipid composition is often dominated by 2-3 lipid species which may be exploited in model systems. For instance, it seems tempting to mimic the composition of the outer leaflet of a mammalian membrane using the three major constituents composed SM, PC and cholesterol to prepare vesicles rather than attempting to prepare membranes with asymmetric lipid composition as found *in vivo*. In order to model the anionic character of bacteria it is thus tempting to employ a binary mixture of zwitterionic and anionic lipids. Indeed, combinations of lipids with PC or PE and PG headgroups have been extensively used to mimic bacterial membranes. In the presented studies of novicidin and alamethicin scaffolded on α- or β-cyclodextrins to constitute a stable synthetic pore construct, we limited ourselves to a binary mixture of 80% DOPC and 20% DOPG to mimic the net negative surface charge of bacteria and used vesicles consisting purely of DOPC to mimic the mainly neutral character of mammalian cell surfaces.

The reason for choosing zwitterionic DOPC rather than a phospholipid with the zwitterionic PE headgroup is twofold. First, PE lipids with unsaturated acyl chains (e.g. C18:1) are not very well suited for bilayer formation due to the propensity to form inverted structures and the use of e.g. 1,2-dipalmitoyl-*sn*-glycero-3-phosphatidylethanolamine (DPPE) or 1-palmitoyl-2-oleoyl-*sn*-glycero-3-phosphoethanolamine (POPE) was not feasible since they are in the gel phase at ambient temperatures. Secondly, the dioleoyl moieties of both DOPC and DOPG lipids does not lead to coexistence of solid and liquid ordered phases under conditions employed which could otherwise lead to isolated domains of highly anionic character.

The following sections describes model membrane morphologies (Figure 7) of importance for these and future studies and include spherical lipid aggregates in the form of micelles, multilamellar vesicles, unilamellar vesicles ranging from approximately 30nm through 200μm, uniform planar bilayers and lipid monolayers which are all valuable models of biomembranes for specific purposes.

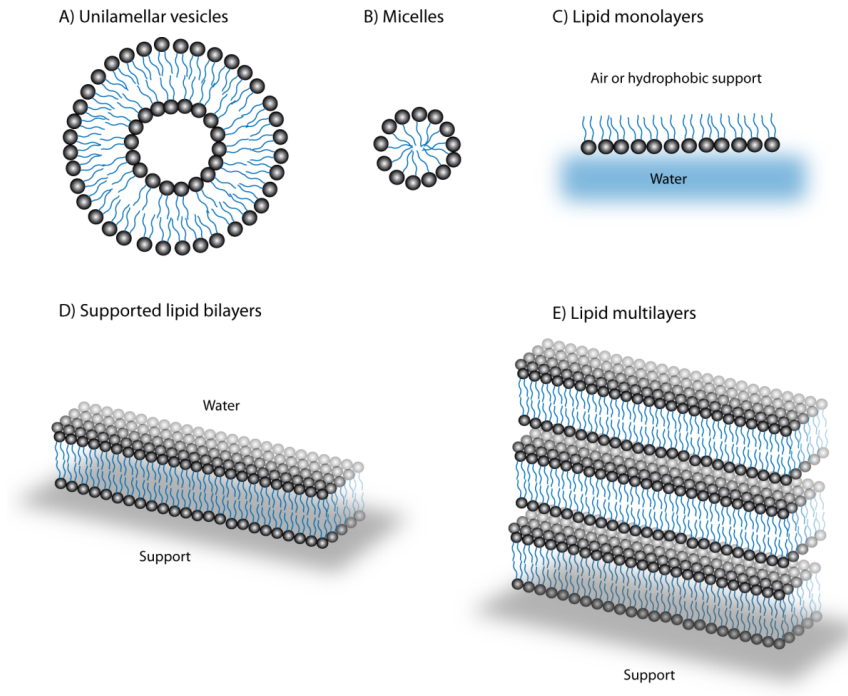

Figure 8 Illustration of commonly used membrane models. (A) Lipid vesicles of varying size can be prepared by sonication, extrusion and electroformation methods to produce vesicles of ~25 nm, 30-800nm and 10-100µm, respectively. (B) Detergents and lysophospholipids containing only one acyl chain may form micellar aggregates. (C) Lipid monolayers may be formed by exposure of lipids to hydrophilic supports or by spreading at the air-water interface. (D) Supported planar bilayers formed by collapse of vesicles on a hydrophilic support separated by a water film. (E) Multilayer membranes form from vesicle suspensions or lipids deposited from organic solvent. Multilayer membranes are separated by a thin water film when hydrated.

Multilamellar vesicles

Multilamellar vesicles (MLVs) serve as the starting point in the preparation of several smaller vesicular structures such as small and large unilamellar vesicles, respectively. When bilayer forming mixtures of phospholipids are dried from organic solvents on a support and rehydrated in aqueous media, large stacked sheets of unilamellar bilayers separated by water are formed as shown in Figure 7E. By gentle hand shaking or vortexing, the multilayer membranes detach and seal to form MLVs in order to avoid energetically unfavorable exposed hydrophobic edges. The internal lamellar structure resembles that of an onion (not shown). Lipid or water soluble molecules can be included in the hydration buffer in order to entrap these molecules within the bilayers or interior of vesicles. However, MLVs are generally not suited for entrapment of water-soluble molecules such as chromophores since the internal volume is largely occupied by multiple bilayers.

Small unilamellar vesicles

The smallest vesicles employed to mimic natural membranes are small unilamellar vesicles (SUVs) of ~25nm which is at or close to the lower size limit possible. The minimum size of vesicles is defined by the lipid shape since the curvature of the inner leaflet in vesicles increase with decreasing vesicle size. Since a high membrane curvature is present in SUVs, approximately double the amount of lipid is present in the outer leaflet compared to the inner one. Since the formation of SUVs is not a spontaneous process due to curvature strain it requires energy to produce such vesicles. Preparation SUVs can be accomplished using a sonication probe. In this case, it is important to immerse the lipid solution in a cooling bath since a high energy is applied to the system which results in sample heating and excessive sonication should therefore be avoided to minimize the risk of sample oxidation and hydrolysis. Further, SUVs are not stable structures and may undergo vesicle fusion and aggregation over time which is why they should be used within a short time after preparation. Since the volume enclosed by SUVs is very small, the encapsulation of water soluble molecules inside vesicles is not favorable compared to larger vesicles. SUVs are especially suited for use in combination with optical techniques since they are less prone to scatter light and increase turbidity of samples compared to larger vesicles [39].

Large unilamellar vesicles

As their name implies, large unilamellar vesicles (LUVs) are larger than SUVs and consists of a single continuous bilayer as shown in Figure 7A. LUVs are usually prepared by extrusion through membranes with defined pore sizes available in the 30 to 800nm range with vesicles of ~100nm most frequently used. The larger size of LUVs compared to SUVs results in an approximate even distribution in numbers of the lipids between the inner and outer leaflet[9]. The starting point in LUV preparation is MLVs which subjected to multiple freeze-thaw cycles leading to the formation of more unilamellar vesicles with an increased internal volume. The size of these vesicles is reduced to their desired size by multiple passages through the membrane pores and result in vesicles of high homogeneity with a size distribution slightly above that of the selected pore size[40, 41]. It should, however, be noted that vesicles produced by extrusion using pores of more than 200nm are less homogenous with respect to size. The larger vesicle size of LUVs result in a lower membrane curvature compared to SUVs and further increases the interval volume which makes them well-suited for entrapment of water-soluble molecules. Entrapment of molecules is generally accomplished by including it in the initial rehydration buffer followed by extrusion as described above. Subsequent purification of the vesicle suspension by gel filtration allows separation of filled vesicles from non-encapsulated molecules [41, 42].

Although LUVs are larger than SUVs and thereby more prone to scatter light, LUVs of ~100nm are still sufficiently small for use in optical techniques. LUVs thus constitute an excellent model system for studies of membrane leakage and protein-membrane interactions.

LUVs containing amphiphilic components such as membrane proteins may be prepared by an alternative approach using detergent removal procedures. This allows the incorporation of proteins whose function would otherwise be lost through exposure to organic solvents or during sonication and extrusion procedures. The protein solubilized in a detergent in which its structure and function is maintained and which satisfies the hydrophobic nature of transmembrane segments serves as the starting point for reconstitution into lipid vesicles. The protein:detergent solution is mixed with lipids in the form of a lipid film or lipid vesicles to create mixed micelles composed by protein, lipid and detergent. Detergent removal may be accomplished by several approaches including dilution to a concentration below the CMC of the detergent, removal of detergent by dialysis, gel filtration or adsorption to polystyrene beads (for a review on methods for detergent removal, refer to reference [43, 44]). During detergent removal, lipid molecules aggregate into bilayers and lipophillic proteins may be embedded in the vesicles. LUVs formed by detergent removal procedures vary in both size and homogeneity depending on various parameters such as lipid, protein and detergent content and detergent removal rate.

Giant unilamellar vesicles

The size of giant unilamellar vesicles (GUVs) are generally in the order of ~10-100µm making them especially suited for studies in which various light microscopy techniques are used including fluorescence microscopy, confocal laser scanning microscopy and micromanipulation methods such as optical tweezers and micropipette techniques owing to their size above the lower limit of resolution for light microscopy of approximately 200nm [45]. The size of GUVs further allow the study of lipid phase separation by fluorescence- and confocal microscopy procedures using specific fluorescent dyes which partition in certain phases or change fluorescent properties.

Several methods for preparation of GUVs exist and the method of choice depends on the problem addressed. A simple and fast procedure to form GUVs involves mixing of lipids in organic medium into the buffer which also contain potential molecules to be entrapped [46]. The organic solvent is removed by vacuum and heating in a rotary evaporator and results in a high concentration of GUVs of mainly unilamellar character. While the method is fast and straightforward, it also includes the use of organic solvents which may still be present in trace amounts even after evaporation.

A more time consuming procedure is the method of gentle hydration. Here, lipid films are formed on glass [47] or Teflon surfaces [48] during evaporation of organic solvents followed by slow hydration of the film in aqueous solution over as much as 48 hours [47]. During the course of rehydration, the lipids swell to form a “cloud” which can be harvested by gentle aspiration [48]. While allowing the use of a large range of buffer compositions it may result in a heterogeneous population of multilamellar vesicles due to the uncontrolled rehydration process [49].

In **paper I** and **IV** presented here, we employed GUVs prepared by electroformation [50, 51]. Lipids are deposited on platinum electrodes from organic solvent which is removed under vacuum. Lipids are rehydrated in the buffer of choice while applying an oscillating current which leads to membrane and fusion of small vesicles into GUVs of ~15-70µm in size. Vesicles prepared by the electroporation method present a more homogeneous size distribution compared to the gentle hydration and solvent evaporation techniques described above and further provide mainly unilamellar vesicles [52]. However, even more homogenous vesicle sizes can be obtained through a refinement of the electroformation procedure though microcontant printing of lipids on ITO glass slides leading to formation of ~13µm GUVs [53]. Another variation of the electroformation procedure in which proteoliposomes are partially dehydrated in the presence of a saturated salt solution yielding exposure of ~75% relative humidity toward the ITO coated glass followed by electroformation [49]. The partial dehydration step overcomes the deleterious effects of the dehydration step which may impair the folding and biological activity of membrane proteins. The incorporation of membrane proteins in GUVs may also be facilitated by vesicle fusion. For instance, bacteriorhodopsin has been incorporated in GUVs through peptide-mediated fusion between LUVs in which BR was incorporated and fused with GUVs [54].

Supported planar bilayers

Planar supported lipid bilayers (SPBs) comprise an interesting model system providing structural and dynamics of free lipid bilayers. Phospholipid vesicles may spontaneously adsorb to solid surfaces and depending on the characteristics of the surface and buffer, they may undergo rupture and fusion to form supported phospholipid bilayers (SPBs) separated from the solid support by a thin water film (Figure 7D), adsorb as intact vesicles or resist adsorption and remain in suspension. The mechanism of SPB formation has been examined extensively using complementary methods such as quartz crystal microbalance with dissipation monitoring (QCM-D), surface plasmon resonance (SPR), fluorescence microscopy, atomic force microscopy (AFM) and dual polarization interferometry (DPI) [55-60]. Bilayers can be formed on surfaces such as glass, mica, silica nitride or SiO_2, whereas vesicles do not rupture on adsorption onto TiO_2, oxidized gold or platinum but result in adsorption of intact vesicle layer or even no adsorption depending on lipid composition such as described for 4:1 mixtures of DOPC and anionic DOPS on SiO_2 due to electrostatic repulsion between the support and the lipids [55, 58, 59, 61, 62]. Recent studies have, however, pointed out the importance of electrostatic attraction and calcium ions by demonstrating bilayer formation from vesicles suspensions on TiO_2 solid support facilitated by calcium [62, 63]. The presence of divalent cations such as calcium or magnesium may thus promote SPB formation from both vesicles consisting of both pure zwitterionic and vesicles containing anionic PS lipids [61]. Several pathways of SPB formation have been suggested including spontaneous rupture of isolated vesicles due to significant deformation on adsorption, cooperative vesicle rupture at certain critical vesicle coverage and vesicle rupture at the edges of bilayer patches which is essentially a combination of the latter.

The ability of lipids to form planar supported lipid bilayers depends largely on the geometry of the employed lipids. Thus, the addition of *non-bilayer* such as those with PE headgroups obstruct bilayer formation on glass surfaces while the successive introduction of methyl groups in PE-Me and PE-Me_2 headgroups has been shown to increase the propensity of bilayer formation since they form lamellar phases similar to DOPC [64]. In **Paper II and IV**, we employed SPBs formed by spontaneous vesicle collapse on SiO_2 and silica nitride surfaces in QCM-D and DPI experiments, respectively. While supported bilayers may also be formed on polymer cushions and freely suspended bilayers on edged surfaces [62], the bilayers formed by spontaneous vesicle collapse has generally been the method of choice in QCM-D and DPI applications [55, 56, 60, 61, 65, 66].

Planar oriented multilayers

Planar oriented lipid multilayers are, in principle, planar supported stacks of bilayers separated by a thin water film (Figure 7E). These multilayer membranes are amenable to techniques such as X-ray and neutron scattering and diffraction techniques, solid-state NMR and oriented circular dichroism; all of which are frequently used to characterize the influence of AMPs of lipid structure and/or *vice versa*. The preparation of solid-supported multilayer membranes is usually done by spreading of lipids from organic solvent or by spin coating [67-69]. In **paper II** and **III**, the deposition from organic solvent involving three steps was chosen: Deposition of lipid and peptide/protein, a drying step and a rehydration step. Lipids may be deposited by spreading of lipid stocks in organic solvent on the desired surface or by transfer of vesicles in aqueous solution.

When lipid multilayers are prepared from organic solvent, lipids are mixed with the peptide at appropriate protein or peptide to lipid ratios and transferred to a support such as the quartz slide from a Hellma 124-QS cell and dried. Care must be taken to spread the lipid evenly on the surface. In this work, 5µl 10mg/ml sample in 1:1 chloroform:methanol was transferred to the glass slide while spreading the it with the tip of a pipette. This procedure was repeated once more to create a lipid film of 100µg and varying peptide content. The deposition of 100-200µg lipid on the surface was chosen since such films are sufficiently transparent to avoid an excessive increase in HT voltage (which is roughly proportional to the absorbance of the film) and thus impair the performance of the CD equipment. Residual solvent is removed in a vacuum dessicator by incubation for at least two hours. An improved method based on naphthalene and organic solvents to prepare aligned multilayer samples to improve the degree of alignment in solid-state NMR studies has been described and applied to describe the orientation of MSI-78 and MSI-594, gramicidin and pardaxin peptides in aligned bilayers [70, 71].

The procedure to prepare lipid multilayers from vesicles in aqueous solution is similar except that the aqueous phase does not evaporate as rapid as often employed organic solvents. Presumably, the preparation of lipid multilayers from aqueous solution may be a result of significant up-concentration of salts and buffer components when dried. Since the same amount of water is not take up on subsequent

hydration, buffer components may lead to artifacts for instance in OCD measurements due to sample absorbance or influence on the interaction of proteins or peptides with lipids.

Rehydration of the lipid film can be accomplished by means of several procedures. A convenient way to obtain a desired degree of hydration is to let samples come to equilibrium with air of a defined relative humidity (RH). Complete hydration (100% RH) is not desired in applications where the sample has to be oriented in a vertical state since membranes may float off the support but saturation may be accomplished by exposing the sample to air which has been bubbled slowly through a water tank.

An alternative method of humidity control is the use of saturated salt solutions. For instance, a vapor pressure corresponding to 97-98% relative humidity (RH) can be obtained by placing a saturated solution of K_2SO_4 inside the chamber whereas a saturated NaCl solution result in ~75% RH and a saturated MgCl2 solution lead to ~33% RH [72]. An alternative approach is the use of PEG solutions to reach a desired hydration level [69]. Besides OCD and solid state NMR studies, aligned lipid bilayers have been employed in X-ray diffraction studies to measure e.g. changes in bilayer thickness and lamellar spacing (bilayer repeat distance) changes in the presence of alamethicin [73].

Micelles

A micelles (Figure 7B) is the aggregate structure formed by detergents, lyso-phospholipids and short-chain phospholipids and cell membrane mimicking phospholipid analogues such as dodecylphosphatidylcholine (DPC) when their concentrations in bulk is raised above their critical micelle concentration (CMC). At the CMC and above, the concentration of monomers remains relatively constant and further addition of detergent will associate into micelles. In contrast, monomers are present at concentrations lower than the CMC. It is important to note that the CMC denote the detergent concentration in bulk solution and not the absolute detergent concentration in a sample. The detergents thus bind to membranes or hydrophobic patches of proteins at low concentrations via the hydrophobic chains of the detergent until it reaches saturation. If the detergent concentration is raised further to the CMC and above, mixed micelle complexes of lipid:detergent, protein:detergent or pure detergent are formed. Micelles play a central role in several scientific and technological applications. In the context of this thesis, micelles have been employed as mimetics of cell membranes in the study of AMPs structures [74-76] and to probe the effect on the structure and activity of proteins such as inactivation, activation or unfolding [77, 78].

2. Antimicrobial peptides and their interaction with lipid membranes

Bacteria are often considered to be malignant organisms and the cause of infectious diseases. Bacteria are indeed the cause of several diseases such as food poisoning, pneumonia or tuberculosis although it must be emphasized that the vast majority of bacteria are harmless or even beneficial for the host. Harmless or beneficial bacteria are often referred to as the normal flora and include more than 500 different bacterial species which are present in at the epithelial linings of the skin, saliva, airways and intestinal tracts [79]. Here, they contribute in maintaining health through synthesis of vitamins, fermentation of ingested foods and conversion of indigestible sugars and even modulate the growth of potentially pathogenic bacteria through competitive exclusion [79, 80].

Colonization by pathogenic bacteria may be prevented by the presence of harmless bacteria through several mechanisms including competition for nutrients, secretion of antimicrobial compounds such as nisin by *Lactococcus lactis* or through stimulation of the host's immune defense system to induce secretion of antimicrobial substances [79, 81]. However, when the immune defense system and normal bacterial flora is no longer sufficient to prevent infection by pathogenic bacteria, infections may also be treated medically by antibiotics.

Infection by pathogenic bacteria are currently treated using antibiotics such as the broad-spectrum antibiotics penicillin, tetracycline, chloramphenicol and streptomycin which targets a wide range of bacteria including both Gram positive and Gram negative bacteria. Such antibiotics interfere with the normal cell cycle of bacteria through inhibition of essential processes such as cell wall, DNA and protein synthesis which inevitably leads to cell death. However, inappropriate use of antibiotics has contributed to the emergence of bacteria which are resistant to conventional antibiotics or even multiple resistances toward several antibiotics[82-84].

In the case of penicillin, which normally acts by preventing synthesis of peptidoglycan in the bacterial cell wall, antimicrobial resistance may arise through increased expression of β-lactamases which hydrolyse the β-lactam ring of penicillin leading to a deactivation of the drug and consequently the inability to synthesize the cell wall component. It is food for thought that the first incidence of antibiotic resistance toward penicillin in S*taphylococcus aureus* was discovered just four years after mass production had started in 1943. Development of antibiotic resistance toward potentially harmful substances in the environment is, however, a direct consequence of natural selection "survival of the fittests" and emphasizes the need for regulation of antibiotic usage in the treatment of infections if antibiotics are ought to remain effective. Despite efforts in regulation of antibiotic usage, the speed at which microbial resistance develops toward new antibiotics in a "use it and lose it" fashion which has led to an urgent need for continuous research and development in order to maintain a pool of effective drugs.

An appealing approach to accommodate the need for new antibiotics is to take advantage of naturally occurring substances in the fight against infections from pathogenic bacteria. In this respect, AMPs have gained attention in the search of alternatives to conventional antibiotics. They have been isolated from all classes of life including vertebrates, invertebrates and plants in which they serve as protective agents against infection of pathogenic microorganisms including bacteria, fungi and have been found to target even viruses, parasites and tumor cells. Whereas conventional antibiotics often target specific functions of the cell, AMPs often kill microorganisms through disruption of the cell membrane which leads to loss of essential biological gradients across membranes and ultimately cell death.

2.1. Characteristics of antimicrobial peptides

AMPs are found and stored in granules of tissues exposed to the environment such as epithelial and blood cells as a first line of defense against infection by pathogens. The peptide sequences are generally relatively short and consist of approximately 10 to hundreds of amino acid residues which show great diversity with respect to secondary structure, charge and amino acid composition [85]. The average length of 1518 known peptides in the antimicrobial peptide database (APD) is approximately 30 residues. The known structures are diverse and range from α-helix to β-sheet, AMPs rich in unusual residues, peptides containing disulphide bridges to combinations of α-helix and β-sheet conformations (Table 2) [85]. Most antimicrobial peptides are cationic and carry an average net positive charge of +3.8 per sequence although also anionic AMPs exist [85]. The net positive charge presented by an excess of lysine (K) and/or arginine (R) residues in AMPs is likely a result of evolution giving organisms presenting cationic antimicrobial peptides an advantage in resisting pathogenic infections since AMPs are targeted preferentially toward the overall negative charge of most bacterial interfaces. In contrast, the more neutral or zwitterionic amphiphiles presented at the surface of host cells and the electrostatic attraction may provide a ready explanation for the specificity of AMPs toward bacteria.

AMPs may be divided into five groups based on their structure and amino acid composition as shown in Table 2. Peptides which contain cysteine residues may form one or more disulphide bridges which, for example, stabilize the antiparallel β-sheet structure of human α-defensin and the combined α-helix/β-sheet structure of human α-defensin (Figure 8). AMPs may also be particularly enriched in unusual amino acid residues such as bovine Indolicidin of which tryptophan constitutes 5 of 13 residues [86-88] and pig cathelicidin PR-39 which carry a large net charge of +10 and further contains 18 proline residues [89]. These residues thus occur approximately 35 and 10 times more often than the average amino acid composition of proteins in the UniprotKB/Swiss-prot protein database, respectively [90]. The structure of AMPs may also be devoid of α-helix and β-sheet conformation and merely be stabilized by the presence of one or more disulphide bridges as in the case of Brevinin-1 and Indolicidin.

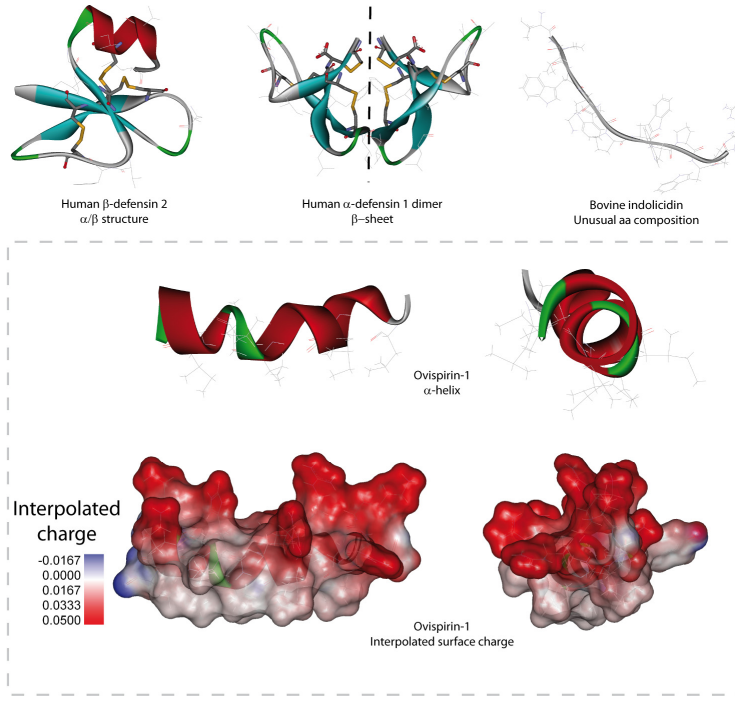

Figure 9 Examples of three-dimensional AMP structures including mixed α/β structure of human β-defensin 2, β-sheet structure of human α-defensin 1, the tryptophan rich bovine indolicidin and α-helical ovispirin-1. Ribbons of α-helical conformations are colored red, β-sheet structures blue, kinks colored green and disulphide bridges orange. The surface charge of ovispirin-1 is shown in the bottom. Images were produced using Accelrys Discovery Studio Visualizer v2.5 and pdb files 1G89 (indolicidin), 1HU5 (ovispirin-1), human α-defensin 1 (3GNY) and human β-defensin 2 (1FD4).

A general feature of AMPs is their segregation of hydrophobic and polar residues as shown by the preferential position of hydrophobic residues at one face of human β-defensin 2 (HBD-2) in Figure 8. This arrangement facilitates dimerization of HBD-2 [91], which minimizes exposure of hydrophobic residues in aqueous environment and further present an amphiphatic structure which allow interaction at the hydrophobic/hydrophilic interface of lipid membranes.

Natural and synthetic linear α-helix antimicrobial peptides constitute a large group of AMPs and include sequences such as magainin, melittin, cecropins, aureins and not least SMAP-29, ovispirin-1 and novispirin AMPs from which *novicidin* (Nc) used in this thesis have evolved [92-103]. Linear α-helical AMPs often attain random coil conformations in aqueous solution and α-helical conformations in which the polar and hydrophobic residues are positioned at opposing faces when presented to hydrophobic environment such as the bacterial membrane or membrane mimicking organic solvents [93-95]. The segregation of polar and hydrophobic residues of α-helix AMPs can conveniently be illustrated by helix wheel projections [104] as illustrated for Nc (Figure 12A, page 39).

Although linear α-helix AMPs share a common secondary structure and segregation of polar and hydrophobic residues, their primary sequences reveal little conservation of individual amino acid residues[105]. On the basis of >150 naturally occurring α-helical AMPs, more than 70% of the sequences displayed a glycine residue at position 1 which initiates an α-helix domain at the N-terminus and more than 50% of the sequences contain a lysine residue at position 8 [34, 35, 105]. Although little positional conservation of individual amino acid residues is observed, a consensus template for the distribution of glycine, hydrophobic, cationic, anionic and neutral residues frequently occurring at individual positions has been suggested [105]. The sequence could thus be described by the presence of one or two hydrophobic residues for every 3-4 amino acid residues separated by basic, acidic or uncharged residues. This is also indicated by the distribution of hydrophobic residues of novicidin by the Kyte-doolittle hydrophobicity scale (Figure 12B) and may also be expected for segregation of hydrophobic and polar residues in an α-helical structure to be possible [105, 106]. The effects of amino acid substitutions in the hydrophobic and polar sectors of the amphiphatic helix on α-helicity and biological activity were further examined. The studies revealed that the absence of large aliphatic residues in the hydrophobic sector completely abolished AMP activity presumably owing to an inefficient insertion in biological membranes [35]. The shallow hydrophobic sector (side chain carbon atoms ≤ 2) further correlated with a reduced propensity to form α-helix structure in SDS micelles [35]. Likewise, effective AMP activity the polar sector was shown to rely on a net charge of +3 to +9 arising from Lys and Arg residues serving to interact with anionic lipid headgroups. Further, the insertion depth of AMPs was suggested to rely on the length of the polar residues facing away from the hydrophobic core. The authors argued that long polar residues may be viewed upon merely as long aliphatic residues with a polar head. Thus, if the carbon chains of polar residues are longer, it allows the main chain of the AMP to penetrate deeper into the hydrophobic core [35]. The studies further assigned the physical interaction of AMPs with the membrane as the principal factor leading to cellular inactivation [35, 105].

Although it may be tempting to hypothesize that effective synthetic peptides with predefined properties may be constructed from such patterns, the activity of AMPs have been shown to be unique for every sequence and even single amino acid substitutions may lead to a change or complete loss of AMP properties such as minimum inhibitory concentration (MIC) against bacteria, hemolytic activity on red blood cells and the ability to permeabilize bacterial membranes [94, 105]. It is therefore crucial to establish further knowledge on the impact of the structure-function relationship between AMPs and membranes.

Table 2 Examples of antimicrobial peptides, their sources and sequences. Data obtained from the Antimicrobial peptide database (APD) [85]. Subscripts on cysteine residues of the sequence denote the residues involved in disulphide bridges.

α-helix	**Source**	**Charge**	**Sequence (% hydrophobic)**
Mastoparan	Insect (Wasp)	+3	INLKALAALAKKIL (71%)
SMAP-29	Animal (Sheep)	+10	RGLRRLGRKIAHGVKKYGPTVLRIIRIAG (37%)
Ovispirin-1	SMAP-29	+7	KNLRRIIRKIIHIIKKYG-NH_2 (39%)
Novicidin	G18F mut. of ovispirin-1	+7	KNLRRIIRKIIHIIKKYF-NH_2 (44%)
Cecropin P1	Animal (Pig)	+5	SWLSKTAKKLENSAKKRISEGIAIAIQGGPR (35%)
Lactoferricin	Human	+9	GRRRRSVQWCAVSQPEATKCFQWQRNMRKVRGPPVSCIKRDSPIQCIQA(36%)
Dermaseptin	Amphibian (Brazilian frog)	+4	GLWSKIKAAGKEAAKAAAKAAGKAALNAVSEAV (57%)
Melittin	Insect (Honeybee)	+5	GIGAVLKVLTTGLPALISWIKRKRQQ (46%)
LL-37	Human	+6	LLGDFFRKSKEKIGKEFKRIVQRIKDFLRNLVPRTES
β-sheet	**Source**	**Charge**	**Sequence (% hydrophobic)**
α-defensin, HNP3	Human	+2	$DC_1YC_2RIPAC_3IAGERRYGTC_3IYQGRLWAFC_2C_1$ (50%)
β-defensin	Animal (Pig)	+6	GPLSCGRNGGVCIPIRCPVPMRQIGTCFGRPVKCCRSW
Protegrin-1	Animal (Pig)	+6	$RGGRLC_1YC_2RRRFC_2VC_1VGR$
Combined α/β	**Source**	**Charge**	**Sequence (% hydrophobic)**
β-defensin (HBD-2)	Human	+7	GIGDPVTCLKSGAICHPVFCPRRYKQIGTCGLPGTKCCKKP (36%)
Unusual aa	**Source**	**Charge**	**Sequence (% hydrophobic)**
Indolicidin	Animal (cow)	+3	ILPWKWPWWPWRR-NH_2 (53%)
Cathelicidin (PR-39)	Animal (pig)	+10	RRRPRPPYLPRPRPPPFFPPRLPPRIPPGFPPRFPPRFP
Disulphide bridges	**Source**	**Charge**	**Sequence (% hydrophobic)**
Brevinin 1	Animal (Frog)	+4	FLPVLAGIAAKVVPALFCKITKKC (66%)
Indolicidin	Animal (cow)	+3	ILPWKWPWWPWRR-NH_2 (53%)

2.2. Impact of antimicrobial peptides on the structure and integrity of lipid membranes

AMPs often attain random coil conformations in aqueous solution and therefore undergo a conformational change on interaction with lipid membranes to separate hydrophobic and polar residues in an amphiphatic structure. The amphiphatic structure presents an ideal structural organization for the interaction with both hydrophobic acyl chains and hydrophilic headgroups of phospholipids, and explains to a large extent the propensity of antimicrobial peptides to interact with lipid membranes[105]. Since most antimicrobial peptides are cationic and bacterial surfaces carry a net negative charge as discussed in previous sections, the major driving force of AMPs toward membranes and negative charges found on the bacterial surface is electrostatic attraction [105, 107]. Apart from promoting initial attraction to membranes, the electrostatic interaction of cationic charges with anionic have further been proposed to play an important role in subsequent structuring and insertion steps in anionic membranes including a deeper penetration into the membrane [34].

The amphiphatic conformation of many monomeric AMPs may not be sufficiently hydrophilic to exist in aqueous solution owing to the hydrophobic effect. If the amphiphatic structure does persist in aqueous solution, peptides such as the human cathelicidin LL-37 form oligomeric structures in which hydrophobic clusters are shielded from the aqueous environment [108]. An oligomeric structure thus requires the organization to be reversed to allow exposure of the hydrophobic residues to the membrane interior and polar residues to the lipid headgroups. Maybe therefore, amphiphatic α-helical AMPs are generally unstructured in solution and adopt the α-helical structure when embedded in phospholipid membranes (Figure 10) [105, 109].

The hydrophobic side chains of the extensively studied AMP magainin 2 from *Xenopus laevis* have been shown to be positioned no closer than 10Å from the bilayer center [96], the closest H_{α} atoms of novicidin (discussed in later sections) have been shown to be positioned 12-13Å from the center of DPC micelles [74], and LL-37 has been shown to penetrate 5-6Å into the hydrophobic core [110]. Figure 9 further shows that the axis of the α-helical AMP Ac-18A-NH_2 is positioned at the approximate level of the glycerol backbone of the phospholipids in the lipid membrane based on X-ray diffraction studies[111]. It thus appears evident that length of the hydrophobic domain of the AMP is shorter than the length of the acyl chains of adjacent lipid molecules, indicating that AMPs often attain a position at a distance from the bilayer center in the surface bound state as also illustrated in Figure 9 and Figure 10. As described in the previous section, the penetration depth may, however, be modulated both by the size of both hydrophobic and polar sectors of the AMP.

Nevertheless, the examples show that amphiphatic helices may act as a spacer between phospholipid headgroups and leave a void in the hydrophobic interior of the membrane. Such free volumes in the membrane are highly unfavourable [112] and may be eliminated by deformation of acyl chains of neighboring lipids and may extend the deformation of lipids in the membrane several nanometers from the

bound peptide[113]. The acyl chain deformations include acyl chain bending, increased *trans*-gauche isomerisation and acyl chain interdigitation (Figure 5 and Figure 10B, C) [114]. Both of these deformations result a decrease in bilayer thickness known as membrane thinning as has been shown for several AMPs including magainin 2 [97], LL-37 [115], Indolicidin [86], MSI-78 [116], melittin and alamethicin [117]. Membrane thickening by AMPs has been observed for AMPs such as PGLa [118] and gramicidin [119] and involves acyl chain stretching to match hydrophobic stretches of the peptides. However, in these cases, the AMPs traversed the bilayer in an inserted state, demonstrating that membrane thinning is not a prerequisite for pore formation [118].

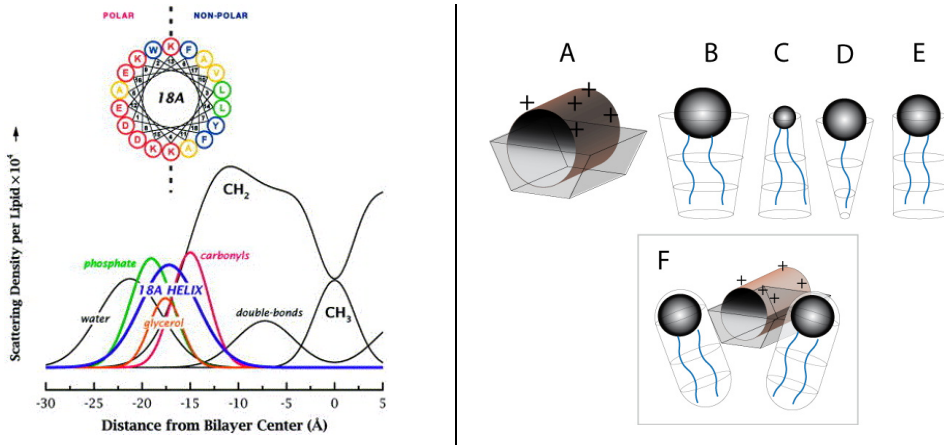

Figure 10 ***Left:*** **Illustration of the transbilayer distribution of non-polar and polar residues of the amphiphatic Ac-18A-NH2 α-helix in fluid DOPC bilayers. The centre of the helical axis is positioned approximately at the level of the glycerol backbone of the phospholipids. Illustration adapted from [111] with permission and the color scheme was established on the basis of the hydrophobicity scale by Wimley and White (1996)[120]. Blue, green, yellow and red color codes denote the highly favorable, moderately favorable, slightly favorable and highly unfavorable partitioning into the hydrophobic core, respectively.** ***Right:*** **Illustration the molecular shape of lipids and cationic α-helical AMPs. A) The wedge shape of a cationic α-helical antimicrobial peptide, (B) the approximate cylindrical shape of e.g. DOPC, (C) the truncated inverted cone shape of diacylglycerol lipids with the smaller PE headgroup, (D) the cone shape of detergents and lysolipids containing only one acyl chain. (E) Interchelation of wedge shaped AMPs into the membrane interface leaves a void below the peptide in the acyl chain region.**

The impact of AMPs on the structure of the membrane may also be viewed upon as changes in the spontaneous membrane curvature owing to the geometrical shape of the membrane lipids and the AMPs [121]. In membranes with high negative curvature strain (e.g. contains a large proportion of PE lipids) from lipids conferring inverted cone shapes, the insertion of AMPs may *reduce* curvature strain since the geometries of the lipids are opposite to PE lipids. However, in membranes with positive or no apparent curvature strain (e.g. PC lipids), the insertion of wedge shaped AMPs or drugs may lead to *increased* positive curvature strain [114]. The induction of positive curvature strain by AMPs has been shown for several AMPs including MSI-78 [122], LL-37 [123], magainin 2 [124] but also the inclusion of lysolipids [125] which confer a cone shape as illustrated in Figure 9D (right).

The considerations above may thus apply to both the local environment surrounding individually bound peptides and the global properties of the membrane. At increasing peptide concentrations profound effects may be observed on the global membrane perspective since modulation of membrane packing and curvature strain may result in membrane defects, transient or stable well-defined pores or loss of membrane integrity (Figure 10) [121, 126]. A common feature of these events is the formation of holes in the membrane which diminish electrochemical gradients essential for cell viability and provide a ready explanation for the antimicrobial activity of AMPs [113]. The three most established models employed in literature to describe the membrane-disruptive properties of AMPs are the Barrel-Stave, toroidal pore and carpet mechanisms (Figure 10) [109, 126]:

The Barrel-stave model describes short-lived membrane pores formed through the insertion of α-helical peptides across the membrane to constitute a helical bundle when a certain threshold concentration of the peptide in the bilayer is reached. The hydrophobic part of the helices is in direct contact with the hydrophobic core while polar residues line the interior of the pore. This arrangement sets high requirements to the peptide in terms of peptide length, structure and amphiphatic properties in order to match the properties of the bilayer as illustrated in Figure 10H. It is therefore not surprising that only few peptides have been experimentally proven to employ the barrel-stave model, although it is frequently discussed in research papers. The most well-known example is alamethicin from the fungus *Trichoderma viride* which accumulate at the bilayer surfaces up to a critical coverage at which it changes orientation from the surface bound state (S) to the inserted (I) state traversing the bilayer. Based on studies of integral membrane proteins and the geometry of the membrane, it has been proposed that 18 to 22 amino acid residues are required for α-helix peptides and approximately 8 residues in β-strand conformation to traverse lipid bilayers depending of acyl chain length [121, 126].

The toroidal pore mechanism has been applied to describe the action of several antimicrobial peptides including magainin 2 [100, 127], LL-37 [123] and aureins [101]. At low concentrations, AMPs employing this mechanism inserts in a surface bound state and result in no or low degree of membrane leakage. Low degrees of membrane leakages may be explained by lateral diffusion of AMPs within the plane of the membrane which may result in temporally high local concentrations of AMP [121]. At higher concentrations, they impose high positive curvature strain in the membrane and shift the orientation of lipid molecules to create continuities between leaflets as shown in Figure 10G. They thereby create a pore structure resembling a torus through which ions and small molecules may readily pass. During pore formation, AMPs reorient along the bilayer normal to the I state but remain associated in the hydrophobic/hydrophilic interface and thus line the pore structure accompanied by the lipid headgroups. In contrast to the Barrel-stave model, the AMP need not to have a specific length owing to the position in the hydrophilic/hydrophobic interface as indicated by the shorter AMP Figure 10G. The occurrence of toroidal pores may further facilitate the flip-flop of AMPs from one leaflet to the other as a result of the membrane continuity as described for magainin 2 [100].

The occurrence of lesser organized aqueous channels of the toroidal pore type with variable size and stability have been suggested to account for the membrane perturbing properties of a variety of AMPs [128]. A similar although less structured toroidal pore form in which only few peptide molecules line the pore in more diffuse orientations has recently been suggested by molecular dynamics simulations (Figure 10F) [129, 130].

The carpet model of membrane disruption involves accumulation of AMPs in the surface bound state throughout the concentration range until a critical membrane coverage is achieved which result in membrane disintegration by disruption of the bilayer curvature [121, 126]. Thus, non-lytic concentrations of the peptide do not result in a reorientation along the bilayer normal to the I state as described for the toroidal pore and barrel-stave models previously described. Loss of membrane integrity is thought to occur through a less defined detergent-like solubilization which may lead to the formation of micelles (Figure 10D-E) which are stabilized by the peptide [113, 121].

Pore formation by the toroidal pore or barrel-stave mechanisms is not a prerequisite for the carpet mechanism. Rather, the accumulation of AMPs in the S state is a common denominator for all modes and the toroidal pore and barrel-stave mechanisms may thus be included in the carpet model. It should be emphasized that the models described above are indeed models and that combinations of these may therefore exist. For instance, the disordered toroidal pore may be described by a combination of the detergent and toroidal pore mechanisms as such as proposed by MD simulations of melittin in bilayers [129]. The exact mechanisms are thus still under debate presumably due to the great variability of AMPs which lead to minute differences in the activity.

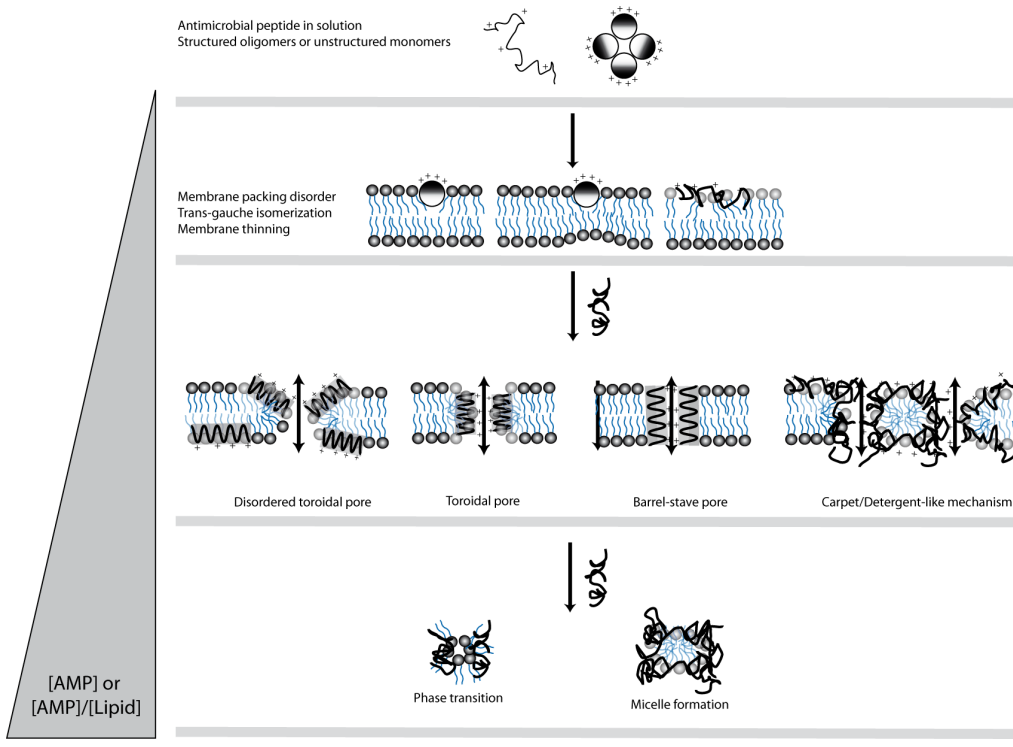

Figure 11 Schematic of antimicrobial peptide interactions with membranes. Peptides in solution containing defined or random coil conformations bind to membranes causing disruption of membrane packing and/or acyl chain interdigitation and membrane thinning. The peptide may also bind in a random coil conformation. Further increases in AMP concentration may lead to formation of toroidal pores in which enforced membrane curvature result in a continuity between leaflets lined by lipid headgroups and AMP in traverse or diffuse orientations. The AMP may also insert via the barrel-stave model to constitute an ion pore with hydrophobic residues directly exposed to the hydrophobic core or induce transient pores in a less defined manner in the carpet/detergent like mechanisms. Further increases may lead to complete membrane disintegration through phase transitions or micelle formation.

3. Mechanisms of microbial resistance

The resistance toward antibiotics may be acquired or an intrinsic property of a given bacteria. Resistance toward antimicrobial agents may arise from alterations in the genetic material through mutations or acquisition of foreign DNA through transformation, viral transduction and conjugation. The transfer of DNA by conjugation is by far the most important of these in the spreading of drug resistance genes in bacteria [131].

From a more functional point of view, resistance may be divided into four groups: First, bacteria may express enzymes which modify or degrade the antibiotic activity such as β-lactamase degradation of the β-lactam ring of penicillin. Second, mutations may result in modifications of the antibiotic target and thereby the mutations diminish the interaction. Third, bacteria may acquire new enzymatic functions which allow the bacteria to by-pass the function of the antiobiotic target. Fourth, the bacteria may remove the antibiotic from the cell using efflux pumps (e.g. tetracycline) or reduce the permeability of the drug (e.g. imipenam).

The occurrence of bacteria is ubiquitous to every habitat on earth including the large number of bacteria present on skin and in the gut flora. In such places, they will have to confront the antimicrobial peptides presented by the host in order to survive and it is therefore unrealistic to expect that no single bacteria can resist antimicrobial peptides[132]. The target of antimicrobial peptides are, however, somewhat different from the target of conventional antibiotics since they primarily target the bacterial membrane. Thereby, strategies of bacteria resistance toward antimicrobial peptides involve mainly the initial attachment to the outermost parts of the cell, the binding to the membrane and the permeabilization of the membrane. Only then, AMPs are able to exert effects on potential intracellular targets.

There has been reports of proteolytic degration of the AMP LL-37 by the metalloprotease aurelysin and a glutamylendopeptidase secreted by *S. aureus*[133]. However, other groups have shown that LL-37 is significantly resistant to proteolytic degradation by proteinase K both in the oligomeric and membrane associated states[108]. Other AMPs such as PR-39 have been suggested to be naturally resistant toward proteolytic degradation owing to their unusual amino acid composition including Arg and Pro rich sequences [134]. However, the proteolytic degradation of LL-37 displayed by *S. aureus* proteases has to be taken into account owing to the ability of bacteria to pass on genes essential for antibiotic resistance.

The initial attachment of AMPs to the outermost surface bacterial cell is affected by the vast majority of anionic components of the bacterial cell wall including LPS, LTA and TA constituents which may act as peptide scavengers through electrostatic interactions. However, such anionic constituents may also participate in the initial attraction of the AMP and bacteria whose surface has no electrostatic affinity or even repel cationic AMPs may have a greater chance of dodging AMPs (Figure 11). Several genes whose expression has been shown to be important for antimicrobial peptide resistance has been identified and several of these act through cell-surface modifications. For example, *S. aureus* has been shown to

substitute TA with D-alanine[135] and strains lacking the responsible expressed gene were more susceptible toward the antimicrobial peptides magainin II and human α-defensin[136]. *S. aureus* has further been shown to confer a gene for substitution of PG headgroups with L-lysine to reduce the net negative surface charge as well as an plasmid encoded efflux pump [137, 138]. *S. typhmurium* and *L. pneumophila* possess genes whose expression leads to an increase Lipid A acylation, thereby reducing the susceptibility to certain AMPs[132]. Further, Lipid A has been shown to be modified by aminoarabinose in *P. mirabilis[139]*.

It is therefore apparent that bacteria have indeed developed mechanisms to resist antimicrobial peptides based on both structural changes of the cell-surface and energy dependent efflux pumps. Since the mechanisms involve both changes of the target sites and efflux pumps, they resemble to some degree the mechanisms involved in the microbial resistance toward conventional antibiotics. These resistance mechanisms thus have to be taken into account in the research and development of new therapeutic agents based on antimicrobial peptides.

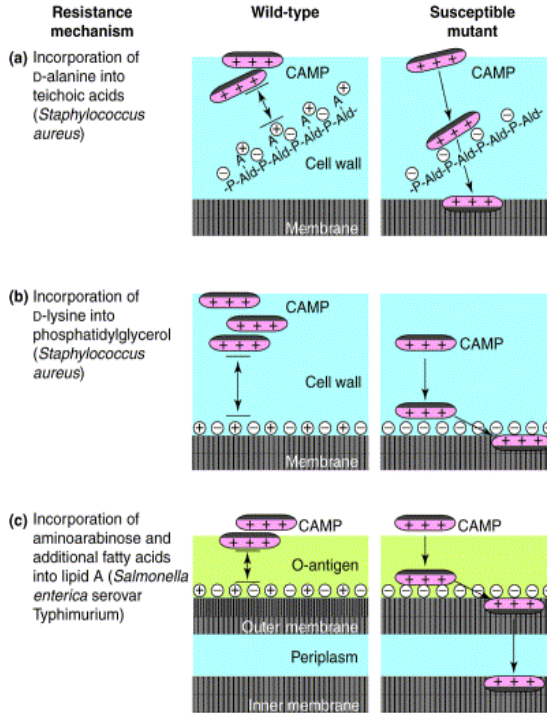

Figure 12 Proposed mechanisms of bacterial resistance toward antimicrobial peptides through cell-surface modifications. In the wild-type bacteria, anionic cell wall constituents such as (a) TA, (b) PG or (c) Lipid A are substituted with positively charged residues which cause electrostatic repulsion of cationic AMPs. Mutants lacking the genes conferring these cell wall modifications display increases susceptibility to cationic AMPs. Adapted from [140] with permission.

4. Intracellular targets of antimicrobial peptides

Previous sections have focused on the membrane and outer surface of bacteria since this of major importance in the scope of this thesis. There is, however, evidence that certain AMPs may exert effects on intracellular targets after passing through the barriers of outer surface and the cell membrane and these will be described briefly here.

A major reason for the designation of the lipid membrane has been studies in which L- and D-enantiomers of AMPs have shown equal abilities to kill bacteria, indicating that no stereospecific receptors are involved in the mechanism[141]. However, certain AMPs such as apidaecin, drosocin and pyrrhocoricin have been suggested to kill bacteria through stereospecific interactions with heat shock proteins residing in the cytoplasm of the cell[142] and are essential for bacterial growth[143]. The inhibition of intracellular processes has also been demonstrated by the ability of pleurocidin isolated from flounder to translocate across the cytoplasma membrane of *E.coli* and inhibit the growth at concentrations where the integrity of the cytoplasma membrane remains unaffected. Thus, membrane integrity was not compromised at concentrations of pleurocidin of up to five times the minimum inhibitory concentration (MIC)[144].

Another peptide, PR-39 isolated from the upper part of the small intestine of pigs, has been shown to kill growing *E.coli* more efficient than nongrowing[89] indicating that essential cell processes are inhibited. Further experiments showed that PR-39 targets DNA and protein synthesis pathways and/or induce protein degradation, the latter also leading to degradation of enzymes required for DNA synthesis[89]. DNA synthesis pathways have also been shown to be of major importance as a target of the tryptophan-rich indolicidin (Table 2). Thus, studies on the morphology of *E.coli* revealed that the peptide induce filamentation of the bacteria. Since this filamentation in bacteria may be caused by inhibition of DNA synthesis, it was investigated whether DNA synthesis was impaired by the AMP. Indeed, it was found that indolicidin inhibits DNA but not RNA and protein synthesis[87].

Further, AMPs may also affect the cell wall synthesis as described for the cationic AMPs Pep 5 and nisin[145]. The authors suggested that the anionic character of the polyanionic TA and LTA constituents of the gram positive cell wall attract AMPs by electrostatics and displace the N-acetylmuramoyl-L-alanine amidase enzyme from the anionic polymer. They thereby inhibit cell wall synthesis which ultimately may lead to destabilization of the cell wall and lysis of cells.

While the intracellular targets comprised by DNA, RNA and protein synthesis, protein folding and cell wall synthesis described above are important for the activity, antimicrobial peptides must, with the exception of cell wall synthesis in gram positive bacteria, first encounter the barriers surrounding the cytoplasm of the bacteria first. Hence, studies of the interaction between AMPs and lipid membranes are important for complete understanding of AMP mechanisms.

5. Novicidin

Novicidin (Nc) is a designed 18-residue designed antimicrobial peptide (KNLRRIIRKGIHIIKKYF-NH_2) in which four lysine and three arginine residues contribute to the net charge of +7. Nc was obtained by a single G18F mutation of ovispirin-1 which in turn has been derived from the N-terminal part of the naturally occurring sheep myeloid antimicrobial peptide 29 (SMAP-29), which is a potent antimicrobial but also shows adverse effects by being highly cytotoxic to human epithelial cells and hemolytic for human erythrocytes [146].

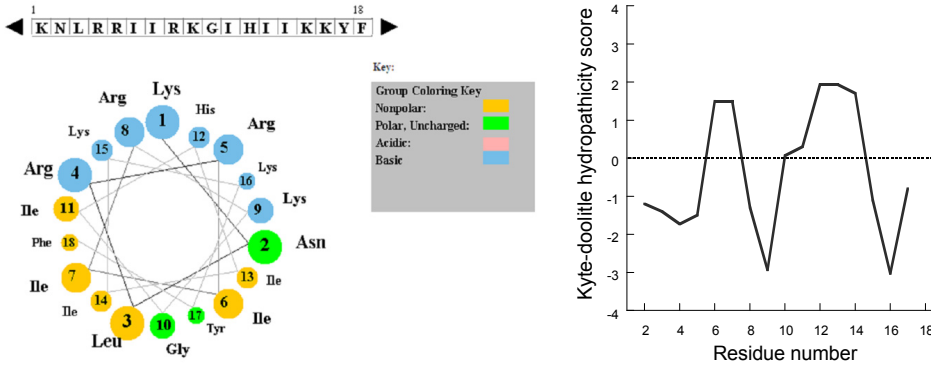

Figure 13 Helical projection wheel and hydropathicity score of the antimicrobial peptide novicidin (Nc). (A) The helical wheel projection of Nc in which hydrophobic residues are clustered at one face and hydrophilic residues on the other. (B) The distribution of hydrophobic and hydrophilic residues according to the Kyte-doolitle hydrophobicity scale [106]. The larger the positive value, the more hydrophobic.

Paper I shows that Nc attains random coil structure in aqueous solution similar to the analogues ovispirin-1, novispirin G-10 and novispirin T-7 [93, 94]. The peptide remains largely in the random coil or weakly helical conformations when subjected to the amphiphatic environment presented by the purely zwitterionic DOPC lipids. In contrast, **Paper I** and **II** clearly show that the secondary structure changes to α-helix structure in the presence of the partially anionic membranes containing 20% of the anionic lipid DOPG. Such structural rearrangements in the presence of amphiphillic environment have also observed for the Nc analogues in solvents set to mimic the bacterial interface. For instance, the α-helix structure was observed in TFE (membrane mimicking solvent) and in the constituents of bacterial cell surfaces including LPS of gram negative bacteria and LTA of gram positive bacteria [94]. Further, Nc analogues attained the α-helix structure in the amphiphillic environments presented by the detergents SDS, LTAC and in pure DOPG lipids [93]. Thus, Nc appear to adopt α-helical structure in which hydrophobic and polar residues are separated at opposing faces only in the presence of the anionic DOPG lipid, whereas Nc is more unstructured in the presence of zwitterionic DOPC.

Paper I showed that calcein release studies revealed that approximately 7 times less Nc was needed to obtain 50% release of calcein from DOPC membranes compared to partially anionic membranes containing 20% DOPG. This clearly indicates that the defined α-helix structure is not a prerequisite for membrane disintegration which, in fact, leads to a decrease in the membrane perturbing activity of Nc. While most studies of linear amphiphatic helices focus on the defined α-helix conformation, MD simulations has recently suggested that also melittin may form pores devoid of defined secondary structure [129] indicating that at least some linear "amphiphatic" AMPs may exert their membrane perturbing activities devoid of a defined secondary structure.

The efficient permeabilization observed in **Paper I** of the zwitterionic PC lipids as a gross model of mammalian membranes may appear counter-intuitive since the target of Nc as well as other AMPs is the net negative bacterial surface. The association of Nc to zwitterionic membranes is expected to occur mainly due to the hydrophobic effect through which hydrophobic residues are shielded from the aqueous solution. Remarkably, interaction of Nc with zwitterionic membranes occur largely in absence of α-helix structure which has previously been attributed an important role as a determinant of the AMP penetration depth since backbone hydrogen bonding in the α-helix conformation reduces the hydrophobicity of the main chain and allow deeper penetration [35]. Indeed, the amino acid composition of Nc comply with the requirements for a deep penetration into the lipid membrane in the α-helical conformation since the aliphatic and polar amino acid residues are generally above 3 carbons in length [35]. Despite of this, Nc do not appear to adopt the well-defined α-helix conformations or penetrate deeply into purely zwitterionic membranes.

In contrast, electrostatic attraction is expected between the 7 positive charges of Nc and anionic constituents of bacterial interfaces. The selectivity of Nc toward anionic membranes was thus investigated in **Paper I** by a novel confocal scanning laser microscopy (CSLM) approach using a binary mixture of pure zwitterionic vesicles and vesicles containing 20% DOPG. Interestingly, Nc showed preferential binding and disruption of the anionic vesicle population while leaving zwitterionic lipids untouched. Electrostatic attraction is thus the major driving force for Nc association to anionic membranes. While such attraction to the anionic vesicle population was to be expected *a priori* due to the net positive charge of Nc, the preferential lysis of this population is important since it suggests that Nc may indeed target anionic interfaces such as the bacterial surface preferentially even in the presence of more neutral mammalian cells. To our knowledge, this approach is first of its kind to describe the discrepancy between AMP binding and vesicle disruption in a heterogeneous population.

The differential behavior of Nc in purely zwitterionic membranes compared to partially anionic membranes was further emphasized by the use of a dansyl labeled Nc in **Paper I**. Stopped flow fluorescence experiments using this variant showed an increase in fluorescence intensity of the dansyl probe during binding to anionic vesicles and was followed by vesicle permeation as determined by calcein dye release. This indicates that the dansyl probe becomes buried in anionic membranes. In contrast, no change in

fluorescence emission was observed in purely zwitterionic membranes indicating that the dansyl group is not buried in zwitterionic membranes. The calcein leakage from zwitterionic membranes thus appear to arise from a more superficial binding that may change the headgroup packing in a more efficient manner compared to the α-helical state of Nc in partially anionic membranes. In order to elucidate the precise mode of interaction between Nc and with purely zwitterionic and partially anionic membranes, further experiments should thus include FTIR, fluorescence anisotropy (e.g. using DPH and TMA-DPH to probe the effect on the membrane at the level of headgroups and hydrocarbon core, respectively) and polarity (e.g. Laurdan generalized polarity) measurements focusing on the packing of acyl chains and headgroups.

The importance of the penetration depth of Nc is further emphasized by our studies using N-terminally acetylated variants of Nc with chain length of 8, 12 or 16 carbons in **paper I.** These studies revealed that C16 acylated Nc partition deeper into lipid bilayers compared to wt Nc presumably owing to the lipid anchor and the induction of α-helix structure of the acetylated variants even in the presence of DOPC lipids. The acetylated Nc variants were further less efficient in permealizing membranes. The adverse effect of Nc acylation was shown to include the antimicrobial activity on *E. coli* suggesting that the deeper penetration of Nc is also less efficient in permeabilizing the membrane. Taken together, this clearly suggests that α-helix propensity may not alone be a determinant of AMP efficiency.

While these data did not provide evidence on the orientation of Nc in partially anionic membranes, the use of oriented circular dichroism (OCD) in **Paper II** consistently showed that the α-helix lies parallel to the membrane surface under conditions where a consistent set of complementary techniques suggest that the lamellar bilayer structure persists. Since an orientation of the α-helix across the membrane is a prerequisite for the Barrel-stave and classical toroidal pore mechanisms of AMP activity, OCD measurements effectively rule out these mechanisms.

Paper II shows that the activity of Nc on partially anionic lipid vesicles may broadly be divided into two regimes. First, calcein dye leakage experiments showed that at low Nc concentration lead to transient permeabilization of anionic membranes whereas general membrane integrity was preserved. Second, several complementary techniques including QCM-D, DPI and fluorescence spectroscopy revealed that at a more general rearrangement of the membrane occurs at higher concentrations.

Although biological membranes are far more complex than the model system employed here, we found a surprisingly good agreement between the concentrations at which lysis of *E.coli* was observed by the release of cytoplasmic β-galactosidase in **Paper I** and the concentration range at which model membranes disintegrate in **Paper II**. However, it is not known how the greater complexity of bacterial membranes affects the activity of AMPs and the viability of bacteria. Bacteria may be affected at significantly lower concentrations than those required for release β-galactosidase from *E.coli* in **Paper I** since release of such an enzyme can only be expected as a result of severe membrane disintegration.

It would therefore be interesting to link the cell viability measured by the minimum inhibitory concentration (MIC) toward gram positive and gram negative strains to the ability to maintain electrochemical gradient essential for bacterial viability. While standard procedures to obtain the MIC are available, the dissipation of transmembrane electrochemical ion gradients may, for instance, be evaluated using potentiometric fluorescent probes such as $(DiOC_2)_3$. While the release of relatively small molecules from bacteria through transient pores is likely to be detrimental for cell viability, much lower concentrations may be required for disruption of electrochemical gradients by transient pore structures compared to the release of β-galactosidase or even smaller molecules with the size of calcein. Thereby, such assays could aid in determining whether a direct link between cell death and the dissipation of electrochemical gradients exist and whether Nc potentially exert inhibitory effects at concentrations lower than those required for cell lysis. In addition, such experiments may validate the credibility of model membranes employed both in this study and commonly employed in literature.

The effect of Nc on the phase transition temperature in DSC experiments of pure DMPC and membranes containing 20% DMPG in **Paper I** further emphasizes the different effect on these membranes. It is especially remarkable that the phase transition temperature from the gel to liquid disordered phase is shifted upwards in partially anionic membranes, indicating a stabilization of the gel phase of partially anionic membranes. This is remarkable since Nc causes leakage but not disintegration of lipid membranes in the liquid disordered phase under similar conditions as shown in **Paper II**.

Interesting experiments including both dimyristol and dipalmitoyl lipids with variations in the headgroup composition are currently conducted in our laboratory and include the determination of phase transition temperatures, membrane permeability, dependence of electrostatic screening by salts and the significance of a defined secondary structure. These experiments combined are likely to result in further insight into the structure-function relationship of Nc and lipid membranes and may be applicable to other AMPs.

6. Alamethicin

Alamethicin (Alm) is an antimicrobial peptide originally derived from the fungus *Trichoderma viride* [147] and is one of the most frequently studied AMPs in literature. Alm consists of 19 residues of which 8 methylated alanine (also termed aminoisobutyric acid, Aib) residues are not included in the standard genetic code placing Alm in a group of peptaibols composed by Aib residues whose N-terminal is often acetylated and the C-terminal is extended with a phenylalaniol residue as in the case of Alm. *In vivo*, Alm is synthesized by a pathway independent on the general peptide translation pathway involving ribosomal activity and depend on a multienzyme complex called ALM synthase [148].

The interaction of Alm with membranes has been the subject of numerous studies and it is now well-established that this hydrophobic α-helical peptide exerts its biological effect via oligomerization and channel formation in the membrane via a mechanism resembling the Barrel-stave mechanism in which Alm binds at the bilayer surface at low concentrations (or peptide/lipid ratios) and reorient along the bilayer

normal at higher concentrations and assembles into a pore [95, 148-154]. However, the exact molecular structure and stoichiometry of Alm pores remains speculative since numerous structures have been proposed and the number of Alm monomers in the pore construct may vary depending on conditions and time [154-156]. A considerable effort has been made to prepare and study chemically-linked alamethicin analogs with linear and cyclic scaffolds to allow characterization of the pore structure, ion selectivity, ion permeation and voltage dependence (Reviewed by G.A. Wooley (2007),[157]). However, investigations with conjugates containing >3 peptides have either employed truncated versions, sequence modified Alms or the linker or template were not of appropriate size or structure for optimal channel formation in membranes [156, 158-160]. Recently, bundles consisting of 6-9 Alm monomers has been proposed to constitute the ion pore described by the Barrel-stave mechanism depending on the chain length of lipids employed [156].

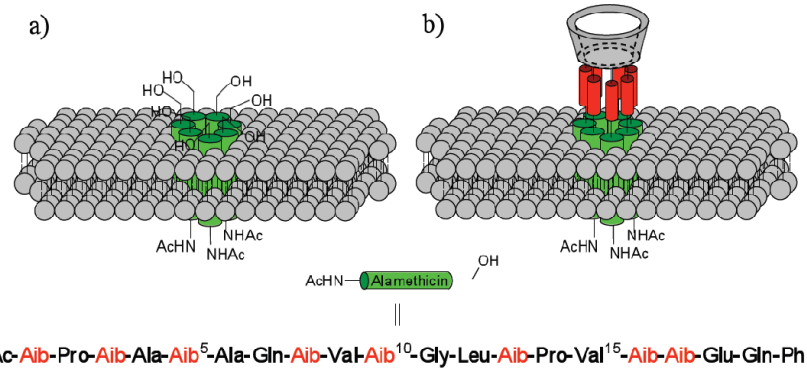

Figure 14 (A) Schematic of the barrel-stave pore constituted by seven transmembrane alamethicin α-helices. (b) Schematic of alamethicin conjugated to cyclodextrin scaffolds to constitute a novel synthetic pore construct through which ions may pass.

Paper III describes the synthesis and biophysical characterization of a new class of crosslinked alamethicin exploiting full length peptides conjugated to α- and β-cyclodextrins from the C- or N-terminal of Alm and compared the membrane-perturbing activity with unmodified Alm. α- and β-cyclodextrins are cyclic oligosaccharides composed by 6 and 7 glucose residues covalently linked through α-1,4 glucosidic linkages, respectively. By covalently linking Alm monomers to each of the primary hydroxyl group of the glucose moieties, the cyclodextrins provide a scaffold for Alm to constitute a novel synthetic pore construct as exemplified in Figure 13.

It is further shown in **paper III**, that while Alm changes conformation when transferred from aqueous environment to a lipidic, Alm scaffolded to α- and β-cyclodextrins is more restricted in terms of structural conformation since the secondary structure were essentially identical in solution and in the presence of lipids whereas Alm undergo a conformational change when transferred from aqueous solution to a lipid environment. Interestingly, we observed that C-terminally linked Alm was approximately 10-fold more

efficient in permeabilizing vesicles and N-terminally linked Alm was 100-fold more efficient although dye leakage occur a lower leakage rate compared to the monomeric peptide. OCD was used to verify the transmembrane orientation of scaffolded Alm helices inserted in multilayer membranes as previously observed for free Alm and confirmed the orientation of Alm helices perpendicular to the membrane [69, 149, 161].

Altogether, **Paper III** demonstrate that crosslinking of AMPs to cyclodextrins may lead to more efficient pores presumably owing to the decreased conformational flexibility and stable structure compared to the free peptides. Scaffolded Alm may thus be described as an artificial nanoscale ion channel which readily interacts with membranes and allow dissipation of gradients across the membrane very efficiently. Since we now have the chemical and biophysical platform for the production and characterization of scaffolded AMPs, it would be interesting to extend these studies to include synthetic pores of other antimicrobial peptides of varying charge, length and hydrophobicity. Further, a wide variety of cyclodextrin derivatives are employed in drug delivery applications [162] which could be employed to modulate the selectivity of ion channels by scaffolded AMPs given that the cyclodextrin moiety will act as a gatekeeper for the pore. It would also be interesting to evaluate the dependence of oligomerization and pore size through the covalent attachment of Alm to cyclodextrins of different size and the ability of ions and drugs to pass through such pores. This is, however, limited by the structure of cyclodextrins since only small cyclodextrins including α-, β- and γ-cyclodextrins (6,7 and 8 glucose residues, respectively) may be described by the "classical" hollow truncated cone whereas larger cyclodextrins show more complex structures [163] and a larger ring size would thus not necessarily result in a larger pore size. However, the width of the pore could be modulated by attaching peptide momers on the wide rim of cyclodextrins although the hydroxyl groups presented here may be more challenging targets for selective substitution with AMPs.

While **Paper III** provides good evidence that the synthetic pore constructs insert in lipid membranes similar to monomeric Alm but in a fixed helix bundle, it would be interesting to carry out single channel ion conductance experiments to probe the membrane permeability at low concentrations. Since Alm conjugates were more efficient in the permeabilization of membranes in **paper III**, they are likely to represent continuously open or long-lasting open channels, the comparison of this preformed pore with monomeric alamethicin requiring would thus be interesting.

Part II: Impact of lipids on protein structure and function

In this second part of this thesis, the attention is turned toward the influence of lipid molecules on the structure and function of equine lysozyme (EL) and *Fusarium solani pisi* cutinase which already possess well-defined structure and functions in aqueous environment devoid of lipids. In the following sections, it is demonstrated that lipids may alter the structure and function proteins. This stands in great contrast to the α-helical antimicrobial peptides studied in this thesis in that they gain structure and function in the presence of an (anionic) amphiphatic environment and generally lack defined structure in aqueous environment.

This part of the thesis is initiated by an introduction to protein (mis)folding and the effect of lipids on the structure of proteins. The work presented in following sections considering **Paper IV**-**VI** describes three cases in which proteins obtain non-native conformations affected by lipids including the conversion of the intrinsically disordered conformation of murine kisspeptin into amyloidal aggregates (**Paper V**), the kinetic trapping and inactivation of *Fusarium solani pisi* cutinase by short-chain phospholipids during refolding from the acid denatured state (**Paper VI**) and the trapping of partially folded states of EL in multimeric equine lysozyme complexes with oleic acid (ELOA) and partial recovery of the native state through interaction with lipid membranes (**paper IV**).

7. Protein (mis)folding

It is generally accepted that the structure and function of proteins is defined by the fold of the native state which, with exceptions, often also correspond to the most thermodynamically stable state under relevant physiological conditions [164, 165].

Anfinsen's dogma predicts that the primary sequence of polypeptide chains together with the aqueous environment contains all information needed to specify the proteins three dimensional structure. The number of possible conformations of a newly synthesized polypeptide chain in random coil conformations is, however, so large that if a polypeptide was to systematically search for all possible conformations toward the native state it would take an astonishing amount of time. Yet, the folding of small proteins into the native fold usually takes much less time and may be in the order of just microseconds [166].

This huge discrepancy in time required for a protein to fold into the native state has been termed Levinthals paradox and suggest that the folding of proteins involve cooperative interactions between amino acid residues which drive the conformation toward increasingly native-like conformations rather than random sampling of polypeptide conformations [167]. The native fold of a protein structure is stabilized by a large number of relatively weak interactions including intramolecular hydrogen bonds, van der Waal's interactions and hydrophobic interactions which all contribute to the stability of the native state - but how are these formed during folding from the random coil conformations of the newly synthesized polypeptide chain?

The concept of the folding funnel (Figure 14) emerged as a tool to understand the self-organization of the polypeptide chain into the native structure [168]. It represents a metaphor for the energy landscape for the continuum of folding states between large number random coil conformations of the unfolded polypeptide chain at the top of the funnel to the thermodynamically more favorable native state with well-defined three-dimensional structure in the bottom of the funnel. The high energy states at the top of the folding funnel are thought lowered through formation of an increasing number of intramolecular contacts toward the native state (Figure 14, purple area) such as the exclusion of water during the formation of a hydrophobic core and the formation of hydrogen bonds within α-helix and β-sheet secondary structure elements.

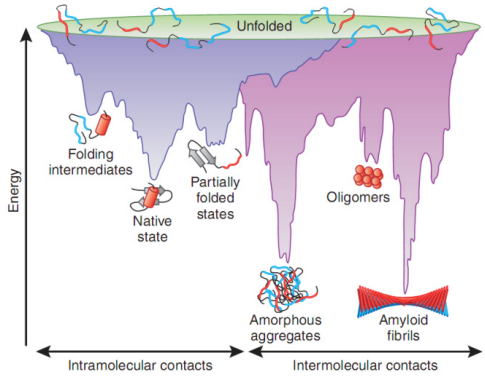

Figure 15 Schematics of the energy landscape of protein (mis)folding. The purple colored area describes the multitude of conformations with increasing number of intramolecular contacts on the way to the native state. The pink area describes folding pathways moving toward amorphous aggregates and amyloid fibrils via intermolecular contacts. A single polypeptide chain may explore the entire folding landscape. Aggregates may form from intermediate folding states formed from proteins destabilized into partially unfolded states or during *de novo* folding. Cytotoxic oligomers may develop as off-pathway intermediates of amyloid formation. Illustration adapted from [165] with permission.

The increasing number of intramolecular contacts decreases the entropy as illustrated by the narrowing of the folding channel and the downward progress in the funnel represents a decrease in the free energy of the system with increasing similarity to the native and most energetically favorable state in the bottom of the folding funnel (Figure 14, purple region). The shape of the folding landscape thus constitute a continuum of folding states which is unique for every protein and defined by the primary sequence of the polypeptide chain as well as surrounding environmental factors. Therefore, the shape of the folding funnel is also thought to be unique for every protein sequence.

The stable energy minimum in the bottom of the folding funnel often also corresponds to the active native state of a protein. However, local energy minima of the folding funnel may be sufficiently large to kinetically trap protein folding in intermediate folding states which may or may not feature characteristics of the native protein such as secondary structure elements or enzymatic activity. Such partially folded intermediates have, for instance, been observed with α-lactalbumin and equine lysozyme which have served as extensively studied models in protein folding and the acylphosphatase of *Sulfolobus solfataricus* which display enzymatic activity even in partially unfolded states [169-174].

Such stable folding intermediates may trap the protein and prevent or slow down the folding of the protein to the native state. If the barriers of the local energy minima cannot be overcome through thermodynamic fluctuations, the interaction with cofactors or chaperones or folding proteins which assists proper folding by stabilizing unfolded or partially folded conformations and prevent aggregation [175, 176]. Nevertheless, several diseases have been shown to arise from the inability of the cell to maintain protein homeostasis – the ability to maintain an active pool of a given protein. Such disease may evolve as a result of the loss of a specific enzymatic activity (e.g. the defective ion transporter causing cystic fibrosis) or development of cytotoxic protein species through protein aggregation into insoluble fibrils or plaques which accumulate in organs such as the brain as shown for Parkinsons and Alzheimers diseases [176, 177].

The formation of amyloid aggregates is fundamentally different from the folding pathway toward the native state. The pink region of Figure 14 illustrates that amyloidal aggregation involves the formation of *intra*molecular between individual polypeptide chains compared to the formation of *inter*molecular bonds within a single polypeptide chain on the way to the native fold. The intramolecular contacts arise through formation of hydrogen bonds in extensive β-sheet structures as illustrated by the thread like appearance of individual β-strands in Figure 14. The formation of amyloids has been suggested to be an intrinsic property of any polypeptide chain especially under mild denaturing conditions which promote partial unfolding thus allowing the polypeptide chain to sample a larger conformational space [178].

It is widely established that amyloid formation typically involves a lag phase in which nuclei accumulate, an elongation phase and a steady state phase. The lag phase is usually very long although environmental factors such a crowded milieu [179], pesticides, metal ions [180] and glucosaminoglucans [181] may also modulate the length of the lag phase. *In vitro*, the lag phase is also often shortened by vigorous shaking which is thought to provide a hydrophobic surface at the air-water interface, increase in temperature, increasing the temperature causing more frequent molecular collisions and exposure of hydrophobic due to molecular fluctuations and partial unfolding, and by using high protein concentrations [182].

Nucleation processes may occur during storage of proteins and is therefore of special interest in biopharmaceutical and other industrial processes in avoiding serious side effects on administration [183, 184]. The lag phase is followed by the elongation phase characterized by a rapid accumulation of fibrillated protein as the nuclei are extended into fibrils. The steady state phase is characterized by equilibrium between highly ordered polymers in amyloid aggregates and monomeric protein. As illustrated by positioning of amyloids at the bottom of a deep well of the folding landscape (Figure 14), amyloidal aggregates are typically very stable structures and more so than the native protein. While these structures are found in senile plaques, it has become increasingly recognized that prefibrillar protein aggregates termed oligomers are the primary cytotoxic species in aggregation diseases [185-187]. These prebrillar species, termed protofibrils, are commonly characterized by high β-sheet content and a heterogeneous distribution of small spherical or tubular assemblies which may in turn assemble into mature fibrils. The protofibrils exert a cytotoxic effect through interaction with phospholipid membranes in which they form

non-specific pores through which essential electrochemical gradients are dissipated and consequently lead to cell death [188].

The cytotoxicity of protein oligomers may, however, not necessarily be detrimental for health as in the case of the diseases above but also bring beneficial properties for the host. In fact, functional amyloids have been found in humans, invertebrates, fungi and not least in bacterial *curli* fibres where they represent a particularly robust material involved in cell adhesion, aggregation and biofilm formation [189-191]. Another example of proteins featuring amyloid like properties is the multimeric protein complex known as HAMLET which specifically target and induce cell death in tumor cells while leaving healthy cells unaffected [192]. HAMLET (human α-lactalbumin made lethal to tumor cells) were initially discovered as an active fraction in milk and subsequently produced *in vitro* by chromatography using an anion exchange column preconditioned with oleic acid (OA) and a preparation method of a HAMLET-like protein complex was recently described under solution conditions [192-194]. HAMLET and related protein complexes with oleic acid are interesting candidates for drug research due to the selectivity of HAMLET toward tumor cells *in vitro* and therapeutic effect against human skin pappilomas virus and human bladder *in vivo* [195-198].

8. Protein-lipid interactions and the implication on structure and function

Part I of this thesis focused on the interaction of antimicrobial peptides with lipid membranes. However, the term lipid may not only be applied to the phospholipids present in lipid membranes but generally to a large and diverse group of molecules related owing to their preferential solubility in non-polar organic solvents and poor solubility in water. Thus, lipids also include fats and oils, waxes, fatty acids, detergents, sterols and certain vitamins. The work presented in this part of the thesis makes use of short-chain (6-9 carbon atoms) zwitterionic phospholipid detergents (C6PC-C9PC), zwitterionic dodecylphosphocholine (DPC) sharing some similarity with phospholipids and the anionic detergent sodium dodecylsulphate (SDS) (see Table 3) which is a known denaturant of proteins.

Detergents have been used in many studies serving as water-soluble lipid mimics; particularly studies aiming to shed light on the mechanisms involved in protein denaturation [77, 174], i.e. the unfolding of proteins by detergents. Despite of this, the mechanism by which proteins interact with detergents is not completely understood [199]. As shown in Table 3, detergents are characterized by their amphiphatic properties in which hydrophobic and hydrophilic parts are segregates similar to the lipids described in part I of this thesis. This is also reflected in the ability of detergents to interact with both hydrophobic patches exposed at the surface, with hydrophobic loops and with amphiphatic α-helices but importantly also electrostatic interaction between cationic or anionic detergents with acidic (Asp and Glu at ~pH<4) and basic (His below ~pH 6, Lys and Arg) residues, respectively.

A major difference between the phospholipids employed in the studies on AMPs and detergents employed in **paper V and VI** and depicted in Table 3 is their ability to self-assemble into micellar aggregates above their critical micelle concentration (CMC). The depicted detergent do thus not form the lamellar structure

characteristic of lipid bilayers but exist as monomers in solution at concentrations below the CMC. The transition from the monomeric state to the aggregated micellar state of non-ionic and zwitterionic detergents is of major importance for protein structure and function and will be discussed below [194].

Table 3 The name, abbreviation, critical micelle concentration (CMC) and structure of detergents employed in this thesis. [a]Approximate CMC values were obtained from the manufacturer (Avanti Polar Lipids), [b]CMC value of SDS obtained from ref [200].

Abbreviation	Name	CMC[a] [mM]	Structure
C6PC	1,2-dihexanoyl-*sn*-glycero-3-phosphocholine	15	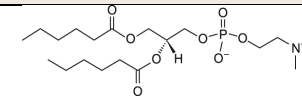
C7PC	1,2-diheptanoyl-*sn*-glycero-3-phosphocholine	1.4	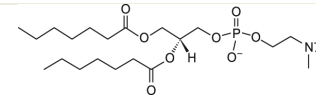
C8PC	1,2-dioctanoyl-*sn*-glycero-3-phosphocholine	0.27	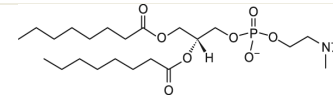
C9PC	1,2-nonanoyl-*sn*-glycero-3-phosphocholine	0.029	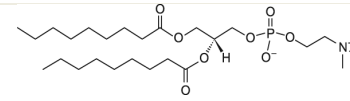
SDS	Sodium dodecyl sulphate	2-8[b]	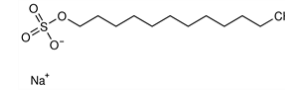
DPC	Dodecylphosphocholine	1.1	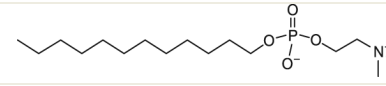

Detergents may interact with soluble proteins through binding to specific binding pockets in proteins designed to occupy hydrophobic ligands or less specific hydrophobic patches on the protein surface. Serum albumin and fatty acid binding protein (FABP) are excellent examples of proteins which are specialized in the binding and transport of fatty acids and hydrophobic compounds [201-204] in binding specific pockets. However, not only fatty acids may bind to albumin but also detergents such as the anionic detergent sodium dodecyl sulphate (SDS). Serum albumin binds three SDS monomers per protein to high affinity sites through a combination of electrostatic interaction and hydrophobic interactions to basic residues having non-polar patches present in the vicinity [205]. Further, albumin binds approximately six SDS molecules through hydrophobic interactions with a lower affinity owing to the lack of electrostatic attraction to basic residues [205]. Remarkably, the interaction of SDS stabilizes the protein as shown by an increase in the stability toward thermal denaturation in DSC experiments through binding in specific binding pockets of the native state [205]. The stability is remarkable since SDS typically binds strongly to globular proteins and

denature proteins through binding to basic residues (Arg, His and Lys) and often induce protein unfolding by introduction of negative charge to the protein arising from the anionic headgroup [206].

Further binding of SDS to serum albumin eventually denatures the protein through binding through non-specific interactions similar to many other globular proteins and saturation of all potential binding sites are typically accomplished when the concentration of free SDS detergent approaches the CMC [206]. In the laboratory, the general property of globular proteins to bind ~1.4g SDS per gram of protein which overwhelm the intrinsic charge of the protein by introducing negative charge is commonly used in the laboratory for analysis of the molecular weight of proteins by SDS-PAGE [206, 207].

In contrast to SDS and other anionic detergents, natural anionic bile salts such as sodium cholate and deoxycholates, non-ionic detergents such as triton X-100 and alkyl glucosides interact with proteins but generally do not unfold them [206]. Thereby, the structure and enzymatic function of proteins is often retained in such detergents making them useful for isolation of membrane proteins. In general, there is evidence that non-ionic, zwitterionic and bile salt detergents in the monomeric state bind, if at all, only weakly to water soluble proteins [174]. Therefore, such detergents may not be expected to affect the stability of proteins. At the time of writing **paper VI**, there was thus no precedence for destabilization or structural rearrangements of water soluble proteins by zwitterionic detergents.

However, the impact of lipids in the form of ionic, zwitterionic and non-ionic detergents on another well-characterized protein, α-lactalbumin (αLA), was recently reported [174]. As shown in Figure 15, the interaction of αLA with anionic SDS was characterized by three regimes in which (0) monomeric SDS bind at low concentrations with no apparent specificity or conformational change of the protein, (1) monomeric SDS bind and induce conformational changes and (2) the interaction with micelles which denatures the protein [174]. The interaction with non-ionic and zwitterionic short-chain phospholipid detergents (C6PC-C9PC) in their monomeric form below the CMC was not detected. However, these detergents induced major conformational changes in αLA above the CMC, indicating that all classes of detergents may destabilize proteins in their micellar form [174].

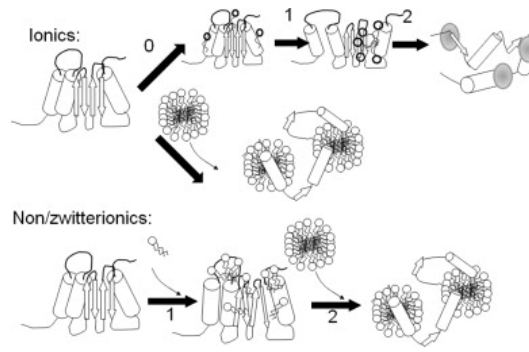

Figure 16 Schematic representation of the differential denaturation of αLA by detergents. The anionic detergent SDS binds to αLA in several steps at concentrations below the CMC. At low concentrations (<0.1 mM), monomeric detergent molecules bind without inducing any major conformational changes (phase 0). Phases 1 and 2 are accompanied by increasing binding of detergent resulting in changes in both secondary and tertiary structure (according to fluorescence and CD) with different kinetics of formation, leading to increased clustering of surfactants on the protein surface. Above the cmc, micelles bind and result in a denatured state. For non-ionic and zwitterionic detergents, no specific binding to αLA is observed and conformational changes indicating protein denaturation occured only above the CMC. Illustration adapted from reference [174] with permission.

Some proteins are particularly resistant toward chemical denaturation by detergent such as SDS. An explanation the profound resistance of such proteins to unfold in the presence of the anionic detergent has been described by the term kinetic stability. The concept of kinetic stability may be explained by means of the two-state unfolding of a protein from the native (N) to the denatured (U) state separated by a transition state (TS) in Figure 16A. Since the height between the N and U states determines the rate of unfolding and the energy required to reach TS is unusually high compared to normal proteins (dotted line), it is essentially trapped in the native state and the protein unfolds extremely slow. The native state of the protein is kinetically trapped.

Similarly, the native protein may resist unfolding even under conditions which favor unfolding of normal proteins as illustrated in Figure 16B (dotted). Here, the energy barrier of the kinetically trapped protein to TS is sufficiently large to significantly slow down unfolding even if the free energy of U may be more favorable than N. Consequently, unfolding the protein is also often irreversible.

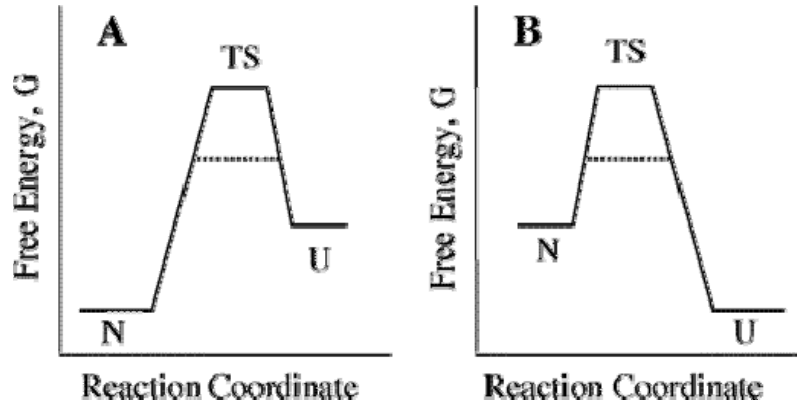

Figure 17 Schematics of the free energy of protein conformations to illustrate the high energy barrier for unfolding of a kinetically stable protein under native (A) and denaturing conditions. The transition state of a normal protein is illustrated by the dashed line and kinetically stable proteins by the full line. Illustration adapted from [208] with permission.

A well-studied example of kinetically trapped proteins is the secreted protein α-lytic protease (αLP) from Lysobacter enzymogenes [209]. When αLP is expressed, it contains an N-terminal sequence required for folding of the protein to the native state. However, once the protein reaches the native state, a region of the N-terminal is cleaved off. The removal of the N-terminal region might be expected to shift the thermodynamic equilibrium further toward the denatured state which is now favored. However, the removal of the N-terminal region results in a high energy barrier toward unfolding and this leaves αLP in an active and kinetically trapped state [210].

Several other proteins including *Thermomyces lanuginosus* lipase [211], pyrrolidone carboxyl peptidase [212], papain, avidin, superoxide dismutase and transthyretin [208]have been identified as kinetically stable proteins. These proteins share important features through a large content of β-sheet structure and a very slow unfolding rate in water.

The resistance toward chemical denaturation of these proteins is of special importance in the context of this thesis. Indeed, the proteins mentioned above have been shown to resist denaturation. Several of these proteins were discovered by their different migration of boiled and non-boiled samples in the presence of SDS. Whereas most proteins denature under such conditions and migrate in a similar pattern irrespective of sample heating, eight kinetically stable proteins was identified by their resistance toward SDS denaturation in the non-boiled sample leading to a different migration in SDS-PAGE relative to the boiled sample [208].

9. Equine lysozyme and structurally related proteins and protein complexes

Lysozymes are widely distributed among animals and plants where they aid in the protection against microbial infections through hydrolyses 1,4-β-linkages between N-acetylmuramic acid and N-acetyl-D-glucosamine of peptidoglycan layers which constitute important structural roles in bacterial cell walls. Thereby, lysozymes are efficient antimicrobial agents toward a range of bacterial strains [213].

Equine lysozyme (EL) is a C-type lysozyme of 129 amino acid residues (14.6kDa) which has the active site of other lysozymes constituted by Glu35 and Asp52 and further contains a conserved calcium binding site characteristic for α-lactalbumins but absent in e.g. human and chicken lysozymes [214, 215]. Due to calcium-binding site and high similarity to α-lactalbumins in terms of sequence and structure, EL has been proposed to be an evolutionary link between lysozymes and α-lactalbumins (αLA) [216, 217]. The crystal structures of EL and αLA proteins shown in Figure 16 further emphasizes the similarity of these proteins both at the structural level and in the position of Trp residues and disulphide bridges. Remarkably, sequence alignment of EL and αLA reveals that 41% of residues are identical and show 62% similarity based on the Blosum62 similarity matrix [218] although the proteins share no similarity in cellular function.

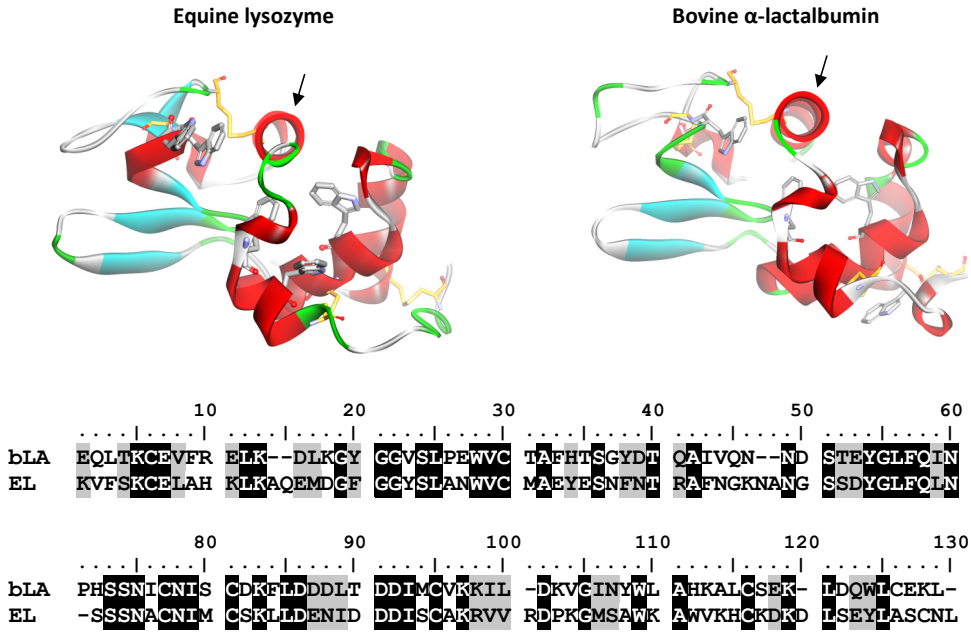

Figure 18 Illustration of the three-dimensional structures of the 129 aa equine lysozyme (PDB file 2EQL) and 123 aa bovine α-lactalbumin (PDB file 1F6R). The structures were made using Accelrys Discovery Studio Visualizer 2.5. The arrows denote helix C of αLA and EL which has been shown to be important for the interaction with membranes for αLA [219]. α-helices are presented in red, β-sheets in blue, loops in green and disulphide bridges in orange. Tryptophan residues are plotted in grey. The sequence alignment below show identical residues with black background, similar residues (based on Blosum62 identity matrix) with grey background.

The calcium binding site consisting of three conserved asparagines residues (D85, 90 and 91 in EL) and two carbonyl groups of the main chain (K82 and N87 in EL) is located at the β-sheet domain and EL displays significantly higher stability toward chemical and temperature denaturation in the calcium-bound apo-form of EL [172].

As shown in Figure 16, EL and αLA consists of two domains of one is composed by four α-helices and the other a β-sheet domain consisting of three beta stands and several loops. As shown by the orange lines in Figure 16, the EL and αLA structures are stabilized by four disulphide bridges. EL contains five Trp residues of which Trp 28, 108 and 11 are buried in the hydrophobic core and Trp63-64 are located closer to the protein surface as shown in Figure 16 [214, 220]. NMR, Trp fluorescence, Trp fluorescence quenching and near-UV CD experiments have suggested that buried Trp residues in EL becomes more exposed to solvent on partial chemical denaturation but remain constrained in a hydrophobic core surrounded by a less structured yet still compact polypeptide chain [170, 172].

Both EL and αLA have been extensively studied as model systems of protein folding since they readily enter partially unfolded states termed molten globules (MG) which are described by a relatively compact structure, well-defined hydrophobic core, native-like secondary structure elements but few tertiary contacts relative to the native protein conformation [170, 172-174, 219, 220]. In the native state, the binding of Ca^{2+} stabilizes the β-sheet domain which includes the calcium binding loop. However, the β-sheet domain is less structured in the MG state compared to the α-helix domain and the conformation of the MG is thus not affected by the presence of Ca^{2+} [172, 214, 220].

The MG state of proteins has been shown not only to be important in understanding the folding pathways leading to the natively folded and active state of proteins, but MGs are also important for alternative folding pathways leading to intermediate or non-native protein structures such as the formation of amyloidal aggregates of lysozymes [221-224].

The MG state of αLA has been shown to interact with phospholipid membranes [219]. More specifically, helix C of αLA (Thr86-Val99; TDDIMCVKKILDKV, indicated by the arrow in Figure 16) displays an amphiphatic character and is involved in association to liposomes. The sequence resembles to a large extent helix C of EL (Figure 16), indicating that these specific residues may also be important for the potential membrane interaction of EL. This is further supported by amide hydrogen-exchange protection studies of EL in the MG state displaying weak H/D exchange protection in helix C [220] (Asp89-Lys103: DDDISCAKRVVRDPK), indicating that this particular helix may also be exposed in the MG state of EL.

Recently, a multimeric protein equine lysozyme complex with oleic acid (ELOA) was produced through partial unfolding on an ion exchange column preconditioned with OA followed by elution in a salt gradient [225] – a process similar to the process described for HAMLET, the protein complex between oleic acid and αLA displaying cytotoxic properties toward tumour cells while sparing healthy cells [192]. The column preparation method has previously been described as a prerequisite in the formation of active HAMLET

which could not be obtained by simple mixing of protein and oleic acid [193]. However, a method in which a tumoricidal complex human αLA and OA was shown to be formed by titration of OA to human αLA at 17 and 45 degrees forming complexes termed LA-OA-17 and LA-OA-45 [194]. While HAMLET has been shown to contain approximately 1 OA per protein monomer, the LA-OA-17 and LA-OA-45 complexes were shown to contain approximately 3 and 9 OA on a monomer basis.

The ELOA complex displays properties common for amyloid oligomers of equine lysozyme and HAMLET through its affinity toward the amyloid specific dye Thioflavin T and Congo red dyes, ring-shaped morphology and cytotoxic effect in cells [192, 224, 225]. The binding of the hydrophobic dye ANS further suggested that hydrophobic patches are exposed on the ELOA surface as also shown with HAMLET [225, 226].

In ELOA, equine lysozyme is present in a partially unfolded state resembling the MG state of EL due to its interaction with oleic acid (Figure 17). Structural characterizations of ELOA by near- and far-UV CD revealed that the protein complex is in a MG state comparable to the acid denatured MG state of EL. Cross peaks between aromatic residues and oleic acid (OA) in NMR studies suggest that the MG state is stabilized through complexation with OA. NMR studies further revealed that the stoichiometry of ELOA varied from 9-48 bound OA per equine lysozyme monomer and that ELOA forms a range of oligomers consisting of 4-30 equine lysozyme monomers [225]. In **paper IV**, we employed the ELOA complex consisting of approximately 32 OA per equine lysozyme monomer. For comparison, HAMLET has been shown to contain approximately one bound OA per protein monomer and HAMLET-like complexes formed by titration of αLa with OA termed LA-OA-17 and LA-OA-45 with numbers referring to the temperature at which the complexes were formed contained approximately 3 and 9 OA, respectively [194, 226].

The cytotoxic effect exerted by ELOA in cells indicate an apoptotic type of cell death since the employed dyes are only accessible to their targets when the integrity of the cytoplasmic membrane is lost [225]. Cell death via apoptosis has also been reported for the related HAMLET complex [192, 227]. HAMLET induces apoptosis in cells through a series of events which include binding at the cell surface, internalization of the complex across the plasma membrane to the cytoplasm and passage to the nucleus through nuclear pore complexes (NPCs) in which it leads to fragmentation of chromatin structure and formation of DNA fragments [192, 198, 227, 228]. The transfer of macromolecules across the cytoplasma membrane and subsequent transfer to the nucleus is remarkable owing the limited permeability of lipid membranes and tight regulation of NPCs. Nevertheless, up to 80% of radiolabeled HAMLET has been observed to accumulate in the nuclear fraction of cells indicating efficient uptake and targeting [227]. While macroscopic events leading to cell death have been described extensively, the mechanisms of individual translocation events across membranes are poorly understood.

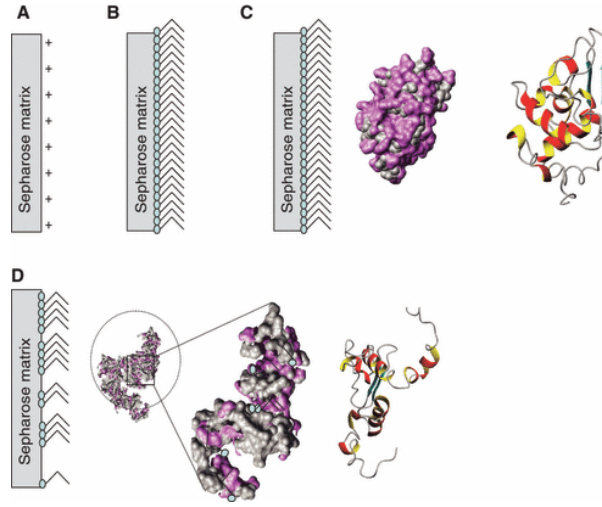

Figure 19 Schematic representation of ELOA formation at the solid-liquid interface by column chromatography. The exposed hydrophilic residues are denoted in purple and hydrophobic residues in grey. In (A-B), the anion exchange matrix is preloaded with oleic acid. In step (C), equine lysozyme interacts with the solid-liquid interface and the hydrophobic residues are exposed and the ELOA complex is formed through interaction with OA and equine lysozyme in (D). The resulting equine lysozyme complex with oleic acid is in a partially unfolded molten globular-like state stabilized by interaction with OA with aromatic residues. Illustration adapted from [225] with permission.

The first step in this complex cascade of events is the interaction with the plasma membrane and the mechanism of interaction and the penetration into cells is therefore essential in understanding the cytotocixity and specificity of protein:oleic acid complexes toward cancer cells. Studies employing SUVs of DPPC and *Chara coralline* plasma membranes have shown that native αLA irreversibly accumulate on membranes and the accumulation is enhanced through complexation with OA in HAMLET [229]. The adsorption of HAMLET on the surface has been suggested to include association and blocking of calcium channels and calcium-activated chloride ion channels followed by the development of a non-selective permeability of the membrane due to non-specific potassium leakage which ultimately initiate the mechanism(s) of HAMLET internalization via non-specific endocytosis pathways [229]. The initial association of HAMLET to membranes is likely mediated by a combination of oleic acid and the partially unfolded state of αLA in HAMLET since H/D exchange studies of membrane-bound αLA shows that specific residues within a single helix is involved in membrane binding and that αLA is in a MG-like form in membrane bound states [219]. While αLA does not traverse membranes, the coupling of the OA cofactor is likely to mediate the internalization.

Recently, a HAMLET analogue produced from recombinant human LA in which all cysteine residues were replaced by alanines and thereby devoid of disulphide bridges was shown to be equally efficient in internalization, in translocation to the nuclei, in killing tumor cells and in the ability to impose DNA

fragmentation compared to HAMLET [230]. Since the alanine analogue lacked disulphide bridges, defined tertiary structure and display similar activity compared to HAMLET it appears that the oleic acid cofactor and not a defined tertiary structure is important for internalization and cytotoxic activity of HAMLET.

In the work presented in **paper IV**, we investigated the interaction of ELOA containing approximately 32 OA per EL monomer and phospholipid membranes of 80% DOPC and 20% anionic DOPG. Our confocal laser scanning microscopy (CLSM) experiments clearly show accumulation of ELOA on membranes containing 20% anionic DOPG lipids under physiological conditions. Native EL showed no accumulation on the surface of membranes despite of the net positive charge (theoretical pI of 8.41 [231]) indicating that complexation with OA increases the affinity to the membrane. Confocal laser scanning microscopy studies in **Paper IV** showed no significant signs of dye leakage which was confirmed by calcein dye leakage with dye leakage levels of 3-6% even under conditions where the OA concentration of the sample exceeded lipid concentration. This was surprising since such low levels of release suggest a small increase in membrane permeability and not vesicle rupture as reported for cells exposed to ELOA for approximately 50 minutes [225]. We further evaluated the propensity of ELOA to internalize into LUVs on exposure to NBD labeled complex followed by quenching of NBD fluorescence by the membrane impermeable dithionite. However, complete quenching of the NBD fluorophore was observed even after prolonged incubation with vesicles (overnight) indicating that ELOA in contrast to HAMLET does not internalize into vesicles.

Using a combination of spectroscopy methods, evaluation of proteolytic resistance and activity assays, **Paper IV** further shows that the interaction with lipid membranes result in a partial refolding toward native-like conformations which display increased proteolytic resistance toward degradation by trypsin and increased lysozyme activity. Together with an apparent equilibrium between bound and free OA in diluted ELOA samples, this suggests that ELOA act via a cargo off-loading mechanism in which it delivers OA to phospholipid membranes and attain more native-like conformations.

Put into the analogy of the folding funnel, these observations suggests that EL becomes partially unfolded to a MG state on the ion exchange column during preparation and move to a higher energy state within the folding funnel. Through the interaction with OA, the MG state of equine lysozyme is stabilized at a local energy minimum and complexation with OA thus prevent ELOA from downward progression within the folding funnel toward the native state. Remarkably, these folding intermediates stabilized by OA in ELOA appear to be thermodynamically stable in solution at room temperature on extended timescales of up to 24 hours [225]. When ELOA is exposed to liposomes, the structural rearrangement and partial recovery of enzymatic activity indicate the loss of oleic acid from the protein complex which allows it to progress downward toward more native-like conformations.

A similar conclusion has been made in studies of HAMLET [232]. Thus, it was shown that the thermal stability of HAMLET was lower than the native protein and that the denaturation of HAMLET is irreversible.

This means that the protein complex is not reformed and HAMLET activity is lost when the sample is cooled. Rather, αLA refolds toward the native state after off-loading the OA cofactor.

Future directions

A question not addressed to detail in studies of both ELOA and HAMLET is the fate of oleic acid. Since the complexation of fatty acids in HAMLET depend largely on the presence of a double bond in the cis-conformation [226], it would be interesting to explore the possibility of including a fraction of fatty acids containing conjugated double bonds such as *cis*-parinaric acid in the protein complexes to allow tracking of these by fluorescence within cells *in vivo* and model membranes *in vitro*. An alternative approach could involve the use of radioactively labeled oleic acid. Through inclusion of fluorescence dyes in lipid membranes such as DPH, fluorescence anisotropy could provide further information on the influence of ELOA on the integrity and packing of lipid membranes. The conformational (dis)order and potential increased mobility of acyl chains as a result oleic acid and/or protein incorporation in the membrane could further be evaluated through changes in frequency and bandwidth of CH_2 stretching bands by FTIR could as a function of protein content [233].

A major difference between the ELOA complex employed in **Paper IV** and studies of HAMLET is the amount of OA associated in the complexes. The ELOA complex in **Paper IV** thus contains approximately 32 oleic acids on a monomer bases at concentrations above approximately 20μM. At lower concentrations, an increasingly large portion of OA dissociates from the complex into its free form in bulk solution. In comparison, the approximately 1, 3 and 9 OA present in HAMLET, LA-OA-17 and LA-OA-45 on a monomer basis [194, 226]. Given that the ELOA complex employed in **paper IV** contains much more OA per EL monomer compared to the stoichiometry of HAMLET and related complexes, it would be interesting to evaluate the difference between ELOA variants with varying OA content and whether this might modify the propensity of the complex to translocate across lipid membranes of various compositions set to mimic individual cell compartments or cancer cells.

In the comparison of EL and αLA, the structural resemblance and propensity of especially the helix C of bovine αLA to interact with membranes in the MG state was mentioned. Owing to the great resemblance of the proteins and the MG state of ELOA stabilized by OA, it would be obvious to conduct NMR H/D exchange experiments with ELOA in the presence liposomes similar to the experiments done with αLA [219] to evaluate whether helix C is also responsible for the interaction of ELOA. Within the context of this thesis, it is interesting that the helix wheel of the C helices of EL and αLA shares the characteristic segregation of polar and hydrophobic residues at opposing faces similar to antimicrobial peptides. Although the segregation may be less distinct than in the case of novicidin, this may explain the propensity of the αLA helix C to interact with membranes. Further owing to the similarity of these proteins, it would be interesting to evaluate potential conformational changes in the structure of HAMLET upon interaction with

membranes as shown in **Paper IV** with ELOA to examine whether structural reorganization is a genuine feature of these complexes.

10. Beta-sheet aggregation of kisspeptin-10

Kisspeptins arise from the expression of the metastasis suppressor gene *Kiss1* (Figure 18) which has been attributed a significant role in the physiological regulation of reproduction and onset of puberty [234]. The expression and signalling of Kiss1 and its receptor Kiss1R have been shown to be essential for the initiation of gonadotropin secretion (luteinizing and follicle stimulating hormones) from GnRH neurones at puberty [234, 235].

In humans, the *Kiss1* gene encodes a precursor protein consisting of 145 amino acids which are thought to be processed by proteolytic presumably by furins or prohormone convertases cleavage into several smaller fragments which are commonly termed kisspeptins [236]. In humans, these fragments constitute both the 54 amino acid protein known as human kisspeptin-54 (hKp-54) as well as truncated versions hKp-10, hKp-13 and hKp-14 amino acid residues which all share a common amidated C-terminus (Figure 18)[235].

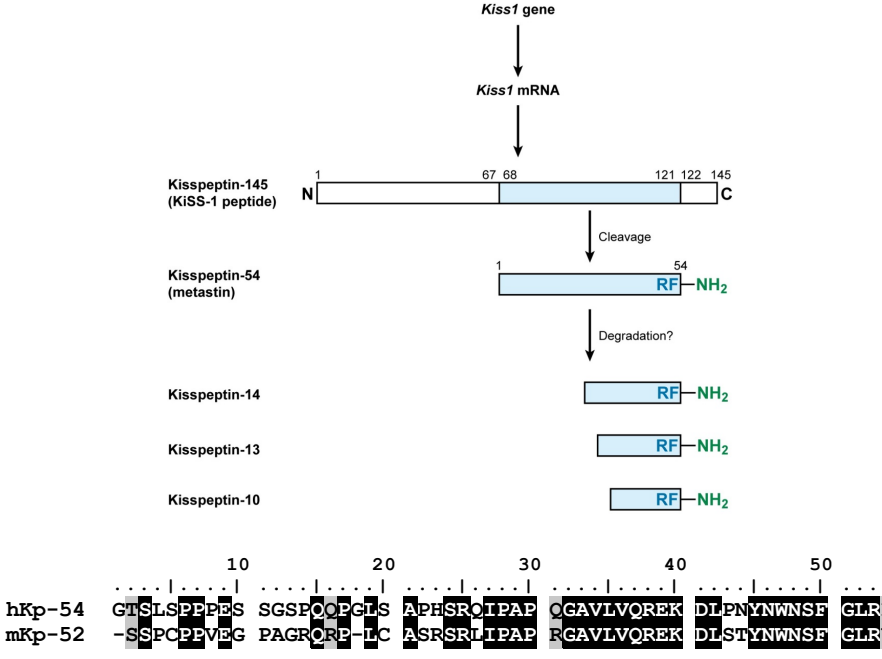

Figure 20 Processing of the human Kiss1 gene. mRNA is transcribed from the *Kiss1* gene and translated to form a the kissptin-145 propeptide. The cleavage site for furins or prohormone convertases that lead to the production of the RF-amidated human kisspeptin-54 (hKp-54), also known as metastin, are indicated by numbers. Shorter peptides (such as hKp-10, -13, and -14) have been detected by mass spectroscopy and have been suggested to be the result of proteolytic cleavage although no obvious cleavage sites have been identified. The hKp-10, -13, and -14 and -54 peptides share a common C terminus and RF-amidated motif with kisspeptin-54. Adapted from Popa et al., (2008)[235] with permissions ©Annual Reviews. Sequence alignment of NCBI accession numbers NP_839991 and Q15726 made in BioEdit v7.0.9 with color coding based on the Blosum62 substitution matrix. Grey shaded residues are similar and black shaded residues are identical.

In rodents, the precursor protein is spliced into a 52 amino acid peptide (murine kisspeptin-52, mKp-52) which show several sequence differences to the hKp-54 sequence (Figure 18). For instance, the putative disulphide bridge between potentially formed between Cys4 and Cys16 [237]. Further, the amidated C terminal is Tyr in rodents compared to the Phe residues in humans. Thus, the only difference between hKp-10 and mKp-10 fragments is a hydroxyl group of the C-terminal amino acid residue. The biological activity has been attributed to the C-terminal fragment of the peptide as indicated by their similarity in binding affinity to the Kiss1 receptor (Kiss1R). The C-terminal has thus been proposed to be responsible for the binding and activation of Kiss1R [237].

Not much is known about the structure of naturally occurring kisspeptin sequences in the blood stream extracellular spaces and nothing is known about their structure in cells. Owing to the storage and secretion of kisspeptins from neuronal secretory vesicles, we initiated studies of mKp-52 serving to probe the effect of the potentially important interaction between kisspeptins and membranes. However, we found that mKp-52 was particularly resistant to the adoption of a defined secondary structure at pH 6.1 even in the presence of 10mM SDS and sodium sulphate as exemplified in Figure 19. However, we observed an α-helix signature in the presence of 60vol-% trifluoroethanol (TFE) which is not remarkable since TFE is known to stabilize α-helix structure in proteins and protein fragments[238].

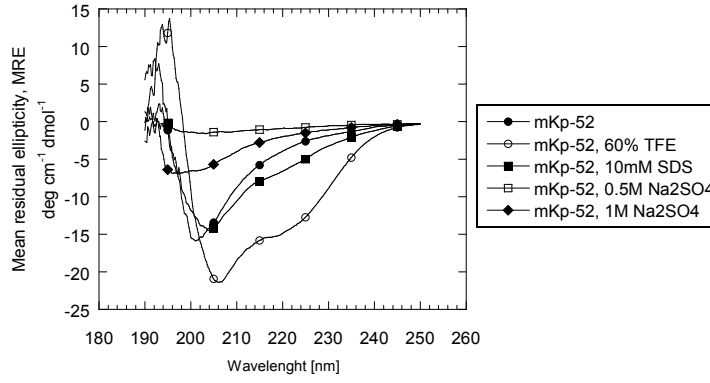

Figure 21 Preliminary studies of mKp-52 showed no sign of defined secondary structure elements in 10mM phosphate buffer pH 6.1. A small change in ellipticity at 222nm was observed in 10mM SDS was observed indicative of a small increase in α-helix content. In 60% TFE which is known to induce α-helix conformations in proteins and peptides [238], the signature of an α-helix was indeed observed. mKp-52 precipitated in the presence of increasing concentrations of sodium sulphate as indicated by the gradual loss of the minimum at ~200nm when going from 0 through 0.5 to 1M sodium sulphate.

The spectra of mKp-52 in 60% TFE differ somewhat from recent studies of hKp-54 in the presence of 0-40% TFE[239] in that hKp-54 did not show appreciable changes in the CD spectrum at these concentrations. They did, however, not extend their studies to 60% corresponding to the spectrum in Figure 19 and the primary sequences differ at several positions (Figure 18) which may explain this difference. The structure of hKp-54 was further evaluated in the presence of SDS and DPC but showed no sign of defined secondary

structure in NMR and CD experiments [239] and is thus in agreement with the results presented in Figure 19. hKp-54 and mKp52 thereby appear to be intrinsically disordered sequences. This may bring advantages in the ability of the kisspeptins to recognize and target a wide range of target proteins. The secondary structure of hKp-10 analogues (S5A and S10A mutants) has further been shown to be mainly of random coil conformation in aqueous buffer at neutral pH, but undergo a structural in the presence of lipid vesicles and membrane mimicking DPC micelles although the data does not suggest a regular secondary structure consistent with our observations with mKp-10 in **paper VI** [240].

Our studies of murine kisspeptin-10 (mKp-10) leading to **paper VI** were initiated to evaluate the structure and interaction with lipids in the form of membrane mimicking dodecylphosphatidylcholine (DPC) micelles and sodium dodecylsulphate (SDS) owing to potentially important interactions between mKp-10 and membranes of secretory granules in which kisspeptins are stored *in vivo.* However, the amphiphiles turned out not to have great influence on the structure of mKp-10 and we therefore turned our attention to the potential of mKp-10 to aggregate into amyloidal aggregates with defined cross-β-sheet structure. To our knowledge, there has been no report of kisspeptins to form amyloids although the propensity of peptides to form amyloidal aggregates has been suggested to be an intrinsic property of the polypeptide chain[241]. The random coil conformations of mKp-10 provide access ready to a number of different conformations and thus explore much of the upper parts in the folding landscape (Figure 14).

Recently, there have been several reports of peptide hormones which can form β-sheet structures under physiological conditions. Particularly, amyloids are formed in the presence of highly sulphonated and naturally occurring glucosaminoglucans such as heparin, indicating a potential role of amyloid deposits of peptide hormones as a physiological storage mechanism [242, 243]. Previously, human secretogranin II has been shown to exhibit aggregation at low pH and in the presence of calcium and aggregation was inhibited by ammonium chloride which neutralizes the pH of acidic intracellular compartments[244]. These conditions are characteristic for the milieu in neuroendocrine secretory granules, suggesting that aggregation is involved in sorting and/or storage of secretogranin to secretory granules[244]. Amyloidal aggregates of peptide hormones are thus likely to be members of the growing number of functional amyloids being discovered.

In preliminary studies leading to **paper V**, we observed no sign of aggregation of mKp-10 under physiological conditions including both pH 7.0 and 5.2 in the presence and absence of 150mM sodium chloride concentrations of sodium chloride and at pH 5.2 in the presence of 10mM calcium and/or 150mM sodium chloride. Thus, we mimicked the milieu both within neuroendocrine secretory granules and physiological conditions surrounding cells. However, **paper V** revealed that mKp-10 may indeed form amyloidal structures under physiological conditions provided by the presence of the polyanionic heparin. The presence of amyloid species was corroborated by the binding of Thioflavin T and through analysis of the secondary structure by FTIR and CD confirming the β-sheet rich conformation common for amyloidal aggregates. We further found that low concentrations below the CMC of the detergents SDS and DPC

inhibited the formation of amyloidal aggregates indicating the binding of these detergents. Thus it appears that low concentrations of the detergents somehow displace the ensemble structure of mKp-10 leading to aggregation to a state which is less prone toward aggregation while heparin has the opposite effect.

Our observations with mKp-10 are thus consistent with the wide-spread propensity of peptide hormones to undergo amyloid aggregation particularly in the presence of of heparin, recently described by Riek and co-workers [242, 243]. They suggested that the amyloidal state could be employed as long-acting deposits of peptide hormones [242, 243]. For this kind of usage, it would be essential to examine whether dissociation of monomers from mKp-10 aggregates occur as demonstrated for several peptides by the authours. Such studies should include the ability and rate of drug release. In this regard, it would also be essential to probe the existence, structure and potentially cytotoxic properties of protofibrillar species which may be released from aggregates.

Further, since our data indicate that amyloidal aggregates are formed with comparable ease at pH 5.2 and 7.0 which corresponding the interior of secretory granules and extracellular space, respectively, it will be essential to identify affectors which allow depolymerisation of amyloidal aggregates if a physiological relevance of amyloids as a storage mechanism is to be established.

11. *Fusarium solani pisi* cutinase

The fungal *Fusarium solani pisi* cutinase is a serine esterase (EC 3.1.1.74) which hydrolyses triglycerides and degrades a waxy extracellular polyester matrix called cutin presented at the surface of plants and further [245, 246]. It is an α/β protein consisting of a central β-barrel of five parallel β-strands surrounded by five α-helices of different length as shown in Figure 20A-B. The active site is composed by Ser120, His188 and Asp175 with the serine residues accessible close to the protein surface as shown in Figure 20C.

The negative charge generated on nucleophillic attack of a substrate is stabilized by the oxyanion binding site [247]. The solvent accessibility of the reactive serine is important in distinguishing between the *F. solani pisi* cutinase from lipases in that the catalytic site of lipases is buried under a surface loop. Lipases thus require interfacial surface activation at lipid-water interfaces which moves the lid and increase accessibility to the active site. The absence of such a lid in *F. solani pisi* cutinase may explain why it does not display surface activation [245]. *F. solani pisi* cutinase is thus active on both monomeric substrates and aggregate lipid structures such as those of triglycerides.

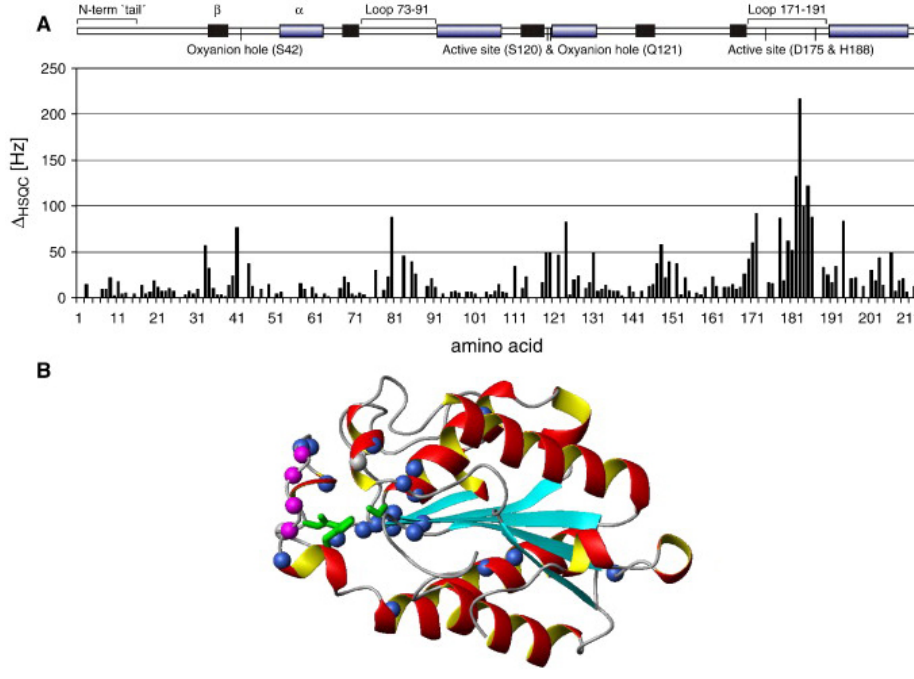

Figure 22 ΔHSQC values for cutinase on interaction with C6PC. (A) ΔHSQC values plotted against the sequence of cutinase. The top base represents secondary structure elements and residues of interest. (B) ΔHSQC of residues interacting with C6PC mapped onto the three-dimentional structure of cutinase (PDB files 1CEX). Magenta spheres denote residues in the flanking loop whose chemical shifts are affected by C6PC (ΔHSQC>100), blue spheres denote residues whose chemical shift is less affected 100Hz≥ΔHSQC≥40Hz and grey the grey signal appear on the addition of cutinase. The active site is shown in green, α-helices in red and β-sheets in blue. Illustration modified from paper VI with permission [248].

The lack of surface activation has, however, been questioned in NMR studies of protein mobility by amide hydrogen protection which show fluctuations between multiple conformations within the binding site, flanking loops and oxyanionion hole[249, 250]. It has thus been suggested that the crystal structure of cutinase represents one conformation and that internal mobility within the active site, oxyanion hole and flanking helices correspond to the interconversion between open and closed conformations [251]. Since the interconversions occur at the µs to ms scale which corresponds approximately to the rate of hydrolysis, the 'breathing' motions may be involved in substrate conversion and the readily accessible active site make it possible for cutinase to exert an activity toward water-soluble esters. The classical view of surface activation in which a pronounced lid restricts the accessibility of the substrate to the active site is thus not displayed by cutinase although inverconversion between different open and closed conformations during substrate turnover are likely [249, 251]. This in agreement with a study employing water-soluble spin-labelled monoglyceride substrate analogues revealing weak surface interactions with micelles which changed the chemical shifts and intramolecular mobility of the flanking loops surrounding the active site including several interactions between hydrophobic residues and the alkyl chains [249].

Owing to its enzymatic function, much focus has been attributed to the interaction of cutinase with lipid substrates or substrate analogues such as the triglyceride analogue phosphonate and micelle forming detergents such as spin-labelled monoglycerides, short-chain zwitterionic phospholipids (C6PC-C9PC, see abbreviations), taurodeoxycholate (TDOC), sodium dodecyl sulphate (SDS), Triton X-100 and dioctyl sulfosuccinate (AOT) to elucidate their effect on protein stability, mobility and activity [78, 249, 251] also including **paper VI**.

Our group has previously shown that non-ionic and zwitterionic detergents strongly activate the *Thermomyces lanuginosus* lipase followed by inhibition at concentrations well below the CMC, indicating that the binding of monomeric detergent is responsible for the increase in activity with no apparent destabilizing effect of the lipase [252]. In direct contrast, no apparent activation and/or inhibition of *F. solani pisi* cutinase by short-chain zwitterionic detergents (C6PC-C9PC) both well below and above the CMC was observed in **paper VI** as probed by the hydrolysis of the substrate analogue *p*-nitrophenol butyrate (pNPB). Remarkably, the thermal stability of cutinase was shown to be decreased markedly at detergent concentrations from approx. half of the CMC and above with an excellent correlation between the CMC (conferred by acyl chain length of the detergent with higher CMC for shorter acyl chains) and the degree of destabilization without affecting the enzymatic activity. Previously, the presence of the non-ionic Triton X-100 micelles form showed no effect on cutinase activity [78].

Paper VI further evaluated the effect of zwitterionic detergents on the refolding of cutinase from the acid denatured state (pH 1.5) to investigate whether the folding pathway of the enzymes is modulated and allow partially folded states to accumulate *en route* to the native state. Off pathway intermediates has previously been described by members of our group during refolding in the presence of low concentrations of strong denaturant [253, 254]. Our stopped flow refolding experiments in **paper VI** showed that the inclusion of zwitterionic detergents with acyl chain length 6-8 at concentrations up to approximately 50% of

the CMC did not affect the folding kinetics of cutinase. At increasing detergent concentrations approaching the CMC, the refolding rate dramatically plunges to very slow refolding rates.

Previously, it has been demonstrated that the refolding from the acid denatured state (pH 1.5) is slower than the corresponding GdmCl state, possibly due to a transient accumulation of aggregates within the dead time of folding [253]. However, we showed that the refolding rate in the presence of the phospholipid analogue DPC was similar irrespectively of the denatured state (GdmCl and pH 1.5 denatured states) in **paper VI,** including the abrupt drop in refolding rates around similar detergent concentration.

The abrupt drop in refolding rate at increasing detergent concentrations above the CMC suggests that detergent micelles traps cutinase in specific non-native conformations during refolding. This was investigated by activity assays employing the substrate analogue p-nitrophenol butyrate (pNBP). When cutinase in the native was incubated with C6PC, C7PC or C9PC, the activity is essentially unchanged. However, if unfolded cutinase was refolded in the presence of C7PC by transfer from pH 1.5 to 4.5, a marked decrease in the enzymatic activity was observed even after incubation of the solution for 1 day. If the detergent was added 15 minutes after the jump from pH 1.5 to 4.5, the activity was much less impaired. **Paper VI** showed that the inhibitory effect of C7PC sets in at a concentration a little below the CMC and consolidates at a concentration of approximately 2x CMC. This indicates that monomeric (<CMC) detergent bind to cutinase and traps it in an inactive state which refolds at an extremely slow rate (hours-days) to the native state. **Paper VI** shows that the secondary structure of the inactivated state displays subtle changes compared to the native state as shown by minor changes in the far UV CD spectrum compared to the native cutinase and cutinase refolded from pH 1.5 in the absence of the zwitterionic detergents.

Taken together the resistance of the native state toward denaturation by zwitterionic detergents and the very slow refolding of cutinase in presence of detergents, the native conformation of cutinase appear to be kinetically trapped by a large energy barrier which prevents it from accesing the native state but is trapped in a compact yet inactive conformation as illustrated in Figure 21. The larger energy barrier is further emphasized by the extremely slow refolding rate of cutinase (~hours-days) in the presence of zwitterionic detergents. Note that cutinase share the common hydralase α/β fold with *Thermomyces lanuginosis* lipiase recently shown to be a kinetically stable enzyme [211] adding cutinase to a continuosly growing list of kinetically stable proteins with a relatively large content of β-sheet structure.

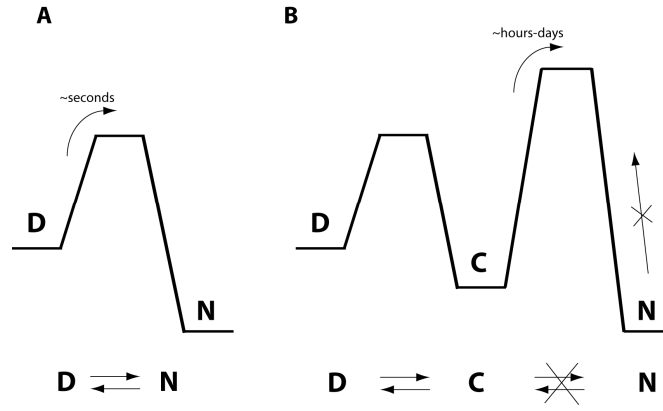

Figure 23 (A) A typical protein which folds on its own to the thermodynamically stable native state (B) in equilibrium with the unfolded state (D). For cutinase, the folding from the acidic denatured state to the native state occurs in the range of a few seconds. (B) In the presence of short-chain zwitterionic detergents at concentration of approximately 0.5xCMC and above, *F. solani pisi* cutinase prefentially folds to a compact (C) yet inactive state and binding of detergent prevent it from rapidly folding to the native state (N). The process does not appear to be reversible since the detergents do not impair activity but merely destabilize cutinase in the N state indicating a large transition barrier from N to C states. Thus, cutinase appear to be kinetically trapped.

Since the publication of **paper V**, a few studies have focused on increasing the stability of *F. solani pisi* cutinase in the presence of detergents [255, 256]. SDS, TDOC and AOT are anionic detergents which are thought to interact with positive charges of the protein by electrostatic attraction. The presence of TDOC at concentrations above the CMC result in a reversible thermal unfolding of the protein up to the melting point of the unaffected protein although cutinase displays a decreased thermal stability when the detergent is present [257]. SDS rapidly unfold cutinase at concentrations both above and below the CMC and lead to slow and irreversible inactivation [78]. The inactive intermediate state can be reactivated by the presence of the non-ionic detergent Triton X-100 [78]. The anionic detergent AOT has further been shown to denature cutinase in a two-state process involving only the native and denatured states [258]. Together, the general destabilizing effect of anionic detergents (e.g. SDS, TDOC and AOT) hamper the application of *F.solani pisi* cutinase as a general ingredient in detergent applications and organic synthesis in non-aqueous solvents for obvious reasons.

Owing to the negative charge of these detergents, it was recently suggested that the stability of cutinase toward anionic detergents could be improved by means of replacing positive charged residues located close to hydrophobic patches or by replacing residues in hydrophobic patches at the surface with less hydrophobic residues and saturation mutagenesis resulted in 24 candidates with a 2-11 fold increase in stability compared to the wild-type protein [255]. The S54D mutation is located far from the active site, shares secondary and tertiary structure with the wildtype protein and displayed highest stability toward AOT with no significant decrease in activity [256]. The importance of residue 54 in the stability toward AOT

is remarkable since no or very little change in chemical shifts of cutinase was observed in the presence of C6PC in **paper VI (**see Figure 20**)**. The introduction of a negative charge (Asp) is thus likely to result in electrostatic repulsion of AOT. A second mutant candidate, L153Q, reduced the exposure of hydrophobic patches accessible at the surface but confer stronger electrostatic interaction with AOT [256]. This residue was not involved significantly in the interaction with zwitterionic detergents in **paper VI (**Figure 20**).** However, the T179C mutation present close to the active site and the disulphide bridge between Cys171 and Cys178 resulted in a conformational change around the Trp residue relative to the wildtype protein, reduced exposure of hydrophobic patches to solvent and conferred increased resistance toward AOT with similar activity levels [255, 256]. This residue is located near one of the flexible flanking loops surrounding the active site (Figure 20) which showed strong changes in chemical shifts in the presence of C6PC in **paper VI**. This indicates that T179 may be important also for the interaction of cutinase with not only anionic but also zwitterionic detergents.

Ongoing research in the laboratory with lipase of *Thermomyces lanuginosus* suggests that the inactivation of *F. solani pisi* cutinase by short-chain phospholipids studied in **paper VI** applies not only to this particular protein but also applies the lipase to since it also displays extremely slow refolding rates in the presence of short-chain phospholipids and detergents (Huabing Wang, personal communication). It will be interesting to evaluate whether detergent binding also occur to the area surrounding the *T. lanuginosus* lipase active site as observed for cutinase or inhibit the folding of other specific parts of this protein.

Part III: Biophysical techniques to study protein-lipid interactions

This section describes various experimental methods which can be used to describe biomolecular interactions. The methods described here are by no means exhaustive but aim to cover most of the aspects which can be encountered in the study the interplay of biomolecules such as proteins, peptides and lipids.

A range of experimental methods have been applied to address the structure and function of proteins and peptides and the integrity of phospholipid membranes in the present work. This thesis clearly shows that no single method can provide the full picture of protein-lipid interactions and their importance for structure and function of both lipids and proteins. The following sections describe biophysical techniques important for the presented work.

12. Circular dichroism

Circular dichroism (CD) is a method measuring the differential absorption of left- and right-hand circularly polarized light absorbed slightly different by a given molecule and is measured using a spectropolarimeter. Proteins and peptides may contain several constituents and characteristics which give rise to preferential absorption of light polarized in one or the other direction.

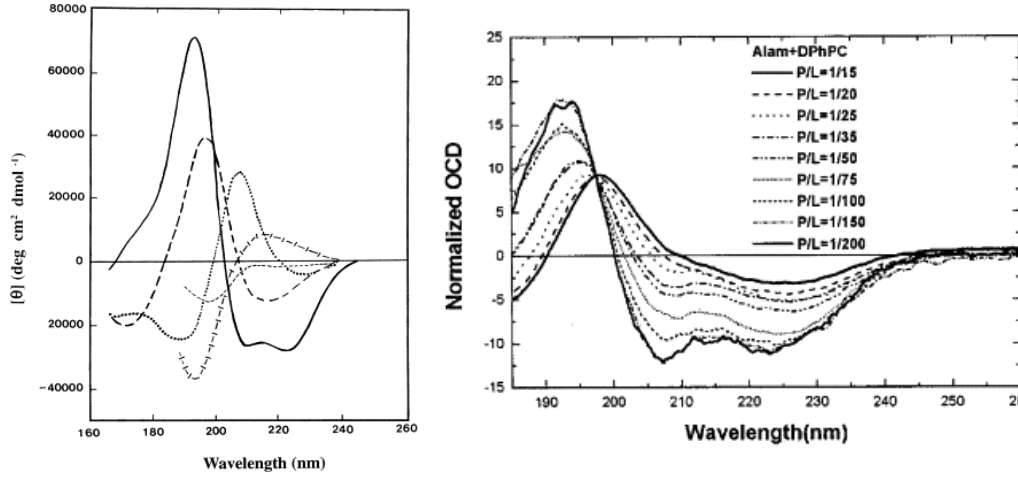

Figure 24 *Left*: Far UV CD spectra of various types of secondary structure including α-helix structure (solid line), antiparallel β-sheet (long dashes), β-turn (dotted line), 3_{10} helices (cross dashed line) and random coil conformations (short dashes). Illustration adapted from [259] with permission. *Right*: Oriented circular dicroism (OCD) spectra of alamethicin in lipid multilayers at varying peptide to lipid ratios (P/L) at full hydration. Spectra normalized at 197nm to have the same isodichroic point. Illustration adapted from [149] with permission.

For instance, aromatic residues constitute a chromophore of proteins and peptides which is especially sensitive to changes in local environment which may be employed to reveal changes in tertiary structure in the Near-UV region. Thus, the spectra in the 260-320nm region arise from the contribution of aromatic

amino acid residues. Conveniently, the contribution of Phe, Tyr and Trp residues are separated into bands positioned between 255-270nm, 275-282nm and 209-305nm, respectively [259]. Thereby, the near UV spectra of proteins may prove valuable fingerprints of the tertiary structure of proteins which can be compared in different milieus. However, near UV CD experiments generally require high concentrations of the protein which may be a limiting factor.

In the Far-UV region (Figure 22, left), the transition dipolar moment of the polypeptide backbone constitutes an important chromophore which can be used in CD to reveal important structural information and allows the assignment of secondary structures such. *β-sheet* thus gives rise to a single minima at approximately 217nm and maximum at approximately 195nm and *α-helices* give rise to minima at approximately 208 and 222nm and a maximum at approximately 190nm. *Random coil conformations* give rise to a negative signal at approximately 200nm. The CD may, however, also be affected by the side chains of aromatic amino residues such as the positive maximum of mKp-10 at approximately 225nm in **paper V** which may be assigned to tyrosine residues owing to their relative abundance in the peptide [260].

The amount of information from CD spectra is by no means comparable to the detailed structures generated by X-ray crystallography and NMR. Nevertheless, CD is an important tool to study structural changes induced by the environment. For instance, protein conformation may change as a response to ligand binding, unfolding or refolding in the presence of denaturants or as a function of temperature.

Circular dichroism has proved its essential role in the present work by showing that a defined α-helical structure is not a prerequisite for the membrane-perturbing activity of Nc (**Paper I-II**) and in the structural characterization of scaffolded Alm (**Paper III**), ELOA (**Paper IV**), murine kisspeptin-10 (**Paper V**) and *F. solani pisi* cutinase (**Paper VI**).

12.1. Oriented circular dichroism

The method of oriented circular dichroism was further implemented in the laboratory and proven useful in determining the α-helix orientation of both novicidin (**Paper II**) and alamethicin scaffolded on cyclodextrins (**Paper III**) relative to the membrane surface. The orientation of AMPs in phospholipid membranes is a key parameter to determine whether AMPs form pore structures as described by the Barrel-stave and toroidal pore mechanisms and the orientation of dipole moments can be addressed by oriented circular dichroism [69]. The method of oriented circular dichroism (OCD) has gained much attention in describing the orientation of α-helix, β-sheet and cyclic AMPs in multilayer membranes [99, 102, 149, 261-266] but also model proteins such as bacteriorhodopsin and α-helix fragments of cytochrome c have been studied [262, 267]. For example, the orientation of alamethicin has been probed as a function of the peptide to lipid ratio (Figure 22, right) [149].

OCD is a relatively simple extension to conventional solution CD measurements and in the current implementation of OCD in our laboratory; a homemade hydration cell was employed. It consists of a copper

cylinder with parallel quartz windows placed at opposing ends to constitute a measuring chamber (Figure 23). Two quartz windows originating from the two halves of a 0.1mm Hellma 124-QS cuvette allows the propagation of light through the cell.

Aligned lipid multilayer membranes were obtained by depositing lipid:AMP mixtures at different peptide to lipid ratios onto the edged half of the Hellma cell from organic solvent which was allowed to dry. Residual solvent was removed by incubation in a vacuum dessicator (P<60mbar) for several hours. In order to control the hydration of multilayer membranes, 50µl of saturated salt solution was placed inside the chamber in an inner Teflon ring and the chamber was sealed using O-rings and Teflon bushings as shown in Figure 23.

The salt solutions employed were saturated potassium sulphate (K_2SO_4) and magnesium chloride ($MgCl_2$) which give rise to relative humidities (RH) of approximately 98% and 33% at equilibrium, respectively [72, 268]. 98% RH was chosen in preference of 100% hydration to avoid that membranes deposited on the quartz slide would flow from the substrate due to its vertical position. 100% hydration could, however, be achieved by covering the multilayer membranes with another substrate but not preferred due to a requirement for longer equilibration times [269]. Although the main interest is data near full hydration (98% RH) which resembling those obtained for fully hydrated membrane [149], the spectra corresponding to the surface bound state may *reversibly* be acquired by exposing the membrane to lower humidities [69, 270]. 98% RH was achieved by overnight equilibration to ensure proper hydration. However, equilibration within the measurement chamber appeared to be very rapid since only few intermediate spectra could be acquired of Alm before the other extreme spectra became apparent when changing to $MgCl_2$ solution (33% RH).

In the case of AMPs, the multilayer lipid membrane thus serves as a medium in which the peptide may insert across the lipid bilayer and thereby align perpendicular to the membrane surface and parallel to the incident light. The OCD method to study the orientation of α-helical proteins and peptides in lipid multilayers was demonstrated using alamethicidin in lipid multilayers [69, 271].

For α-helices, the absorption of light occur in two directions, namely absorption of light propagating parallel to the helix and one in which light propagating perpendicular to the helix. In the setup employed, the incident light is oriented perpendicular to the aligned multilayers deposited on the quartz slide. The CD spectrum of a peptide oriented in a surface bound state (S) can be recognized by a strong negative signal at approximately 208nm and a less profound adsorption band at approximately 222-228nm. If the helix axis is reoriented along the bilayer normal such that the incident light propagates in the direction of the helix, the opposite signal is observed, namely a strong band at approximately 222-228nm and almost no intensity at approximately 208nm. If the aligned multilayers are placed perpendicular to the incident light, a reduction in the intensity at ~208nm indicates that the helix is in a preferred orientation parallel to the incident light and thus perpendicular to the membrane surface. On the contrary, the presence of a strong band at

approximately 208nm means that the peptide is oriented in a preferential surface bound state perpendicular to the incident light. The absorption bands of β-strands all lie parallel to the axis of that β-strands which implies that the overall intensity of the spectrum is reduced when β-strands change from a parallel to a perpendicular orientation relative to the direction of the incident light. It is, however, important to note that transitions observed by OCD can originate from both conformational changes within the secondary structure elements of the peptide and reorientation along the bilayer normal.

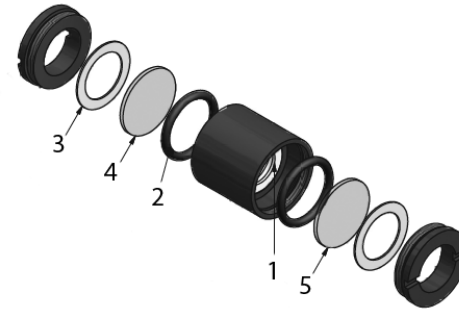

Figure 25 Hydration cell employed for oriented circular dichroism studies of AMP orientation in multilayer membranes at defined vapor pressures. The cell consists of a copper cylinder with (1) a Teflon bushing in which 50µl saturated salt solution was placed, (2) O-rings, (3) two teflon discs, (4) the planar component of a 0.1mm Hellma 124-QS cuvette and (5) the hollow part of the 0.1mm Hellma 124-QS cuvette. The cell was assembled and sealed by the two threaded end-pieces. Lipid multilayers were formed be deposition of lipids from organic solvents followed by hydration to ~33% or ~98% relative humidity using saturated $MgCl_2$ and K_2SO_4 solutions, respectively.

13. Fluorescence spectroscopy

Fluorescence is the phenomenon observed when a chromophore is excited through the absorption of light and then emits light at a lower energy level than the incident light (Figure 24A). The absorption of light causes an electron to jump to a discrete singlet excited state from which energy quickly is dissipated to lower energy states through collisional events with the surroundings. When the surroundings are no longer capable of accepting the larger energy difference toward the 'relaxed' ground state, it may undergo spontaneous emission of light at a lower energy than the incident light. Since the energy, *E*, of light is defined by $E = \frac{hc}{\lambda}$ where h is Planck's constant, *c* is the speed of light and λ is the wavelength of light, the lower energy state corresponds to a larger wavelength. The difference between the wavelengths of the incident light and the emitted light at maximum intensity has been termed the stoke's shift (Figure 24B).

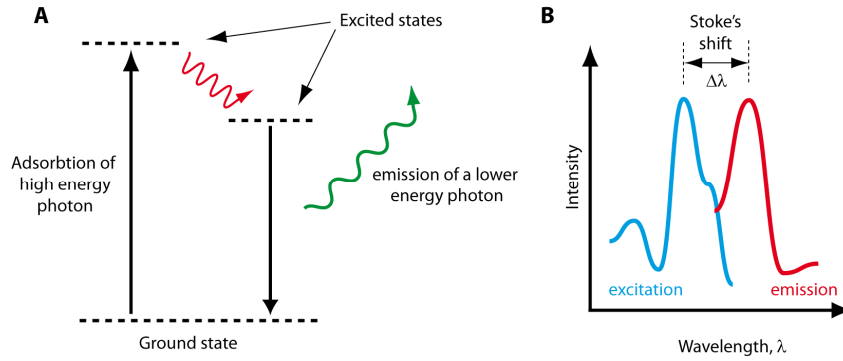

Figure 26 Principles of fluorescence emission. (A) When a molecule in the relaxed ground state adsorbs a photon of light and causes an electron to jump to an excited state, some of the energy is dissipated to surrounding molecules and the excited electron drops to a lower, but still excited, energy level (red line). If the surrounding molecules may not accept difference in the energy level between the lower excited state and the ground state, it may reach the ground state through emission of light at a lower energy level (i.e. longer wavelength) compared to the incident light. (B) The difference in wavelength between the incident light and the emitted light of lower energy is termed the stoke's shift.

Fluorescence spectroscopy is a highly versatile tool for various purposes as emphasized by its use in confocal scanning laser microscopy with fluorescent probes (**Paper I,IV**), calcein dye leakage (**Paper I-III, IV**) and generalized polarity determined using environment sensitive probe Laurdan (**Paper II**).

13.1. Flourescence as a tool to probe membrane permeability

The effect of antimicrobial peptides on the integrity of lipid membranes can be monitored through the inclusion of a fluorescent dye within vesicles. Once membranes are perturbed by AMPs through pore formation or less defined membrane disruption events by the carpet mechanism, the entrapped fluorophore is released to bulk solution and change fluorescence properties. This can, for instance, be accomplished by (i) using the fluorescent probe calcein which self-quenches at high concentrations (≥70μM) inside the vesicles and display an increase in fluorescence when diluted into bulk solution or (ii) by entrapment of a terbium (Tb^{3+}) inside vesicles and addition of dipicolinic acid (DPA) on the external side of vesicles. The Tb3+/DPA chelate is approximately 10000-fold more fluorescent than Tb^{3+} alone.

In **Paper I-III and IV**, the self-quenching fluorophore calcein was entrapped in 100nm LUVs to monitor the degree of permeabilization by AMPs and ELOA, although the latter turned out not to permeabilize membranes to appreciable levels. When membrane integrity of vesicles is disturbed by e.g. the presence of AMPs and consequently results in a dilution of calcein into bulk solution, self-quenching is abolished and an increase in fluorescence emission can be observed as a function of protein/peptide concentration. In order to obtain the maximum level of release the surfactant Triton X-100 was added to the vesicles resulting in complete dye release and maximum fluorescence.

13.2. Fluorescence as a tool to monitor protein conformation

Fluorescence spectroscopy of proteins and peptides relies primarily on the presence of tryptophan (Trp, W) residues whereas phenylalanine (Phe, F) and tyrosine (Tyr, Y) fluoresce to a smaller extent. Trp fluorescence is especially important in fluorescence spectroscopy since it is sensitive to the polarity of the local environment around. It is one of the 20 standard amino acids but is a relatively rare (natural abundance 1.07% [90]) and the intrinsic Trp fluorescence of many proteins thus relies on only single or few Trp residues.

The study of Trp residues by fluorescence spectroscopy may provide information of changes in protein conformation or binding of ligands in the local environment of the residue. Trp residues are usually selected by excitation at 295nm where Tyr and Phe residues are not excited. The dependence of the local environment of Trp residues is shown by changes in the fluorescence emission wavelength. Thus, a red-shifted emission maximum generally corresponds to the transfer of Trp residues to a more solvent exposed position in the protein whereas a blue-shift indicates the transfer to a more buried position. The maximum emission intensity is typically located within the ~330-360nm range.

The presence of several Trp residues such as the five Trp residues of EL or Trp residues near several potential binding sites may, however, give rise to complicated changes in the emission spectra. If no Trp residues are present, one has to rely on either introduction of Trp residues through mutagenesis or coupling of chromophores such as NBD or dansyl groups. Certain prostetic groups such as heme of peroxidases and hemoglobin may also be employed for fluorescence studies.

In **Paper I**, a dansyl group was attached at the N-terminal Lys residue and used to monitor the interaction with lipid membranes since the fluorescence emission intensity is increased when embedded inside membranes. In **Paper IV**, the intrinsic Trp fluorescence emission constituted by five Trp residues in equine lysozyme were used in combination with CD, proteolysis and activity assays to show the formation of more native-like conformations of ELOA on interaction with lipid membranes.

13.3. Fluorescence as a tool to monitor lipid membrane properties

Whereas the intrinsic properties of fluorescent amino acid residues of peptides and proteins are valuable tools in the study protein conformations and protein binding to membranes, fluorescence spectroscopy can also be employed to report environment changes in the membrane as the result of protein or peptide binding. The bulk of naturally occurring lipids do not show fluorescent properties with the exception of few and rare lipids such as *cis*-parinaric acid and decosahexanoic acid which feature fluorescent properties owing to their conjugated double bonds. However, fluorescent dyes such as LAURDAN or DPH may be included at low concentration in the lipid membrane and used as a reporter of membrane fluidity, polarity

and order. It is important to limit the amount of probe in order to avoid artifacts due to potential changes in membrane properties by the presence of the fluorescent probe.

In **paper II**, the environmentally sensitive dye Laurdan was employed to monitor the polarity at the hydrophobic/hydrophilic interface in membranes [272-274]. In lipid bilayers, the fluorescent probe laurdan is anchored to the bilayer via its acyl chain and the naphthalene chromophore is positioned near the glycerol backbone of lipids at the interface between the hydrophilic headgroups and the hydrophobic membrane interior [272]. The fluorescence emission maxima of laurdan in lipid bilayers have been shown to depend on the dipolar relaxation of the probe to the solvent. It is thus sensitive to the phase state of the lipids being blue-shifted in the gel phase (tight packing, low solvent accessibility) and red-shifted (lower energy, larger wavelength) in the liquid disordered phase (loose packing, higher solvent accessibility) where a small number of water molecules in the membrane interface have been attributed to the relaxation [272]. The shift of the emission maximum of laurdan can be quantified by the generalized polarity (GP) function:

$$GP = \frac{I_R - I_B}{I_R + I_B}$$

Where I_R and I_B is the emission intensity of the red- and blue-shifted component, respectively. Since the fluorescence emission of laurdan is highly sensitive to the degree of water penetration to the membrane, an increase in laurdan GP suggests a decreased water penetration to the probe whereas a decrease in laurdan GP suggests increased water penetration. This has not only been attributed to different lipid phases[52, 272], but also to monitor the decreased water penetration into bilayers containing cholesterol[275] and to monitor the mechanical strain in lipid vesicles of different size revealing lower GP values with decreasing vesicle size[274].

In **paper II**, we employed laurdan GP to demonstrate a decrease in water penetration to the bilayer interface at increasing Nc concentrations as an indication of a tighter headgroup packing.

While not included in the papers described here, the use of anisotropy probes in membranes could reveal important information about the mobility and fluidity of lipid bilayers. This could, for instance, involve the fluorescent probe DPH and the derivative TMA-DPH in anisotropy measurements since these probes can be employed to probe the fluidity in the hydrocarbon core and at the membrane surface [276]. Thus, they can distinguish between AMP effects exerted on the membrane surface only and the modulation of membrane fluidity deeper into the membrane.

In anisotropy, the fluorescent probe is excited by linearly polarized light which preferentially excite molecules whose transition moment is aligned parallel to the incident polarization vector. The fluorescence emission is recorded at polarization both parallel and perpendicular to the polarization of the incident light. The anisotropy (r) denoting the rotational diffusion of the fluorophore can then be calculated [277]:

$$r = \frac{I_{||} - GI_{\perp}}{I_{||} + 2GI_{\perp}}$$

Where $I_{||}$ and $I_{\perp}$ are the emission intensities of the vertical (II) and horizontal ($\perp$) polarizations when the sample is excited using vertically polarized light.

The rotational diffusion of the DPH fluorophore is dependent on the surrounding environment. Thus, the mobility (and thereby the diffusional rotation) of the probe would be greater in a liquid disordered bilayer compared to a bilayer in the gel phase. This may be exploited to probe the effect of AMPs on bilayer fluidity.

14. Quartz crystal microbalance with dissipation (QCM-D)

The QCM-D technique measures the mass adsorbed on a surface by measuring the change in resonance frequency of an oscillating quartz crystal. While early QCM equipment was used in vacuum or gas phases, the technique evolved and is now also used in liquid environment; for instance in the study of interaction of bilayer formation on solid support [56, 57], adsorption kinetics [278-280] and conformational changes of adsorbed proteins [281].

The QCM-D technique relies on the piezoelectric properties of quartz which is deformed when an alternating current is connected to the electrodes and *vice versa*. QCM sensors are typically operated at their natural frequency and odd-number multiples thereof (i.e. 1*n*, 3*n*, 5*n*, …, 13*n* with *n* being the natural frequency; typically 5 Mhz).

Initial studies on molecular interactions using QCM were based on the simplest implementation as a mass sensor based on the Sauerbrey relation described in 1959 which relates a decrease in resonance frequency, *Δf* to the mass change [282]:

$$\Delta m_{acoustic} = \frac{C}{n}\Delta f_n$$

n is the overtone number, *C* = -17.7ng $cm^{-2}Hz^{-1}$) is the mass sensitivity constant for an AT-cut crystal with a fundamental frequency of 5 MHz. Note that the frequency shifts and masses observed in QCM measurements are sensitive to all materials which are coupled to the oscillation of the crystal which include both molecules directly associated to the surface and molecules which are associated with them and thus "trapped" in the oscillation. The latter typically constitute water and buffer molecules.

The interpretation of QCM data using the sauerbrey equation is valid for rigid films which do reduce the oscillating motion of the sensor significantly. Thus, the relation is valid only for thin, homogeneous and rigid films which do not cause large energy losses.

In quartz crystal microbalance with dissipation monitoring (QCM-D), the energy dissipation (energy loss) is quantified by disconnecting the alternating current while monitoring the decrease in the oscillation amplitude and thus provides a tool to describe how biomaterials adsorbed at the solid-liquid interface dampen the resonator (Figure 25, left). The dissipation parameter thus describes the viscoelastic properties of the system and provides additional aid in the analysis of data.

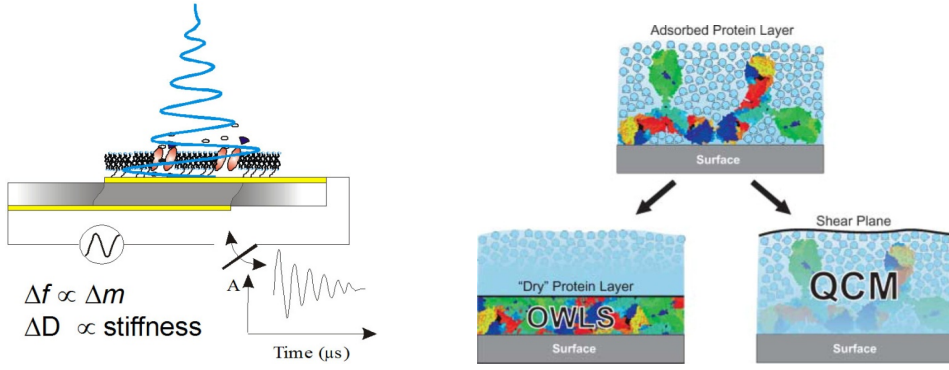

Figure 27 Right: Principles of quartz crystal microbalance with dissipation monitoring. The crystal is brought to oscillation at a specific resonance frequency governed by the properties of the crystal and potentially associated mass adsorbed at the surface by applying an alternative current on the electrodes positioned at opposing faces of the crystal. Changes in deposited mass can be monitored by the change in resonance frequency, Δf. The energy dissipation is monitored by disconnection of the alternating current by monitoring the amplitude decay of the oscillation and provides a measure of the viscoelastic properties of the adsorbed film. Picture used with permission from Q-Sense. Left: Illustration of the fundamental difference between optical methods and quartz crystal microbalance with dissipation. QCM-D identify the mass coupled to the oscillation of the quartz crystal including trapped water and buffer constituents whereas optical methods detect only the 'dry' mass associated such as proteins. Illustration adapted from [283] with permission.

The viscoelastic properties of adsorbed films may be obtained by the use of viscoelastic modeling to provide estimates of film thickness, density, shear modulus and shear viscosity [284]. The acoustic mass coupled to the oscillation is obtained by the product of the thickness and density ($m_{acoustic}$ =thickness x density) and typically provide a larger estimate of the mass of adsorbed biomolecules compared to optical methods such as surface plasmon resonance and dual polarization interferometry since QCM-D senses the associated mass and coupled water and buffer components as illustrated in the right hand side of Figure 25 [283, 285, 286].

The theoretical model makes use of both frequency and energy dissipation data recorded at multiple harmonics. Data interpretation requires prior knowledge of either the effective density or the effective thickness in order to obtain qualified estimates on the viscoelastic properties of an adsorbed film. While these estimates can be obtained from complementary techniques, several studies have shown that estimates of $m_{acoustic}$ are independent on the initial qualified "guess" of effective density [287] within a biological relevant range of the adsorbed species (i.e. approximately 1.0-1.6g/cm^3).

QCM-D was used to probe the interaction and impact of novicidin and ELOA in **paper II** and **paper IV** on preformed supported lipid bilayers. Few studies of antimicrobial peptides using QCM-D can be found in literature and to our knowledge; **paper II** is the first to employ lipids in the liquid disordered phase to study the interaction with AMPs.

The shear-wave resonance of a 5 Mhz AT-cut quartz crystal extends approximately 250nm into the liquid phase from the crystal surface at the natural frequency and the distance decreases with increasing overtone numbers. This difference in penetration depth has been exploited to probe the mass distribution of AMPs across the lipid bilayers and to evaluate whether these peptides merely associate to the surface of bilayer or distribute evenly across the membrane indicative of pore formation or translocation to the leaflet closest to the sensor surface. For instance, the antimicrobial peptides maculatin 1.1, caerin 1.1, aureins and two variants apidaecin has been shown to bind on the surface of lipid bilayers as shown by overtone spreading and to insert across the lipid membrane as shown by essentially equal frequency responses across all observed overtones, respectively [103, 288]. While QCM-D thus provides a qualitative description of the mass distribution, the overtone spreading itself does, however, not offer a discrete measure of the mass distribution. The reasons for *not* choosing an interpretation of the novicidin with SPBs in analogy with the cases described above are two-fold. First, the authors of both papers employed lipids in the gel phase which could restrict insertion of AMPs in such bilayers. Second, the surface coupling of a 19-mer peptide was recently shown to dramatically increase in the hydration of the film [289] on the basis of a combined QCM-D and reflectrometry study. This is consistent with our observations with our data from both QCM-D and complementary techniques. Further, the use of backward washing procedures to avoid further injection of peptide residing in the flow system showed that incubation with high concentrations of novicidin followed by washing led to removal of material from the surface as an indication on significant membrane rearrangements.

In **Paper IV**, the interaction of multimeric equine lysozyme complexes with oleic acid (ELOA) was shown to dissociate bilayers from the sensor surface. In **paper IV**, we employed dissipation-frequency (*Df*) plots for a qualitative description of the protein-bilayer interaction. By plotting the energy dissipation against the resonance frequency, changes in the adsorbed film may be elucidated [290]. Our interpretation that bilayers dissociate is were based on trajectory in the *Df* landscape which resembled *the reverse* of bilayer formation and observations from calcein dye leakage and confocal laser scanning microscopy that ELOA which did not suggest in membrane disruption even at high protein concentrations.

Paper II employed QCM-D to monitor the effect of Nc on the integrity of preformed supported lipid bilayers and was found to be highly consistent with complementary techniques.

15. Dual Polarization Interferometry (DPI)

DPI is a surface technique which uses polarized laser light passing through a set of stacked waveguides. When the polarized laser light exits the waveguides and combined, it forms a two-dimensional interference pattern (Figure 26). The surface of one of these waveguides is employed as the sensing waveguide whereas the other serves as a reference. When molecules are adsorbed on the surface of the sensing waveguide, they change the refractive index of the material within the evanescent field and cause a phase shift of the light passing through the sensing waveguide. This results in a shift in the two-dimensional interference pattern ("fringes" which arise when the light beams are combined [291]. The resulting fringe pattern is the result of constructive (light) and deconstructive (dark) interference caused by the phase difference of the propagating waves.

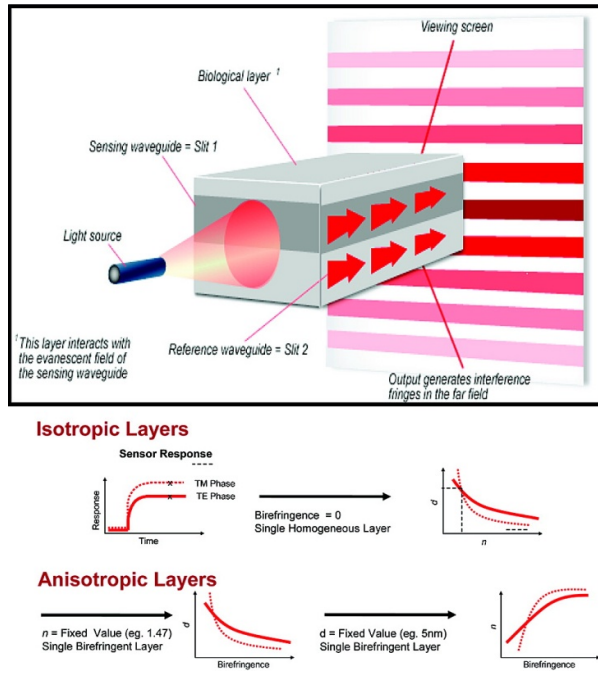

Figure 28 Principles of dual polarization interferometry (DPI) and the application on isotropic layers. Laser light of transverse electric and transverse magnetic polarizations are led through two stacked waveguides of which one serve as the sensing and one as the reference waveguide. When the lightwave of the two waveguides exit and are combined, an interference pattern is the result of constructive and destructive interference. When molecules are adsorbed on the sensing waveguide, they interact with the evanescent field and change the phase of the light passing through the sensing waveguide and ultimately the fringe pattern. From these changes, the thickness and refractive index of the adsorbed layer can be determined for anisotropic layers. If one of these values are known, the degree of anisotropy (birefringence) can be estimated. Illustration adapted from [55] with permission.

The polarization of the incident light is further rotated during measurements providing two polarization modes (Transverse electric and Transverse magnetic polarizations, TE and TM) which can be employed to calculate the refractive index and thickness of an adsorbed film. For anisotropic films such as lipid bilayers, the refractive indexes for the two polarizations modes are different and thus yield another parameter to estimate. However, if either the thickness or isotropic refractive index of the sample is known to a good estimate, the degree of anisotropy can be evaluated. The degree of anisotropy is described by the difference between refractive indexes perpendicular and parallel to the surface and termed birefringence[55]. In recent papers, DPI has been employed both to describe the process of vesicle collapse and to describe the interaction of an artificial antimicrobial peptide to lipid bilayers[55, 65].

In **paper II**, DPI is employed to describe the loss of bilayer integrity at increasing Nc concentrations as shown by a drop in birefringence. There are, however, uncertainties involved with estimating the mass of lipid bilayers[55] and should be considered as approximate values only. However, there is good agreement between mass estimates obtained during interaction of novicidin and SPBs using both QCM-D and DPI under similar conditions in **paper II**.

References

1. Singer, S.J. and G.L. Nicolson, *The fluid mosaic model of the structure of cell membranes.* Science, 1972. **175**(4023): p. 720-731.
2. Benga, G. and R.P. Holmes, *Interactions between components in biological membranes and their implications for membrane function.* Progress in biophysics and molecular biology, 1984. **43**(3): p. 195.
3. Cevc, G., *Membrane electrostatics.* BBA-Reviews on Biomembranes, 1990. **1031**(3): p. 311-382.
4. van Meer, G., D.R. Voelker, and G.W. Feigenson, *Membrane lipids: where they are and how they behave.* Nature reviews. Molecular cell biology, 2008. **9**(2): p. 112.
5. Mouritsen, O.G., *Life--as a matter of fat: the emerging science of lipidomics*. 2005: Springer Verlag.
6. Zasloff, M., *Antimicrobial peptides of multicellular organisms.* Nature, 2002. **415**(6870): p. 389-395.
7. Epand, R.M., *Membrane lipid polymorphism: relationship to bilayer properties and protein function.* Methods in molecular biology (Clifton, NJ), 2007. **400**: p. 15.
8. Marsh, D., *Lateral pressure profile, spontaneous curvature frustration, and the incorporation and conformation of proteins in membranes.* Biophysical journal, 2007. **93**(11): p. 3884-3899.
9. Cullis, P.R. and M.J. Hope, *Physical properties and functional roles of lipids in membranes.* Biochemistry of lipids, lipoproteins and membranes, 1996. **31**: p. 1–33.
10. Cevc, G., *Phospholipids handbook*. 1993: CRC.
11. Cullis, P.R. and B. De Kruijff, *Lipid polymorphism and the functional roles of lipids in biological membranes.* BBA-Reviews on Biomembranes, 1979. **559**(4): p. 399-420.
12. Heerklotz, H., *The microcalorimetry of lipid membranes.* Journal of Physics Condensed Matter, 2004. **16**(15): p. 441-468.
13. Lewis, R.N., D.A. Mannock, and R.N. McElhaney, *Differential scanning calorimetry in the study of lipid phase transitions in model and biological membranes: practical considerations.* Methods in molecular biology (Clifton, NJ), 2007. **400**: p. 171.
14. Bagatolli, L.A., *To see or not to see: lateral organization of biological membranes and fluorescence microscopy.* BBA-Biomembranes, 2006. **1758**(10): p. 1541-1556.
15. Veatch, S.L. and S.L. Keller, *Seeing spots: complex phase behavior in simple membranes.* BBA-Molecular Cell Research, 2005. **1746**(3): p. 172-185.
16. Morein, S., et al., *Wild-type Escherichia coli Cells Regulate the Membrane Lipid Composition in a``Window''between Gel and Non-lamellar Structures.* Journal of Biological Chemistry, 1996. **271**(12): p. 6801.
17. Huijbregts, R.P.H., A. de Kroon, and B. de Kruijff, *Rapid transmembrane movement of C6-NBD-labeled phospholipids across the inner membrane of Escherichia coli.* BBA-Biomembranes, 1996. **1280**(1): p. 41-50.
18. Homan, R. and H.J. Pownall, *Transbilayer diffusion of phospholipids: dependence on headgroup structure and acyl chain length.* Biochimica et biophysica acta, 1988. **938**(2): p. 155.
19. Pomorski, T. and A.K. Menon, *Lipid flippases and their biological functions.* Cellular and molecular life sciences, 2006. **63**(24): p. 2908-2921.
20. Sud, M., et al., *LMSD: LIPID MAPS structure database.* Nucleic Acids Research, 2007. **35**(Database issue): p. D527.
21. Devaux, P.F. and R. Morris, *Transmembrane asymmetry and lateral domains in biological membranes.* Traffic, 2004. **5**(4): p. 241-246.
22. Zachowski, A., *Phospholipids in animal eukaryotic membranes: transverse asymmetry and movement.* Biochemical Journal, 1993. **294**(Pt 1): p. 1.

23. Suttmann, H., et al., *Antimicrobial peptides of the Cecropin-family show potent antitumor activity against bladder cancer cells.* BMC urology, 2008. **8**(1): p. 5.
24. Ran, S. and P.E. Thorpe, *Phosphatidylserine is a marker of tumor vasculature and a potential target for cancer imaging and therapy* 1.* International Journal of Radiation Oncology* Biology* Physics, 2002. **54**(5): p. 1479-1484.
25. Kruyssen, F.J., W.R. De Boer, and J.T. Wouters, *Effects of carbon source and growth rate on cell wall composition of Bacillus subtilis subsp. niger.* Journal of Bacteriology, 1980. **144**(1): p. 238.
26. Fischer, W., *Lipoteichoic acid and lipids in the membrane of Staphylococcus aureus.* Medical microbiology and immunology, 1994. **183**(2): p. 61-76.
27. Goldfine, H., *Lipids of prokaryotes- Structure and distribution.* Current topics in membranes and transport, 1982. **17**: p. 1-43.
28. Goldfine, H., *Bacterial membranes and lipid packing theory.* The Journal of Lipid Research, 1984. **25**(13): p. 1501.
29. de Cock, H., et al., *Non-lamellar structure and negative charges of lipopolysaccharides required for efficient folding of outer membrane protein PhoE of Escherichia coli.* Journal of Biological Chemistry, 1999. **274**(8): p. 5114.
30. Lugtenberg, E.J. and R. Peters, *Distribution of lipids in cytoplasmic and outer membranes of Escherichia coli K12.* Biochimica et biophysica acta, 1976. **441**(1): p. 38.
31. Österberg, F., et al., *Lipid extracts from membranes of Acholeplasma laidlawii A grown with different fatty acids have a nearly constant spontaneous curvature.* Biochimica et Biophysica Acta (BBA)/Lipids and Lipid Metabolism, 1995. **1257**(1): p. 18-24.
32. Garab, G., et al., *Self-regulation of the lipid content of membranes by non-bilayer lipids: a hypothesis.* Trends in plant science, 2000. **5**(11): p. 489-494.
33. Sprong, H., P. van der Sluijs, and G. van Meer, *How proteins move lipids and lipids move proteins.* Nature Reviews Molecular Cell Biology, 2001. **2**(7): p. 504-513.
34. Zelezetsky, I., et al., *Controlled alteration of the shape and conformational stability of -helical cell-lytic peptides: effect on mode of action and cell specificity.* Biochemical Journal, 2005. **390**(Pt 1): p. 177.
35. Zelezetsky, I. and A. Tossi, *Alpha-helical antimicrobial peptides—using a sequence template to guide structure–activity relationship studies.* BBA-Biomembranes, 2006. **1758**(9): p. 1436-1449.
36. Matsuzaki, K., et al., *Interactions of an antimicrobial peptide, magainin 2, with outer and inner membranes of Gram-negative bacteria.* BBA-Biomembranes, 1997. **1327**(1): p. 119-130.
37. Silvestro, L., J.N. Weiser, and P.H. Axelsen, *Antibacterial and antimembrane activities of cecropin A in Escherichia coli.* Antimicrobial agents and chemotherapy, 2000. **44**(3): p. 602.
38. Christensen, B., et al., *Channel-forming properties of cecropins and related model compounds incorporated into planar lipid membranes.* Proc. Natl. Acad. Sci. USA, 1988. **85**(14): p. 5-072.
39. Matsuzaki, K., et al., *Optical characterization of liposomes by right angle light scattering and turbidity measurement.* BBA-Biomembranes, 2000. **1467**(1): p. 219-226.
40. Olson, F., et al., *Preparation of liposomes of defined size distribution by extrusion through polycarbonate membranes.* Biochimica et biophysica acta, 1979. **557**(1): p. 9.
41. Gregoriadis, G., *Liposome technology: Liposome preparation and related techniques*. 2006: Informa HealthCare.
42. Tristan, R., et al., *Liposome retention in size exclusion chromatography.* BMC Biotechnology, 2005. **5**.
43. Ollivon, M., et al., *Vesicle reconstitution from lipid–detergent mixed micelles.* BBA-Biomembranes, 2000. **1508**(1-2): p. 34-50.
44. Seddon, A.M., P. Curnow, and P.J. Booth, *Membrane proteins, lipids and detergents: not just a soap opera.* BBA-Biomembranes, 2004. **1666**(1-2): p. 105-117.

45. Hell, S.W., *Breaking Abbe's barrier: Diffraction-unlimited resolution in far-field microscopy'.* Cytometry Part A: p. 742-742.
46. Moscho, A., et al., *Rapid preparation of giant unilamellar vesicles.* Proc. Natl. Acad. Sci. USA, 1996. **93**: p. 11443**–**11447.
47. Darszon, A., et al., *Reassembly of protein-lipid complexes into large bilayer vesicles: Perspectives for membrane reconstitution.* Proceedings of the National Academy of Sciences, 1980. **77**(1): p. 239.
48. Needham, D., T.J. McIntosh, and E. Evans, *Thermomechanical and transition properties of dimyristoylphosphatidylcholine/cholesterol bilayers.* Biochemistry, 1988. **27**(13): p. 4668-4673.
49. Girard, P., et al., *A new method for the reconstitution of membrane proteins into giant unilamellar vesicles.* Biophysical journal, 2004. **87**(1): p. 419-429.
50. Angelova, M.I. and D.S. Dimitrov, *Liposome electroformation.* Faraday Discussions of the Chemical Society, 1986. **81**: p. 303-311.
51. Angelova, M.I., et al., *Preparation of giant vesicles by external AC electric fields. Kinetics and applications.* Prog. Colloid Polym. Sci, 1992. **89**: p. 127-131.
52. Bagatolli, L.A., T. Parasassi, and E. Gratton, *Giant phospholipid vesicles: comparison among the whole lipid sample characteristics using different preparation methods A two photon fluorescence microscopy study.* Chemistry and Physics of Lipids, 2000. **105**(2): p. 135-147.
53. Taylor, P., et al., *A novel technique for preparation of monodisperse giant liposomes.* Chemical Communications, 2003. **2003**(14): p. 1732-1733.
54. Kahya, N., et al., *Reconstitution of membrane proteins into giant unilamellar vesicles via peptide-induced fusion.* Biophysical Journal, 2001. **81**(3): p. 1464-1474.
55. Mashaghi, A., et al., *Optical Anisotropy of Supported Lipid Structures Probed by Waveguide Spectroscopy and Its Application to Study of Supported Lipid Bilayer Formation Kinetics.* Analytical Chemistry, 2008. **80**(10): p. 3666-3676.
56. Keller, C.A. and B. Kasemo, *Surface specific kinetics of lipid vesicle adsorption measured with a quartz crystal microbalance.* Biophys.J., 1998. **75**(3): p. 1397-1402.
57. Keller, C.A., et al., *Formation of Supported Membranes from Vesicles.* Physical Review Letters, 2000. **84**(23): p. 5443-5446.
58. Reimhult, E., F. Hook, and B. Kasemo, *Vesicle adsorption on SiO[sub 2] and TiO[sub 2]: Dependence on vesicle size.* The Journal of Chemical Physics, 2002. **117**(16): p. 7401-7404.
59. Reimhult, E., F. Hook, and B. Kasemo, *Intact Vesicle Adsorption and Supported Biomembrane Formation from Vesicles in Solution: Influence of Surface Chemistry, Vesicle Size, Temperature, and Osmotic Pressure.* Langmuir, 2003. **19**(5): p. 1681-1691.
60. Richter, R., A. Mukhopadhyay, and A. Brisson, *Pathways of Lipid Vesicle Deposition on Solid Surfaces: A Combined QCM-D and AFM Study.* Biophysical Journal, 2003. **85**(5): p. 3035-3047.
61. Richter, R.P. and A.R. Brisson, *Following the formation of supported lipid bilayers on mica: a study combining AFM, QCM-D, and ellipsometry.* Biophysical journal, 2005. **88**(5): p. 3422-3433.
62. Richter, R.P., R. Berat, and A.R. Brisson, *Formation of solid-supported lipid bilayers: an integrated view.* Langmuir, 2006. **22**(8): p. 3497-3505.
63. Rossetti, F.F., et al., *Interactions between Titanium Dioxide and Phosphatidyl Serine-Containing Liposomes: Formation and Patterning of Supported Phospholipid Bilayers on the Surface of a Medically Relevant Material.* Langmuir, 2005. **21**(14): p. 6443-6450.
64. Hamai, C., et al., *Effect of average phospholipid curvature on supported bilayer formation on glass by vesicle fusion.* Biophysical journal, 2006. **90**(4): p. 1241-1248.
65. Yu, L., et al., *Interaction of an artificial antimicrobial peptide with lipid membranes.* Biochimica et Biophysica Acta (BBA) - Biomembranes. **In Press, Corrected Proof**.
66. Seantier, B., et al., *Dissipation-enhanced quartz crystal microbalance studies on the experimental parameters controlling the formation of supported lipid bilayers.* J.Phys.Chem.B Condens.Matter Mater.Surf.Interfaces.Biophys., 2005. **109**(46): p. 21755-21765.

67. Mennicke, U. and T. Salditt, *Preparation of solid-supported lipid bilayers by spin-coating.* Langmuir, 2002. **18**(21): p. 8172-8177.
68. Seul, M. and M.J. Sammon, *Preparation of surfactant multilayer films on solid substrates by deposition from organic solution.* Thin Solid Films, 1990. **185**(2): p. 287-305.
69. Wu, Y., H.W. Huang, and G.A. Olah, *Method of oriented circular dichroism.* Biophysical Journal, 1990. **57**(4): p. 797-806.
70. Hallock, K.J., et al., *An innovative procedure using a sublimable solid to align lipid bilayers for solid-state NMR studies.* Biophysical journal, 2002. **82**(5): p. 2499-2503.
71. Ramamoorthy, A., et al., *Solid-state NMR investigation of the membrane-disrupting mechanism of antimicrobial peptides MSI-78 and MSI-594 derived from magainin 2 and melittin.* Biophysical journal, 2006. **91**(1): p. 206-216.
72. Winston, P.W. and D.H. Bates, *Saturated solutions for the control of humidity in biological research.* Ecology, 1960: p. 232-237.
73. Wu, Y., et al., *X-ray diffraction study of lipid bilayer membranes interacting with amphiphilic helical peptides: diphytanoyl phosphatidylcholine with alamethicin at low concentrations.* Biophysical journal, 1995. **68**(6): p. 2361-2369.
74. Franzmann, M., D. Otzen, and R. Wimmer, *Quantitative Use of Paramagnetic Relaxation Enhancements for Determining Orientations and Insertion Depths of Peptides in Micelles.* Chembiochem: a European journal of chemical biology, 2009.
75. Wang, G., *Structure, dynamics and mapping of membrane-binding residues of micelle-bound antimicrobial peptides by natural abundance 13C NMR spectroscopy.* BBA-Biomembranes, 2009.
76. Ikura, T., G. Nobuhiro, and F. Inagaki, *Refined structure of melittin bound to perdeuterated dodeclylphoscholine micelles as studied by 2D-NMR and distance geometry calculation.* Proteins: Structure, Function, and Bioinformatics. **9**(2): p. 81-89.
77. Otzen, D.E., *Protein unfolding in detergents: effect of micelle structure, ionic strength, pH, and temperature.* Biophysical journal, 2002. **83**(4): p. 2219-2230.
78. Pocalyko, D.J. and M. Tallman, *Effects of amphipaths on the activity and stability of Fusarium solani pisi cutinase.* Enzyme and Microbial Technology, 1998. **22**(7): p. 647-651.
79. Sears, C.L., *A dynamic partnership: Celebrating our gut flora.* Anaerobe, 2005. **11**(5): p. 247-251.
80. O'Hara, A.M. and F. Shanahan, *The gut flora as a forgotten organ.* EMBO reports, 2006. **7**(7): p. 688.
81. Zanetti, M., *Cathelicidins, multifunctional peptides of the innate immunity.* Journal of leukocyte biology, 2004. **75**(1): p. 39.
82. Bennett, P.M., *Plasmid encoded antibiotic resistance: acquisition and transfer of antibiotic resistance genes in bacteria.* British Journal of Pharmacology, 2008. **153**(S1): p. S347.
83. Ochman, H., J.G. Lawrence, and E.A. Groisman, *Lateral gene transfer and the nature of bacterial innovation.* Nature, 2000. **405**(6784): p. 299-304.
84. Nikaido, H., *Multidrug resistance in bacteria.* Annual Review of Biochemistry, 2009. **78**: p. 119-146.
85. Wang, G., X. Li, and Z. Wang, *APD2: the updated antimicrobial peptide database and its application in peptide design.* Nucleic Acids Research, 2008.
86. Shaw, J.E., et al., *Mechanisms of antimicrobial peptide action: studies of indolicidin assembly at model membrane interfaces by in situ atomic force microscopy.* Journal of Structural Biology, 2006. **154**(1): p. 42-58.
87. Subbalakshmi, C. and N. Sitaram, *Mechanism of antimicrobial action of indolicidin.* FEMS microbiology letters, 1998. **160**(1): p. 91-96.
88. Ha, T.H., et al., *Interaction of Indolicidin with Model Lipid Bilayer: Quartz Crystal Microbalance and Atomic Force Microscopy Study.* Langmuir, 2000. **16**(2): p. 871-875.
89. Boman, H.G., B. Agerberth, and A. Boman, *Mechanisms of action on Escherichia coli of cecropin P1 and PR-39, two antibacterial peptides from pig intestine.* Infect. Immun., 1993. **61**(7): p. 2978-2984.
90. Boutet, E., et al., *Uniprotkb/swiss-prot.* database. **2**: p. 3.

91. Hoover, D.M., et al., *The structure of human β-defensin-2 shows evidence of higher order oligomerization.* Journal of Biological Chemistry, 2000. **275**(42): p. 32911.
92. Skerlavaj, B., et al., *SMAP-29: a potent antibacterial and antifungal peptide from sheep leukocytes.* FEBS Letters, 1999. **463**(1-2): p. 58-62.
93. Wimmer, R., et al., *Versatile Interactions of the Antimicrobial Peptide Novispirin with Detergents and Lipids.* Biochemistry, 2006. **45**(2): p. 481-497.
94. Sawai, M.V., et al., *Impact of single-residue mutations on the structure and function of ovispirin/novispirin antimicrobial peptides.* Protein Engineering, 2002. **15**(3): p. 225.
95. Bechinger, B., *Structure and functions of channel-forming peptides: magainins, cecropins, melittin and alamethicin.* Journal of Membrane Biology, 1997. **156**(3): p. 197-211.
96. Matsuzaki, K., et al., *Orientational and aggregational states of magainin 2 in phospholipid bilayers.* Biochemistry, 1994. **33**(11): p. 3342-3349.
97. Ludtke, S., K. He, and H. Huang, *Membrane thinning caused by magainin 2.* Biochemistry, 1995. **34**(51): p. 16764-16769.
98. Münster, C., et al., *Grazing incidence x-ray diffraction of highly aligned phospholipid membranes containing the antimicrobial peptide magainin 2.* European Biophysics Journal, 2000. **28**(8): p. 683-688.
99. Ludtke, S.J., et al., *Cooperative membrane insertion of magainin correlated with its cytolytic activity.* Biochim. Biophys. Acta, 1994. **1190**: p. 181-184.
100. Matsuzaki, K., et al., *An antimicrobial peptide, magainin 2, induced rapid flip-flop of phospholipids coupled with pore formation and peptide translocation.* Biochemistry, 1996. **35**(35): p. 11361.
101. Cheng, J.T.J., et al., *Effect of Membrane Composition on Antimicrobial Peptides Aurein 2.2 and 2.3 From Australian Southern Bell Frogs.* Biophysical Journal, 2009. **96**(2): p. 552-565.
102. Pan, Y.L., et al., *Characterization of the structure and membrane interaction of the antimicrobial peptides aurein 2.2 and 2.3 from Australian southern bell frogs.* Biophysical journal, 2007. **92**(8): p. 2854-2864.
103. Mechler, A., et al., *Specific and Selective Peptide-Membrane Interactions Revealed Using Quartz Crystal Microbalance.* Biophysical Journal, 2007. **93**(11): p. 3907-3916.
104. Schiffer, M. and A.B. Edmundson, *Use of helical wheels to represent the structures of proteins and to identify segments with helical potential.* Biophysical Journal, 1967. **7**(2): p. 121-135.
105. Giangaspero, A., L. Sandri, and A. Tossi, *Amphipathic α-helical antimicrobial peptides.* European Journal of Biochemistry, 2001. **268**(21): p. 5589-5600.
106. Kyte, J. and R.F. Doolittle, *A simple method for displaying the hydropathic character of a protein.* Journal of Molecular Biology, 1982. **157**(1): p. 105-132.
107. Shai, Y., *Mechanism of the binding, insertion and destabilization of phospholipid bilayer membranes by a-helical antimicrobial and cell non-selective membrane-lytic peptides.* Biochim. Biophys. Acta, 1999. **1462**(1-2): p. 55–70.
108. Oren, Z., et al., *Structure and organization of the human antimicrobial peptide LL-37 in phospholipid membranes: relevance to the molecular basis for its non-cell-selective activity.* Biochemical Journal, 1999. **341**(Pt 3): p. 501.
109. Ramamoorthy, A., *Beyond NMR spectra of antimicrobial peptides: dynamical images at atomic resolution and functional insights.* Solid State Nuclear Magnetic Resonance, 2009.
110. Henzler-Wildman, K.A., et al., *Perturbation of the Hydrophobic Core of Lipid Bilayers by the Human Antimicrobial Peptide LL-37.* Biochemistry, 2004. **43**(26): p. 8459-8469.
111. Hristova, K., et al., *An amphipathic -helix at a membrane interface: a structural study using a novel X-ray diffraction method.* Journal of molecular biology, 1999. **290**(1): p. 99-117.
112. Israelachvili, J.N., S. Marcelja, and R.G. Horn, *Physical principles of membrane organization.* Quarterly reviews of biophysics, 1980. **13**(2): p. 121.

113. Bechinger, B. and K. Lohner, *Detergent-like actions of linear amphipathic cationic antimicrobial peptides.* BBA-Biomembranes, 2006. **1758**(9): p. 1529-1539.
114. Pabst, G., *Global properties of biomimetic membranes: perspectives on molecular features.* Biophysical Reviews and Letters, 2006. **1**(1): p. 57-84.
115. Sevcsik, E., et al., *How lipids influence the mode of action of membrane-active peptides.* BBA-Biomembranes, 2007. **1768**(10): p. 2586-2595.
116. Mecke, A., et al., *Membrane Thinning Due to Antimicrobial Peptide Binding: An Atomic Force Microscopy Study of MSI-78 in Lipid Bilayers.* Biophysical Journal, 2005. **89**(6): p. 4043-4050.
117. Chen, F.Y., M.T. Lee, and H.W. Huang, *Evidence for membrane thinning effect as the mechanism for peptide-induced pore formation.* Biophysical journal, 2003. **84**(6): p. 3751-3758.
118. Pabst, G., et al., *Membrane thickening by the antimicrobial peptide PGLa.* Biophysical Journal, 2008. **95**(12): p. 5779-5788.
119. Harroun, T.A., et al., *Experimental evidence for hydrophobic matching and membrane-mediated interactions in lipid bilayers containing gramicidin.* Biophysical journal, 1999. **76**(2): p. 937-945.
120. Wimley, W.C. and S.H. White, *Experimentally determined hydrophobicity scale for proteins at membrane interfaces.* nature structural biology, 1996. **3**(10): p. 842-848.
121. Bechinger, B., *Rationalizing the membrane interactions of cationic amphipathic antimicrobial peptides by their molecular shape.* Current Opinion in Colloid & Interface Science, 2009. **14**(5): p. 349-355.
122. Hallock, K.J., D.K. Lee, and A. Ramamoorthy, *MSI-78, an analogue of the magainin antimicrobial peptides, disrupts lipid bilayer structure via positive curvature strain.* Biophysical journal, 2003. **84**(5): p. 3052-3060.
123. Henzler Wildman, K.A., D.-K. Lee, and A. Ramamoorthy, *Mechanism of Lipid Bilayer Disruption by the Human Antimicrobial Peptide, LL-37.* Biochemistry, 2003. **42**(21): p. 6545-6558.
124. Matsuzaki, K., et al., *Relationship of Membrane Curvature to the Formation of Pores by Magainin 2.* Biochemistry, 1998. **37**(34): p. 11856-11863.
125. Epand, R.M. and R.F. Epand, *Calorimetric detection of curvature strain in phospholipid bilayers.* Biophysical journal, 1994. **66**(5): p. 1450-1456.
126. Shai, Y., *Mode of action of membrane active antimicrobial peptides.* Biopolymers, 2002. **66**(4): p. 236-248.
127. Ludtke, S.J., et al., *Membrane Pores Induced by Magainin.* Biochemistry, 1996. **35**(43): p. 13723-13728.
128. Wu, M., et al., *Mechanism of Interaction of Different Classes of Cationic Antimicrobial Peptides with Planar Bilayers and with the Cytoplasmic Membrane of Escherichia coli.* Biochemistry, 1999. **38**(22): p. 7235-7242.
129. Sengupta, D., et al., *Toroidal pores formed by antimicrobial peptides show significant disorder.* BBA-Biomembranes, 2008. **1778**(10): p. 2308-2317.
130. Leontiadou, H., A.E. Mark, and S.J. Marrink, *Antimicrobial peptides in action.* J. Am. Chem. Soc, 2006. **128**(37): p. 12156-12161.
131. Sefton, A.M., *Mechanisms of antimicrobial resistance: their clinical relevance in the new millennium.* Drugs, 2002. **62**(4): p. 557-566.
132. Yeaman, M.R. and N.Y. Yount, *Mechanisms of antimicrobial peptide action and resistance.* Pharmacological reviews, 2003. **55**(1): p. 27-55.
133. Sieprawska-Lupa, M., et al., *Degradation of human antimicrobial peptide LL-37 by Staphylococcus aureus-derived proteinases.* Antimicrobial agents and chemotherapy, 2004. **48**(12): p. 4673.
134. Shinnar, A.E., K.L. Butler, and H.J. Park, *Cathelicidin family of antimicrobial peptides: proteolytic processing and protease resistance.* Bioorganic Chemistry, 2003. **31**(6): p. 425-436.

135. Peschel, A., et al., *The D-alanine residues of Staphylococcus aureus teichoic acids alter the susceptibility to vancomycin and the activity of autolytic enzymes.* Antimicrobial agents and chemotherapy, 2000. **44**(10): p. 2845.
136. Peschel, A., et al., *Inactivation of the dlt Operon inStaphylococcus aureus Confers Sensitivity to Defensins, Protegrins, and Other Antimicrobial Peptides.* Journal of Biological Chemistry, 1999. **274**(13): p. 8405.
137. Kupferwasser, L.I., et al., *Plasmid-mediated resistance to thrombin-induced platelet microbicidal protein in staphylococci: role of the qacA locus.* Antimicrobial agents and chemotherapy, 1999. **43**(10): p. 2395.
138. Peschel, A., et al., *Staphylococcus aureus resistance to human defensins and evasion of neutrophil killing via the novel virulence factor MprF is based on modification of membrane lipids with l-lysine.* Journal of Experimental Medicine, 2001. **193**(9): p. 1067.
139. McCoy, A.J., et al., *Identification of Proteus mirabilis mutants with increased sensitivity to antimicrobial peptides.* Antimicrobial agents and chemotherapy, 2001. **45**(7): p. 2030.
140. Peschel, A., *How do bacteria resist human antimicrobial peptides?* Trends in microbiology, 2002. **10**(4): p. 179-186.
141. Wade, D., et al., *All-D amino acid-containing channel-forming antibiotic peptides.* Proc. Natl. Acad. Sci. USA, 1990. **87**(12): p. 4761-4765.
142. Otvos Jr, L., et al., *Interaction between heat shock proteins and antimicrobial peptides.* Biochemistry(Washington), 2000. **39**(46): p. 14150-14159.
143. Bukau, B. and G.C. Walker, *Mutations altering heat shock specific subunit of RNA polymerase suppress major cellular defects of E. coli mutants lacking the DnaK chaperone.* The EMBO Journal, 1990. **9**(12): p. 4027.
144. Patrzykat, A., et al., *Sublethal concentrations of pleurocidin-derived antimicrobial peptides inhibit macromolecular synthesis in Escherichia coli.* Antimicrobial agents and chemotherapy, 2002. **46**(3): p. 605.
145. Bierbaum, G. and H.G. Sahl, *Autolytic system of Staphylococcus simulans 22: influence of cationic peptides on activity of N-acetylmuramoyl-L-alanine amidase.* Journal of bacteriology, 1987. **169**(12): p. 5452.
146. Sawai, M.V., et al., *Impact of single-residue mutations on the structure and function of ovispirin/novispirin antimicrobial peptides.* Protein Engineering, 2002. **15**(3): p. 225.
147. Meyer, C.E. and F. Reusser, *A polypeptide antibacterial agent isolated from Trichoderma viride.* Experientia, 1967. **23**(2): p. 85.
148. Leitgeb, B., et al., *The history of alamethicin: a review of the most extensively studied peptaibol.* Chemistry and Biodiversity, 2007. **4**(6): p. 1027-1051.
149. Chen, F.-Y., M.-T. Lee, and H.W. Huang, *Sigmoidal Concentration Dependence of Antimicrobial Peptide Activities: A Case Study on Alamethicin.* 2002. **82**(2): p. 908-914.
150. Andrew Woolley, G. and B.A. Wallace, *Model ion channels: gramicidin and alamethicin.* Journal of Membrane Biology, 1992. **129**(2): p. 109-136.
151. He, K., et al., *Neutron scattering in the plane of membranes: structure of alamethicin pores.* Biophysical journal, 1996. **70**(6): p. 2659-2666.
152. Qian, S., et al., *Structure of the alamethicin pore reconstructed by X-ray diffraction analysis.* Biophysical Journal, 2008. **94**(9): p. 3512-3522.
153. Huang, H.W. and Y. Wu, *Lipid-alamethicin interactions influence alamethicin orientation.* Biophysical Journal, 1991. **60**(5): p. 1079-1087.
154. Constantin, D., et al., *Interaction of alamethicin pores in DMPC bilayers.* Biophysical journal, 2007. **92**(11): p. 3978-3987.
155. Peter Tieleman, D., B. Hess, and M.S.P. Sansom, *Analysis and evaluation of channel models: simulations of alamethicin.* Biophysical journal, 2002. **83**(5): p. 2393-2407.

156. Pan, J., S. Tristram-Nagle, and J.F. Nagle, *Alamethicin Aggregation in Lipid Membranes.* Journal of Membrane Biology, 2009. **231**(1): p. 11-27.
157. Woolley, G.A., *Channel-forming activity of alamethicin: effects of covalent tethering.* Chemistry and Biodiversity, 2007. **4**(6): p. 1323.
158. Matsubara, A., et al., *Ion-channels of cyclic template-assembled alamethicins that emulate the pore structure predicted by the barrel-stave model.* Chemical Communications, 1996. **1996**(17): p. 2069-2070.
159. Duclohier, H., et al., *Channel properties of template assembled alamethicin tetramers.* Journal of Peptide Science, 2003. **9**(11-12): p. 776-783.
160. Wassner, A.J., et al., *Synthesis and ion conductance behavior of a tetrameric alamethicin ion channel.* Org. Lett, 2002. **4**(10): p. 1647-1649.
161. Bürck, J., et al., *Conformation and Membrane Orientation of Amphiphilic Helical Peptides by Oriented Circular Dichroism.* Biophysical Journal, 2008. **95**(8): p. 3872-3881.
162. Challa, R., et al., *Cyclodextrins in drug delivery: an updated review.* Aaps Pharmscitech, 2005. **6**(2): p. 329-357.
163. Larsen, K.L., *Large cyclodextrins.* Journal of Inclusion Phenomena and Macrocyclic Chemistry, 2002. **43**(1): p. 1-13.
164. Dobson, C.M., A. Sali, and M. Karplus, *Protein folding: a perspective from theory and experiment.* Angewandte Chemie. International edition in English, 1998. **37**(7): p. 868-893.
165. Hartl, F.U. and M. Hayer-Hartl, *Converging concepts of protein folding in vitro and in vivo.* Nature Structural & Molecular Biology, 2009. **16**(6): p. 574-581.
166. Kubelka, J., J. Hofrichter, and W.A. Eaton, *The protein folding 'speed limit'.* Current Opinion in Structural Biology, 2004. **14**(1): p. 76-88.
167. Levinthal, C., *Are there pathways for protein folding.* J. Chim. Phys, 1968. **65**(1): p. 44-45.
168. Dill, K.A. and H.S. Chan, *From Levinthal to pathways to funnels.* Nature Structural Biology, 1997. **4**(1): p. 10-19.
169. Bemporad, F., et al., *Biological function in a non-native partially folded state of a protein.* The EMBO Journal, 2008. **27**: p. 1525-1535.
170. Morozova-Roche, L.A., et al., *Structural characterisation and comparison of the native and A-states of equine lysozyme.* Journal of Molecular Biology, 1997. **268**(5): p. 903-921.
171. Morozova, L.A., et al., *Structural basis of the stability of a lysozyme molten globule.* Nature Structural & Molecular Biology, 1995. **2**(10): p. 871-875.
172. Van Dael, H., et al., *Partially folded states of equine lysozyme. Structural characterization and significance for protein folding.* Biochemistry, 1993. **32**(44): p. 11886-11894.
173. Kuwajima, K., *The molten globule state of alpha-lactalbumin.* The FASEB Journal, 1996. **10**(1): p. 102-109.
174. Otzen, D.E., P. Sehgal, and P. Westh, *α-Lactalbumin is unfolded by all classes of surfactants but by different mechanisms.* Journal of Colloid And Interface Science, 2009. **329**(2): p. 273-283.
175. Ulrich Hartl, F. and J. Martin, *Molecular chaperones in cellular protein folding.* Current Opinion in Structural Biology, 1995. **5**(1): p. 92-102.
176. Powers, E.T., et al., *Biological and chemical approaches to diseases of proteostasis deficiency.* Annual Review of Biochemistry, 2009. **78**: p. 959-991.
177. Chiti, F. and C.M. Dobson, *Protein misfolding, functional amyloid, and human disease.* 2006.
178. Dobson, C.M., *Protein folding and misfolding.* Nature, 2003. **426**(6968): p. 884-890.
179. Uversky, V.N., et al., *Accelerated -synuclein fibrillation in crowded milieu.* FEBS letters, 2002. **515**(1-3): p. 99-103.
180. Uversky, V.N., et al., *Synergistic effects of pesticides and metals on the fibrillation of -synuclein: implications for Parkinson's disease.* Neurotoxicology, 2002. **23**(4-5): p. 527-536.

181. Cohlberg, J.A., et al., *Heparin and Other Glycosaminoglycans Stimulate the Formation of Amyloid Fibrils from [alpha]-Synuclein in Vitro†.* Biochemistry, 2002. **41**(5): p. 1502-1511.
182. Sluzky, V., et al., *Kinetics of insulin aggregation in aqueous solutions upon agitation in the presence of hydrophobic surfaces.* Proceedings of the National Academy of Sciences of the United States of America, 1991. **88**(21): p. 9377.
183. Frokjaer, S. and D.E. Otzen, *Protein drug stability: a formulation challenge.* Nature Reviews Drug Discovery, 2005. **4**(4): p. 298-306.
184. Morozova-Roche, L. and M. Malisauskas, *A false paradise-mixed blessings in the protein universe: the amyloid as a new challenge in drug development.* Current medicinal chemistry, 2007. **14**(11): p. 1221-1230.
185. Lambert, M.P., et al., *Diffusible, nonfibrillar ligands derived from A 1–42 are potent central nervous system neurotoxins.* Proceedings of the National Academy of Sciences of the United States of America, 1998. **95**(11): p. 6448.
186. Hartley, D.M., et al., *Protofibrillar intermediates of amyloid beta-protein induce acute electrophysiological changes and progressive neurotoxicity in cortical neurons.* Journal of Neuroscience, 1999. **19**(20): p. 8876.
187. Klein, W.L., G.A. Krafft, and C.E. Finch, *Targeting small A oligomers: the solution to an Alzheimer's disease conundrum?* TRENDS in Neurosciences, 2001. **24**(4): p. 219-224.
188. Stefani, M. and C. Dobson, *Protein aggregation and aggregate toxicity: new insights into protein folding, misfolding diseases and biological evolution.* Journal of Molecular Medicine, 2003. **81**(11): p. 678-699.
189. Larsen, P., et al., *Amyloid adhesins are abundant in natural biofilms.* Environmental microbiology, 2007. **9**(12): p. 3077-3090.
190. Barnhart, M.M. and M.R. Chapman, *Curli biogenesis and function.* 2006.
191. Otzen, D. and P.H. Nielsen, *We find them here, we find them there: functional bacterial amyloid.* Cellular and Molecular Life Sciences, 2008. **65**(6): p. 910-927.
192. Hakansson, A., et al., *Apoptosis Induced by a Human Milk Protein.* Proceedings of the National Academy of Sciences, 1995. **92**(17): p. 8064-8068.
193. Svensson, M., et al., *Conversion of a-lactalbumin to a protein inducing apoptosis*, in *Proceedings of the National Academy of Sciences*. 2000, National Acad Sciences. p. 4221-4226.
194. Knyazeva, E.L., et al., *Who Is Mr. HAMLET? Interaction of Human α-Lactalbumin with Monomeric Oleic Acid.* Biochemistry, 2008. **47**: p. 13127-13137.
195. Gustafsson, L., et al., *Treatment of Skin Papillomas with Topical alpha-Lactalbumin-Oleic Acid*. 2004. p. 2663-2672.
196. Mossberg, A.K., et al., *Bladder cancers respond to intravesical instillation of HAMLET (human alpha-lactalbumin made lethal to tumor cells).* Int J Cancer, 2007. **121**(6): p. 1352-1359.
197. Mok, K.H., et al., *HAMLET, protein folding, and tumor cell death.* Biochemical and Biophysical Research Communications, 2007. **354**(1): p. 1-7.
198. Svanborg, C., et al., *HAMLET kills tumor cells by an apoptosis-like mechanism-cellular, molecular, and therapeutic aspects.* Advances in cancer research, 2003. **88**: p. 1-29.
199. Xiang, J., et al., *Interaction of cellulase with sodium dodecyl sulfate at critical micelle concentration level.* Colloids and Surfaces B: Biointerfaces, 2006. **49**(2): p. 175-180.
200. Fuguet, E., et al., *Critical micelle concentration of surfactants in aqueous buffered and unbuffered systems.* Analytica Chimica Acta, 2005. **548**(1-2): p. 95-100.
201. Zunszain, P.A., et al., *Crystal structural analysis of human serum albumin complexed with hemin and fatty acid.* BMC Structural biology, 2003. **3**(1): p. 6.
202. Ghuman, J., et al., *Structural basis of the drug-binding specificity of human serum albumin.* Journal of molecular biology, 2005. **353**(1): p. 38-52.

203. Chmurzyñska, A., *The multigene family of fatty acid-binding proteins (FABPs): function, structure and polymorphism.* J Appl Genet, 2006. **47**(1): p. 39-48.
204. Kaikaus, R.M., N.M. Bass, and R.K. Ockner, *Functions of fatty acid binding proteins.* Cellular and Molecular Life Sciences (CMLS), 1990. **46**(6): p. 617-630.
205. Nielsen, A.D., K. Borch, and P. Westh, *Thermochemistry of the specific binding of C12 surfactants to bovine serum albumin.* Biochimica et Biophysica Acta (BBA)/Protein Structure and Molecular Enzymology, 2000. **1479**(1-2): p. 321-331.
206. Jones, M.N., *Surfactant interactions with biomembranes and proteins.* Chemical Society Reviews, 1992. **21**(2): p. 127-136.
207. Shapiro, A.L., E. Vinuela, and J.V. Maizel Jr, *Molecular weight estimation of polypeptide chains by electrophoresis in SDS-polyacrylamide gels.* Biochemical and biophysical research communications, 1967. **28**(5): p. 815.
208. Manning, M. and W. Colon, *Structural Basis of Protein Kinetic Stability: Resistance to Sodium Dodecyl Sulfate Suggests a Central Role for Rigidity and a Bias Toward [beta]-Sheet Structure†.* Biochemistry, 2004. **43**(35): p. 11248-11254.
209. Cunningham, E.L., et al., *Kinetic stability as a mechanism for protease longevity.* Proceedings of the National Academy of Sciences, 1999. **96**(20): p. 11008.
210. Cunningham, E.L. and D.A. Agard, *Disabling the folding catalyst is the last critical step in -lytic protease folding.* Protein Science: A Publication of the Protein Society, 2004. **13**(2): p. 325.
211. Andersen, K.K., *Protein-surfactant interactions : the interplay between structure, stability and kinetics*, in *Dept. Life Sciences*. 2009, Aalborg University: Aalborg.
212. Kaushik, J.K., K. Ogasahara, and K. Yutani, *The unusually slow relaxation kinetics of the folding-unfolding of pyrrolidone carboxyl peptidase from a hyperthermophile, Pyrococcus furiosus.* Journal of molecular biology, 2002. **316**(4): p. 991-1003.
213. Hughey, V.L. and E.A. Johnson, *Antimicrobial activity of lysozyme against bacteria involved in food spoilage and food-borne disease.* Applied and Environmental Microbiology, 1987. **53**(9): p. 2165.
214. Tsuge, H., et al., *A structural study of calcium-binding equine lysozyme by two-dimensional 1H-NMR.* Biochimica et biophysica acta, 1991. **1078**(1): p. 77.
215. Tsuge, H., et al., *Crystallographic Studies of a Calcium Binding Lysozyme from Equine Milk at 2.5 AResolution.* Journal of Biochemistry, 1992. **111**(2): p. 141.
216. Acharya, K.R., et al., *Models of the three-dimensional structures of echidna, horse, and pigeon lysozymes: Calcium-binding lysozymes and their relationship with -lactalbumins.* Journal of protein chemistry, 1994. **13**(6): p. 569-584.
217. Nitta, K., et al., *The calcium-binding property of equine lysozyme.* FEBS letters, 1987. **223**(2): p. 405.
218. Henikoff, S. and J.G. Henikoff, *Amino acid substitution matrices from protein blocks.* Proceedings of the National Academy of Sciences, 1992. **89**(22): p. 10915.
219. Agasøster, A.V., et al., *The Interaction of Peripheral Proteins and Membranes Studied with -Lactalbumin and Phospholipid Bilayers of Various Compositions*.* Journal of Biological Chemistry, 2003. **278**(24): p. 21790-21797.
220. Morozova, L.A., et al., *Structural basis of the stability of a lysozyme molten globule.* Nature Structural Biology, 1995. **2**(10): p. 871-875.
221. Gharibyan, A.L., et al., *Lysozyme amyloid oligomers and fibrils induce cellular death via different apoptotic/necrotic pathways.* Journal of molecular biology, 2007. **365**(5): p. 1337-1349.
222. Malisauskas, M., et al., *Does the Cytotoxic Effect of Transient Amyloid Oligomers from Common Equine Lysozyme in Vitro Imply Innate Amyloid Toxicity?* Journal of Biological Chemistry, 2005. **280**(8): p. 6269.
223. Booth, D.R., et al., *Instability, unfolding and aggregation of human lysozyme variants underlying amyloid fibrillogenesis.* Nature, 1997. **385**(6619): p. 787-793.

224. Malisauskas, M., et al., *Amyloid protofilaments from the calcium-binding protein equine lysozyme: formation of ring and linear structures depends on pH and metal ion concentration.* Journal of molecular biology, 2003. **330**(4): p. 879-890.
225. Wilhelm, K., et al., *Protein oligomerization induced by oleic acid at the solid/liquid interface - equine lysozyme cytotoxic complexes.* FEBS Journal, 2009. **276**(15): p. 3975-3989.
226. Svensson, M., et al., *Lipids as cofactors in protein folding: Stereo-specific lipid–protein interactions are required to form HAMLET (human -lactalbumin made lethal to tumor cells).* Protein Science: A Publication of the Protein Society, 2003. **12**(12): p. 2805.
227. Håkansson, A., et al., *Multimeric α-lactalbumin from human milk induces apoptosis through a direct effect on cell nuclei.* Experimental cell research, 1999. **246**(2): p. 451-460.
228. Hallgren, O., et al., *HAMLET triggers apoptosis but tumor cell death is independent of caspases, Bcl-2 and p53.* Apoptosis, 2006. **11**(2): p. 221-233.
229. Zherelova, O., et al., *Interaction of antitumor α-lactalbumin—oleic acid complexes with artificial and natural membranes.* Journal of Bioenergetics and Biomembranes, 2009. **41**(3): p. 229-237.
230. Pettersson-Kastberg, J., et al., *α-Lactalbumin, Engineered to be Nonnative and Inactive, Kills Tumor Cells when in Complex with Oleic Acid: A New Biological Function Resulting from Partial Unfolding.* Journal of Molecular Biology, 2009. **394**(5): p. 994-1010.
231. Gasteiger, E., et al., *Protein identification and analysis tools on the ExPASy server.* The proteomics protocols handbook, 2005: p. 571–607.
232. Fast, J., et al., *Stability of HAMLET—A kinetically trapped -lactalbumin oleic acid complex.* Protein Science: A Publication of the Protein Society, 2005. **14**(2): p. 329.
233. Mendelsohn, R., et al., *Raman and Fourier transform infrared spectroscopic studies of the interaction between glycophorin and dimyristoylphosphatidylcholine.* Biophysical Journal, 1982. **37**(1): p. 83.
234. Smith, J.T. and I.J. Clarke, *Kisspeptin expression in the brain: catalyst for the initiation of puberty.* Reviews in Endocrine & Metabolic Disorders, 2007. **8**(1): p. 1-9.
235. Popa, S.M., D.K. Clifton, and R.A. Steiner, *The Role of Kisspeptins and GPR54 in the Neuroendocrine Regulation of Reproduction.* Annual Review of Physiology, 2008. **70**(1): p. 213-238.
236. Aparicio, S., *Kisspeptins and GPR54—The new biology of the mammalian GnRH axis.* Cell Metabolism, 2005. **1**(5): p. 293-296.
237. Ohtaki, T., et al., *Metastasis suppressor gene KiSS-1 encodes peptide ligand of a G-protein-coupled receptor.* Nature, 2001. **411**(6837): p. 613-617.
238. Shiraki, K., K. Nishikawa, and Y. Goto, *Trifluoroethanol-induced Stabilization of the [alpha]-Helical Structure of [beta]-Lactoglobulin: Implication for Non-hierarchical Protein Folding.* Journal of Molecular Biology, 1995. **245**(2): p. 180-194.
239. Shin, R., et al., *Nuclear magnetic resonance and circular dichroism study of metastin (Kisspeptin-54) structure in solution.* Clinical and Experimental Metastasis, 2009. **26**(6): p. 527-533.
240. Lee, J.Y., et al., *Molecular interaction between kisspeptin decapeptide analogs and a lipid membrane.* Archives of biochemistry and biophysics, 2009.
241. Dobson, C.M., *The structural basis of protein folding and its links with human disease.* Philosophical Transactions of the Royal Society B: Biological Sciences, 2001. **356**(1406): p. 133-145.
242. Maji, S.K., et al., *Amyloid as a depot for the formulation of long-acting drugs.* PLoS Biol, 2008. **6**(2): p. e17.
243. Maji, S.K., et al., *Functional amyloids as natural storage of peptide hormones in pituitary secretory granules.* Science Signaling, 2009. **325**(5938): p. 328.
244. Gerdes, H.H., et al., *The primary structure of human secretogranin II, a widespread tyrosine-sulfated secretory granule protein that exhibits low pH-and calcium-induced aggregation.* Journal of Biological Chemistry, 1989. **264**(20): p. 12009-12015.

245. Martinez, C., et al., *Fusarium solani cutinase is a lipolytic enzyme with a catalytic serine accessible to solvent.* 1992.
246. Mannesse, M.L.M., et al., *Cutinase from Fusarium solani pisi Hydrolyzing Triglyceride Analogs. Effect of Acyl Chain Length and Position in the Substrate Molecule on Activity and Enantioselectivity.* Biochemistry, 1995. **34**(19): p. 6400-6407.
247. Martinez, C., et al., *Cutinase, a lipolytic enzyme with a preformed oxyanion hole.* Biochemistry, 1994. **33**(1): p. 83-89.
248. Sehgal, P., et al., *Modulation of cutinase stability and structure by phospholipid detergents.* Biochimica et Biophysica Acta (BBA) - Proteins & Proteomics, 2007. **1774**(12): p. 1544-1554.
249. Poulsen, K.R., et al., *The Interaction of Fusarium solani pisi Cutinase with Long Chain Spin Label Esters†.* Biochemistry, 2006. **45**(30): p. 9163-9171.
250. Prompers, J.J., et al., *Backbone Dynamics of Fusarium solani pisi Cutinase Probed by Nuclear Magnetic Resonance: The Lack of Interfacial Activation Revisited†.* Biochemistry, 1999. **38**(17): p. 5315-5327.
251. Prompers, J.J., et al., *NMR Studies of Fusarium solani pisi Cutinase in Complex with Phosphonate Inhibitors†.* Biochemistry, 1999. **38**(19): p. 5982-5994.
252. Mogensen, J.E., P. Sehgal, and D.E. Otzen, *Activation, Inhibition, and Destabilization of Thermomyces lanuginosus Lipase by Detergents.* Biochemistry, 2005. **44**(5): p. 1719-1730.
253. Otzen, D.E., et al., *Aggregation as the basis for complex behaviour of cutinase in different denaturants.* BBA-Proteins and Proteomics, 2007. **1774**(2): p. 323-333.
254. Melo, E.P., et al., *Trehalose favors a cutinase compact intermediate off-folding pathway.* Biochemistry, 2003. **42**(24): p. 7611-7617.
255. Brissos, V., et al., *Improving activity and stability of cutinase towards the anionic detergent AOT by complete saturation mutagenesis.* Protein Engineering Design and Selection, 2008.
256. Brissos, V., et al., *Biochemical and structural characterisation of cutinase mutants in the presence of the anionic surfactant AOT.* BBA-Proteins and Proteomics, 2008. **1784**(9): p. 1326-1334.
257. Creveld, L.D., et al., *DSC studies of Fusarium solani pisi cutinase: consequences for stability in the presence of surfactants.* Biophysical Chemistry, 2001. **92**(1-2): p. 65-75.
258. Ternström, T., et al., *Unfolding and inactivation of cutinases by AOT and guanidine hydrochloride.* BBA-Proteins and Proteomics, 2005. **1748**(1): p. 74-83.
259. Kelly, S.M., T.J. Jess, and N.C. Price, *How to study proteins by circular dichroism.* BBA-Proteins and Proteomics, 2005. **1751**(2): p. 119-139.
260. Krittanai, C. and W.C. Johnson, *Correcting the circular dichroism spectra of peptides for contributions of absorbing side chains.* Analytical biochemistry, 1997. **253**(1): p. 57-64.
261. Yang, L., et al., *Barrel-stave model or toroidal model? A case study on melittin pores.* Biophysical Journal, 2001. **81**(3): p. 1475-1485.
262. de Jongh, H.H.J., E. Goormaghtigh, and J.A. Killian, *Analysis of circular dichroism spectra of oriented protein-lipid complexes: toward a general application.* Biochemistry, 1994. **33**(48): p. 14521-14528.
263. Heller, W.T., et al., *Multiple States of β-Sheet Peptide Protegrin in Lipid Bilayers.* Biochemistry, 1998. **37**(49): p. 17331-17338.
264. Weiss, T.M., et al., *Two States of Cyclic Antimicrobial Peptide RTD-1 in Lipid Bilayers.* Biochemistry, 2002. **41**(31): p. 10070-10076.
265. Ladokhin, A.S. and S.H. White, *'Detergent-like'permeabilization of anionic lipid vesicles by melittin.* BBA-Biomembranes, 2001. **1514**(2): p. 253-260.
266. Dave, P.C., et al., *Interaction of Alamethicin with Ether-Linked Phospholipid Bilayers: Oriented Circular Dichroism, 31P Solid-State NMR, and Differential Scanning Calorimetry Studies.* Biophysical Journal, 2005. **89**(4): p. 2434-2442.

267. de Jongh, H.H.J., R. Brasseur, and J.A. Killian, *Orientation of the. alpha.-helixes of apocytochrome c and derived fragments at membrane interfaces, as studied by circular dichroism.* Biochemistry, 1994. **33**(48): p. 14529-14535.
268. Hunt, J.F., et al., *Spontaneous, pH-Dependent Membrane Insertion of a Transbilayer [alpha]-Helix.* Biochemistry, 1997. **36**(49): p. 15177-15192.
269. Lee, M.T., F.Y. Chen, and H.W. Huang, *Energetics of pore formation induced by membrane active peptides.* Biochemistry, 2004. **43**(12): p. 3590-3599.
270. Heller, W.T., et al., *Effect of changing the size of lipid headgroup on peptide insertion into membranes.* Biophysical journal, 1997. **73**(1): p. 239-244.
271. Olah, G.A. and H.W. Huang, *Circular dichroism of oriented alpha helices. I. Proof of the exciton theory.* The Journal of Chemical Physics, 1988. **89**(4): p. 2531-2538.
272. Parasassi, T., et al., *Laurdan and Prodan as polarity-sensitive fluorescent membrane probes.* Journal of Fluorescence, 1998. **8**(4): p. 365-373.
273. De Vequi-Suplicy, C.C., C.R. Benatti, and M.T. Lamy, *Laurdan in fluid bilayers: position and structural sensitivity.* Journal of fluorescence, 2006. **16**(3): p. 431-439.
274. Zhang, Y.L., J.A. Frangos, and M. Chachisvilis, *Laurdan fluorescence senses mechanical strain in the lipid bilayer membrane.* Biochemical and Biophysical Research Communications, 2006. **347**(3): p. 838-841.
275. Parasassi, T., et al., *Cholesterol modifies water concentration and dynamics in phospholipid bilayers: a fluorescence study using Laurdan probe.* Biophysical Journal, 1994. **66**(3, Part 1): p. 763-768.
276. Jasniewski, J., et al., *Fluorescence anisotropy analysis of the mechanism of action of mesenterocin 52A: speculations on antimicrobial mechanism.* Applied Microbiology and Biotechnology, 2008. **81**(2): p. 339-347.
277. Lakowicz, J.R., *Principles of Fluorescence Spectroscopy. 1999.* Kluwer Academic/Plenum Publisher, New York, Kap. **9**.
278. Otzen, D.E., M. Oliveberg, and F. Höök, *Adsorption of a small protein to a methyl-terminated hydrophobic surfaces: effect of protein-folding thermodynamics and kinetics.* Colloids and Surfaces B: Biointerfaces, 2003. **29**(1): p. 67-73.
279. Höök, F., et al., *Energy dissipation kinetics for protein and antibody-antigen adsorption under shear oscillation on a quartz crystal microbalance.* Langmuir, 1998. **14**(4): p. 729-734.
280. Zhou, C., et al., *Human Immunoglobulin Adsorption Investigated by Means of Quartz Crystal Microbalance Dissipation, Atomic Force Microscopy, Surface Acoustic Wave, and Surface Plasmon Resonance Techniques.* Langmuir, 2004. **20**(14): p. 5870-5878.
281. Höök, F., et al., *Structural changes in hemoglobin during adsorption to solid surfaces: Effects of pH, ionic strength, and ligand binding.* Proceedings of the National Academy of Sciences of the United States of America, 1998. **95**(21): p. 12271.
282. Sauerbrey, G., *Verwendung von Schwingquarzen zur W„gung d nner Schichten und zur Mikrow„gung.* Zeitschrift f r Physik A Hadrons and Nuclei, 1959. **155**(2): p. 206-222.
283. Voros, J., *The Density and Refractive Index of Adsorbing Protein Layers.* Biophysical Journal, 2004. **87**(1): p. 553-561.
284. Voinova, M.V., et al., *Viscoelastic acoustic response of layered polymer films at fluid-solid interfaces: Continuum mechanics approach.* Arxiv preprint cond-mat/9805266, 1998.
285. Höök, F., et al., *A comparative study of protein adsorption on titanium oxide surfaces using in situ ellipsometry, optical waveguide lightmode spectroscopy, and quartz crystal microbalance/dissipation.* Colloids and Surfaces B: Biointerfaces, 2002. **24**(2): p. 155-170.
286. Voinova, M.V., M. Jonson, and B. Kasemo, *Missing mass effect in biosensor's QCM applications.* Biosens Bioelectron, 2002. **17**(10): p. 835-841.

287. Larsson, C., M. Rodahl, and F. H""k, *Characterization of DNA immobilization and subsequent hybridization on a 2D arrangement of streptavidin on a biotin-modified lipid bilayer supported on SiO2.* Anal.Chem, 2003. **75**(19): p. 5080-5087.
288. Piantavigna, S., et al., *Cell Penetrating Apidaecin Peptide Interactions with Biomimetic Phospholipid Membranes.* International Journal of Peptide Research and Therapeutics, 2009. **15**(2): p. 139-146.
289. Edvardsson, M., et al., *QCM-D and Reflectometry Instrument: Applications to Supported Lipid Structures and Their Biomolecular Interactions.* Analytical Chemistry, 2008. **81**(1): p. 349-361.
290. Rodahl, M., et al., *Simultaneous frequency and dissipation factor QCM measurements of biomolecular adsorption and cell adhesion.* Faraday Discuss, 1997. **107**: p. 229-246.
291. Swann, M.J., et al., *Dual-polarization interferometry: an analytical technique to measure changes in protein structure in real time, to determine the stoichiometry of binding events, and to differentiate between specific and nonspecific interactions.* Anal.Biochem., 2004. **329**(2): p. 190-198.

Part V: Scientific papers of the thesis

Paper I:

Divorcing Folding from Function: How acylation affects the Membrane-Perturbing Properties of an Anti-microbial Peptide?

Brian Vad, Line Aagot Thomsen, Kresten Bertelsen, Magnus Franzmann, Jan Mondrup Pedersen, Søren B. Nielsen, Thomas Vosegaard, Zuzana Valnickova, Troels Skrydstrup, Jan J. Enghild, Reinhard Wimmer, Niels Chr. Nielsen and Daniel E. Otzen.
Biochim Biophys Acta Biomembranes Proteins and Proteomics *In press*

Biochimica et Biophysica Acta xxx (2009) xxx–xxx

Contents lists available at ScienceDirect

Biochimica et Biophysica Acta

journal homepage: www.elsevier.com/locate/bbapap

Divorcing folding from function: How acylation affects the membrane-perturbing properties of an antimicrobial peptide

Brian Vad [a,b], Line Aagot Thomsen [b], Kresten Bertelsen [c], Magnus Franzmann [b], Jan Mondrup Pedersen [c], Søren B. Nielsen [a,d], Thomas Vosegaard [c], Zuzana Valnickova [a], Troels Skrydstrup [c], Jan J. Enghild [a], Reinhard Wimmer [b], Niels Chr. Nielsen [c,*], Daniel E. Otzen [a,b,*]

[a] Center for Insoluble Protein Structures (inSPIN), Interdisciplinary Nanoscience Center (iNANO) and Department of Molecular Biology, Gustav Wieds Vej 10C, University of Aarhus, DK – 8000 Aarhus C, Denmark
[b] Department of Biotechnology, Chemistry and Environmental Engineering, Aalborg University, Sohngaardsholmsvej 49, DK – 9000 Aalborg, Denmark
[c] Center for Insoluble Protein Structures (inSPIN), Interdisciplinary Nanoscience Center (iNANO) and Department of Chemistry, Langelandsgade 140, University of Aarhus, DK – 8000 Aarhus C, Denmark
[d] Department of Food Science, Faculty of Agricultural Sciences, University of Aarhus, Blichers Allé, DK – 8830 Tjele, Denmark

ARTICLE INFO

Article history:
Received 22 October 2009
Received in revised form 24 November 2009
Accepted 8 December 2009
Available online xxxx

Keywords:
Novicidin
Membrane permeabilization
Confocal laser scanning microscopy
Circular dichroism
Liquid- and solid-state NMR
Peptide acylation

ABSTRACT

Many small cationic peptides, which are unstructured in aqueous solution, have antimicrobial properties. These properties are assumed to be linked to their ability to permeabilize bacterial membranes, accompanied by the transition to an α-helical folding state. Here we show that there is no direct link between folding of the antimicrobial peptide Novicidin (Nc) and its membrane permeabilization. N-terminal acylation with C8–C16 alkyl chains and the inclusion of anionic lipids both increase Nc's ability to form α-helical structure in the presence of vesicles. Nevertheless, both acylation and anionic lipids reduce the extent of permeabilization of these vesicles and lead to slower permeabilization kinetics. Furthermore, acylation significantly decreases antimicrobial activity. Although acyl chains of increasing length also increase the tendency of the peptides to aggregate in solution, this cannot rationalize our results since permeabilization and antimicrobial activities are observed well below concentrations where aggregation occurs. This suggests that significant induction of α-helical structure is not a prerequisite for membrane perturbation in this class of antimicrobial peptides. Our data suggests that for Nc, induction of α-helical structure may inhibit rather than facilitate membrane disruption, and that a more peripheral interaction may be the most efficient permeabilization mechanism. Furthermore, acylation leads to a deeper embedding in the membrane, which could lead to an anti-permeabilizing "plugging" effect.

1. Introduction

Over the past two decades, more than 800 antimicrobial peptides (AMPs) have been reported from sources as diverse as animals, plants, insects, and fungi [1–4]. As parts of the innate immune system in vertebrates, AMPs are often the first line of defence against an invading organism, and thus show activity against a broad range of targets. Microorganisms do not easily evolve resistance to them, making them of great interest as alternatives to small-molecule antibiotics. Over the recent few years significant resources have been directed towards their commercialization. So far, only a few products have succeeded, while several promising candidates have been halted because of adverse effects or effects similar to existing antibiotics [5]. The lack of success most likely reflects limited understanding of their mechanism of action and microbial specificity. At present the common procedure is to search for naturally occurring AMPs and then subsequently mutate them to change their specificity [6–10]. More detailed insight into AMP activity may ultimately allow design *in silico* [11].

Many AMPs are understood to target the bacterial plasma membrane directly rather than through receptors (though there are a growing number of exceptions such as lantibiotic peptides that target lipids in the bacterial septum and thus inhibit cell division [12] and defensins with viral targets [13]). They do so in a variety of ways, including a barrel-stave model, a carpet model, and a toroidal-pore model [14]. In the barrel-stave model, the peptides completely traverse the membrane by pore formation, quickly ruining the

Abbreviations: AMP, antimicrobial peptide; CD, circular dichroism; Nc, Novicidin; Nc-CX, N-terminally acylated Nc where X refers to the number of carbon atoms in the acyl chain; PRE, paramagnetic relaxation enhancement

* Corresponding authors. Otzen is to be contacted at the Center for Insoluble Protein Structures (inSPIN) Interdisciplinary Nanoscience Center (iNANO) and Department of Molecular Biology, Gustav Wieds Vej 10C, University of Aarhus, DK – 8000 Aarhus C, Denmark. Tel.: +45 89 42 46 50; fax: +45 86 12 31 78. Nielsen, Tel.: +45 89 42 38 41; fax: +45 86 19 61 99.
E-mail addresses: ncn@inano.dk (N.C. Nielsen), dao@inano.dk (D.E. Otzen).

1570-9639/$ – see front matter © 2009 Elsevier B.V. All rights reserved.
doi:10.1016/j.bbapap.2009.12.006

electrochemical gradient and killing the cell [15]. This mode of action is mostly driven by hydrophobic interactions between an amphipathic peptide and the lipid's acyl chains and is therefore less specific towards membranes of different lipid compositions [15]. A minimum of 22 and 8 amino acids is necessary to straddle the bacterial membrane for an α-helical- and a β-sheet peptide, respectively. In the carpet model, the positively charged peptides cover the membrane surface in a carpet-like fashion until they reach a concentration where they permeabilize the cell by disrupting the membrane curvature [16]. As opposed to the barrel-stave model, the peptide does not need to assume a specific oligomeric structure and the peptides are always in contact with the lipid headgroups at the interface with the acyl chains. This mode of action is more sensitive to the lipid headgroup charge, explaining why it is more specific towards the negatively charged surface of bacteria [17–19]. Finally, the toroidal-pore model is a mixture between the carpet model and the barrel-stave model. Defined pores are formed as in the barrel-stave model but the peptides lie in the lipid headgroup-acyl chain interface. This is possible because the peptides induce a sharp bending of the lipids so that lipid headgroups can line the interior of the pore.

It may be possible to modulate the mode of antimicrobial action, and thus the spectrum of applications, by modifying the AMPs with acyl chains, since this modification will increase AMP hydrophobicity and potentially also its membrane affinity. This has been studied in two different approaches: Makovitzki et al. [20] synthesized tetrapeptides with acyl chains of length 8–16 (number carbons in the acyl chain) and found that the tetrapeptides conferred bacterial species specificity while their aggressiveness correlated with acyl chain length. The same group also showed that conjugation of the AMP magainin with acyl chains of length 7, 11, and 16 had important effects on magainin activity, with the membrane permeabilizing ability increasing uniformly with chain length [21]. Furthermore, the attachment of the acyl chains also resulted in a change of the secondary structure of magainin-C11 and magainin-C16 (magainin with acyl chains of lengths 11 and 16, respectively) in solution from that of the wildtype magainin. While magainin-C7, like the wild type, was disordered and monomeric in solution, both magainin-C11 and magainin-C16 adopted α-helical structure. Magainin-C11 was only α-helical above a threshold concentration indicating detergent-like properties in which the protein assumed an α-helical structure in the micellar state. In contrast, magainin-C16 remained α-helical at all investigated concentrations, suggesting that the longer acyl chain was able to sequester the hydrophobic residues in the folded magainin at the monomer level. C-terminal modification with biotin through a single or tandemly coupled caproyl group had no significant effect on gramidicin structure or function [22], and modification with a palmitoyl only group slightly reduces the gramicidin's lipid-perturbing properties, consistent with the peptide's high tendency to associate with the lipid even in the unacylated form [23].

For non-acylated peptides that are unstructured in solution, membrane binding is generally accompanied by the formation of α-helical structure in order to satisfy hydrogen-bonding requirements in a less hydrophilic environment [24]. One might therefore expect that membrane-binding properties and thus antimicrobial properties should correlate with the ability to form α-helical structures in a membrane environment. However, it has been shown for designed antimicrobial peptides composed of a mixture of α- and β-amino acids [25] (but not for peptides containing β-amino acids alone [26]) that there is no correlation between helical propensity and antimicrobial activity.

To explore in greater detail how acylation can modulate membrane-binding properties, and whether helical propensities of peptides with α-amino acids correlate with membrane permeabilization, we report here a detailed study on the effect of acylation on the AMP Novicidin (Nc) [7,27–30]. This AMP is a variant of the 18-residue Ovispirin, which in turn is derived from the N-terminal region of the cathelicidin peptide SMAP-29 from sheep. Ovispirin showed unacceptably high haemolytic activity, but the mutation Ile10→Gly (Novispirin) reduced this to more appropriate levels. Subsequently, the C-terminal mutation Gly18→Phe (giving the peptide Novicidin, abbreviated Nc, sequence KNLRR IIRKG IHIIK KYF) led to improved efficacy towards microorganisms (personal communication, Hans Henrik Kristensen). Novispirin and Nc are unstructured in solution but readily adopt α-helical structures in the presence of anionic lipids and detergents, as well as to a smaller extent in the presence of cationic and zwitterionic detergents [31], in agreement with its amphipathic character (Fig. 1A). We focus on the structural and vesicle-disruptive properties of Nc (denoted Nc wt in its unmodified form), its N-terminally acylated derivatives and a Dansyl-labelled version of Nc. Surprisingly, we find that the induction of measurable amounts of α-helical structure is not a prerequisite for membrane permeabilizing properties and that acylation actually reduces permeabilization efficiency. We suggest that a more peripheral membrane contact may be the most productive mode of action for at least some AMPs.

2. Materials and methods

2.1. Chemicals

DMPC (1,2-di-myristoyl-sn-glycero-3-phosphocholine), DHPC (1,2-di-hexanoyl-sn-glycero-3-phosphocholine), DMPG (1,2-di-myristoyl-sn-glycero-3-[phospho-rac-(1-glycerol)]), DOPC (1,2-di-oleoyl-sn-glycero-3-phosphocholine) and DOPG (1,2-di-oleoyl-sn-glycero-3-[phospho-rac-(1-glycerol)]) were from Avanti Polar Lipids (Alabaster, AL). Protected amino acids, 1,2-ethane dithiole (EDT), triisopropylsylane (TIPS), di-chloromethane (DCM), dimethylformamide (DMF), N,N-diisopropylethylamine (DIPEA), 1H-benzotriazolyl)-1,1,3,3-tetramethyl-uronium hexafluorophosphate (HBTU), octanoic, dodecanoic- and hexadecanoic acid, and *O*-(7-azabenzotriazol-1-yl)-*N*,*N*,*N*′,*N*′-tetramethyl-uronium hexafluorophosphate (HATU) were from Iris Biotech (Marktredwitz, Germany). Acetonitrile chromasolv gradient grade, trifluoroacetic acid (TFA), sucrose 99.5% purity and D (+) glucose 99.5% purity were from Sigma (St. Louis, MO). DiIC18(3), Alexa-488 hydrazide (Alexa^{488}), Alexa-633 hydrazide (Alexa^{633}) and BL21(DE3) were from Invitrogen (Carlsbad, California). Calcein disodium salt was from Fluka (Buchs, Switzerland). Deuterated dodecylphosphocholine (DPC-d_{38}) was from Cambridge Isotope Laboratories Inc. (Andover, MA). Gd-(DTPA-BMA) was generously provided by Klaus Zangger. Recombinant Nc wt peptide (prepared as described [31] and used for all experiments that involved non-derivatized Nc) was generously provided by Dr. Hans Henrik Kristensen.

2.2. Peptide synthesis, acylation and purification

Synthesis of the acylated Nc peptides was carried out in two steps. Firstly, the 18-residue Nc peptide was synthesized on an automatic CEM liberty microwave assisted peptide synthesizer (Matthews, North Carolina) by solid-phase synthesis using standard Fmoc chemistry on Wang resin. Secondly, the fatty acid was attached to the N-terminus of the resin-bound peptide also using Fmoc chemistry. To prepare dansyl-Nc, Nc was manually acylated with the dansyl moiety. Further synthesis and purification details are provided in the Supplementary information.

2.2.1. Preparation of LUV liposomes

LUVs (large unilamellar vesicles) containing calcein were prepared from stock solutions of lipids dissolved in methanol and dried overnight in a Heto VR-1 centrifuge vacuum drier. Lipids were then resuspended by vortexing in 20 mM Tris HCl, pH 7.5 containing 40 mM calcein sodium salt, to a final concentration of 10 g/l (~14 mM), exposed to at least seven cycles of freezing in liquid nitrogen, followed by thawing in a 50 °C water bath, before extrusion through a 200 nm

Please cite this article as: B. Vad, et al., Divorcing folding from function: How acylation affects the membrane-perturbing properties of an antimicrobial peptide, Biochim. Biophys. Acta (2009), doi:10.1016/j.bbapap.2009.12.006

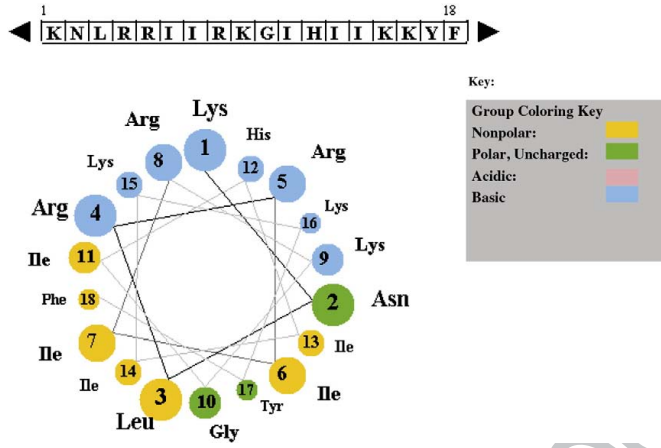

Fig. 1. Sequence of Novicidin and a helical projection highlighting its amphipathic character.

pore filter 12 times using a 10 ml thermo barrel extruder (Northern Lipids, Vancouver, Canada). The lipid solutions were run on a PD10 column pre-equilibrated with 20 mM Tris HCl, pH 7.5. Eluent fractions were gathered and tested by fluorescence measurements with and without the addition of Triton X-100 to test for calcein release. Those with the highest signal-to-background ratio were selected for further use. All extruded vesicles were used on the same day that they were made.

2.2.2. GUV liposomes and laser confocal microscopy measurements

GUVs (giant unilamellar vesicles) were prepared by the electroformation method originally described by Angelova and Dimitrov [32] and observed with a LSM 510 scanning confocal microscope (Zeiss GmbH, Jena, Germany). Further details are provided in the Supplementary information.

2.3. Manual calcein release assay

All fluorescence measurements were conducted on an LS55 fluorimeter essentially as described [33]. Further details are provided in the Supplementary information.

2.4. Stopped-flow measurements

Kinetic experiments were carried out on an Applied Photophysics SX-18MV reaction analyzer (Applied Photophysics, Leatherhead, Surrey) in fluorescence detection mode. For the calcein release measurements, the solution was excited at 490 nm and a 510-nm glass filter was used to measure emission intensity. The calcein vesicles and peptides were mixed in 10:1 volume ratio and at least three measurements were averaged for each concentration. Final concentrations of lipid were around 50 μM while final peptide concentrations varied from 0.2 μM to 72 μM. In measurements using Dansyl-Nc, the samples were excited at 335 nm and a 530-nm glass filter was used. The lipid concentration was held constant at 20 μM while the peptide concentration was varied from 1 to 10 μM.

2.5. Secondary structural changes measured by CD spectroscopy

Circular dichroism studies were performed on a Jasco J-810 spectropolarimeter (Jasco Spectroscopic Co., Hachioji City, Japan) with a Jasco PTC-348W1 temperature control unit. Scan speed was set to 100 nm/min, slit width 2 nm. All experiments were carried out in 20 mM Tris–HCl pH 7.5, at 25 °C using a 1 mm quartz cuvette. The measurements were conducted as one-pot titrations with an initial peptide concentration of 200 μM and stepwise addition of lipids. After the addition of each new lipid aliquot, the sample was allowed to equilibrate for at least 1 min before a spectrum was recorded. Samples at each concentration were measured in three scans and averaged to yield the final spectrum. Background spectra without peptide were subtracted and the CD signal was corrected for dilution.

2.6. Differential scanning calorimetry (DSC)

LUVs for use in DSC experiments were prepared by dissolving and mixing appropriate amounts of DMPC and DMPG yielding pure DMPC and 80:20 w/w% DMPC:DMPG in 1:1 chloroform:methanol, respectively. 10 mg lipid was transferred to a glass vial and solvent was removed under a stream of nitrogen gas followed overnight incubation in a vacuum desiccator ($p < 60$ mbar) to remove trace amounts of solvent. Lipids were rehydrated in 10 mM sodium phosphate pH 8.0 to produce a 10 mg/ml lipid solution and LUVs were subsequently formed by extrusion through 100-nm polycarbonate filter by 15 passages through a MiniExtruder (Avanti Polar Lipids, Alabaster, CA). The phase behavior of LVUs was studied using a Microcal VP-DSC scanning microcalorimeter (Northampton, MA, USA). Samples were prepared by mixing peptide and buffer in appropriate ratios followed by addition of pre-formed LUVs to obtain a lipid concentration of 1 mg/ml and varying peptide content from pure lipid to 1:20 Nc:lipid (molar ratios). Heating and cooling scans were performed between 5 and 45 °C at a scan rate of 60 °C/h and prescan thermal equilibration for 15 min using 10 mM sodium phosphate buffer pH 8.0 as the reference sample. The high feedback mode was used to ensure correct recording of sharp peaks. The DSC cell was pressurized to ~30 psi throughout the experiment.

2.7. Peptide lipid binding measured by fluorescence anisotropy

The excitation was set to 335 nm and emission was measured at 515 nm in a 200 μl Hellma quartz cuvette. Slit width was set to 7.5 nm for both the vertical and horizontal filters. For each sample the G-Factor was measured before measuring the anisotropy. Dansyl-Nc concentration was held constant at 25 μM and increasing amounts of lipid was added. The samples were mixed by pipetting and allowed to equilibrate for 2 min before measuring anisotropy.

Please cite this article as: B. Vad, et al., Divorcing folding from function: How acylation affects the membrane-perturbing properties of an antimicrobial peptide, Biochim. Biophys. Acta (2009), doi:10.1016/j.bbapap.2009.12.006

2.8. Interaction of Nc variants with E. coli cells

Cell permeabilization assays and minimal inhibitory concentration (MIC) assays were performed essentially as described [34,35] but with modifications described in the Supplementary information.

2.9. Solution-state NMR experiments

NMR samples containing 1 mM Nc-C16 or 2 mM Nc were dissolved in 90 mM DPC-d_{38}, 10 mM phosphate buffer, 0.05% sodium azide, 5% D_2O, pH 6 to a final volume of 500 µl. All NMR measurements were conducted at 37 °C on a Bruker DRX600 spectrometer (Bruker BioSpin, Rheinstetten, Germany) operating at a field strength of 14.1 T, equipped with a TXI(H/C/N) probe with triple-axis gradients. The PRE measurements of Nc-C16 were performed as previously described in detail [36]. Further details are provided in the Supplementary information.

2.10. Solid-state NMR

The NMR bicelle samples were made from DMPC, DHPC, and DMPG. All experiments were performed on a Bruker Avance 400 spectrometer operating at 9.4 T corresponding to 400 MHz for protons. Further details are provided in the Supplementary information.

3. Results

3.1. Interaction of Nc and acyl derivatives with lipids

We start by analyzing the degree to which zwitterionic (DOPC) and mixed, partially anionic (80DOPC:20DOPG) lipid vesicles induce structure in the different Nc variants. These vesicles were used as simple mimics of the mammalian plasma membrane (predominantly zwitterionic) and the outer leaflet of the bacterial cell membrane (at least 25% anionic lipid in *E. coli*). The secondary structure of Nc and the acylated derivatives (termed Nc-CX, where X refers to the number of carbon atoms in the acyl chain) was monitored by far-UV CD. Fig. 2A shows the CD spectra of Nc, Nc-C8, Nc-C12, and Nc-C16. Nc, Nc-C8, and low concentrations (40 µM) of Nc-C12 display CD spectra characteristic of a random coil. At high concentrations (200 µM), the CD spectrum of Nc-C12 changes to a distinct α-helical profile with minima at 209 and 222 nm. Nc wt and Nc-C8 remain unstructured at 200 µM (data not shown). The CD spectrum of Nc-C16 is primarily α-helical over the entire accessible concentration range (20–200 µM).

In the presence of 0–2 mg/ml DOPC, Nc shows only a slight change in its CD spectrum, retaining the features of a random coil structure (data not shown) though there is a small increase in ellipticity between 0 and 2 mg/ml lipid (Fig. 2B). This agrees with the observation that high (several hundred mM) concentrations of non-ionic and zwitterionic surfactant are required to induce helical structure in the closely related peptide Novispirin [31]. In contrast, Nc-C8 and Nc-C12 both change from random coil to α-helical structure with increasing concentrations of lipid over the range probed (the spectrum for Nc-C8 shown in Fig. 2A). In the presence of 80DOPC:20DOPG vesicles, the spectra of Nc, Nc-C8, and Nc-C12 changed dramatically from random coil to α-helix (representative spectra shown in Fig. 2A, summarized in Fig. 2C). The ellipticity at 208 nm, which is indicative of α-helical structure, shows a reasonably linear increase with lipid concentration, apart from a more hyperbolic behavior for Nc-C12 in DOPC (Fig. 2B). As we have previously reported for Novispirin [31], this slope most likely represents the initial linear stage of a hyperbolic binding curve, whose slope (summarized in Table 1) is directly proportional to the lipid binding affinity. To avoid artifacts from light scattering, we did not record data at higher lipid concentrations.

For both lipid compositions, Nc wt shows the lowest lipid affinity of all the peptides (measured in terms of α-helix induction), although

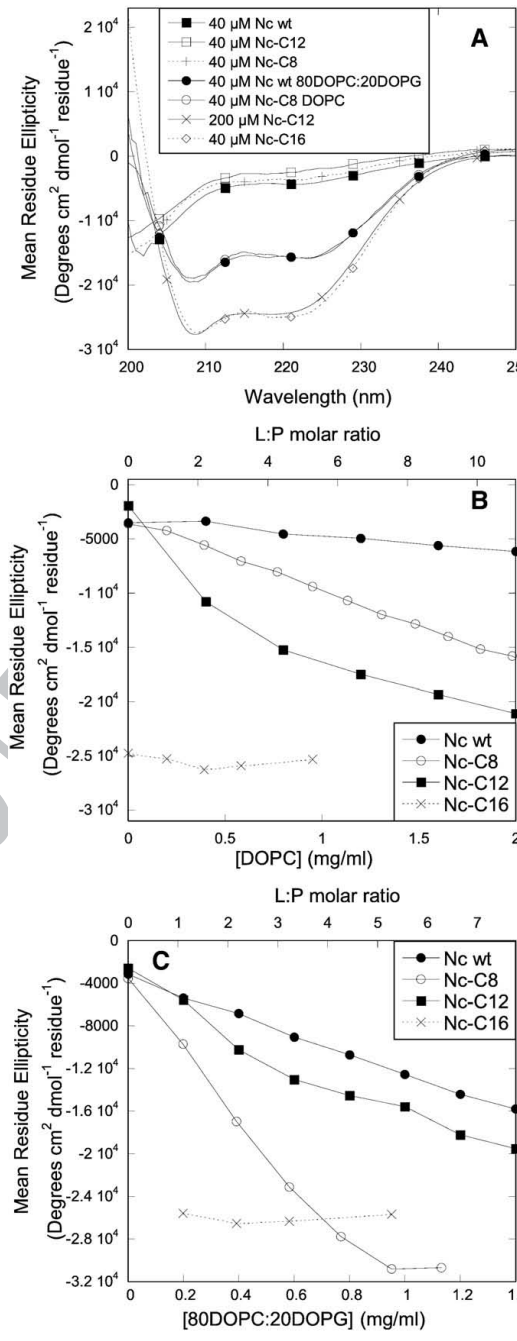

Fig. 2. (A) CD spectra of Nc and acylated derivatives in 20 mM Tris–Cl pH 7.5: 40 µM Nc wt, 40 µM Nc-C8, 40 µM Nc-C12, 200 µM Nc-C12, 40 µM Nc-C16, 40 µM Novicidin in 80DOPC:20DOPG vesicles and 40 µM Nc-C8 in pure DOPC vesicles. Development of CD spectra at 208 nm with the addition of increasing concentrations of (B) DOPC and (C) 80DOPC:20DOPG to Nc wt, Nc-C8, Nc-C12 and Nc-C16.

Please cite this article as: B. Vad, et al., Divorcing folding from function: How acylation affects the membrane-perturbing properties of an antimicrobial peptide, Biochim. Biophys. Acta (2009), doi:10.1016/j.bbapap.2009.12.006

Table 1
Increase in ellipticity at 208 nm of Nc peptides as a function of lipid concentration (units of molar ellipticity per mg/ml lipid × 10^{-3}).[a,b]

Peptide	DOPC	80DOPC:20DOPG
Nc wt	−1.21	−8.98
Nc-C8	−6.56	−29.56
Nc-C12	−8.84[c]	−11.87
Nc-C16	−0.58	−1.15

[a] All data carried out in 20 mM Tris–HCl pH 7.5 at 25 °C. Fits based on data shown in Fig. 2.
[b] These values are not actual affinity constants (since the ellipticity generally increases linearly and does not level off to a plateau level over the concentration range tested) but serve to illustrate the degree to which different lipids can increase the secondary structure of the Nc peptides over the experimentally accessible concentration range.
[c] Data have been fitted to a parabolic equation to derive the slope at zero molar lipid.

it has a clear preference for 80DOPC:20DOPG vesicles where the slope (corresponding to the binding affinity) is ~7 times higher. Nc-C12 has slightly greater affinity for DOPC than Nc-C8, but the switch to 80DOPC:20DOPG vesicles only increases Nc-C12 affinity by around 30% while that of Nc-C8 increases 5-fold. The CD spectra of Nc-C16 remained essentially unchanged by the addition of both lipid types. The reduced effect of anionic lipids likely reflects the increased propensity of the acylated peptides to form α-helical structures on their own (see Discussion).

3.2. Acylation leads to a marked decrease in the efficiency of lipid permeabilization

We now turn to a functional analysis of the Nc peptides, *i.e.* their ability to permeabilize vesicles, using a manual calcein release assay.

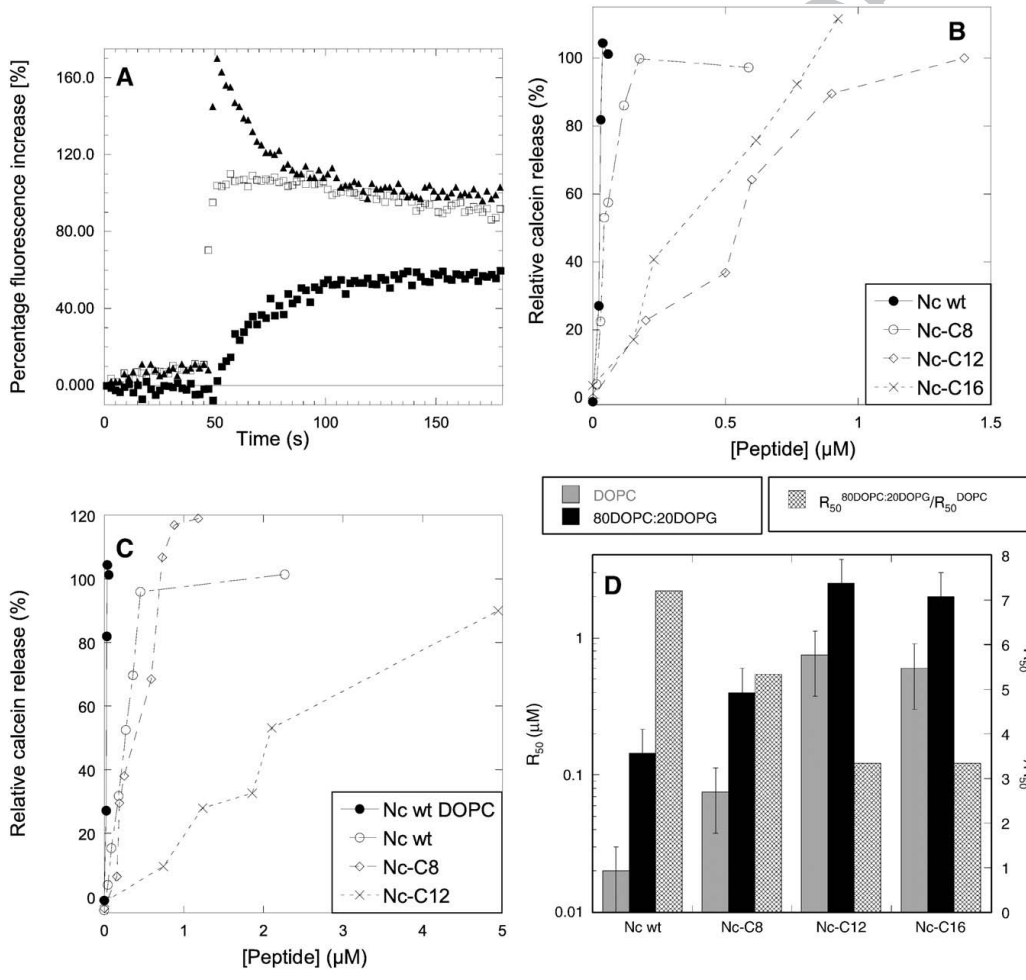

Fig. 3. (A) Typical time profile of calcein release by Nc and derivatives. Signal normalised relative to signal upon the addition of Triton X-100 (see Materials and methods). With the addition of Nc and acylated derivatives to calcein-loaded vesicles three distinct calcein release patterns are observed in steady-state fluorescence measurements. A slow release leading with the curve displaying second order characteristics (■), a fast release with a fluorescence increase between 0- and 100% (□), and finally a fast release with an overshoot which after ~1 min reach decreases to 100% (▲). Injection occurs in all cases at 50 s. (B and C) Nc and the acylated derivatives were added to calcein-loaded vesicles composed of (B) DOPC and (C) 80DOPC:20DOPG (data for Nc in DOPC included for comparison). The normalised maximum fluorescence was plotted as a function of protein concentration. (D) Peptide concentrations needed for 50% calcein release (R_{50}) from DOPC vesicles and 80DOPC:20DOPG vesicles and the ratio between these two values. Errors based on duplicate measurements.

Please cite this article as: B. Vad, et al., Divorcing folding from function: How acylation affects the membrane-perturbing properties of an antimicrobial peptide, Biochim. Biophys. Acta (2009), doi:10.1016/j.bbapap.2009.12.006

We prepared LUVs containing calcein at a concentration (50 mM) in which calcein fluorescence is self-quenched, and measured the release of calcein as function of peptide concentration, using the addition of Triton X-100 to obtain the fluorescence level associated with 100% release. The presence of calcein did not affect the ability of lipids to induce structural changes in the peptides (data not shown), nor did Triton X-100 influence the fluorescence of calcein (data not shown).

Three distinct calcein release patterns were observed (Fig. 3A): (*i*) instantaneous (<10 s) calcein release, followed by a steady baseline (mainly seen for acylated Nc), (*ii*) relatively rapid release of calcein which could be described by first order kinetics with a plateau being reached after a few minutes (mainly seen for wt Nc), or (*iii*) rapid overshoot of fluorescence to a value well above that of free calcein, followed by a decrease to a signal corresponding to roughly 100% calcein release (seen at high concentrations of all 4 peptides)The fraction of calcein released as a function of peptide concentration in the two different lipid compositions is illustrated in Fig. 3B–C. The efficacy of release is quantified by the amount of peptide needed to effectuate 50% calcein release (R_{50}). In all cases, very high concentrations of peptide lead to a drop in calcein release (data not shown), possibly due to vesicle aggregation (*vide infra*).

The ranking order of the lipolytic effect of the peptides is as follows (summarized in Fig. 3D): Nc > Nc-C8 > Nc-C16 > Nc-C12. For all of the peptides, it was apparent that R_{50} increased in 80DOPC:20DOPG vesicles. The ratio $R_{50}^{\mathrm{DOPC:DOPG}}/R_{50}^{\mathrm{DOPC}}$ (the higher this ratio, the greater the preference for DOPC) decreased in the order Nc > Nc-C8 > Nc-C12 ~ Nc-C16, reaching a plateau of around 3 for Nc-C12 and Nc-C16. This indicates that the more hydrophobic the peptide, the lower the preference for DOPC vesicles. For Nc-C8 and Nc-C12 these permeabilization data contrast with the structural data provided by CD, which reveal that acylation decreases the preference for 80DOPC:20DOPG vesicles in terms of inducing α-helicity.

3.3. Exposure of *E. coli* to Nc variants shows that acylation reduces the efficacy of Nc as an antimicrobial peptide

To compare the data on synthetic vesicles with Nc's biological targets, *i.e.* bacteria, we measured the lysis of *E. coli* at different concentrations of the Nc variants. Lysis was measured by the release of cytosolic β-galactosidase, monitored by the hydrolysis of the chromogenic substrate *o*-nitrophenyl galactose. All peptides lead to the same level of release at concentrations around 20–40 μM (Fig. 4A), but differ at lower concentrations. When we quantify this as $[\mathrm{Nc\text{-}X}]^{50\%}$, the concentration of Nc at which release is 50% of the maximal value, we obtain a value of ~1 μM for Nc wt and values of 5–7 μM for all 3 acylated peptides. An even clearer picture emerges from MIC (minimal inhibitory concentration) assays (Fig. 4B), which reveal that Nc-C8 has a ~3-fold reduction in efficacy compared to Nc wt, while Nc-C12 and Nc-C16 hardly have any inhibitory effect at all. Thus, both in calcein assays and biological assays, unacylated Nc permeabilizes membranes more efficiently than acylated Nc. This membrane-lysing activity does not have any unwanted side effect, since hemolysis assays do not reveal any of the Nc peptides to have lytic activities against red blood cells at concentrations up to several mM (data not shown).

3.4. Fluorescence anisotropy measurements show that Nc mobility is decreased upon mixing with DOPC and 80DOPC:20DOPG vesicles

The calcein release measurements indicate that Nc binds to and permeabilizes both neutral and partially anionic vesicles, although CD titration data show that α-helical structure is only induced in the partially anionic vesicles. This suggests that induction of α-helix structure in peptides that are unstructured in solution is not a prerequisite for AMP action. To monitor binding independent of

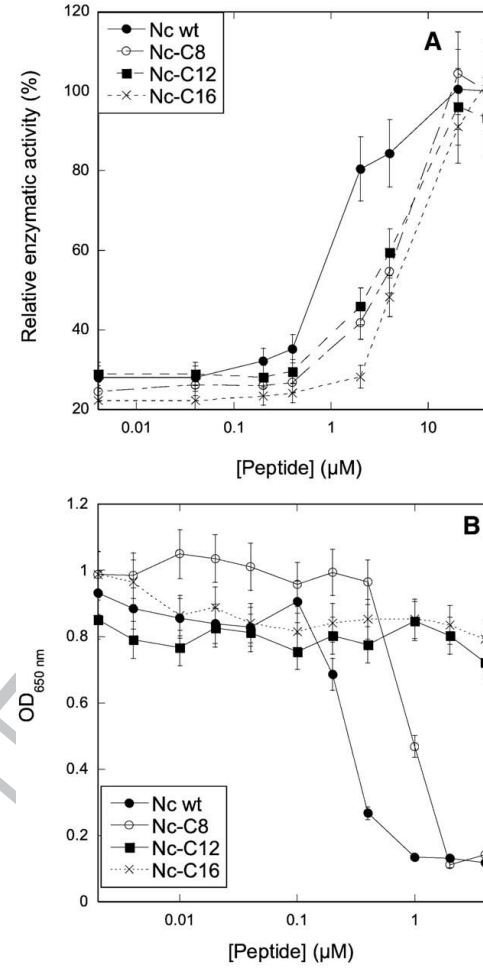

Fig. 4. (A) Degree of release of β-galactosidase from *E. coli* by different concentrations of Nc and acylated variants hereof. Errors in individual measurements ~7% based on duplicate measurements. (B) MIC assay performed on *E. coli* using different concentrations of Nc and acylated variants hereof. Errors in individual measurements ~15% based on duplicate measurements. Clearly Nc wt is the most effective at reducing *E. coli* growth while Nc-C12 and Nc-C16 hardly have any effect at all.

folding, we used a Dansyl-labelled variant of unacylated Nc (Dansyl-Nc) to measure how the fluorescence anisotropy of the dansyl group changes as lipid is added. Immobilization of the peptide on the vesicle surface is expected to lead to a significant increase in anisotropy. Upon increasing the concentrations of lipid, we observe a hyperbolic binding curve which for both DOPC and 80DOPC:20DOPG vesicles reaches a plateau at a lipid:protein molar ratio of ~250 (Fig. 5A). Lipids were added stepwise to a single Dansyl-Nc solution. We were able to probe higher lipid:peptide ratios than in the CD experiments because of the low concentrations of Dansyl-Nc required for these experiments. To obtain reproducible results, we had to let the system equilibrate for a few minutes before recording anisotropy, particularly at the lower concentrations. This is most likely due to reorganization of the lipids into micellar-like structures as we can see from our calcein release measurements that the binding happens on a much

Please cite this article as: B. Vad, et al., Divorcing folding from function: How acylation affects the membrane-perturbing properties of an antimicrobial peptide, Biochim. Biophys. Acta (2009), doi:10.1016/j.bbapap.2009.12.006

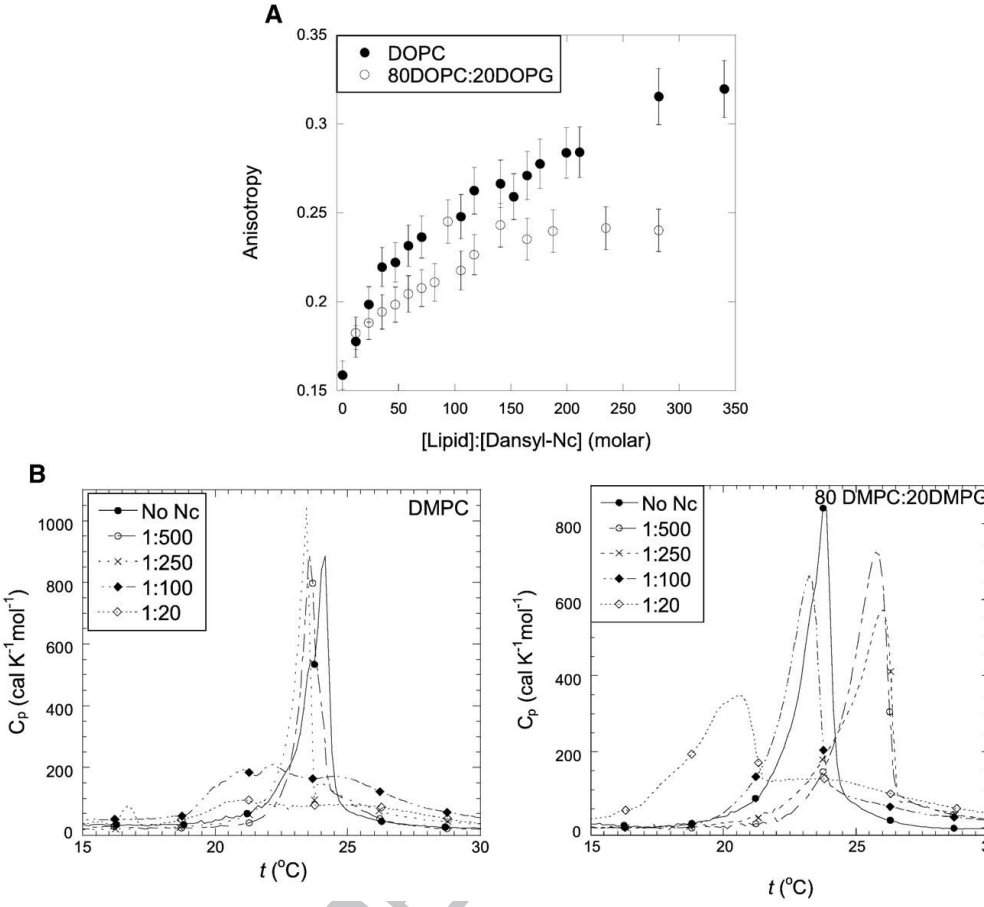

Fig. 5. (A) Anisotropy measurements of Dansyl-Nc in increasing concentrations of pure DOPC and 80DOPC:20DOPG. The vesicles were allowed to equilibrate for 1 min before each measurement. (B) DSC scans of DMPC and 80DMPC:20DMPG at different peptide–lipid ratios. Legend indicates Nc wt:lipid ratio (molar ratio).

faster timescale. We observe a slightly larger increase in fluorescence anisotropy for the DOPC vesicles. This could tentatively be interpreted as increased propensity to aggregate and thus permeabilize these vesicles compared to 80DOPC:20DOPG vesicles (cf. Fig. 3D). Alternatively, the peptide could be localized in a deeper and more ordered part of the bilayer in the DOPC vesicles, leading to a more pronounced effect on the lipid transition (see below).

3.5. DSC experiments reveal Nc interactions with both lipid types

Further evidence for the strong interaction of Nc with zwitterionic as well as partially anionic vesicles comes from differential scanning calorimetry experiments, where we monitor the phase transition temperature t_m in the presence of different concentrations of Nc. Here we use DMPC and 80DMPC:20DMPG where the transition temperature (23 °C in the absence of peptide) is experimentally accessible. Even at P:L ratios as low as 1:500, Nc wt has a marked effect on the transition (Fig. 5B) but the details are different for the two lipids: for DMPC, t_m declines by a few degrees as we go from 1:500 to 1:250 P:L and is replaced by a much broader transition at 1:100 and 1:25 P:L. For 80DMPC:20DMPG, there is a rise in t_m at the two lowest P:L ratios followed by a decline; the broad transition is only observed at the highest P:L.

3.6. Dansyl-labelled Nc highlights differences in peptide insertion into different lipids

We combined the time-resolution of stopped-flow kinetics with the environmental sensitivity of a Dansyl fluorophor, attached to the N-terminus of unacylated Nc, to investigate the coupling between peptide binding and calcein release. The Dansyl probe increases the hydrophobicity of Nc and this might be expected to lead to an increased partitioning into the membrane. Accordingly, Dansyl-Nc shows a ~3-fold higher affinity towards DOPC and 80DOPC:20DOPG vesicles compared to Nc wt, measured in terms of increased α-helicity (data not shown). However, Dansyl-Nc shows the same 6–7 fold preference for 80DOPC:20DOPG over DOPC as Nc wt does (Table 1), making it a valid probe for measuring binding to different membrane types. When Dansyl-Nc is mixed with DOPC vesicles, we observe a slight increase in Dansyl fluorescence prior to vesicle disruption (indicated by the increase in calcein fluorescence), indicating a modest degree of peptide interaction with the membrane before disruption (Fig. 6A). However,

Please cite this article as: B. Vad, et al., Divorcing folding from function: How acylation affects the membrane-perturbing properties of an antimicrobial peptide, Biochim. Biophys. Acta (2009), doi:10.1016/j.bbapap.2009.12.006

when Dansyl-Nc is added to 80DOPC:20DOPG vesicles, we observe a 10-fold higher increase in Dansyl fluorescence (compared to DOPC), which also precedes vesicle disruption (Fig. 6B). This increased Dansyl fluorescence in 80DOPC:20DOPG vesicles compared to DOPC vesicles indicates that Novicidin undergoes a greater change in environmental polarity when it inserts into 80DOPC:20DOPG vesicles. This suggests that Nc inserts more deeply into the 80DOPC:20DOPG membrane than into the pure DOPC membrane. We also observe an additional increase in Dansyl fluorescence during the process of calcein release from 80DOPC:20DOPG vesicles, suggesting a further rearrangement of Dansyl-Nc in the 80DOPC:20DOPG membrane upon vesicle disruption.

3.7. Nc peptides cause vesicle leakage, aggregation and lysis

Confocal laser scanning microscopy (CLSM) with giant unilamellar vesicles (GUVs) provides an alternative way of elucidating the mechanism of action of the different peptides, since we can focus on individual vesicles rather than measuring ensemble changes. The GUVs contained a lipid fluorophor (DiIC18) and were loaded with membrane impermeable water-soluble fluorophors (Alexa^{488} for 80DOPC:20DOPG vesicles and Alexa^{633} for DOPC vesicles), allowing us to monitor changes in both membrane integrity and permeability. The increased imaging facilities come at the expense of kinetic resolution, because diffusion limitation led to typical lag times of 10–15 min until the added peptide reached the field of vision, which makes it unrealistic to compare with the time profile provided by stopped-flow experiments. As illustrated in Fig. 7 and summarized in Table 2, the interactions between peptide and vesicle could be classified into three groups: (i) slow leakage that led to complete release of the vesicle content over 5–10 min, leaving an empty but intact vesicle behind; (ii) vesicle aggregation where the vesicles clump together, without necessarily facilitating the release of trapped fluorophor and (iii) vesicle lysis, causing immediate release of the vesicle content and complete loss of vesicle structure. Within the framework of current models for AMP action, (i) is most simply interpreted as pore formation and (iii) as the carpet model for membrane lysis, whereas (ii) represents an alternative class of interactions which do not occur in the absence of Nc and which to our knowledge has not been described before using CLSM. Images recorded at different stages of the process are provided in the Supplementary material.

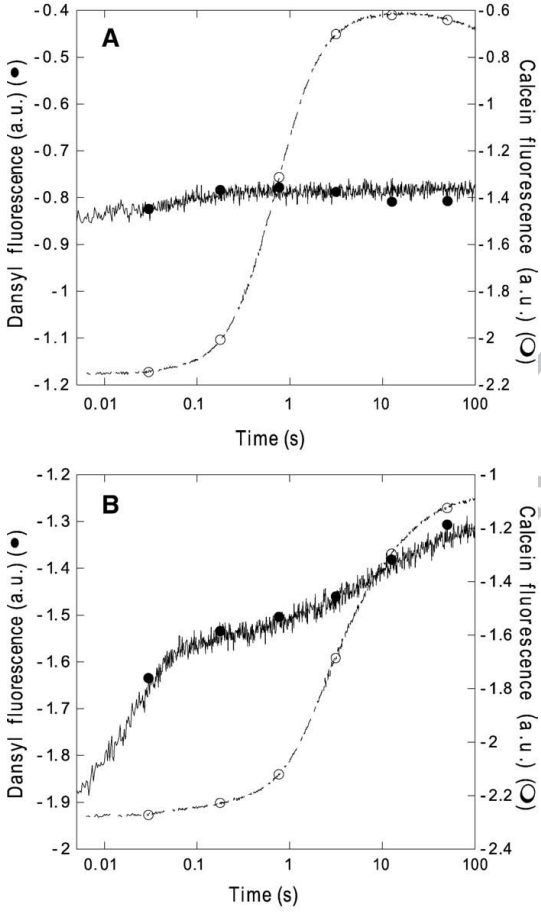

Fig. 6. Stopped-flow analysis of Nc interactions with lipids. Upon the addition of Dansyl-Nc we observe an increase for the dansyl fluorescence for both vesicles composed of DOPC (A) and 80DOPC:20DOPG (B) before an increase in the calcein fluorescence. In DOPC vesicles, there is a small increase in dansyl fluorescence due to binding (up to 0.1 s) followed by release of vesicle contents over 0.1–10 s. For the 80DOPC:20DOPG vesicles, there is a large fluorescence increase from the dansyl probe up to ~0.1 s and an additional slower increase up to 100 s (possibly due to lipid rearrangements) while calcein release occurs over the period 1–100 s.

Nc wt added to DOPC vesicles caused both vesicle lysis and aggregation (Table 2). The fused vesicles seemed partially stabilized, as they were the last to rupture and little to no leakage was observed. For Nc, it was clear that there was a higher degree of vesicle aggregation when the vesicles contained 20% DOPG. The aggregation of both vesicle types caused partial entrapment of the water-soluble probe and leads to larger particles with greater light-scattering properties. This could very well explain the overshoot in steady-state measurements at high concentrations that was more prominent with 80DOPC:20DOPG vesicles. For both vesicle types, both lysis of the vesicles and slow leakage was observed during and after the aggregation of the vesicles. The increase in vesicle aggregation observed with 80DOPC:20DOPG vesicles might be explained by favorable electrostatic interactions between adsorbed (cationic) Nc and neighbouring (anionic) vesicles. We have also observed aggregation of the related peptide Novispirin in the presence of different concentrations of SDS [31].

The addition of Nc-C8 to either DOPC vesicles or 80DOPC:20DOPG vesicles did not cause vesicle aggregation to any observable degree, but we did observe vesicle lysis. Vesicle leakage was only evident for 80DOPC:20DOPG vesicles. The leaky vesicles retained their structural integrity despite the fact that they did not aggregate, in contrast to observations with Nc. Nc-C12 did not cause slow leakage from neither DOPC nor 80DOPC:20DOPG vesicles but resulted in vesicle lysis, and, in contrast to Nc-C8, also led to vesicle aggregation. Thus, vesicle aggregation seems to be independent of whether the peptide causes lysis or leakage. For Nc-C16 the vesicle leakage behavior was comparable to that of Nc for both DOPC and 80DOPC:20DOPG vesicles but Nc-C16 caused an equally high degree of aggregation of vesicles irrespective of their lipid composition.

We also investigated the behavior of Nc when presented with a mixed population of different vesicles. In the presence of both DOPC and 80DOPC:20DOPG vesicles, we see a clear preference for the vesicles containing DOPG. We distinguish between the two vesicle types by filling them separately with different water-soluble fluorophores (Alexa^{488} for DOPC versus Alexa^{633} for 80DOPC:20-DOPG). While the 80DOPC:20DOPG vesicles behave more or less in the vesicle mixture as we have observed for neat 80DOPC:20DOPG vesicles (both aggregation, lysis and leakage are observed), we only observe rupturing of a few of the DOPC vesicles in the mixture. This indicates that the 80DOPC:20DOPG vesicles compete effectively

Please cite this article as: B. Vad, et al., Divorcing folding from function: How acylation affects the membrane-perturbing properties of an antimicrobial peptide, Biochim. Biophys. Acta (2009), doi:10.1016/j.bbapap.2009.12.006

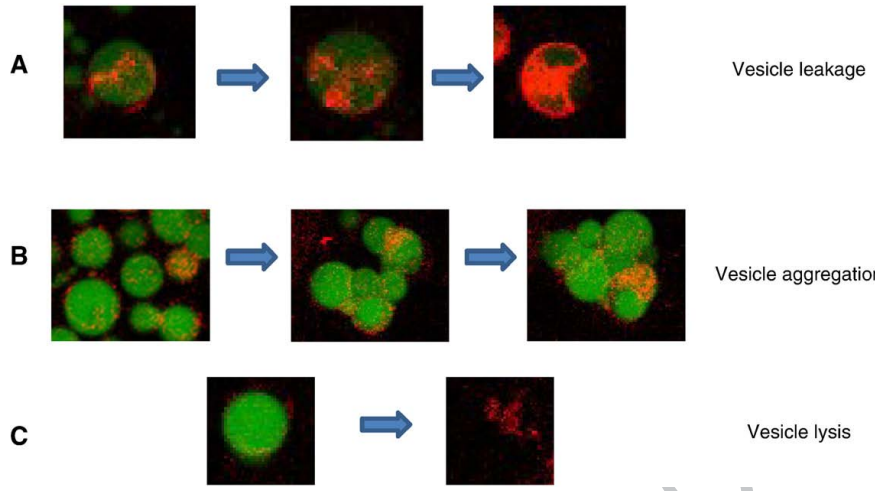

Fig. 7. Representative multicolour fluorescence images of Alexa^{488} (green colour) loaded lipid vesicles with DiIC18 (red colour) incorporated in the membrane obtained by confocal laser scanning microscopy. In the presence of Nc and acylated derivatives, we observe three distinct modes of action, namely (A) vesicle leakage, (B) vesicle aggregation and (C) vesicle lysis. The relative preferences for the three modes of action are summarized in Table 2. The arrows represent the flow of time, but the length of time is not specified due to different kinetics with different peptides and lipids. (For interpretation of the references to colour in this figure legend, the reader is referred to the web version of this article.)

with pure DOPC vesicles in attracting free Nc (see Supplementary material).

3.8. Nc-C16 is more deeply embedded in micelles than Nc wt

In order to analyze the effect of acylation on Nc's anchoring in amphiphilic environments, we have used solution-state NMR to determine the structure and extent of insertion of Nc-C16 in zwitterionic (DPC) micelles. The structure was determined with traditional homonuclear 2D-spectra for the proton shift assignment and $^{1}H-^{13}C$-HSQC natural abundance spectra for the C^{α} and C^{β} shift assignment. Key values of the structure calculation are listed in Table 3. The structure of Nc-C16 consists of a single slightly bent amphipathic α-helix with the acyl chain attached to the N-terminal part of the peptide (Fig. 8A). Similar structures have been reported for the homologous peptides Ovispirin and Novispirin in SDS micelles [37–39]. The only NOE cross peaks between the peptide and the attached acyl group that could be assigned were the correlation between the H^{N} of residues 1–3 and the protons located on the fatty acid α-carbon atom. In the calculated structures the acyl chain therefore appears highly flexible without this necessarily being correct.

To determine the relative insertion depths of Nc and Nc-C16 in DPC micelles, samples with the micelle bound peptides were titrated with the paramagnetic agent Gd(DTPA-BMA) that is known not to interact with peptides and micelles [36,40]. T_1 relaxation values for the H^{α} protons in the peptides were calculated from peak volumes of cross peaks with the H^{α} atom appearing in the indirect dimension of inversion-recovery weighted NOESY spectra. The R_1 relaxation rates of the H^{α} atoms measured at different concentration of Gd(DTPA-

Table 2
Summary of confocal laser scanning microscopy experiments with Nc and acylated derivatives, indicating the propensities of the peptides for three different kinds of vesicle interactions (illustrated in Fig. 7).[a]

Peptide	DOPC vesicles	80DOPC:20DOPG vesicles
Vesicle leakage		
Nc wt	+	+++
Nc-C8	−	+
Nc-C12	−	−
Nc-C16	+	+++
Vesicle aggregation		
Nc wt	+	+++
Nc-C8	−	−
Nc-C12	++	+
Nc-C16	+++	+++
Vesicle lysis		
Nc wt	++	+
Nc-C8	+++	++
Nc-C12	+++	+++
Nc-C16	++	+

[a] For practical reasons, all experiments were performed at pH 6 and at 15 °C. The degree of leakage, aggregation and lysis was based on a relative comparison between the different samples.

Table 3
Quality criteria for the calculated Nc-C16 structures.

Number of distance constraints	271
Of which intraresidual	136
Of which sequential	69
Of which medium-range ($2 \leq \Delta_{res} \leq 4$)	66
Number of angle constraints[a]	26
Of which φ	13
Of which ψ	13
CYANA residual target function	0.89 ± 0.04 Å^2
Distance restraints violated by more than 0.2 Å	0
Angle restraints violated more than 5°[b]	0
rmsd residues 2–17[c]	0.13 ± 0.08 Å
% of residues in Ramachandran plot	
In most favored regions	91.5
Less favored regions	7.6
Generously allowed regions	0.9
Disallowed allowed regions	0

[d]As calculated by PROCHECK_NMR.
[a] Only those derived from TALOS.
[b] Per molecule.
[c] For backbone atoms C′, C^{α} and N, as calculated by CYANA from the pairwise rmsd values of each of the 20 structures against a mean structure.

Please cite this article as: B. Vad, et al., Divorcing folding from function: How acylation affects the membrane-perturbing properties of an antimicrobial peptide, Biochim. Biophys. Acta (2009), doi:10.1016/j.bbapap.2009.12.006

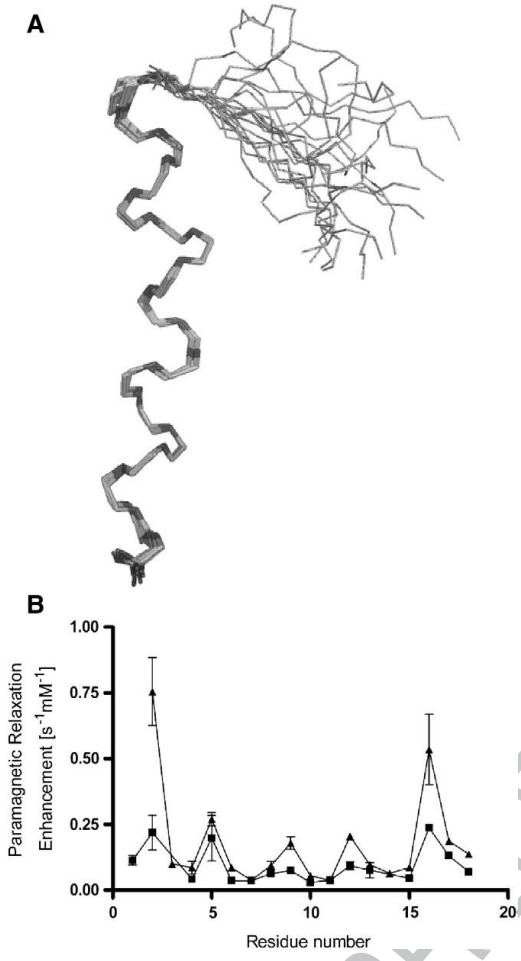

Fig. 8. (A) Structure of Nc-C16 in the presence of DPC. Superposition of the 20 backbone conformers with the lowest cyana target function representing the 3D NMR structure. The bundle is obtained by superimposing the backbone C^{α}, C, and N atoms of residues 2–17. The carbon atoms of the acyl chain are clearly seen extending from the N-terminal part of the peptide. (B) PRE values of H^{α} nuclei of Nc (▲) and Nc-C16 (■) as a function of residue numbers. Error bars indicate variations in PRE values obtained from fitting several peaks.

BMA) were subsequently plotted against the concentration of the paramagnetic agents giving the paramagnetic relaxation enhancement (PRE) values of the atoms.

In Fig. 8B the H^{α} PRE values of Nc and Nc-C16 can be seen as a function of the residue numbers. The PRE curves of both peptides give a wavelike pattern with a wavelength of either 3 or 4 residues between the maxima of the PRE curves which for both peptides are located at the residues Asn-2, Arg-5, Lys-9, His-12 and Lys-16 corresponding to the hydrophilic side of the amphipathic helix.

As the PRE values depend on the inverse of the sixth power of the distance between the hydrogen and the paramagnetic atom [40], the results shows that the hydrophilic side of the helix is facing the outside of the micelle as expected. The PRE values of the Nc atoms are significantly larger than the corresponding atoms in Nc-C16 which clearly indicates that the acylated variant of Novicidin is buried deeper into the micelles. This difference is most pronounced for Asn2 in the N-terminal part of the peptides where the acyl chain of Nc-C16 is attached, which suggests that the hydrophobic acyl chain of Nc-C16 is pulling the N-terminus of the peptide towards the hydrophobic core of the micelle. This increased immersion then appears to be transmitted along the helix backbone to the rest of the peptide all the way to the C-terminus, probably reflecting an overall increase in the membrane partitioning coefficient.

3.9. Solid-state NMR experiments reveal stronger interactions of acylated Nc with lipids

We now turn from Nc–detergent to Nc–lipid interactions using oriented-sample solid-state NMR spectroscopy. Atomic-resolution details on the insertion of the different variants of Nc into different phospholipids may be obtained by recording ^{1}H–^{13}C PISEMA spectra [41] of natural abundance samples with the peptides reconstituted into bicelles (formed by DMPC:DMPG:DHPC lipids at different ratios) produce bicelles with the right size and charge properties. Note that DMPC:DMPG based membranes was chosen instead of DOPC:DOPG membranes to follow known recipes [42] for production of stable bicelles. To the best of our knowledge, such recipes are not established for DOPC/DOPG membranes. Accordingly, direct comparison of biophysical and solid-state NMR data has to be conducted under the precaution that lipid chain-length and saturation may influence details of the membrane–peptide interactions. The DMPC:DMPG:DHPC bicelles orient in a strong magnetic field with the bicelle normal perpendicular to the field direction, enabling measurement of anisotropic (i.e., orientation-dependent) chemical shift and dipole–dipole coupling interactions for the various CH_n groups in the lipids. Accordingly, the ^{1}H–^{13}C PISEMA experiments may be used correlate orientation-dependent ^{13}C chemical shifts with ^{1}H–^{13}C dipole–dipole couplings for the abundant lipid molecules as demonstrated previously for other systems by Ramamoorthy and coworkers [43,44]. By monitoring the positions and lineshapes of the resonances for various lipid carbons in 2D PISEMA spectra, it is possible to probe small differences in local dynamics and orientation of the lipid functional groups and thereby get information about the influence of the peptides on the various parts of the lipids. This is illustrated in Fig. 9, with Fig. 9A showing a representative full 2D PISEMA spectrum of DMPC:DHPC bicelles containing Nc wt (molar ratios Nc wt:DMPC:DHPC 1:57:18), Fig. 9B the molecular structure of DMPC with indication of three representative functional groups, and Fig. 9C–H excerpts for these functional groups from 2D PISEMA spectra recorded using different lipid:peptide systems. The full PISEMA spectrum demonstrates correlation between ^{1}H–^{13}C dipole–dipole couplings (giving rise to multiplets/splittings in the horizontal direction) and ^{13}C chemical shifts for the highly abundant lipid CH_n groups. Variations in the orientation-dependent dipole–dipole coupling and chemical shifts upon mixing in peptides to the membranes will probe peptide:lipid interactions with spatial resolution through observation of distinct signals for the various lipid carbons.

The PISEMA spectrum excerpts (Fig. 9C–H) originate from samples with pure lipid (red line), lipid and Nc wt (green line), lipid and Nc-C8 (blue line), and lipid and Nc-C16 (magenta line) with the lipids being either pure zwitterionic bicelles (DMPC together with DHPC, Fig. 9C–E) or a mixtures of zwitterionic and anionic bicelles (molar ratios Nc:DMPC:DMPG:DHPC 1:46:10.6:17.7, Fig. 9F–H). The spectra report the perturbation of headgroup (C_{α}), a central carbon (C_3), and a terminal acyl carbon (C_{14}) according to the structural model given in Fig. 9B. In addition to contour plots from relevant parts of the 2D PISEMA spectra for the four different samples, the individual panels also contain sum projections (left and top) onto the ^{13}C chemical shift axis (vertical) and the ^{1}H–^{13}C dipolar axis (horizontal). The individual panels also contain (right and bottom) the corresponding traces taken through the maximum point of the 2D spectra for the peptide-free

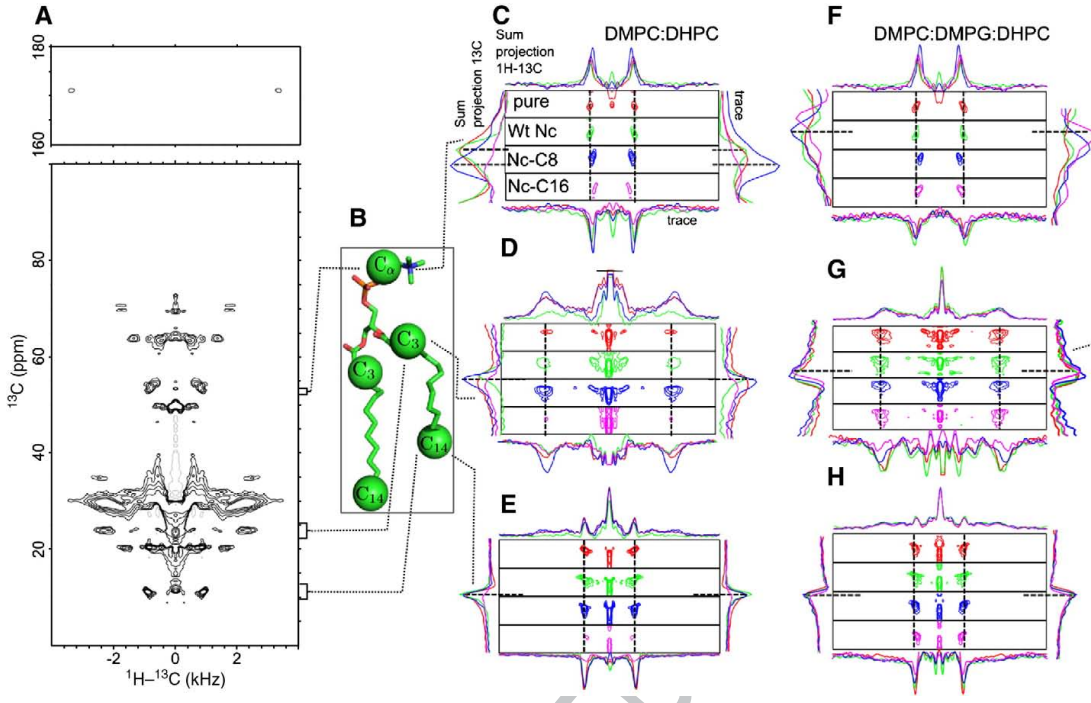

Fig. 9. Solid-state NMR spectra of Novicidin and acetylated variants in pure and mixed lipids. (A) Full ^{1}H–^{13}C dipole–dipole couplings versus ^{13}C chemical shift correlated PISEMA spectrum of DMPC:DHPC bicelles including Nc wt (molar ratios Nc:DMPC:DHPC of 1:57:18). (B) Molecular model of DMPC with indication of the C_α, C_3, and C_{14} carbons through which excerpts of PISEMA spectra (C–H) are taken. (C–H) Each panel describes four different bicelle samples containing either; pure lipid bicelle (red), lipid and Nc wt (green), lipid and Nc-C8 (blue) and lipid with Nc-C16 (magenta). Each panel consists of an excerpt from 2D ^{1}H–^{13}C PISEMA spectra of DMPC:DHPC or DMPC:DMPG:DHPC bicelles as well as sum projections and traces along the position of the pure bicelle for both the ^{1}H dimension and the ^{13}C dimension. (C–E) describe the spectral changes observed for zwitterionic bicelles. (F–H) describe the spectral changes observed for a mixture of zwitterionic and anionic bicelles (molar ratios Nc:DMPC:DMPG:DHPC 1:46:10.6:17.7). The focus is on three representative regions describing the lipid head group (C, F), the central part of the lipid molecule (D, G), and the lipid tail region (E, H). (For interpretation of the references to colour in this figure legend, the reader is referred to the web version of this article.)

bicelles. While changes in the local environment (structure/orientation and time averaged dynamics) may be monitored from the 2D contours as well as the projections, it is evident that most sensitivity towards minor changes in peak positions will be probed through the traces. Note that all samples were prepared with approximately the same peptide concentration. Furthermore, the calcein release data (Fig. 3) suggest that Nc will display stronger interactions with zwitterionic vesicles than with the mixed zwitterionic and anionic vesicles. However, the CD data (Fig. 2) suggest that 80DOPC:20DOPG vesicles bind Nc more strongly.

From the upper panels in Fig. 9C–H, it becomes evident that Nc as well as the acylated Nc variants interact with the headgroup of both types of lipids. This is seen from the position and shape of the contours, and very clearly from the traces taken at the position of the resonance in the pure lipid spectra. A closer inspection of the spectra provides a more diverse set of observations for a deeper penetration of the peptides into the various lipids. From Fig. 9C–E column, it is seen that Nc-C16 interacts with all carbon sites of the zwitterionic lipids and thereby may adapt a transmembrane (or transiently transmembrane) configuration with significant effect on the carbons on the central region of the lipids. Note that in the absence of NMR signals from the peptide, we cannot determine whether it is the acyl chain or the peptide backbone that is transmembrane. In contrast, it appears that largely only the headgroup region (C_α and C_3 carbons) are affected by the peptides with shorter or no acylation. Turning to the DMPC:DMPG:DHPC lipid bicelles (Fig. 9F–H column), it appears that the perturbing effect from the various peptides on the local environment of the lipids are somewhat less pronounced (weaker interactions) and to a large extend only influence the headgroup region. For the Nc wt sample only a slight shift in the resonance position is observed for the α and β (not shown) carbons, indicating a relatively weak perturbation as compared to the interaction with the pure bicelles.

The observed changes (summarized in Table 4) overall indicate that Novicidin and its acylated variants mainly interact with the surface of bicelles composed of zwitterionic and anionic lipids, while more pronounced interactions are observed for the pure zwitterionic

Table 4
Summary of peptide induced-perturbation of CH_n groups in the headgroup (C_α), central (C_3), and tail (C_{14}) regions of zwitterionic (DMPC) and mixed zwitterionic and anionic (DMPC:DMPG) bicelles.[a]

	Peptide	DMPC	DMPC:DMPG (4:1)
Headgroup (C_α)	Nc	++	+
	Nc-C8	+++	++
	Nc-C16	+++	++
Central (C_3)	Nc	++	−
	Nc-C8	++	+
	Nc-C16	++	++
Tail (C_{14})	Nc	−	−
	Nc-C8	−	−
	Nc-C16	+++	+

[a] See labelling of lipid functional groups in Fig. 9G.

Please cite this article as: B. Vad, et al., Divorcing folding from function: How acylation affects the membrane-perturbing properties of an antimicrobial peptide, Biochim. Biophys. Acta (2009), doi:10.1016/j.bbapap.2009.12.006

lipids. In the latter case is seems that addition of acyl chains accelerates the interaction with perturbation of the inner parts of the membrane for the Nc-C16 acylation. We note that the $^{1}H–^{13}C$ PISEMA experiments do not provide information on whether this transmembrane perturbation is caused by the formation of ion channels (barrel stave) or static/transient incorporation of monomer/oligomers of acylated peptides. We note that, in full consistency with the NMR observations, the biophysical measurements report the strongest membrane perturbation for the DOPC vesicles, with the requirement of less peptide to penetrate/perturb the vesicles relative to the 80DOPC:20DOPG vesicles — although this appears to occur with very little induction of secondary structure.

4. Discussion

4.1. Acylation promotes higher-order assemblies and α-helical structure

The CD spectra of Nc and the acylated derivatives in buffered solution clearly show that the C12 and C16 acyl chains changed the peptide structure. Nc-C12 is random coil at 40 μM but α-helical at 200 μM, whereas Nc-C16 was α-helical at all measured concentrations (10–100 μM). For Nc-C12, this can be explained by the peptides arranging in a surfactant like fashion (aided by the acyl chain's desire to avoid an aqueous environment) with a critical micelle concentration (CMC) between 40 and 200 μM. Micelle formation results in an α-helical structure, as described by Makovitzki et al. [20]. For Nc-C16, the CMC is either below the peptide concentration tested in this study (i.e. <10 μM) or the structure is stabilized in a different fashion, possibly existing only as a monomer. Solution-state NMR experiments on pure samples of Nc-C12 and Nc-C16 in the absence of lipids showed that both derivatives at ~1 mM in aqueous buffer formed aggregates that did not yield any useful NMR signals (M. F. and R. W., unpublished data). However, when dispersed in DPC, Nc-C16 yielded well-defined NMR spectra. In addition, Dufour et al. [45] have studied linearized versions of the lipopeptide surfactin and found that C10, C14, and C18 surfactin had CMC values of 1113, 301, and 8 μM respectively. These values are consistent with our own observations and also support the Nc-C16 micellization. In principle, the acyl chain could also pack against the peptide at the monomer level provided a suitably hydrophobic binding surface was available as suggested by Makovitzki et al. [20]. A helix projection of Nc (Fig. 1) highlights a perfectly amphipathic helix with a sharp distinction between a hydrophobic face (only interrupted by Gly10) and a cationic face, where the acyl chain is attached to first residue placed in the middle of the cationic face. Nevertheless, Nc-C16's apparent micellization suggests that the C16 chain engages in inter- rather than intramolecular packing. It is likely that the precise site of attachment of the acyl chain will dictate whether it is more favorable for the chain to dock against the peptide, engage with other acyl chains in an intermolecular micellar arrangement, or even combine the two types to form small micelles that also incorporate the peptide, as suggested for the lipopeptides elegantly developed by Privé et al. [46].

It is worth considering how these aggregative tendencies may influence subsequent vesicle interactions: We have a system with two defined states, one monomeric where the peptide has a random conformation, the other most likely multimeric where the peptide has an α-helical structure. Let us assume that the peptide initially inserts as a monomer into the lipid bilayer (even if it binds as a multimer it is likely to rearrange its higher-order arrangement in the bilayer, and possibly monomerize, due to the change in environment). In that case binding will need to be preceded by micelle dissociation above the CMC of the lipopeptide micelle (which is <10 μM for Nc-C16 and between 40 and 200 μM for Nc-C12). Detergent micellar dynamics typically involve two relaxation processes, namely the dissociation of monomer from micelles (on the μs scale) and micelle break-up (on the minute scale depending on the biophysical properties of the detergent) [47]. Thus, we do not consider it likely that monomer dissociation from micelles is rate-limiting for the kinetics of binding of acylated Nc to membranes.

Furthermore, we do not expect the acylated peptides' aggregation tendencies to play significant roles in their membrane permeabilizing and antimicrobial properties for three reasons: Firstly, these activities are measured at very low concentrations where aggregation in solution is very insignificant for Nc-C8 and Nc-C12 and likely also very low for Nc-C16. Secondly, there is no difference between Nc-C12 and Nc-C16's permeabilizing and antimicrobial activities despite significant differences in aggregation potential. Thirdly, Nc-C8 can be considered a non-aggregating peptide under all our measured conditions and its permeabilizing and antimicrobial activities lie neatly between the unacylated Nc wt and the Nc-C12 and Nc-C16 peptides.

Any changes in membrane disruption kinetics are therefore most likely to reflect changes in the binding to the membrane and/or structural rearrangements in this environment. Let us address these issues.

4.2. Changes in secondary structure caused by the addition of lipids

Nc folding in vesicles is strongly dependent on the lipid headgroup. Nc remains largely random coil in DOPC, but 80DOPC:20DOPG vesicles induce α-helical structure. However, the increase in secondary structure does not in itself favor permeabilization but makes it less efficient. These data can be interpreted in two ways: either Nc binds to a smaller extent to DOPC than to 80DOPC:20DOPG vesicles but the peptide molecules that do bind are much more efficient at permeabilizing DOPC than 80DOPC:20DOPG. Alternatively, Nc binds to DOPC vesicles but in a disordered conformation. We favor the latter interpretation, since we know from three independent techniques (calcein release, fluorescence anisotropy and DSC) that Nc binds at least as well to DOPC vesicles as to 80DOPC:20DOPG vesicles. The differences in structure may reflect different arrangements on the vesicle surface and/or membrane traversion, as suggested also by the different DSC profiles towards zwitterionic versus partially anionic vesicles. One scenario could be that Nc is loosely attached to DOPC vesicles, allowing it to remain relatively unstructured and thus cover a larger surface on the vesicle, while in 80DOPC:20DOPG vesicles Nc is buried at the headgroup-acyl chain interface, favoring an amphipathic α-helix structure. This is consistent with our stopped-flow experiments with Dansyl-Nc where we observe a higher degree of interaction with 80DOPC:20DOPG vesicles both prior to and after vesicle disruption. Our solid-state NMR observations also show that Nc mainly interacts with the lipid headgroups. Previously we observed that the closely related peptide Novispirin was able to bind to the positively charged surfactant LTAC to a more superficial extent than to the complementary SDS micelles, highlighting different levels of interaction [31]. Other studies also indicate that binding and permeabilization can be separate processes, and that binding alone is not sufficient for membrane permeabilization. For example, the amyloid-β peptide can bind to both crystalline and liquid disordered phases but only permeabilize the liquid disordered state [48].

Acylated peptides are α-helical in the presence of zwitterionic vesicles, suggesting that the acyl chain causes the peptides to adsorb to the vesicles in a manner that facilitates the formation of α-helix. One could imagine that the acyl chains work as “anchors” that pull the peptides into the headgroup-acyl chain interface where it then folds into an α-helix, supported by our PRE-data which indicate deeper penetration into micelles by Nc-C16 than Nc wt (Fig. 8B). This anchoring effect may also explain our solid-state NMR observation where we not only observe perturbation of the lipid head groups but also effects in the central and tail parts of the lipids — where α-helical secondary structure would support membrane penetration (static or transient). Graham and Phillips [49] reported that adsorption of rigid

Please cite this article as: B. Vad, et al., Divorcing folding from function: How acylation affects the membrane-perturbing properties of an antimicrobial peptide, Biochim. Biophys. Acta (2009), doi:10.1016/j.bbapap.2009.12.006

molecules to lipid membranes caused a slower increase in surface pressure compared to flexible molecules. Thus increased peptide rigidity induced by α-helix formation (in combination with "plugging" effects mentioned below) could explain the decreased tendency to disrupt vesicles. In addition, the increased submersion into the lipid bilayer will make the acylated peptides less sensitive to the nature of the headgroup and will thus decrease the preference for zwitterionic lipids shown by Nc.

4.3. Changes in lipid specificity caused by acylation

In the steady-state fluorescence measurements of vesicle disruption, we observe that Nc causes calcein release from DOPC vesicles at 7-fold lower concentration than those needed for disruption of 80DOPC:20DOPG vesicles. Solid-state NMR data also reveal a stronger interaction between the peptide and the DMPC membranes than the DMPC:DMPG membranes. Peptide acylation increases the concentrations needed for vesicle disruption, and leads to a decreased preference for zwitterionic vesicles compared to partially anionic vesicles (Fig. 3D). However, this decreased functional efficiency does not reflect a lower degree of overall binding to vesicles, as we need less lipid to induce changes in secondary structure for both Nc-C8 and Nc-C12 compared to Nc. To explain this apparent discrepancy, we speculate that the peptide's N-terminal acyl chain to some degree is able to counteract membrane disruption. The observed faster release rates for acylated peptides could then could then be explained by the higher surface concentration of peptide that has been able to accumulate up to this level without disrupting the membrane because of the "plugging" effects of the acyl chain which help retain membrane integrity (see model in Fig. 10). The "plugging" effect could very well be what we observe in the solid-state NMR spectra. It is clear that Nc-C16 interacts with central parts of the lipid bilayer as seen in Fig. 9E and H. We note that from the present NMR data, we cannot distinguish whether it is the peptide itself or it is its acyl chains that interact with the central parts of the lipids. Data which could be interpreted in the same light have been observed for the lipopeptide surfactin where an increase in acyl chain length lowers the surface pressure of vesicles [50]. *In vivo* these effects would presumably lead to a decrease in the haemolytic activity of the peptide as the outer leaflet of red blood cell is primarily composed of the zwitterionic phosphatidylcholine and phosphatidylethanolamine [51].

The decreased preference of acylated Nc for zwitterionic lipids differs significantly from the work of Dathe et al. [52] and Wieprecht et al. [53], who report an increased affinity towards zwitterionic vesicles as a result of increased hydrophobicity. However, in their studies they have made point mutations in order to increase the hydrophobicity, rather than acylating the peptide. As with the acylated variants, this emphasizes the separation of folding and function.

4.4. Vesicle aggregation

The overshoot observed in our calcein release assay is presumably a scattering effect caused by vesicle aggregation. Apparently the

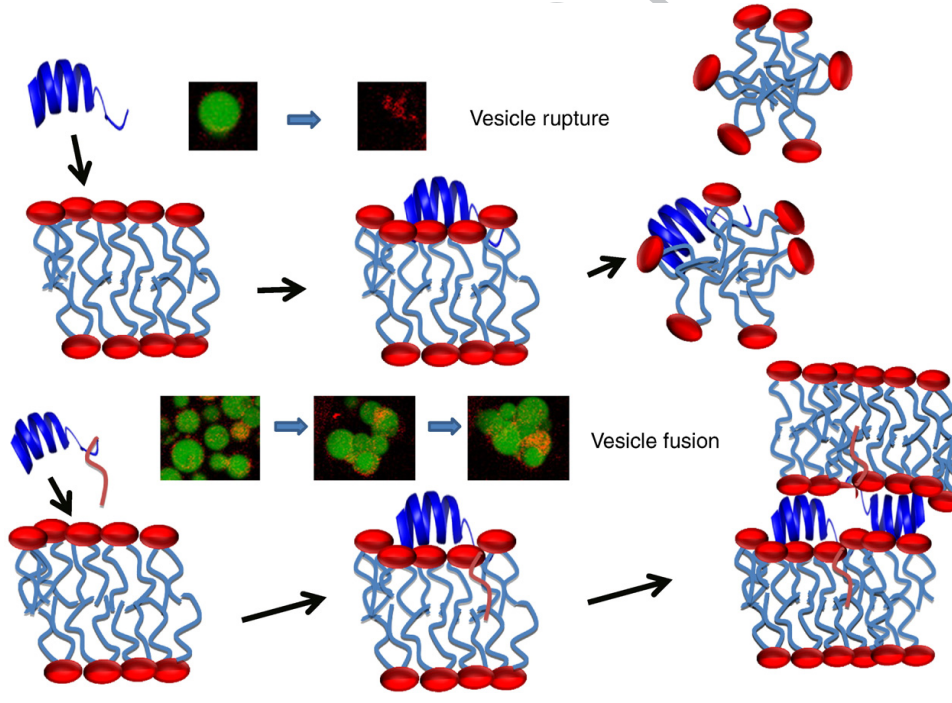

Fig. 10. A schematic model to illustrate why much less Nc wt is required compared to the acylated versions to cause the same degree of vesicle permeabilization. Nc wt (blue) attaches peripherally to DOPC vesicles since there is no significant change in the secondary structure upon binding although we still observe vesicle disruption. In the presence of DOPG, Nc is submerged more extensively in the bilayer, most likely at the acyl chain headgroup interface, leading to increased α-helix structure and an increase in the fluorescence of the dansyl-labelled Nc prior to vesicle disruption. The acylation of Nc (acyl chain in pink) pulls the peptide deeper into the DOPC vesicles as we have formation of α-helix. Nevertheless the insertion is different from that in 80DOPC:20DOPG vesicles, since there are still clear differences in the vesicle disruption kinetics and concentrations needed for the two types of vesicles. The acyl chain helps to counteract the vesicle destabilizing effect of the peptide, leading to the need for higher concentrations of peptides to disrupt the vesicles, irrespective of the lipids used. (For interpretation of the references to colour in this figure legend, the reader is referred to the web version of this article.)

Please cite this article as: B. Vad, et al., Divorcing folding from function: How acylation affects the membrane-perturbing properties of an antimicrobial peptide, Biochim. Biophys. Acta (2009), doi:10.1016/j.bbapap.2009.12.006

vesicle aggregates are subsequently dissolved as we observe the overshoot to decrease over time. This is confirmed in our CLSM experiments where we in some cases clearly observe vesicle aggregation followed by vesicle disruption. Peptide induced aggregation of vesicles has been reported previously for antimicrobial peptides such as Cryptidin-4 and polylysine, measured by FRET and dynamic light scattering [54–56]. The aggregation is believed to be driven primarily by preferential electrostatic interactions, bilayer deformation, and lipid head group dehydration [56,57]. We do observe a link between the aggregation and the acylation, since increasing chain lengths increase the aggregation (though Nc-C8 has reduced aggregation capability compared to non-acylated Nc). One explanation could be that the previously suggested plugging effect, in combination with exposure of cationic side-chains on the surface which can attract neighbouring anionic vesicles, gives the peptide–lipid complexes time to interact and subsequently aggregate. Our working model for the effect of Novicidin on membranes is summarized in Fig. 10.

4.5. In a mixed population of vesicles charge interactions are the governing forces of peptide–lipid interactions

Confocal laser scanning microscopy experiments on the mixed populations of purely zwitterionic and zwitterionic-anionic vesicles (Supplementary material) reveal that peptides show a marked preference towards the (partially) negatively charged DOPC:DOPG vesicles over the zwitterionic DOPC vesicles. This preference differs from our calcein release measurements but does not contradict them. Rather, they simply reveal that long-range interactions in solution, mediated by electrostatics, can be sufficient to trap peptides on or close to a membrane surface for subsequent folding and membrane interactions. Although the visualization of vesicle contents release by peptides and small molecules has been reported previously [58–61], to our knowledge this is the first example of the microscope-based analysis of mixed vesicle populations. This allows us to compare the affinity of wildtype and modified peptides for a specific lipid composition in the presence of competing lipids, and thus ultimately model complex *in vivo* systems, such as the human digestive tract, where the antimicrobial peptides are exposed to a diverse range of possible targets [62,63].

Acknowledgements

We are very grateful to Drs. Hans Henrik Kristensen and Per Holse Mygind, Novozymes A/S, for generous donations of Nc as well as for useful discussions. This work was supported by the Danish National Research Foundation through the Center for Insoluble Protein Structures (inSPIN). B.S.V. and M.F. are supported by pre-doctoral grants co-financed by Aalborg University and the Villum Kann Rasmussen Foundation through BioNET. The NMR laboratory at Aalborg University is supported by the Obel Foundation.

Appendix A. Supplementary data

Supplementary data associated with this article can be found, in the online version, at doi:10.1016/j.bbapap.2009.12.006.

References

[1] J.D. Hale, R.E. Hancock, Alternative mechanisms of action of cationic antimicrobial peptides on bacteria, Expert Rev. Anti Infect. Ther. 5 (2007) 951–959.
[2] K. Lohner, S.E. Blondelle, Molecular mechanisms of membrane perturbation by antimicrobial peptides and the use of biophysical studies in the design of novel peptide antibiotics, Comb. Chem. High Throughput Screen. 8 (2005) 241–256.
[3] M. Zasloff, Antimicrobial peptides of multicellular organisms, Nature 415 (2002) 389–395.
[4] K.A. Brogden, Antimicrobial peptides: pore formers or metabolic inhibitors in bacteria? Nat. Rev. 3 (2005) 238–250.
[5] Y.J. Gordon, E.G. Romanowski, A.M. McDermott, A review of antimicrobial peptides and their therapeutic potential as anti-infective drugs, Curr. Eye Res. 30 (2005) 505–515.
[6] J. Andra, J. Howe, P. Garidel, M. Rossle, W. Richter, J. Leiva-Leon, I. Moriyon, R. Bartels, T. Gutsmann, K. Brandenburg, Mechanism of interaction of optimized Limulus-derived cyclic peptides with endotoxins: thermodynamic, biophysical and microbiological analysis, Biochem. J. 406 (2007) 297–307.
[7] O. Taboureau, O.H. Olsen, J.D. Nielsen, D. Raventos, P.H. Mygind, H.H. Kristensen, Design of novispirin antimicrobial peptides by quantitative structure–activity relationship, Chem. Biol. Drug Des. 68 (2006) 48–57.
[8] S. Pistolesi, R. Pogni, J.B. Feix, Membrane insertion and bilayer perturbation by antimicrobial peptide CM15, Biophys. J. 93 (2007) 1651–1660.
[9] M.A. Fazio, L. Jouvensal, F. Vovelle, P. Bulet, M.T. Miranda, S. Daffre, A. Miranda, Biological and structural characterization of new linear gomesin analogues with improved therapeutic indices, Biopolymers 88 (2007) 386–400.
[10] C. Landon, F. Barbault, M. Legrain, L. Menin, M. Guenneugues, V. Schott, F. Vovelle, J.L. Dimarcq, Lead optimization of antifungal peptides with 3D NMR structures analysis, Protein Sci. 13 (2004) 703–713.
[11] O. Taboureau, O.H. Olsen, J.D. Nielsen, D. Raventós, P.H. Mygind, H.-H. Kristensen, Design of Novispirin antimicrobial peptides by quantitative structure–activity relationship, Chem. Biol. Drug Des. 68 (2006) 48–57.
[12] H.E. Hasper, N.E. Kramer, J.L. Smith, J.D. Hillman, C. Zachariah, O.P. Kuipers, B. De Kruijff, E. Breukink, An alternative bactericidal mechanism of action for lantibiotic peptides that target lipid II, Science 313 (2006) 1636–1637.
[13] M.E. Quiñones-Mateu, M.M. Ledermann, Z. Feng, B. Chakraborty, J. Weber, H.R. Rangel, M.L. Marotta, M. Mirza, B.L. Jiang, P. Kiser, K. Medvik, S.F. Sieg, A. Weinberg, Human epithelial beta-defensins 2 and 3 inhibit HIV-1 replication, AIDS 17 (2003) F39–F48.
[14] Y. Shai, Z. Oren, From "carpet" mechanism to de-novo designed diastereomeric cell-selective antimicrobial peptides, Peptides 22 (2001) 1629–1641.
[15] G. Ehrenstein, H. Lecar, Electrically-gated ionic channels in lipid bilayers, Rev. Biophys. 10 (1977) 595–623.
[16] Y. Pouny, D. Rapaport, A. Mor, P. Nicolas, Y. Shai, Interaction of antimicrobial dermaseptin and its fluorescently labeled analogues with phospholipid membranes, Biochemistry 31 (1992) 12416–12423.
[17] E. Gazit, A. Boman, H.G. Boman, Y. Shai, Interaction of the mammalian antibacterial peptide cecropin P1 with phospholipid vesicles, Biochemistry 34 (1995) 11479–11488.
[18] Y. Pouny, Y. Shai, Interaction of D-amino acid incorporated analogues of pardaxin with membranes, Biochemistry 31 (1992) 9482–9490.
[19] Y. Shai, Molecular recognition between membrane-spanning polypeptides, Trends Biochem. Sci. 20 (1995) 460–464.
[20] A. Makovitzki, D. Avrahami, Y. Shai, Ultrashort antibacterial and antifungal lipopeptides, Proc. Natl. Acad. Sci. USA 103 (2006) 15997–16002.
[21] D. Avrahami, Y. Shai, Conjugation of a magainin analogue with lipophilic acids controls hydrophobicity, solution assembly, and cell selectivity, Biochemistry 41 (2007) 2254–2263.
[22] F. Separovic, S. Barker, M. Delahunty, R. Smith, NMR structure of C-terminally tagged gramicidin channels, Biochim. Biophys. Acta 1416 (1999) 48–56.
[23] T.C. Vogt, J.A. Killian, B. De Kruijff, The influence of acylation on the lipid structure modulating properties of the transmembrane polypeptide gramicidin, Biochim. Biophys. Acta 1193 (1994) 55–61.
[24] S.H. White, W.C. Wimley, Membrane protein folding and stability: physical principles, Ann. Rev. Biophys. Biomol. Struct. 28 (1999) 319–365.
[25] M.A. Schmitt, B. Weisblum, S.H. Gellman, Unexpected relationships between structure and function in alpha, beta-peptides: antimicrobial foldamers with heterogeneous backbones, J. Am. Chem. Soc. 126 (2004) 6848–6849.
[26] T.L. Raguse, E.A. Porter, B. Weisblum, S.H. Gellman, Structure–activity studies of 14-helical antimicrobial beta-peptides: probing the relationship between conformational stability and antimicrobial potency, J. Am. Chem. Soc. 124 (2002) 12774–12785.
[27] H. Khandelia, Y.N. Kaznessis, Molecular dynamics simulations of helical antimicrobial peptides in SDS micelles: what do point mutations achieve? Peptides 26 (2005) 2037–2049.
[28] M.V. Sawai, A.J. Waring, W.R. Kearney, P.B.J. McCray, W.R. Forsyth, R.I. Lehrer, B.F. Tack, Impact of single-residue mutations on the structure and function of ovispirin/novispirin antimicrobial peptides, Prot. Eng. 15 (2002) 225–232.
[29] F. Jacobsen, A. Mohammadi-Tabrisi, T. Hirsch, D. Mittler, P.H. Mygind, C.P. Sonksen, D. Raventos, H.H. Kristensen, S. Gatermann, M. Lehnhardt, A. Daigeler, H.U. Steinau, L. Steinstraesser, Antimicrobial activity of the recombinant designer host defence peptide P-novispirin G10 in infected full-thickness wounds of porcine skin, J. Antimicrob. Chemother. 59 (2007) 493–498.
[30] H. Khandelia, Y.N. Kaznessis, Molecular dynamics investigation of the influence of anionic and zwitterionic interfaces on antimicrobial peptides' structure: implications for peptide toxicity and activity, Peptides 27 (2006) 1192–1200.
[31] R. Wimmer, K. Andersen, B. Vad, M. Davidsen, S. Mølgaard, L.W. Nesgaard, H.-H. Kristensen, D.E. Otzen, Versatile interactions of the antimicrobial peptide Novispirin with detergents and lipids, Biochemistry 45 (2006) 481–497.
[32] M.I. Angelova, D.S. Dimitrov, Liposome electroformation, Faraday Discuss. Chem. Soc 81 (1986) 301–311.
[33] B. Vad, K. Bertelsen, C.H. Johansen, J.M. Pedersen, T.S. Skrydstrup, N.C. Nielsen, D.E. Otzen, Pardaxin permeabilizes vesicles more efficiently by pore formation than by disruption, Biophys. J. in press.
[34] S.B. Nicholas, K.D. Philipson, Cardiac expression of the Na(+)/Ca(2+) exchanger NCX1 is GATA factor dependent, Am. J. Physiol. 277 (1999) H324–H330.
[35] C.M. Kusuma, J.F. Kokai-Kun, Comparison of four methods for determining lysostaphin susceptibility of various strains of Staphylococcus aureus, Antimicrob. Agents Chemother. 49 (2005) 3256–3263.

Please cite this article as: B. Vad, et al., Divorcing folding from function: How acylation affects the membrane-perturbing properties of an antimicrobial peptide, Biochim. Biophys. Acta (2009), doi:10.1016/j.bbapap.2009.12.006

[36] M. Respondek, T. Madl, C. Gobl, R. Golser, K. Zangger, Mapping the orientation of helices in micelle-bound peptides by paramagnetic relaxation waves, J. Am. Chem. Soc. 129 (2007) 5228–5234.
[37] M.V. Sawai, A.J. Waring, W.R. Kearney, P.B. McCray Jr., W.R. Forsyth, R.I. Lehrer, B.F. Tack, Impact of single-residue mutations on the structure and function of ovispirin/novispirin antimicrobial peptides, Protein Eng. 15 (2002) 225–232.
[38] R. Wimmer, K.K. Andersen, B. Vad, M. Davidsen, S. Molgaard, L.W. Nesgaard, H.H. Kristensen, D.E. Otzen, Versatile interactions of the antimicrobial peptide novispirin with detergents and lipids, Biochemistry 45 (2006) 481–497.
[39] V.C. Kalfa, H.P. Jia, R.A. Kunkle, P.B. McCray Jr., B.F. Tack, K.A. Brogden, Congeners of SMAP29 kill ovine pathogens and induce ultrastructural damage in bacterial cells, Antimicrob. Agents Chemother. 45 (2001) 3256–3261.
[40] G. Pintacuda, M.A. Keniry, T. Huber, A.Y. Park, N.E. Dixon, G. Otting, Fast structure-based assignment of 15N HSQC spectra of selectively 15N-labeled paramagnetic proteins, J. Am. Chem. Soc. 126 (2004) 2963–2970.
[41] C.H. Wu, A. Ramamoorthy, S.J. Opella, High-resolution heteronuclear dipolar solid-state NMR spectroscopy, J. Magn. Reson. 109 (1994) 270–272.
[42] A.A. De Angelis, S.J. Opella, Bicelle samples for solid-state NMR of membrane proteins, Nat. Protoc. 2 (2007) 2332–2338.
[43] S. Dvinskikh, U. Dürr, K. Yamamoto, A. Ramamoorthy, A high-resolution solid-state NMR approach for the structural studies of bicelles, J. Am. Chem. Soc. 128 (2006) 6326–6327.
[44] S. Dvinskikh, U. Dürr, K. Yamamoto, A. Ramamoorthy, High-resolution 2D NMR spectroscopy of bicelles to measure the membrane interaction of ligands, J. Am. Chem. Soc. 129 (2007) 794–802.
[45] S. Dufour, M. Deleu, K. Nott, B. Wathelet, P. Thonart, M. Paquot, Hemolytic activity of new linear surfactin analogs in relation to their physico-chemical properties, Biochim. Biophys. Acta 1726 (2005) 87–95.
[46] C.-L. McGregor, L. Chen, N.C. Pomroy, P. Hwang, S. Go, A. Chakrabartty, G.G. Privé, Lipopeptide detergents designed for the structural study of membrane proteins, Nat. Biotechnol. 21 (2003) 171–176.
[47] A. Patist, J.R. Kanicky, P.K. Shukla, D.O. Shah, Importance of micellar kinetics in relation to technological processes, J. Colloid Interface Sci. 245 (2002) 1–15.
[48] P.T. Wong, J.A. Schauerte, K.C. Wisser, H. Ding, E.L. Lee, D.G. Steel, A. Gafni, Amyloid-b membrane binding and permeabilization are distinct processes influenced separately by membrane charge and fluidity, J. Mol. Biol. 386 (2009) 81–96.
[49] D.E.G.a.M.C. Phillips, Proteins at liquid interfaces: I. Kinetics of adsorption and surface denaturation, J. Colloid Interface Sci. 7 (1979) 403–414.
[50] M. Eeman, A. Berquand, Y.F. Dufrene, M. Paquot, S. Dufour, M. Deleu, Penetration of surfactin into phospholipid monolayers: nanoscale interfacial organization, Langmuir 22 (2006) 11337–11345.
[51] A.J. Verkleij, R.F. Zwaal, B. Roelofsen, P. Comfurius, D. Kastelijn, L.L. van Deenen, The asymmetric distribution of phospholipids in the human red cell membrane. A combined study using phospholipases and freeze-etch electron microscopy, Biochim. Biophys. Acta 323 (1973) 178–193.
[52] M. Dathe, T. Wieprecht, H. Nikolenko, L. Handel, W.L. Maloy, D.L. MacDonald, M. Beyermann, M. Bienert, Hydrophobicity, hydrophobic moment and angle subtended by charged residues modulate antibacterial and haemolytic activity of amphipathic helical peptides, FEBS Lett. 403 (1997) 208–212.
[53] T. Wieprecht, M. Dathe, M. Beyermann, E. Krause, W.L. Maloy, D.L. MacDonald, M. Bienert, Peptide hydrophobicity controls the activity and selectivity of magainin 2 amide in interaction with membranes, Biochemistry 36 (1997) 6124–6132.
[54] K. Matsuzaki, M. Fukui, N. Fujii, K. Miyajima, Permeabilization and morphological changes in phosphatidylglycerol bilayers induced by an antimicrobial peptide, tachyplesin I, Colloid Polym. Sci. 271 (1993) 901–908.
[55] G. Fujii, S. Horvath, S. Woodward, F. Eiserling, D. Eisenberg, A molecular model for membrane fusion based on solution studies of an amphiphilic peptide from HIV gp41, Protein Sci. 1 (1992) 1454–1464.
[56] J.E. Cummingsa, T.K. Vanderlick, Aggregation and hemi-fusion of anionic vesicles induced by the antimicrobial peptide cryptidin-4, Biochim. Biophys. Acta 1768 (2007) 1796–1804.
[57] T. Stegmann, R.W. Doms, A. Helenius, Protein-mediated membrane fusion, Annu. Rev. Biophys. Biophys. Chem. 18 (1989) 187–211.
[58] S.T. Henriques, A. Quintas, L.A. Bagatolli, F. Homble, M.A. Castanho, Energy-independent translocation of cell-penetrating peptides occurs without formation of pores. A biophysical study with pep-1, Mol. Membr. Biol. 24 (2007) 282–293.
[59] E.E. Ambroggio, F. Separovic, J.H. Bowie, G.D. Fidelio, L.A. Bagatolli, Direct visualization of membrane leakage induced by the antibiotic peptides: maculatin, citropin, and aurein, Biophys. J. 89 (2005) 1874–1881.
[60] Y. Tamba, M. Yamazaki, Single giant unilamellar vesicle method reveals effect of antimicrobial peptide magainin 2 on membrane permeability, Biochemistry 44 (2005) 15823–15833.
[61] Y. Tamba, S. Ohba, M. Kubota, H. Yoshioka, H. Yoshioka, M. Yamazaki, Single GUV method reveals interaction of tea catechin (−)-epigallocatechin gallate with lipid membranes, Biophys. J. 92 (2007) 3178–3194.
[62] L.R. Montes, A. Alonso, F.M. Goni, L.A. Bagatolli, Giant unilamellar vesicles electroformed from native membranes and organic lipid mixtures under physiological conditions, Biophys. J. 93 (2007) 3548–3554.
[63] L. Dethlefsen, M. McFall-Ngai, D.A. Relman, An ecological and evolutionary perspective on human-microbe mutualism and disease, Nature 449 (2007) 811–818.

Please cite this article as: B. Vad, et al., Divorcing folding from function: How acylation affects the membrane-perturbing properties of an antimicrobial peptide, Biochim. Biophys. Acta (2009), doi:10.1016/j.bbapap.2009.12.006

Paper II:

Impact of the antimicrobial peptide Novicidin on membrane structure and integrity

Søren B. Nielsen and Daniel Otzen
Manuscript submitted

Impact of the antimicrobial peptide Novicidin on membrane structure and integrity

Søren B. Nielsen[1,2] and Daniel E. Otzen[1*]

[1] Interdisciplinary Nanoscience Center (iNANO), Department of Molecular Biology, University of Aarhus, Gustav Wieds Vej 10C, DK – 8000 Aarhus C

[2] Department of Food Science, Faculty of Agricultural Sciences, University of Aarhus, Blichers Allé, DK - 8830 Tjele

* To whom correspondence should be addressed. E-mail dao@inano.dk, tel. + 45 89 42 50 46, fax + 45 86 12 07 40.

Abbreviations: Novicidin, Nc; OCD, oriented circular dichroism; QCM-D, quartz crystal microbalance with dissipation; DPI, Dual polarization interferometry; GP, generalized polarity

Running title: Impact of Novicidin on membrane organization

ABSTRACT

We have studied the impact of the 18-residue cationic antimicroial peptide Novicidin (Nc) on the structure and integrity of partially anionic lipid membranes using oriented circular dichroism (OCD), quartz crystal microbalance with dissipation (QCM-D), dual polarization interferometry (DPI), calcein dye leakage and fluorescence spectroscopy. OCD consistently showed that Nc is bound in an α-helical, surface bound state over a range of peptide to lipid (P/L) ratios up to ~1:15. Realignment of Nc at higher P/L ratios correlates to loss of membrane integrity as shown by Laurdan fluorescence spectroscopy and by loss of lipid alignment in DPI analysis. Laurdan generalized polarity shows a decrease in water accessibility or mobility in the hydrophobic/hydrophilic interface of the lipid membrane, consistent with rearrangement of lipid packing. QCM-D studies on the interaction of Nc with lipid membranes emphasize the importance of including the dissipation factor in data analysis, revealing formation of a highly hydrated film after exposure to ≥3μM Nc. Our findings suggest a carpet mechanism of membrane disruption in which peptide binding first induces leakage at a critical surface concentration, probably through formation of transient pores or transient disruption of the membrane integrity, followed by more extensive membrane disintegration at higher P/L ratios.

Keywords: quartz crystal microbalance with dissipation; supported lipid bilayers; antimicrobial peptide; oriented circular dichroism; calcein dye leakage

INTRODUCTION

Antimicrobial peptides (AMPs) constitute an integral part of the innate immune system. They have been isolated from a broad range of species and show a wide spectrum of antimicrobial activity against bacteria, fungi, and viruses [1]. The interest in AMPs from both scientific and industrial perspectives is driven by the development of resistance among pathogens toward conventional antibiotics [2]. AMPs have been divided into several groups according to structure, charge and the presence of specific amino acid residues. Most AMPs are cationic [3] and with few exceptions (*e.g.* [4, 5]) exert their activity through binding to the bacterial cell surface. The anionic membrane has been described as the major driving force in binding of cationic antimicrobial peptides. In contrast, lipids in the outer part of membranes in mammals are mainly neutral. This difference in charge provides the basis for the selectivity of cationic peptides toward bacteria. AMPs interacting with lipid membranes may form membrane pores in which hydrophobic amino acid residues directly interact with the hydrophobic core of the membrane whereas charged residues project into the pore interior. This model has been described as the barrel-stave mechanism due to the formation of an ion channel (barrel) composed by several peptide helices (staves) inserted across the bilayer [6]. Other models suggest that membrane disruption does not necessarily require insertion into the hydrophobic core of membranes. In the toroidal pore model, AMPs accumulate on the membrane surface until critical membrane coverage is achieved. At this point, the positive membrane curvature becomes large enough to create continuities between the inner and outer leaflets. In this case, the AMP remains associated with the headgroups and line the pore [7]. Another proposed mechanism in which AMPs accumulate at the surface until membrane disintegration is the carpet mechanism. In this model, the peptide accumulate on the surface until the membrane is destabilized sufficiently through a detergent-like disintegration or solubilization of the membrane [8].

Novicidin (Nc) belongs to a large group of linear cationic α-helical peptides, which also counts well-studied AMPs such as cecropins, mellitin, magainin and LL37 among its members. Nc was developed for reduced cytotoxicity by a single G18F mutation of ovispirin-1 which in turn was inspired by the sheep myeloid antimicrobial peptide (SMAP) 29. Ovispirin-1 and the novispirin G-10 and T7 derivatives thereof has been shown to adopt weak helical or random coil structures in phosphate buffers, but assume an α-helical conformation in the presence of organic alcohols such as trifluoroethanol (which are assumed to mimic the lipid-water interface [9]), as well as outer membrane lipids such as lipopolysaccharides and lipoteichoic acid found in the polyanionic cell

surfaces of Gram-negative and Gram–positive bacteria, respectively [10]. Nc also forms an α-helical conformation in 20% 1,2-dioleoylphosphatidylglycerol (DOPG) and 80% 1,2-dioleoylphosphatidylcholine (DOPC) [11]. However, the membrane disrupting ability of Nc has been shown not to require an α-helical fold, and Nc showed a greater level of permeabilizing activity towards DOPC vesicles than vesicles containing 20% DOPG. Nevertheless, Nc preferentially ruptures giant unilamellar vesicles (GUVs) containing 20% DOPG in a mixed population of pure DOPC and GUVs containing 20% DOPG [11].

Our previous work with Nc has focused mainly on the peptide's structural changes in an amphiphilic environment [11-13]. Here we analyze the interaction of Nc with anionic lipid membranes with a host of complementary techniques in order to describe the rearrangements at the membrane level. We describe the orientation of the α-helical structure in lipid membranes using oriented circular dichroism (OCD) and describe the membrane perturbation using quartz crystal microbalance with dissipation (QCM-D) to measure the mass and determine the reversibility of peptide binding to supported lipid bilayers. Dual polarization interferometry (DPI) is used to show a significant decrease in the order of the lipid film on interaction with Nc. Further, vesicle perturbation was monitored by calcein dye leakage and changes in membrane environment upon peptide binding were monitored by the membrane embedded fluorescent probe Laurdan. These data together establish the primary mode of interaction between Nc and negatively charged membranes. We find that the α-helix of Nc remains in the surface bound state and rearranges only at very high peptide to lipid ratios due to loss of membrane integrity. Binding of Nc result in decreased water accessibility in the lipid headgroup region and distortion in lipid alignment. These observations correlate to a loss of membrane integrity and indicate that the membrane disruptive effect of Nc occurs via the carpet mechanism.

MATERIALS AND METHODS

Materials: 1,2-dioleoylphosphatidylcholine (DOPC) and 1,2-dioleoylphosphatidylcholine (DOPG) were purchased in powder form from Avanti Polar Lipids (Alabaster, AL). 6-dodecanoyl-2-dimethylaminonaphthalene (Laurdan) was obtained from Molecular Probes (Eugene, Oregon, USA). Chloroform (Sigma, St. Louis, USA) and methanol (Sigma, Steinheim, Germany) were of 99% purity or higher. Triton X-100 and Calcein disodium salt were obtained from Fluka (Buchs, Switzerland). Novicidin (Nc) was a generous gift from Drs. Per Holse Mygind and Hans Henrik Kristensen, Novozymes A/S. Nc concentration was determined using a calculated extinction coefficient at 280 nm of 1490 M^{-1} cm^{-1} [14].

Preparation of large unilamellar vesicles: 100nm large unilamellar vesicles (LUVs) were made by preparing a dry lipid film (5mg lipid) composed of 80:20 w/w% DOPC:DOPG through evaporation of the chloroform solvent in a stream of nitrogen gas. The lipid film was rehydrated in 20mM Tris-Cl pH 7.5 buffer also containing 70mM calcein when lipids were applied for calcein release studies or 5mM CaCl2 when applied for QCM experiments. In DPI experiments, lipids were prepared in 10mM HEPES, 150mM NaCl, 2mM $CaCl_2$ pH 7.4. The lipids were subjected to 5 freeze-thaw cycles using liquid nitrogen and 40°C water bath before the lipid suspension was extruded using 15 times through a 100nm polycarbonate membranes using the Avanti polar lipids MiniExtruder (Avanti Polar Lipids Inc., Alabaster, AL) as described by the manufacturer.

Calcein dye leakage: Calcein dye leakage was monitored at 25^{o}C using a Varian Cary Eclipse spectrofluorometer (Varian, Palo Alto, CA) equipped with a thermostatted 4-cell holder with stirring. Calcein was excited at 490nm and emission was monitored at 515nm using 2.5nm slits and medium PMT voltage (600V). Samples were stirred with magnetic bars at maximum speed. Prior to the fluorescence measurement, 500µl 5mg/ml calcein-loaded LUVs were loaded on a PD-10 desalting column (GE Healthcare) to purify vesicles with entrapped calcein from free calcein. Vesicles were eluted in aliquots of 500µl and the calcein vesicle containing fractions were pooled and diluted 400x into 50µM non-labelled LUVs. 750µl vesicle suspension was transferred to cuvette and baseline fluorescence was recorded (F_0). A 10µl aliquot of Nc was added to monitor calcein release by Nc (leading to the calcein fluorescence intensity F). Subsequent addition of 10µl 2% Triton X-100 yielded the maximum possible calcein release (with fluorescence intensity F_{max}). The amount of released calcein was calculated by the following equation:

Dye leakage = $(F-F_0) / (F_{max} - F_0) * 100\%$ (1)

Laurdan generalized polarity: Laurdan fluorescence was monitored at 25°C with a Perkin Elmer LS55 spectrofluorometer (Perkin Elmer A/S, Hvidovre, Denmark) equipped with a stirred cell holder set operated at highest stirring speed. LUVs containing Laurdan were prepared by the procedure described above except that 0.5 mol % Laurdan was added to lipids before drying out the lipid film with nitrogen gas. Vesicles were diluted to 50µM in 20mM Tris-Cl pH 7.5 and 750µl aliquots were transferred to a cuvette and titrated with aliquots of 10µM Nc in the same buffer while measuring the emission spectra from 400-550nm between peptide additions using excitation at 350nm and 7.5nm slits for both excitation and emission.

To quantify the emission spectral changes, the Laurdan excitation generalized polarity (GP) was defined as:

$GP = (I_B - I_R) / (I_B + I_R); \quad -1 < GP < 1$ (2)

where I_B is the emission intensity at the blue-shifted peak at 437nm and I_R is the emission intensity of the red-shifted peak at 483nm.

Quartz crystal microbalance: Quartz crystal microbalance with dissipation monitoring (QCM-D) measurements were performed with the Q-sense E4 system (Q-sense AB, Västra Frölunda, Sweden). 14 mm 5 MHz At-cut sensor crystals with SiO_2 coating (QSX 303, Q-sense AB, Västra Frölunda, Sweden) were used. The E4 system was thermostatted at 25°C.

Changes in resonance frequency (Δf) and energy dissipation (ΔD) upon addition of samples were measured simultaneously using Q-soft v2.0.1 on four channels at four different overtones of the natural frequency (3^{rd}, 5^{th}, 7^{th}, 9^{th} and 11^{th} overtones corresponding to 15, 25, 35, 45 and 55Mhz resonance frequencies, respectively). Unless otherwise stated, all displayed changes in frequency and dissipation refer to the 3^{rd} overtone.

Each experiment consisted of the following procedures: Sensor crystals were cleaned by immersion in 2% SDS solution for at least 30 minutes at room temperature, rinsed in MQ H_2O and dried in a stream of nitrogen gas. The crystals were then subjected to UV/Ozone treatment for 10 minutes, rinsed in MQ H_2O and blown dry with nitrogen gas before mounting them in the QCM chambers. Sensor crystals were equilibrated in 20mM Tris-Cl pH 7.5 and supported lipid bilayers were formed by spontaneous collapse of LUVs (100µg/ml lipid) in the same buffer plus 5mM $CaCl_2$ to facilitate

vesicle collapse. LUVs were applied at 200µl/min using an Ismatec Reglo peristaltic pump (Ismatec SA, Glattbrugg, Switzerland) followed by wash in 20mM Tris-Cl pH 7.5, a brief wash in 20mM HEPES-KOH pH 7.4, 150mM NaCl to remove non-specifically bound lipid from the flow system and the system was finally equilibrated in 20mM Tris-Cl pH 7.5. 350µl Nc in the same buffer was injected at 200µl/min to ensure complete exchange of the chamber contents on injection. Subsequent washing was carried out in the reversed direction (so the solution only contained buffer plus the small amounts of Nc that had not bound in the initial transfer of Nc solution to the crystal) to evaluate the reversibility of interaction without further supply of Nc to the chamber.

Data analysis was carried out using Q-tools v3.0.6.213 (Q-sense AB, Västra Frölunda, Sweden) in two different approaches.

Firstly, we used Sauerbrey relation [15], which describes the linear relation between the recorded resonance frequency and the mass of the adlayer, provided the film is sufficiently thin and rigid:

$$\Delta m_{Sauerbrey} = \frac{C}{n}\Delta f_n \qquad (3)$$

C is the sensitivity constant ($17.7 ng \cdot cm_2^{-1} \cdot Hz^{-1}$) for the 5 Mhz AT-cut quartz crystals employed in this study, n is the overtone number and Δf_n the frequency shift at the n^{th} harmonic (n=1,3,5 …). A density of $1.05 g/cm^3$ (an average of the density of bilayers and water) was assumed.

Secondly, we used the Voigt viscoelastic model, provided by the Q-tools software, to provide a mathematical fit based on mechanical elements [16]. The Voigt model represent the adsorbed layer by a mechanical model described through estimates of thickness (d_{eff}), density (ρ_{eff}), shear elasticity (μ_{eff}) and shear viscosity (η_{eff}) and thus extends the Sauerbrey solution to include viscoelastic effects. Under the assumption that the adsorbed film is uniform with respect to thickness, density and that the film does not slip, we have employed the Voigt model to estimate thickness, shear elasticity and shear viscosity using QCM frequency and dissipation data from the 3^{rd}, 5^{th}, 7^{th} and 9^{th} harmonics. A fixed density of $1.05 g/cm^3$ was assumed. Note that, the mass per area (ng/cm^2) determined by the product of thickness and density ($\Delta m = d_{eff} \times \rho_{eff}$) did not change with a biologically relevant density range from 1.0 (water) and $1.6 g/cm^3$.

Dual polarization interferometry (DPI): DPI measurements were used to investigate the interaction between supported lipid bilayers composed by 80:20 w/w% DOPC:DOPG and Nc.

DPI measurements were made on a *Ana*Light BIO200 (Farfield Group Ltd, UK) system using unmodified AnaChip waveguides cleaned with 10% Helmanex and 2% SDS. For a thorough description on the implications of using DPI in the study of anisotropic films such as supported lipid bilayers see [17, 18].

Experiments were initialized using 10mM HEPES, 150mM NaCl pH 7.4 followed by formation of supported lipid bilayers by exposure to ~100µg/ml 80:20 w/w% DOPC:DOPG in 10mM HEPES pH 7.4, 150mM NaCl, 2mM $CaCl_2$. The running buffer was changed to 20mM Tris-Cl pH 7.5 and Nc concentrations from 0.00125-20.48µM were injected. DPI experiments were made at 20°C.

Data analysis was carried as described by [18]. In brief, the refractive index was fixed at 1.47 and we used a dn/dc value of 0.135 which corresponds to a constant layer density of ~1.01g/cm^3.

Solution circular dichroism: Solution CD experiments were carried out using a Jasco J-810 spectropolarimeter at 25°C. Spectra were recorded from 260-185nm in continous scanning mode with a response time of 1s, 0.2nm steps, a bandwidth of 2nm and a scan speed of 100nm/min. 10 spectra were accumulated and averaged to increase the signal to noise ratio. Each spectrum was corrected by subtracting the lipid spectrum background. 200µl 2mM LUVs consisting of either pure DOPC or 80:20 w/w% DOPC:DOPG was placed in a 1mm path length cuvette and aliquots of Nc was added to obtain peptide to lipid ratios from 1:240 to 1:6 while obtaining the CD spectrum between each addition. The mean residual ellipticity (MRE) ($[\theta]$) was calculated using equation 4:

$$[\theta] = \frac{100\theta M_r}{clNN_A} \qquad (4)$$

where θ is the CD signal in mdeg, M_r is the molecular weight, c is the peptide concentration in mg/ml, l is the pathlength in cm and N_A is the number of amino acid residues of the peptide (18). The MRE at 222nm was used to evaluate the degree of α-helicity.

Oriented circular dichrosim: The procedure of OCD measurements has been described by [19, 20]. Stock solutions of Nc (from a freeze-dried 50 mg/ml solution with 20 mM Tris-Cl pH 7.5) and 80:20 w/w% DOPC:DOPG were prepared in 1:1 chloroform:methanol in various peptide to lipid ratios. The lipid concentration was kept at 10mg/ml so that addition of 2 rounds of 5µl sample (allowing evaporation of the solvent after each addition) to round quartz cell (0.1mm Hellma 124-QS) resulted in deposition of 100µg lipid and 3.3 to 60µg Nc corresponding to ~1:90 and ~1:5 molar ratios, respectively. The solvent was evaporated in a desiccator under vaccum (P<60mbar)

for at least one hour to remove residual solvent. The lipid film was rehydrated by vapor diffusion in a humidity chamber containing a saturated solution of K_2SO_4 or $MgCl_2$ to obtain a vapor pressure equivalent to ~98% or ~33% relative humidity (RH) at 25°C [21, 22]. These hydration levels are denoted full or low hydration, respectively. The OCD spectra of alamethicin at 100% and ~98% RH are identical [20]. After overnight equilibration, cells were transferred to our sample container (Fig. S1 in Supplementary Information) containing 50µl of the same salt solution to maintain the desired RH. The OCD spectra of samples was measured with the incident light perpendicular to the plane of the sample surface and the OCD spectra of pure lipid were measured separately and subtracted from samples. OCD spectra were collected using the synchrotron radiation circular dichroism (SRCD) facility at the Institute for Storage Ring Facilities (ISA) at Aarhus University, Denmark by averaging at least three spectra at eight different angles in order to eliminate artefacts arising from linear dichroism and birefringence phenomena. Additional spectra were recorded using a Jasco J-810 spectropolarimeter by scanning from 260-185 in 0.2nm steps. Other parameters were: 2nm bandwidth, 2 sec response time, 100nm/min scan speed and accumulation of at least 5 scans. Data analysis was done with CDtool v1.4 [23]. Because the actual amount of peptide present in the beam could not be determined, spectra were normalized at 224nm [24].

RESULTS

Nc binds in an orientation parallel to the membrane plane

To determine how Nc is positioned in membrane bilayers, we carried out synchrotron radiation-based oriented circular dichroism experiments of Nc in aligned lipid multilayers. The procedure allows the determination of surface (S) bound or inserted (I) states of antimicrobial peptides corresponding to a parallel or perpendicular orientation of the peptide relative to the bilayer, respectively [19]. The synchrotron source allowed us to record spectra reliably down to ~175 nm and thus obtain the complete contours of the peak centered around 190 nm (Fig. 1A). Aligned lipid multilayers were formed on quartz slides in the presence of Nc at P/L ratios ranging from 1:90 to 1:5 using a 80:20 w/w% DOPC:DOPG lipid mixture. This mimics the 15-20% negatively charged PG headgroups of *Escherishia coli* membranes [25] and also induces a much higher level of α-helical structure in Novicidin [11, 12]. The OCD spectra of Nc are normalized to the negative minimum at 224nm [24] (Fig. 1A).

The OCD spectra of Nc at full hydration at P/L ratios ranging from 1:90 to 1:15 showed essentially the same features, described by two negative minima at ~ 208 and 222nm and a positive maximum at ~ 190nm. This indicates that the peptide orientation remains oriented parallel to the membrane plane (*i.e.* the S state [19]), even at P/L ratios as high as 1:15. Dehydration of the membranes facilitated by saturated $MgCl_2$ salt solution (leading to a reduction in relative humidity from 98 to 33%) did not result in changes of the OCD spectra at 1:30 and 1:50 P/L ratios (data not shown). Thus reorientation of Nc along the bilayer normal does not occur under these conditions.

At 1:10 and 1:5 P/L ratios, the minimum at 208nm red-shifts slightly to 209nm and the intensity decreases slightly. A similar decrease in peak amplitude at ~208 nm relative to the 224nm peak was obtained using pure DOPC multilayer membranes (data not shown). The ~190nm band red-shifts to ~195nm which is characteristic for α-helices which orient along the direction of the incident light.. Altogether, these observations reveal a reorientation of the peptide helix similar to the OCD of other peptides [20, 24, 26]. However, whereas the intensity of the ~208nm peak disappears for these peptides (1:15 in DPPC, >1:30 in 1:1 DMPC:DMPG and >1:30 in DLPC, respectively), the intensity of the ~209 nm peak of Nc at P/L ~1:5 and 1:10 remains comparable to the intensity of the 224nm peak. This indicates that a reorientation to the fully inserted state does not occur; rather, Nc

is only partially inserted in a tilted state at these high P/L ratios. Similar behavior has been observed for PGLa and MSI-103 which aligned in a tilted state in DMPC bilayers [27].

We recorded solution CD spectra at similar P/L ratios to determine if changes in secondary structure could affect OCD measurements. In pure DOPC vesicles (Fig. 1B), the mean residue ellipticity (MRE) at 208nm remained constant at approximately -11.5 deg cm^2dmole^{-1} in the P/L range from ~1:240-1:20, consistent with the previously observed superficial binding of Nc to these vesicles [11]. The presence of anionic DOPG headgroups induces an increase in the α-helicity of Nc (Fig. 1B). At higher P/L ratios there is a decrease in α-helicity for Nc in 80:20 w/w% DOPC:DOPG which approached the MRE in 100% DOPC although the ratio between the intensity at 222 and 208nm remained constant. In view of the high P:L ratio we ascribe this decrease to the loss of helix-inducing lipid binding sites for Nc, which means that an increasing fraction of the Nc remains unstructured in the aqueous phase or converts to a non-helical binding mode such as the one it assumes in the presence of DOPC. It seems unlikely that perfectly aligned multilayers persist at these ratios although membranes remained visually homogeneous.

To probe the effect of lipid chain length, we used OCD to evaluate the orientation of Nc in multilayers consisting of 80:20 w/w% DLPC:DLPG and DMPC:DMPG, respectively, at 1:15 P/L ratio. The clear bands with a maximum at ~193nm and minima at ~208 and ~222nm (Fig. S2) are consistent with an S-state orientation. This indicates that lipid chain length, *i.e.* the thickness of the hydrocarbon layer underlying the interfacial region, does not affect the preference for the S state. Reorientation of short peptides such as the 16 aa aurein 2.2 and 2.3 from the surface bound (S) state to tilted (T) or inserted (I) states have been observed at P/L ratios ranging from 1:120 to 1:30 depending on lipid composition [24, 28]. Nevertheless, our data clearly indicate that the 18 residues of Nc remain associated in S state even at relatively high peptide to lipid ratios of ~1:15 independent of lipid composition. The surface bound state is in agreement with the position of Nc in DPC micelles as recently determined by quantitative paramagnetic relaxation enhancement approaches [13].

Quartz crystal microbalance and dual polarization interferometry show saturable surface binding of Nc to supported lipid bilayers

The interaction between Nc and lipid bilayers was further assessed using a quartz crystal microbalance with dissipation, which sensitively monitors changes in surface mass and

viscoelasticity associated with binding and surface-modifying reactions [29, 30]. In each experiment, supported planar bilayers were prepared by spontaneous vesicle collapse on silica coated sensor crystals *in situ* (Fig. S3). The process of spontaneous vesicle collapse to form supported planar bilayers (SPBs) has been extensively studied elsewhere [31-36]. Here, we formed SPBs composed of 80:20 w/w% DOPC:DOPG by collapse of 100nm LUVs. The advantage of this system is that we are well above the phase transition temperature (-18 and-20^{o}C for DOPG and DOPC, respectively), in contrast to DMPC or DMPC:DMPG mixtures, where the transition temperatures (around ~23^{o}C in solution) may even be increased in SPBs due to the stabilizing crystal surface. To remove non-specifically bound lipid from the flow system, it was necessary to include a brief washing with 150mM NaCl in the same buffer to remove lipids bound unspecifically to tubing in the flow system. After buffer exchange back to the original 20mM Tris-Cl pH 7.5, the resulting bilayers showed a uniform frequency shift of approximately -24 Hz and dissipation values below ~0.2x10^{-6}, indicating the formation of a uniform lipid bilayer on top of the silica surface.

Fig. 2A and 2B show representative traces of Δf and ΔD at the 3rd harmonic of such injections onto the SPBs. Exposure of SPBs to 1 (not shown) and 2µM peptide concentration resulted in a small decrease in resonance frequency, indicative of mass removal. The minor changes observed suggest that bilayer integrity is essentially unaffected by the presence of Nc at these concentrations. At $\geq$ 3 µM Nc, there was a much greater decrease in frequency (Δf) upon peptide injection. Δf stabilized at -36±0.9 Hz at 10-20 µM Nc. Assuming that the Sauerbrey relation (eq. 3) holds, this corresponds to a coupled mass of 638±14 ng/cm^2.

However, we observed changes in dissipation values (ΔD) of up to ~2x10^{-6} on injection of 3-10µM Nc and 4.3 x10^{-6} on injection of 20µM Nc (Fig. 2B). This indicates the formation of a highly hydrated film as a result of either (i) a peptide layer on top of the bilayer resulting in additional water trapped in the oscillation or (ii) rearrangement of the lipid bilayer as a result of peptide binding. Characterization of hydrated films by the Sauerbrey equation often underestimates the coupled mass due to viscous losses [16, 37]. We therefore employed Voigt viscoelastic modeling [16], in which we combine changes in frequency and dissipation, to quantify the lipid film as shown for the injection of 5µM Nc (Fig. 2C and Fig. S4) and summarized for 3-20µM injections (Fig. 2D). This allows us to evaluate the validity of the Sauerbrey equation in this study. As expected from a hydrated adlayer, Voigt modeling resulted in mass estimates upon addition of Nc which are only slightly larger than those obtained using the simpler Sauerbrey relation. The small differences

between the 3rd overtone estimate by Sauerbrey and Voigt modeling clearly indicate that the Sauerbrey relation effectively describes the mass of the combined film in the presence of Nc, despite its neglect of viscous losses. The 11th overtone displays a slightly smaller mass estimate. This discrepancy is due to the difference in the penetration depth of the oscillation in non-rigid films which decreases with increasing overtone numbers. Since the Sauerbrey estimate at the 3rd harmonic extends furthest into solution and is in good agreement with Voigt modeling, the following data refer to data of the 3rd harmonic.

The data for subsequent buffer rinsing (indicated by arrows in Figs. 2A and 2B) in Fig 2C highlight the necessity of employing Voigt modeling. While the Sauerbrey relation gives a decrease in adlayer mass at the 3µM injection, whose magnitude depends inversely on the overtone number, a dramatic increase in coupled mass is observed by Voigt modeling. The high dissipation values observed upon rinsing with buffer together with the mass increase suggests that a structural rearrangement of the film has occurred, transforming it from a relatively rigid bilayer (which obeys the Sauerbrey relation to a good approximation) to a soft, highly hydrated film. The mass estimates obtained (a) using the Sauerbrey relation at the 3rd overtone and (b) through Voigt modeling for all concentrations with the exception of 1 and 2 µM injections (for which overtone separation was insufficient for modeling) are shown in Fig. 2D as the average mass ± S.E.M of three replicates. Voigt modeling suggested film estimates similar to those obtained using the Sauerbrey relation on the frequency of the 3rd harmonics on injection of 3-20µM Nc (Fig. 2D), confirming that the Sauerbrey relation can be employed to a good approximation for the binding of Nc. However, subsequent buffer rinsing consistently resulted in larger mass estimates by Voigt modeling at 3- 20 µM Nc. These data suggest that irreversible rearrangements of the bilayer occur subsequent to interaction with Nc, leading to the formation of a highly hydrated film after removal of Nc by rinsing.

It is important to stress that both Sauerbrey and Voigt models describe the whole film including water and buffer components which are coupled to the oscillation. In cases where water and molecules are “trapped” in the oscillating film due to inhomogeneities or cavities, these will not behave as bulk medium. This means that the parameters obtained from either model describe the adlayer as well as coupled molecules, and it is thus not possible to separate the contributions from bilayers, Nc and water molecules. In contrast to QCM-D, optical techniques such as dual polarization interferometry (DPI) are sensitive only to the non-hydrated species adsorbed on the

surface. DPI allows determination of mass, density and thickness of biomolecules adsorbed at the solid-liquid interface from changes in the refractive index of the adsorbed film and recent progress has allowed description of isotropic films such as lipid bilayers [17, 18]. To study transitions in film mass and bilayer order further, we therefore carried out DPI experiments in which Nc was injected on supported lipid bilayers of the same 80:20 w/w% DOPC:DOPG lipid mixture.

Fig. 3 shows the change in mass and birefringence within the bilayer after addition of Nc. Injection of Nc at concentrations below 2µM caused no or little change in film mass whereas subsequent injections of higher concentrations lead to a marked increase in bilayer mass. It should be emphasized that the DPI mass values reported cannot be considered as precise measurements due to uncertainties regarding the $(dn/dc)_{lipid}$ and ρ_{lipid} [18]. We do, however, find it reassuring that DPI mass estimates are nearly super-imposable on QCM-D estimates during peptide interaction. Washing steps between Nc injections in DPI analysis did not reveal appreciable changes in mass estimates (data not shown) in contrast to the significant increase in acoustic mass observed by QCM-D. As only QCM-D is sensitive to water molecules coupled to the adsorbed film [38, 39], this emphasizes that significant water uptake accompanies Nc interactions with the membrane.

DPI further showed a decrease in birefringence from an initial value of ~0.016 at concentrations below 2µM to < 0.01 on injecting ≥10µM Nc, indicating a gradual distortion in the alignment of lipid acyl chains [17]. The initial birefringence is in good agreement with that of pure DOPC membranes [18].

In summary, the loss of bilayer alignment at concentrations ≥2µM observed by DPI is in excellent agreement with gradual membrane disintegration as suggested by QCM-D estimates after rinsing.

Membrane disruption by Nc results in decreased water accessibility to the lipid headgroup-tail interface

To further characterize the membrane-disrupting effects of Nc from the membrane perspective, we employed calcein dye leakage and Laurdan generalized polarity measurements. Calcein dye leakage from phospholipid vesicles is a well established method to study the permeability of small molecules through lipid membranes. In our experiments, maximum calcein leakage was evaluated by addition of Triton X-100 to ensure complete lysis of vesicles in the end of each experiment.

The membrane pertubation activity of Nc was examined by incubation with calcein-loaded vesicles at various P/L ratios (typical time courses shown in Fig. S5). Fig. 4A shows the dye leakage as a function of the peptide to lipid ratio. Incubation of Nc at P/L ratios up to ~1:1000 did not cause calcein leakage. 50% calcein dye leakage was obtained at P/L ratios of ~1:150 and maximum dye leakage by Nc was observed at an approximate P/L ratio of ~1:100. These concentrations are well below those where OCD data indicate a reorientation of Nc in the lipid bilayers, and clearly suggest that a transverse orientation of Nc is not required for membrane permeabilization. The realignment of Nc observed by OCD at P/L ratios above ~1:15 must therefore be caused by loss of membrane integrity rather than insertion across the lipid membrane.

Another way to study membrane rearrangements is to use the amphiphilic probe Laurdan, which partitions to the interface between polar headgroups and the hydrophobic core of lipid membranes. Laurdan fluorescence emission is sensitive to changes in the polarity of the surrounding environment and reports on the accessibility and mobility of water molecules in the vicinity of the probe [40-43]. Both accessibility and mobility of water molecules are defined by the packing of lipid membranes. Fig. 4B shows Laurdan's emission spectrum in 80:20 w/w% DOPC:DOPG membranes. The spectrum is very close to that of Laurdan in pure DOPC [44]. Addition of Nc to 80:20 w/w% DOPC:DOPG vesicles results in a gradual blue-shift of the emission spectrum at P/L ratios above ~1:60. The blue-shift of Laurdan emission indicates a decrease in the accessibility of water molecules at the interface between polar headgroups and the hydrophobic core. Consequently, Nc appears to modulate membrane packing.

The change in membrane environment on interaction with Nc can thus be followed through the evolution of Laurdan generalized polarity defined by $(I_{483}-I_{437})/(I_{483}+I_{437})$ as shown in Fig. 4A. An increase in Laurdan GP was observed at P/L ratios above ~1:60, continuing until saturation at P/L ratios around ~ 1:10. We note that the apparent modulation of membrane packing observed by Laurdan GP is in excellent agreement with the concentration range at which bilayer integrity is modulated in QCM-D and DPI measurements (~3-20µM) despite the fact that we are comparing Laurdan data on vesicles in solution with QCM-D and DPI data on supported planar bilayers. Interestingly, membrane leakage does not appear to be associated directly with membrane disintegration as calcein dye leakage approaches 100% just before the onset of membrane rearrangement. Together with the apparent inability of Nc to reorient along the bilayer normal (according to OCD experiments), the results suggests that transient pores may be formed at the

lower P/L ratios leading to increased membrane permeability, whereas membrane disintegration occurs at larger P/L values.

DISCUSSION

The OCD data presented here (Fig 1A) clearly demonstrate that Nc orients parallel to the membrane surface at P/L ratios below ~1:15, in agreement with the position in DPC micelles in a recent paramagnetic relaxation enhancement study [13]. In that particular study, Hα atoms of hydrophobic residues of Nc were shown to position at a minimum distance of 12-13 Å from the center of DPC micelles employed in the study. Charged groups (Lys, Asn, Arg, His) were located in the DPC/water interface. This surface localization implies that Nc will act as a wedge between lipid molecules, creating local discontinuities in the bilayer. In the head group region, the peptide thus acts as a spacer which separates lipid molecules and further creates an energetically unfavorable gap at the level of the acyl chains, as previously described for magainin and its analogue MSI-78 [45, 46]. These effects may in part counteracted by dehydration of head groups and through *e.g. trans-gauche* isomerizations or acyl chain interdigitation in order to render the membrane curvature less positive.

Our Laurdan fluorescence studies presented here show a blue-shift of the Laurdan emission spectrum in the P/L range from ~1:100 to ~1:10. The blue-shift of Laurdan emission (leading to an increase in Laurdan GP) suggests a decrease in the motional freedom of polar moieties embedded in the vicinity of the probe. This has been associated with a closer packing of phospholipids, leading to a reduction in the water accessibility at the hydrophobic/hydrophilic interface where Laurdan is located [40, 42, 47]. Similarly, Laurdan GP was found to increase with increasing size of pure DOPC vesicles [40], since relaxation of membrane strain through an increase in vesicle size caused phospholipid head groups to pack closer in the outer leaflet and thus exclude or reduce the mobility of water. We observe an increase in mechanical strain on insertion of Nc in lipid bilayers as indicated by the increase in GP. Induction of mechanical strain by the presence of Nc is further supported by our DPI data (Fig. 3) which show a decrease in the alignment of lipid chains at concentrations (≥2μM) comparable to the concentration range where head groups packing is affected (Fig 4A).

Whereas the addition of Nc at P/L ratios below ~1:100 was shown to induce leakage from calcein-filled vesicles, higher P/L ratios were required to induce more severe membrane defects, leading to complete disruption at P/L ratios of ~1:10 and above (Fig 4A). In the P/L range of ~1:90 to ~1:15 we didnot, however, observe evidence of peptide reorientation along the bilayer normal by OCD as required in the barrel-stave and toroidal pore mechanisms. Such behavior has previously been

observed in a solid state NMR study of peptides MSI-594 and MSI-78 (derived from magainin 2 and melittin, respectively) in which the peptides were shown to orient nearly parallel to the surface at concentrations where pores were present [48]. We employed supported lipid bilayers using two differente techniques to study the interaction with Nc. In QCM-D measurements we observe an initial binding of Nc to the surface whereas the membrane is fundamentally disturbed only after rinsing with buffer. Note that supported lipid bilayers are formed prior to exposure to Nc and that lipid bilayers may be stabilized by the support. In contrast, calcein leakage and Laurdan GP experiments were conducted using lipid vesicles free in solution. The methods further differ since we have a fixed but unknown amount of lipid in DPI and QCM-D measurements which makes it difficult to obtain precise P/L ratios. However, we observed excellent agreements of the membrane disruptive activity of Nc as a function of the absolute Nc concentration in both Laurdan GP, QCM-D and DPI measurements.

Complete membrane disintegration appears to occur at P/L ratios of ~1:10, corresponding to ~5µM Nc as shown by apparent plateau of Laurdan GP. This is in excellent agreement with DPI and QCM-D results showing the development of highly hydrated films after exposure to 3-20µM Nc and loss of lipid alignment (Fig 2D and Fig 3). Solution CD of Nc showed a strong induction of α-helicity in Nc at P/L ratios below ~1:100, whereas a decrease in α-helicity was observed at higher ratios approaching that of pure DOPC vesicles at ~1:10 (Fig. 1B). Phosphocholine headgroups occupy approximately 62Å^2 [49] in the bilayer which is approximately 6 times lower than that occupied by each Novicidin molecule in an amphipathic orientation in the membrane plane. The gradual loss of secondary structure in CD is thus expected to be saturation of binding, since the lipid surface is being increasingly populated by Nc and approaches saturation at these P/L ratios.

The P/L range of membrane rearrangements observed by Laurdan GP, DPI and QCM-D occur within the same P/L range as the change in secondary structure of Nc, thereby indicating that membrane disintegration occur only at relatively high surface coverages of approximately 5-10% and above, where the area covered by the lipid-bound Novicidin molecules approaches that of the total vesicle surface area.

As summarized in Fig. 5, these results account for a detergent-like mechanism of membrane disruption for Nc. Nc accumulates at the membrane surface in an orientation parallel to the membrane surface. At P/L ratios of ~1:1000, the membrane is sufficiently destabilized to cause leakage from calcein vesicles ultimately leading to loss of membrane integrity at P/L ratios above

~1:100 and complete membrane disintegration at ~1:10. We find it very encouraging that the concentration dependent interaction and membrane-disruptive activity of Nc with artificial membranes in this study is highly comparable to the *in vivo* activity against *E.coli* previously reported by our group [11].

ACKNOWLEDGEMENTS

We thank Brian Vad and Søren Vrønning Hoffmann for valuable discussions and help with practical issues. We thank Farfield Ltd for valuable discussions and help with the DPI instrument.

REFERENCES

[1] M. Zasloff, Nature 415 (2002) 389.
[2] R. E. W. Hancock, H. G. Sahl, Nature biotechnology 24 (2006) 1551.
[3] Z. Wang, G. Wang, Nucleic acids research 32 (2004) D590.
[4] Y.-Q. Xiong, M. R. Yeaman, A. S. Bayer, Antimicrob. Agents Chemother. 43 (1999) 1111.
[5] H. G. Boman, B. Agerberth, A. Boman, Infect. Immun. 61 (1993) 2978.
[6] M. S. Sansom, Progress in biophysics and molecular biology 55 (1991) 139.
[7] K. Matsuzaki, O. Murase, N. Fujii, K. Miyajima, Biochemistry 35 (1996) 11361.
[8] Z. Oren, Y. Shai, Biopolymers (Peptide Science) 47 (1998) 451.
[9] V. E. Bychkova, A. E. Dujsekina, S. I. Klenin, E. I. Tiktopulo, V. N. Uversky, O. B. Ptitsyn, Biochemistry 35 (1996) 6058.
[10] M. V. Sawai, A. J. Waring, W. R. Kearney, P. B. Cray Jr, W. R. Forsyth, R. I. Lehrer, B. F. Tack, Protein Engineering 15 (2002) 225.
[11] B. S. Vad, L. A. Thomsen, K. Bertelsen, M. Franzmann, J. M. Pedersen, T. Vosegaard, Z. Valnickova, T. S. Skrydstrup, J. J. Enghild, R. Wimmer, N. C. Nielsen, D. E. Otzen, Biochim. Biophys. Acta In press (2009).
[12] R. Wimmer, K. Andersen, B. Vad, M. Davidsen, S. Mølgaard, L. W. Nesgaard, H.-H. Kristensen, D. E. Otzen, Biochemistry 45 (2006) 481.
[13] M. Franzmann, D. Otzen, R. Wimmer, Chembiochem: a European journal of chemical biology (2009).
[14] E. Gasteiger, C. Hoogland, A. Gattiker, S. Duvaud, M. R. Wilkins, R. D. Appel, A. Bairoch, The proteomics protocols handbook (2005) 571.
[15] G. Sauerbrey, Z.Phys 155 (1959) 206.
[16] M. V. Voinova, M. Rodahl, M. Jonson, B. Kasemo, Arxiv preprint cond-mat/9805266 (1998).
[17] L. Yu, L. Guo, J. L. Ding, B. Ho, S. Feng, J. Popplewell, M. Swann, T. Wohland, BBA-Biomembranes 1788 (2009) 333.
[18] A. Mashaghi, M. Swann, J. Popplewell, M. Textor, E. Reimhult, Analytical Chemistry 80 (2008) 3666.
[19] Y. Wu, H. W. Huang, G. A. Olah, Biophysical Journal 57 (1990) 797.
[20] F.-Y. Chen, M.-T. Lee, H. W. Huang, 82 (2002) 908.
[21] J. F. Hunt, P. Rath, K. J. Rothschild, D. M. Engelman, Biochemistry 36 (1997) 15177.
[22] P. W. Winston, D. H. Bates, Ecology (1960) 232.
[23] J. G. Lees, B. R. Smith, F. Wien, A. J. Miles, B. A. Wallace, Analytical biochemistry 332 (2004) 285.
[24] Y. L. Pan, J. T. J. Cheng, J. Hale, J. Pan, R. E. W. Hancock, S. K. Straus, Biophysical journal 92 (2007) 2854.
[25] S. Morein, A. S. Andersson, L. Rilfors, G. Lindblom, Journal of Biological Chemistry 271 (1996) 6801.
[26] L. Yang, T. A. Harroun, T. M. Weiss, L. Ding, H. W. Huang, Biophysical Journal 81 (2001) 1475.
[27] J. Bürck, S. Roth, P. Wadhwani, S. Afonin, N. Kanithasen, E. Strandberg, A. S. Ulrich, Biophysical Journal 95 (2008) 3872.
[28] J. T. J. Cheng, J. D. Hale, M. Elliot, R. E. W. Hancock, S. K. Straus, Biophysical Journal 96 (2009) 552.
[29] K. Glasmästar, C. Larsson, F. Höök, B. Kasemo, J. Coll. Interface Sci. 246 (2002) 40.
[30] P. H. Justesen, T. Kristensen, T. Ebdrup, D. E. Otzen, J. Coll. Int. Sci. 279 (2004) 399.
[31] C. A. Keller, B. Kasemo, Biophys.J. 75 (1998) 1397.
[32] C. A. Keller, K. Glasmästar, V. P. Zhdanov, B. Kasemo, Physical Review Letters 84 (2000) 5443.
[33] R. Richter, A. Mukhopadhyay, A. Brisson, Biophysical Journal 85 (2003) 3035.
[34] R. P. Richter, A. Brisson, Langmuir 20 (2004) 4609.
[35] E. Reimhult, F. Hook, B. Kasemo, Langmuir 19 (2003) 1681.
[36] E. Reimhult, F. Hook, B. Kasemo, The Journal of Chemical Physics 117 (2002) 7401.

[37] C. Larsson, M. Rodahl, F. Höök, Anal. Chem. 75 (2003) 5080.
[38] F. Höök, B. Kasemo, T. Nylander, C. Fant, K. Sott, H. Elwing, Anal.Chem 73 (2001) 5796.
[39] F. Höök, J. Vörös, M. Rodahl, R. Kurrat, P. Böni, J. J. Ramsden, M. Textor, N. D. Spencer, P. Tengvall, J. Gold, Colloids and Surfaces B: Biointerfaces 24 (2002) 155.
[40] Y. L. Zhang, J. A. Frangos, M. Chachisvilis, Biochemical and Biophysical Research Communications 347 (2006) 838.
[41] C. C. De Vequi-Suplicy, C. R. Benatti, M. T. Lamy, Journal of fluorescence 16 (2006) 431.
[42] T. Parasassi, E. K. Krasnowska, L. Bagatolli, E. Gratton, Journal of Fluorescence 8 (1998) 365.
[43] T. Parasassi, M. Di Stefano, M. Loiero, G. Ravagnan, E. Gratton, Biophysical Journal 66 (1994) 763.
[44] T. Parasassi, E. Gratton, W. M. Yu, P. Wilson, M. Levi, Biophysical journal 72 (1997) 2413.
[45] B. Bechinger, BBA-Biomembranes 1712 (2005) 101.
[46] K. J. Hallock, D. K. Lee, A. Ramamoorthy, Biophysical journal 84 (2003) 3052.
[47] T. Parasassi, G. D. Stasio, A. Miccheli, F. Bruno, F. Conti, E. Gratton, Biophysical chemistry 35 (1990) 65.
[48] A. Ramamoorthy, S. Thennarasu, D. K. Lee, A. Tan, L. Maloy, Biophysical journal 91 (2006) 206.
[49] G. Cevc, *Phospholipids handbook*. CRC: 1993.

FIGURE LEGENDS

Figure 1: Oriented CD spectra of Nc.

(A) Oriented CD spectra of Nc in 80:20 w/w% DOPC:DOPG multilayers at different peptide:lipid (P/L) ratios. Arrows indicate direction of increasing P/L values. The spectra were normalized such that the intensities of all spectra at 208nm are the same. The spectra show that Nc remains oriented parallel to the surface at P/L ratios from 1:90 to 1:20. A red-shift of the ~190nm peak is observed at P/L ≥ 1:15 and the relative intensity of the 222nm band increases at P/L 1:10, revealing a partial loss of alignment in the surface bound state at this high peptide content.

(B) Solution CD of Nc in 100nm 80:20 w/w% DOPC:DOPG or 100% DOPC LUVs at P/L ratios of ~1:240 to ~1:6.

Figure 2: Interaction of Nc with supported lipid bilayers

QCM-D analysis of the concentration dependency of Nc interaction with supported lipid bilayers and reversibility of interaction by rinsing (arrows) in the reverse direction to avoid further injection of Nc.

(A) Changes in frequency (divided by the overtone) at the 3rd harmonic on injection of 2-20µM Nc.

(B) Energy dissipation at the 3rd harmonic on injection of 2-20µM Nc.

(C) Evaluation of the validity of the Sauerbrey relation by comparison with Voigt-model assuming a single layer film with a density of 1050 kg/m^3 at 3µM Nc concentration. The Voigt model reveals a highly hydrated film after washing, which is not described by the Sauerbrey equation.

(D) Estimates of Sauerbrey mass of bilayer and bilayers exposed to Nc and mass estimates by Voigt modeling after subsequent rinsing. Estimates are average of three experiments ± std.error.

Figure 3: Nc causes disorder in supported lipid bilayers

DPI analysis of the concentration dependency of Nc interaction with supported lipid bilayers. The birefringence (o) show significant reduction in lipid order at peptide concentrations above 1.3µM coinciding with increasing film mass (●), indicating membrane disintegration by Nc.

Figure 4: Nc permeabilizes membranes well before it disrupts the bilayer significantly.

(A) Laurdan generalized polarity measurements (■) and calcein dye leakage (□) as a function of the P/L ratio. Laurdan GP was defined as GP = $(I_{437}-I_{483})/(I_{437}+I_{483})$. The Nc concentration in Laurdan GP is given on the upper-axis for reference. (B) Emission spectra of Laurdan in the presence of Nc (normalized at wavelength with maximum intensity). The arrow indicates the direction of the blue-shift at increasing peptide to lipid ratios.

Figure 5: Mechanism of Nc interaction with anionic membranes.

(1) At low concentrations of Nc, it binds in a surface bound state and does not lead to sufficient interruption of the membrane to cause leakage. (2) At increasing concentration, the membrane is disturbed sufficiently to form transient pores although the overall integrity of the membrane is preserved and Nc remain in a surface bound state. (3) At higher concentrations, the membrane is significantly disturbed and disintegrates in a detergent-like manner.

Fig 1A

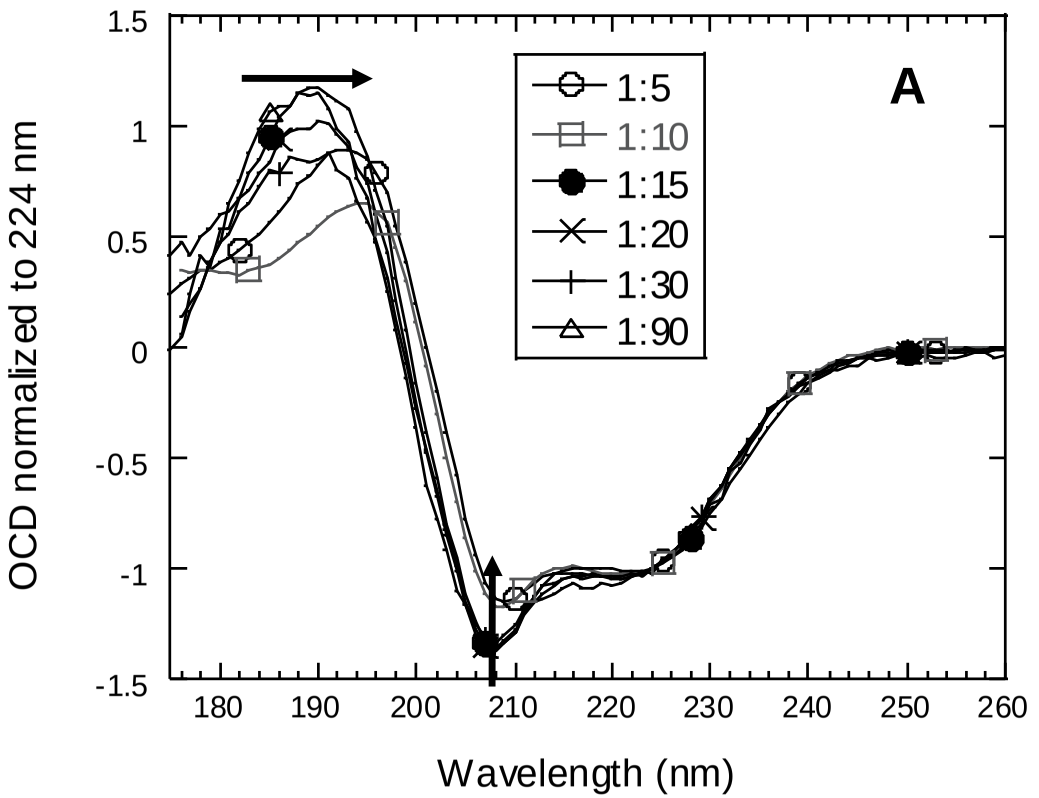
1.5
1
0.5
0
-0.5
-1
-1.5
180
190
200
210
220
230
240
250
260
OCD normalized to 224 nm
Wavelength (nm)
1:5
1:10
1:15
1:20
1:30
1:90
A

Fig 1B

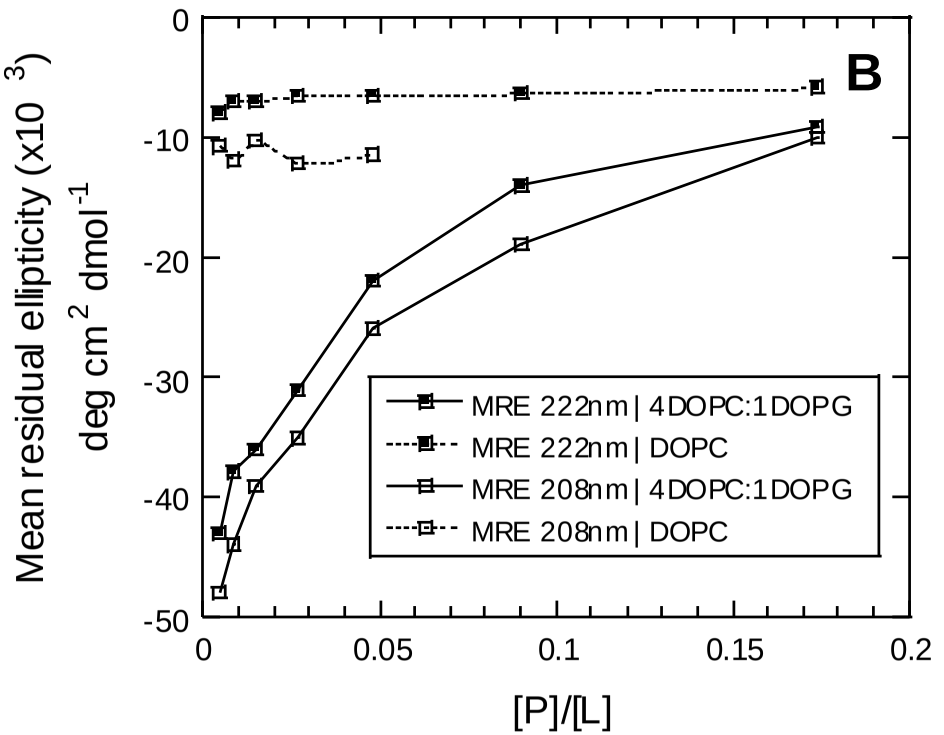
B
Mean residual ellipticity (x10 3)
deg cm 2 dmol-1
0
-10
-20
-30
-40
-50
0
0.05
0.1
0.15
0.2
[P]/[L]
MRE 222nm | 4DOPC:1DOPG
MRE 222nm | DOPC
MRE 208nm | 4DOPC:1DOPG
MRE 208nm | DOPC

Figure 2A

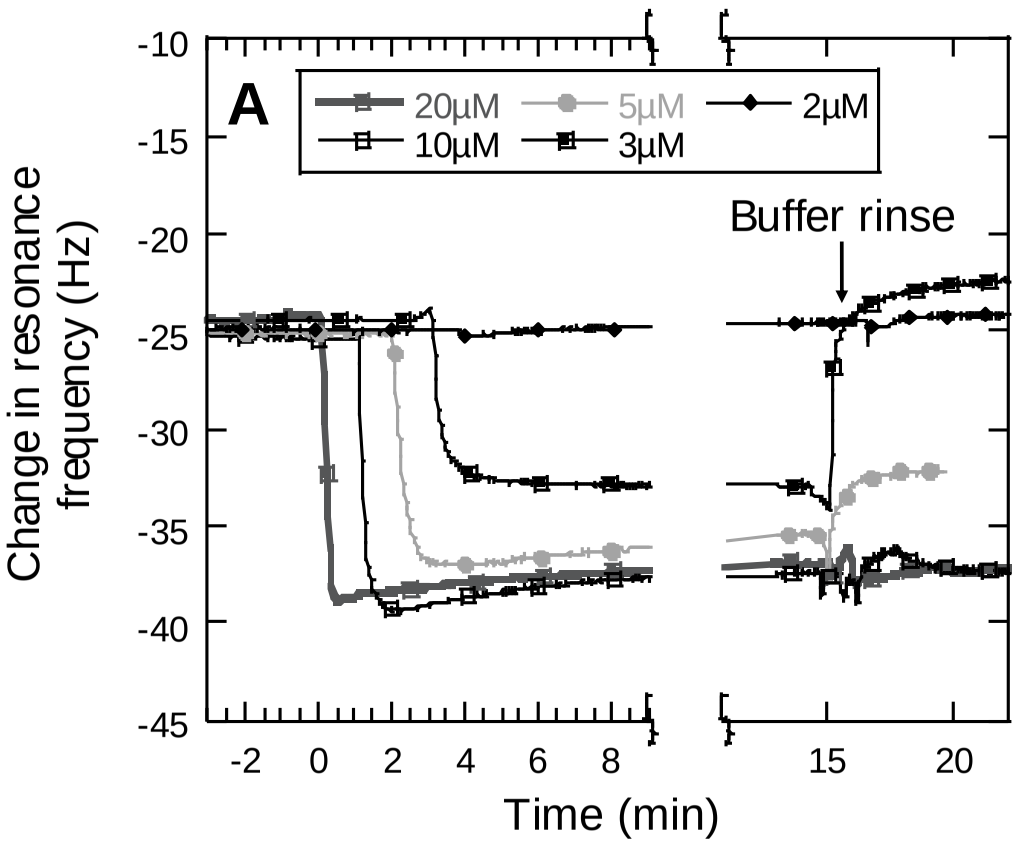
A
20µM
5µM
2µM
10µM
3µM
Buffer rinse
Change in resonance frequency (Hz)
-10
-15
-20
-25
-30
-35
-40
-45
-2
0
2
4
6
8
15
20
Time (min)

Figure 2B

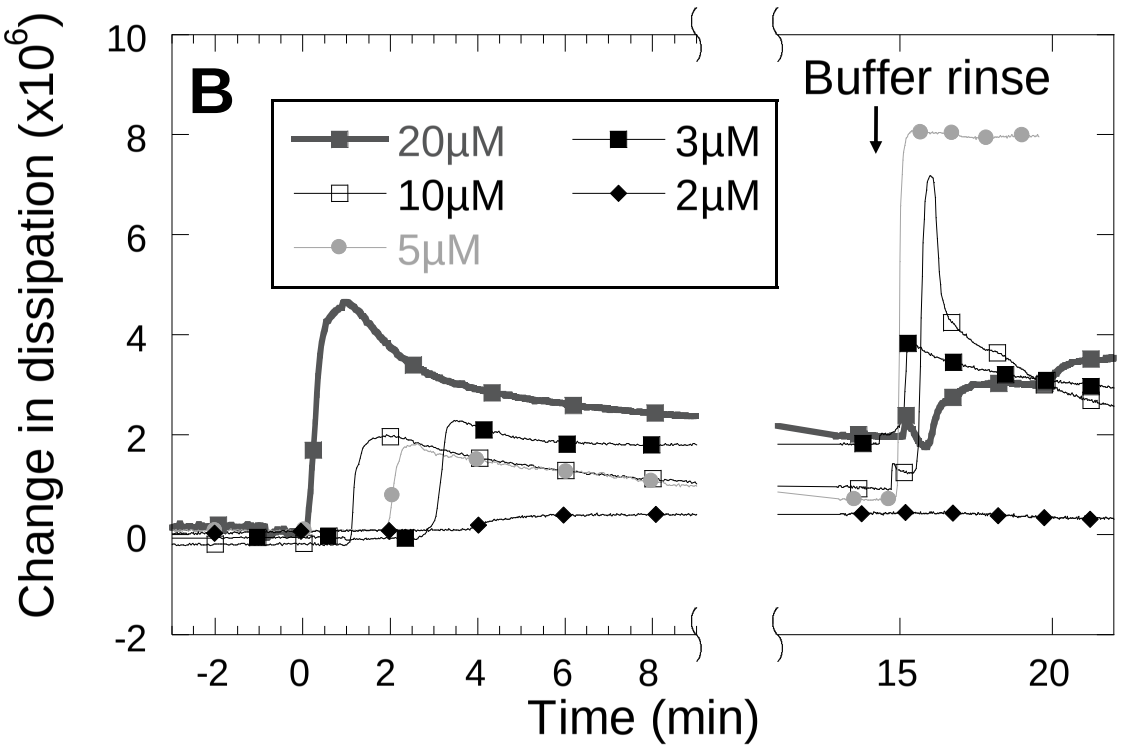
B
20μM
10μM
5μM
3μM
2μM
Buffer rinse
Change in dissipation (x10^6)
Time (min)
10
8
6
4
2
0
-2
-2
0
2
4
6
8
15
20

Figure 2C

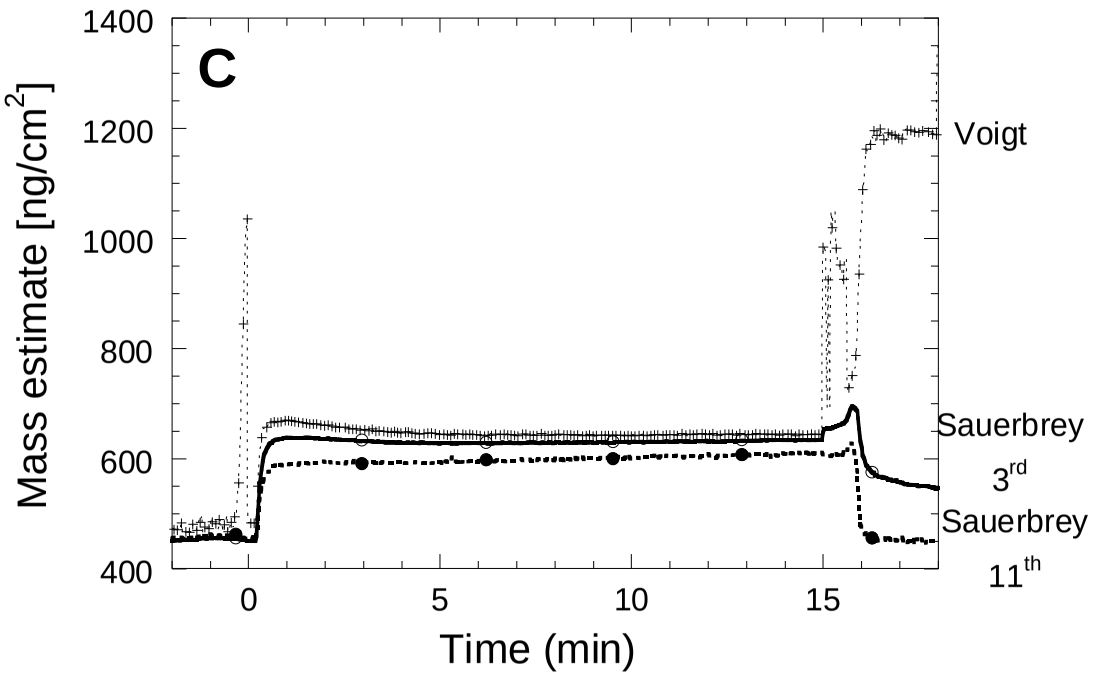
C
Mass estimate [ng/cm^2]
1400
1200
1000
800
600
400
0
5
10
15
Time (min)
Voigt
Sauerbrey 3rd
Sauerbrey 11th

Figure 2D

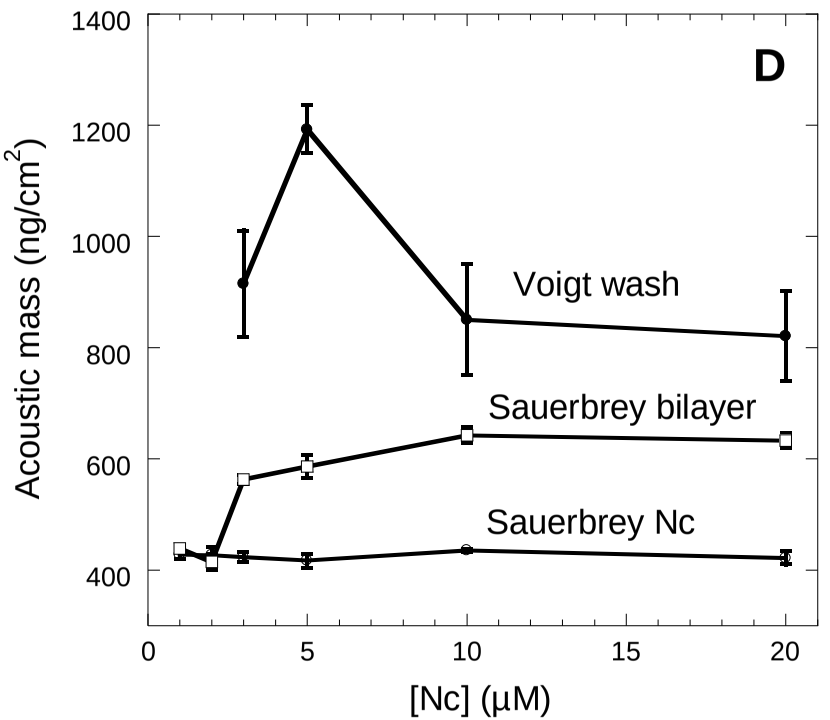
D
Acoustic mass (ng/cm^2)
1400
1200
1000
800
600
400
0
5
10
15
20
[Nc] (µM)
Voigt wash
Sauerbrey bilayer
Sauerbrey Nc

Figure 3

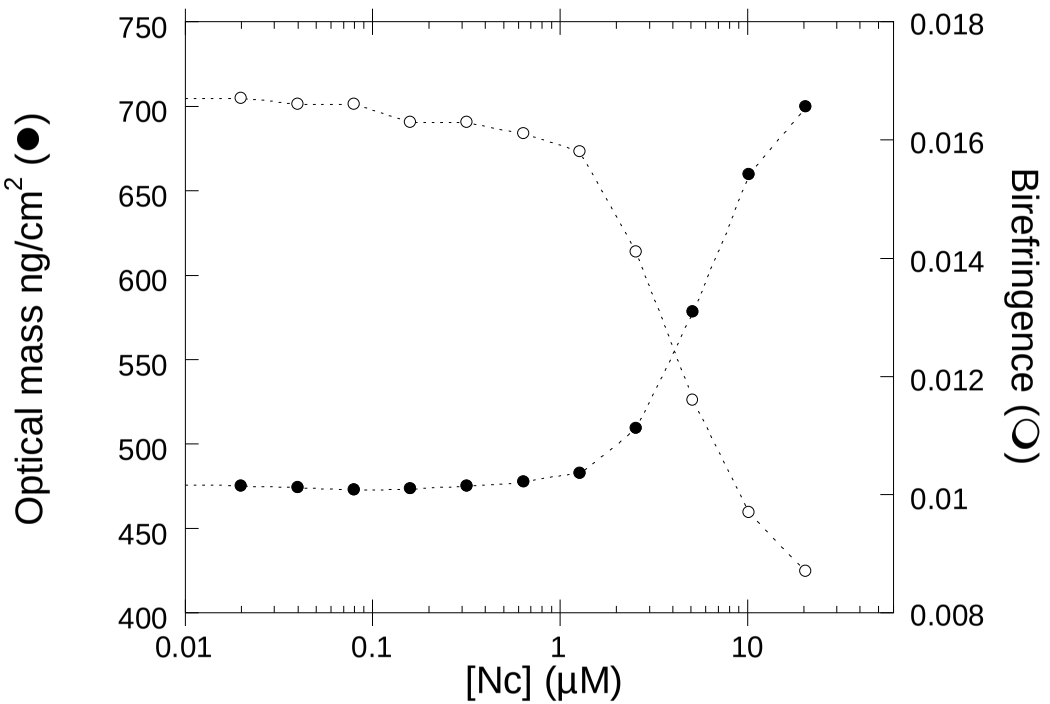
Optical mass ng/cm^2 (●)
Birefringence (○)
[Nc] (μM)
750
700
650
600
550
500
450
400
0.018
0.016
0.014
0.012
0.01
0.008
0.01
0.1
1
10

Fig 4A

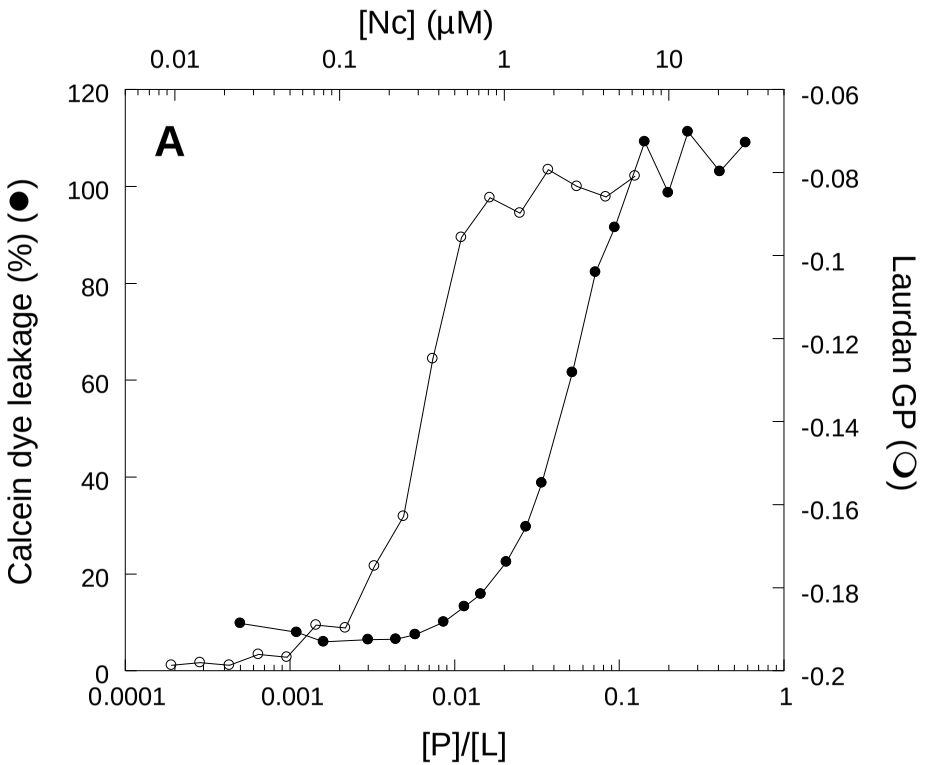
[Nc] (μM)
0.01
0.1
1
10
A
Calcein dye leakage (%) (●)
Laurdan GP (○)
120
100
80
60
40
20
0
-0.06
-0.08
-0.1
-0.12
-0.14
-0.16
-0.18
-0.2
0.0001
0.001
0.01
0.1
1
[P]/[L]

Figure 4B

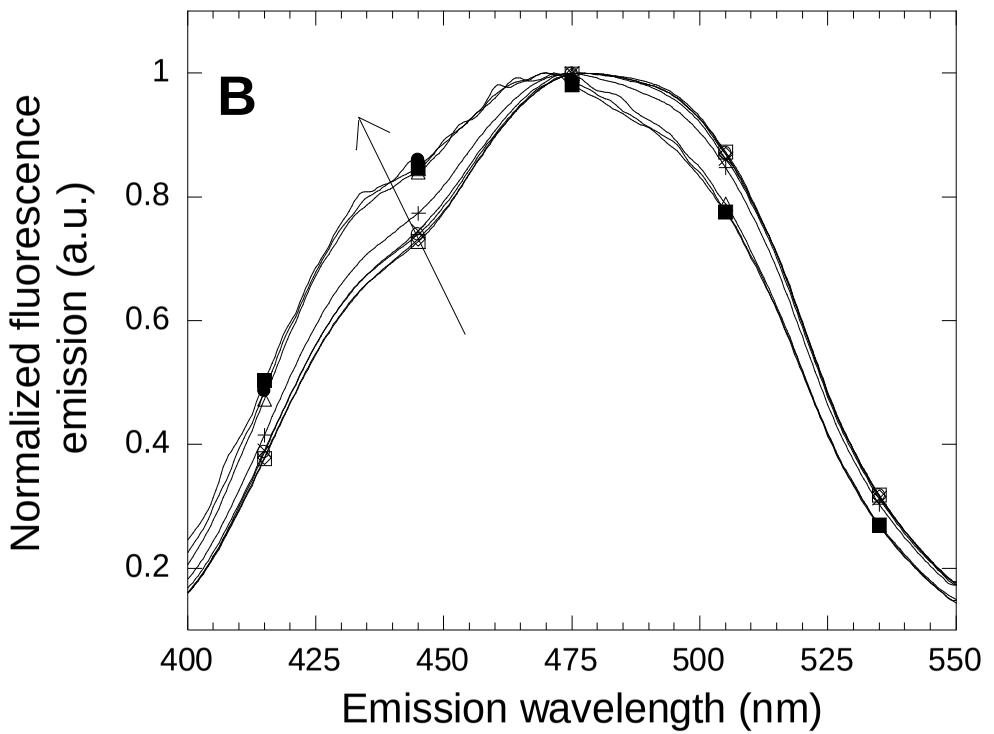
B
Normalized fluorescence emission (a.u.)
1
0.8
0.6
0.4
0.2
400
425
450
475
500
525
550
Emission wavelength (nm)

Figure 5

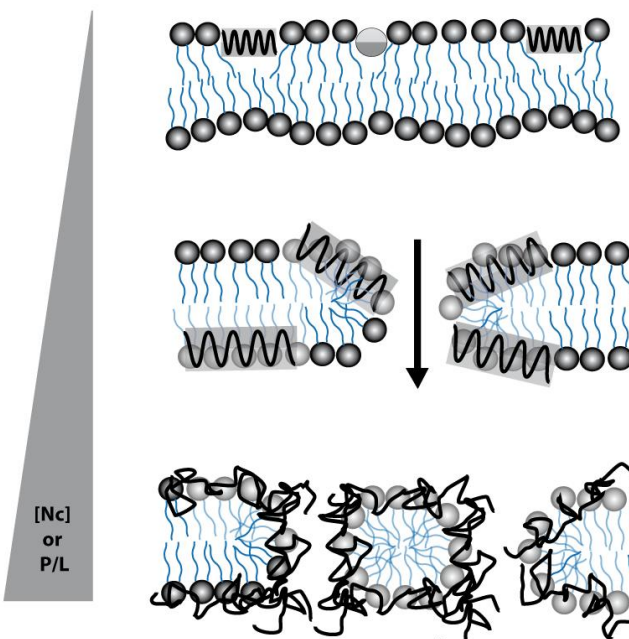

1) Nc binding
* Nc surface bound (OCD) 1:90 > P/L < 1:10
* No calcein leakage at P/L < 1:1000

2) Pore formation
* Calcein leakage P/L > 1:1000
* Intact vesicles (DLS) P/L < 1:100

3) Membrane disintegration
* Loss of secondary structure (CD) P/L > 1:240
* Loss of lipid order (DPI) > 2μM
* Tighter headgroup packing (Laurdan) at P/L > 1:100
* Membrane disintegration (QCM-D) > 3μM
* Complete calcein leakage at P/L > 1:100

Paper III:

Effective Membrane Channel Forming Properties of Alamethicin:Cyclodextrin Conjugates

Claudia U. Hjørringgard, Brian S. Vad, Søren B. Nielsen, Niels Chr. Nielsen, Daniel E. Otzen and Troels Skrydstrup
Manuscript submitted

Channel-forming Peptides

DOI: 10.1002/anie.200((will be filled in by the editorial staff))

Cyclodextrin-Scaffolded Alamethicin with Efficient Membrane Permeabilizing Properties**

Claudia U. Hjørringgaard, Brian S. Vad, Søren B. Nielsen, Thomas Vosegaard, Niels Chr. Nielsen, Daniel E. Otzen and Troels Skrydstrup**

Antimicrobial peptides (AMPs) represent a class of potential antibiotics, which are found among all classes of life as part of the innate immune response against fungi, viruses and both Gram-positive and Gram-negative bacteria.[1] Most of the AMPs disrupt the bacterial membrane leading to cell lysis, making it difficult for the bacteria to develop resistance against these peptides, in contrast to conventional small-molecule antibiotics, which have very specific binding sites in the cellular metabolism. The two main common membrane-disrupting models of the AMPs are the carpet and pore-formation mechanisms; the latter is subdivided into barrel-stave and toroidal pore mechanisms. [1e, 2]

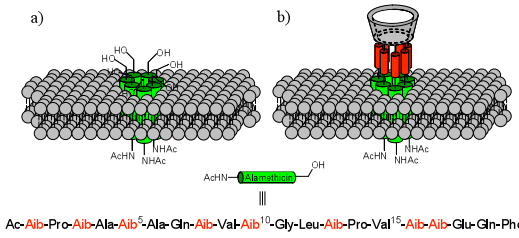

Figure 1. Models of a) an alamethicin channel and b) a cyclodextrin scaffolded alamethicin channel linked at the C-terminal.

One of the most frequently studied AMPs is the 19-mer peptide of fungal origin, alamethicin (Alm), which is acetylated at the N-terminus and extended with phenylalaninol at the C-terminus (Figure 1).[3] This peptide is a member of the peptaibol-family, which contains on average 40% of the helix-inducing aminoisobutyric acid (Aib) residue.[4] While it is well-established that this hydrophobic α-helical peptide exerts its biological effect via oligomerization and channel formation in the membrane (Figure 1a), the precise molecular structure of these pores still remains speculative[5] but recent NMR and MD investigations suggest that they are highly dynamic and non-uniform by nature.[6] The covalent tethering of alamethicin to a suitable cyclic template such as a cyclodextrin (CD) (Figure 1b) could lead to more stable membrane channels which are uniform in structure and therefore possibly more active than the free monomer, in particular a lower concentrations. Furthermore, these conjugates could provide suitable models for solid-state NMR studies of membrane channels composed of a predefined number of peptide units. Although considerable efforts have already been made to prepare and study chemically-linked alamethicin analogs with linear or cyclic scaffolds other than CDs,[7] investigations with conjugates containing >3 peptides either used truncated or residue modified alamethicins or the linker or template were not of appropriate size or structure for optimal channel formation in membranes.[8]

In this Communication, we report on the synthesis of a new class of templated alamethicins exploiting the full length peptides conjugated to α- and β-cyclodextrins from the C- or N-terminal, which can be assembled exploiting Click chemistry.[9] These templated AMPs, containing up to 7 alamethicins, possess the same membrane-induced structural changes as alamethicin according to circular dichroism, but display remarkably improved efficacy of membrane permeabilization compared to the non-templated peptide, as determined by calcein release experiments. These preliminary results suggest that the combination of antimicrobial peptides with a cyclodextrin scaffold is ideal for inducing stable membrane channel formation.

The choice of the cyclodextrin scaffold for these studies was made on the basis of the different ring sizes available in bulk quantities for cyclic oligosaccharides containing from 6 to 8 glucose units (α-, β- and γCD), and the ease of selective modification of the primary C6-hydroxyl group of the individual glucose units.[10] Alamethicin:CD conjugates varying in the number of peptides from 6 to 8 (as well as higher ratios for less abundant higher-size CDs) are therefore in principle accessible with this scaffold class. Covalent linking of the peptide to CD was conceived to proceed by a known transformation of the C6-hydroxyl groups to the corresponding azides[11] followed by a Cu-catalyzed cycloaddition with an alkyne conjugated alamethicin possessing an appropriate linker length.

The synthesis of the alkyne-containing linker covalently attached to either the N-terminal or the C-terminal end of alamethicin using a combination of solid-phase peptide synthesis and solution phase chemistry is depicted in Scheme 2. For the C-terminal functionalization, the synthetic route commenced with the trityl resin preloaded with bis-(aminoethyl)ethylene glycol (Scheme

[*] C. U. Hjørringgaard, Assoc. Prof. Dr. T. Vosegaard, Prof. Dr. N. C. Nielsen, Prof. Dr. T. Skrydstrup
Center for Insoluble Protein Structures (inSPIN), Interdisciplinary Nanoscience Center (iNANO) and Department of Chemistry, Aarhus University, Langelandsgade 140, 8000 Aarhus C, Denmark
Fax: (+45) 8619 6199
E-mail: ts@chem.au.dk

Dr. B. S. Vad, S. B. Nielsen, Prof. Dr. Daniel E. Otzen
Center for Insoluble Protein Structures (inSPIN), The Interdisciplinary Nanoscience Center, Department of Molecular Biology, Aarhus University, Gustav Wieds Vej 10C, 8000 Aarhus C, Denmark
E-mail: dao@inano.dk

[**] We thank the Danish National Research Foundation, the Lundbeck Foundation, the Carlsberg Foundation, the iNANO and OChem Graduate Schools and Aarhus University for generous financial support of this work.

Supporting information for this article is available on the WWW under http://www.angewandte.org or from the author.((Please delete if not appropriate))

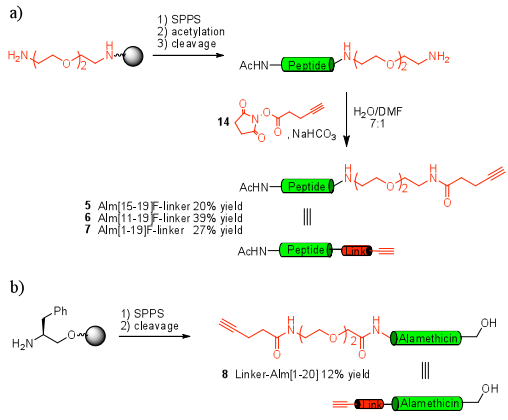

Scheme 2. Synthesis of the alkyne-containing linker attached to the peptide at a) the C-terminal b) the N-terminal.

2a). We have recently reported a fully automated solid-phase synthesis of peptaibols exploiting both microwave and double coupling of amino acids positioned after an α,α-dialkylated amino acid.[12] This methodology allowed us to rapidly prepare the resin bound Alm in which the phenylalaninol unit was replaced by phenylalanine. Subsequent TFA-mediated liberation of the peptide with the linker from the resin and further functionalization of the primary amine with *N*-succinimidyl-4-pentynoate completed the synthesis of the alkyne-linked alamethicin **7**. Two truncated versions of the peptaibol were also prepared as shown with compounds **5** and **6** containing, respectively, the amino acid residues 15–19 and 11–19 of Alm. These were synthesized as model systems for the conjugation studies, and also for investigations of the channel-forming properties of the shortened peptide derivatives.

The N-terminally linked alamethicin variant **8** was prepared by a fully automated synthesis starting from the trityl resin preloaded with phenylalaninol (Scheme 2b). Subsequent peptide coupling to install the full alamethicin structure was followed by double coupling of 8-(9-fluorenylmethyloxycarbonyl amino)-3,6-dioxaoctanoic acid under standard conditions, liberation of the primary amine and coupling with pentynoic acid. Cleavage from the resin with TFA provided the desired alkyne:peptide conjugate **8** in acceptable yields.

Considerable efforts were made to identify suitable reaction conditions for effectively promoting the Cu(I)-catalyzed alkyne-azide cycloaddition (CuAAC) for assembling the alamethicin-cyclodextrin conjugates. The results of the CuAAC are depicted in Table 1. Best reaction conditions were found using 20 mol% CuI and excess triethylamine in dry DMF at 70°C. While the cycloadditions with the alkynes **5** and **6** (entries 1 and 2) were finished after 4 hours, the same reactions with the full-length alamethicin–alkynes, **7** and **8**, to either the modified α- or βCD required longer reaction times for completion (entries 3–6).

To remove the copper ions, the metal scavenging resin Quadrapure™ IDA was then added. Purification of the synthesized conjugates **9** and **10** was accomplished by semi-preparative reverse phase HPLC and the compounds were characterized by MALDI-TOF MS. HPLC purification of the full-length conjugates linked at the C-terminal, AlmCαCD (**12**) and AlmCβCD (**11**), or at the N-terminal, AlmNαCD (**14**) and AlmNβCD (**13**), with molecular weights reaching up to 16.6 kDa was not suitable. However, this could be accomplished by gel filtration chromatography providing the desired macromolecules.

Characterization of conjugates by MALDI-TOF MS revealed that these compounds also contained to a certain extent CD conjugates with one less peptide.[13] Furthermore, and dependent

Table 1. CuAAC between the alkyne containing peptides and the azido CD-scaffolds.

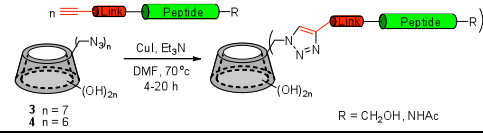

Entry	CD-scaffold		Alkyne	Time	Product (Yield)
1	**3**	**5**	Ac-VUUEQF	4 h	**9** (51%)[a]
2	**3**	**6**	Ac-GLUPVUUEQF	4 h	**10** (46%)[a]
3	**3**	**7**	Ac-UPUAUAQUVUGLUPVUUEQF	o/n[b]	**11** (49%)[c]
4	**4**	**7**	Ac-UPUAUAQUVUGLUPVUUEQF	o/n[b]	**12** (60%)[c]
5	**3**	**8**	UPUAUAQUVUGLUPVUUEQ-Phol	20 h	**13** (89%)[c]
6	**4**	**8**	UPUAUAQUVUGLUPVUUEQ-Phol	20 h	**14** (86%)[c]

[a] Isolated yields after RP-HPLC purification. [b] o/n = overnight. [c] Isolated yields after gel filtration chromatography.

on the structure of the conjugate, one to three copper ions were included in these scaffolded peptides (See Supplementary Information). This is most likely related to the large size of the structures, which impedes copper extraction and the high content of triazoles that can act as ligands for copper. Nevertheless, we assumed that these modifications would not influence the overall assessment of the membrane permeabilizing properties of these Alm:CD conjugates.

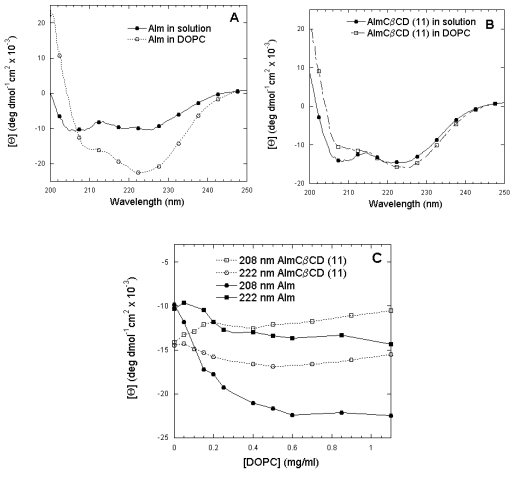

Figure 2.Circular dichroism spectra of a) alamethicin and b) alamethicin-β-CD conjugate linked at the C-terminal. c) Comparison of the ellipticity of Alm and AlmCβCD at different DOPC concentrations.

Coupling of Alm to a scaffold could be expected to impart lower flexibility and fewer conformational degrees of freedom when interacting with membranes. We used far-UV circular dichroism to follow the changes in the secondary structure of Alm alone and the various conjugates when exposed to the zwitterionic lipid di-oleoyl-phosphatidyl choline (DOPC). Qualitatively similar results were obtained with vesicles containing 80% DOPC + 20% of the anionic lipid di-oleoyl-phosphatidyl glycerol (DOPG). In solution, Alm and the alkyne-linked peptide **7** show minima of equal magnitude at 205 and 225 nm but undergo a large spectroscopic change upon binding to DOPC, leading to a deep minimum at 222–226 nm and a shoulder at 208 nm (shown for Alm in Fig. 2A). In contrast, the four full-length alamethicin:CD conjugates AlmCαCD (**12**), AlmCβCD (**11**), AlmNβCD (**13**) and AlmNαCD (**14**) only show minor changes upon switching from solution to DOPC (shown for AlmCβCD in Fig. 2B). The solution spectra of these constructs are more similar to their lipid spectra than to the solution spectrum of Alm, indicating that the scaffolding has induced a structure that is similar to the lipid-state. This may be seen more clearly in Fig. 2C where the ellipticity at the two minima 208 and 222 nm are plotted versus increasing DOPC concentration. The ellipticity changes are clearly smaller for scaffolded than for free Alm, although the titration is completed at roughly the same lipid concentration for both constructs, indicating an essentially unaltered lipid affinity.

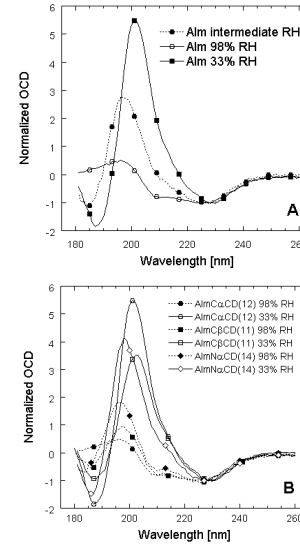

Figure 3. Oriented circular dichroism of a) alamethicin in multilayer membranes. [Peptide]/[Lipid] = 1/50 and b) AlmCβCD (**11**), AlmCαCD (**12**) and AlmNαCD (**14**) in multilayer membranes. [Peptide]/[Lipid] = 1/15.

To probe the orientation of the peptides in the lipid, we recorded oriented circular dichroism spectra of free and scaffolded Alm in multilayer membranes composed of 80% DOPC:20% DOPG lipids under conditions of controlled humidity.[14] With this technique, it is possible to distinguish between helical orientations parallel and perpendicular to the membrane plane, since the orientation parallel to the membrane gives rise to a negative signal at ~208 nm, which is much less pronounced in the perpendicular orientation.[15] Under low humidity conditions (33% relative humidity, RH), free Alm adopts an orientation parallel to the membrane plane which changes to the inserted state perpendicular to the membrane plane on hydration of the membrane (98% RH) (Fig. 3A), leading to a pronounced minimum at 186 nm and a maximum around 202 nm. Similar changes are seen for C-terminally linked Alm conjugates, AlmCαCD (**12**) and AlmCβCD (**11**) (Fig. 3B). For the N-terminally linked Alm conjugates, AlmNαCD (**14**) and AlmNβCD (**13**), the maximum is slightly blue-shiftet to 198 nm, indicating that the helices are inserted in a preferentially perpendicular but slightly tilted state. The four Alm:CD conjugates reorient along the bilayer under low humidity conditions (33% RH), indicating that the CD scaffold does not interfere with the peptide's ability to change orientation.

Finally, we examined the ability of the scaffolded Alm to permeabilize DOPC vesicles. We used the calcein release assay, in which calcein is entrapped within vesicles at a concentration high enough to cause self-quenching of its fluorescence.[16] Permeabilization of vesicles leading to calcein release into the exterior dilutes the calcein sufficiently to induce a strong increase in fluorescence, which can be followed in real time. Complete release is affected by the addition of Triton X-100, allowing us to normalize data.

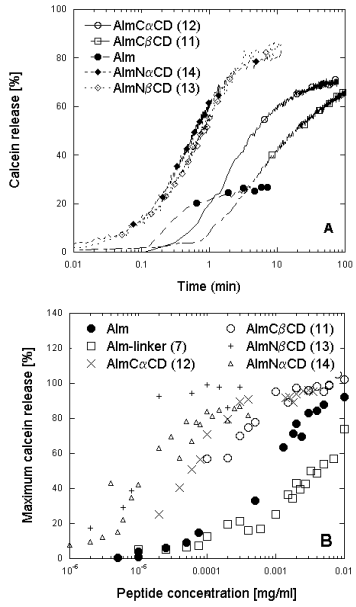

Figure 4. **A**) Calcein release assay. [Peptide]/[Lipid] = 1/1000. **B**) Maximum calcein release at different peptide concentrations.

The kinetics of release of calcein varies among the different constructs at comparable concentrations. The C-terminally linked Alm conjugates AlmCαCD (**12**) and AlmCβCD (**11**) take up to ten-fold longer time than Alm alone to reach a fluorescence plateau, whereas the N-terminally linked Alm conjugates AlmNαCD (**14**) and AlmNβCD (**13**) are just as rapid as the free peptide (Fig. 4A). However, it is striking that in all cases scaffolded Alm is significantly more efficient than free Alm on a mass basis (Fig. 4B); the amount of peptide needed to effect 50% release is reduced 10-fold (relative to Alm alone) for the C-terminally linked conjugates and *an impressive 100-fold* for the N-terminally linked conjugates.[17] This ranking is observed in both zwitterionic and partially anionic lipids. Furthermore, the C-terminally linked alamethicins require higher protein concentrations to permeate anionic vesicles. The preference for zwitterionic lipids has also previously been observed for the cationic AMPs pardaxin and novicidin.[18] However, we do not observe this effect to the same extent with N-terminally linked alamethicins, suggesting that it is linked to the mode of insertion rather than the linking to cyclodextrin. These results support our initial assumption that less conjugated alamethicin is needed to permeate vesicles due to a higher local concentration of peptide. The difference observed for the C-and N-terminally linked alamethicin is perhaps due to a difference in the insertion mechanism. Nevertheless, the full-length alamethicin is a prerequisite for lysis, since a β-CD scaffold coupled to the truncated peptide corresponding to residues 11-19 of alm showed essentially no (0-3%) permeabilization of DOPC and 80% DOPC:20% DOPG vesicles.

In summary, the channel-forming peptide, alamethicin has been synthesized with an alkyne group linked to either the C- or N-terminal. The alkyne containing peptides were then attached to a cyclodextrin scaffold by use of Click chemistry. The membrane permeabilizing properties of the conjugates proved to be highly effective and lysis experiments revealed a 100-fold increase in activity for the most active conjugate in comparison to the free peptide. Further work is in progress to examine other antimicrobial peptide-cyclodextrin conjugates such as novicidin, as well as to examine in more detail the conformational preferences and channel structures of conjugates by NMR studies. This work will be reported in due course.

Experimental Section

An example of the synthesis of alamethicin:cyclodextrin conjugates: Per-6-(4-(*N*-(2-(2-(Alm[1-20]aminomethoxy)ethoxy)-ethyl)pent-4-ylamide)-1*H*-1,2,3-triazol-1-yl)-β-cyclodextrin (13)

Hepta-6-azido-β-cyclodextrin (0.8 mg, 0.62 mmol) was dissolved in dry DMF (0.01 M) under an atmosphere of argon. The alkyne containing peptide (**8**, 10 mg, 4.65 mmol, 1.1 eq. pr. azide) and Et_3N (1.73 mL, 12.4 mmol) were added and the reaction mixture was deoxygenated by bubbling through with argon for 15 min. CuI (0.2 mg, 1.0 mmol, 20 mol% according to the alkyne) was added and the reaction mixture was heated to 70°C and stirred for 20 h. Quadrapure™ IDA resins (0.16 mmol/g) were added and shaken over night. The resins were filtered off and the reaction mixture evaporated *in vacuo*. The crude product was dissolved in MeCN/NH_3(aq,2.5%), lyophilized and purified by gel filtration chromatography using a Superdex™ 200 10/300 column with 20% MeCN in 2.5% NH_3(aq) as the eluent. The flow rate was 0.5 mL/min. The product was isolated as a light blue solid (8.9 mg, 89%). MALDI-TOF MS $C_{749}H_{1204}N_{182}O_{224}$ [M+3*Na^++3*Cu^{2+}-8*H^+]; calculated 16582.5, found 16581.1.

Received: ((will be filled in by the editorial staff))
Published online on ((will be filled in by the editorial staff))

Keywords: Click chemistry · peptides · cyclodextrin · circular dichroism · antimicrobial

[1] a) J. D. Hale, R. E. Hancock, *Expert Review of Anti-infective Therapy* **2007**, 5, 951; b) K. Lohner, S. E. Blondelle, *Combinatorial Chemistry & High Throughput Screening* **2005**, *8*, 241; c) M. Zasloff, *Nature* **2002**, *415*, 389; d) K. A. Brogden, *Nat. Rev. Microbiol.* **2005**, *3*, 238; e) P. Hamill, K. Brown, H. Jenssen, R. E. Hancock, *Curr. Opin. Biotechnol.* **2008**, *19*, 628; f) W. van't Hof, E. C. I. Veerman, E. J. Helmerhorst, A. V. N. Amerongen, *Biol. Chem.* **2001**, *382*, 597; g) O. Toke, *Biopolymers* **2005**, *80*, 717; h) A. Giuliani, G. Pirri, S. F. Nicoletto, *Central European Journal of Biology*, **2007**, *2*, 1.

[2] a) Y. Shai, Z. Oren, *Peptides* **2001**, *22*, 1629; b) L. Yang, T. A. Harroun, T. M. Weiss, L. Ding, H. W. Huang, *Biophys. J.* **2001**, *81*, 1475; c) G. Baumann, P. J. Mueller, *J. Supramol. Struct.* **1974**, *2*, 538; d) S. J. Ludtke, K. He, W. T. Heller, T. A. Harroun, L. Yang, H. W. Huang, *Biochemistry* **1996**, *35*, 13723.

[3] a) C. E. Meyer, F. Reusser, *Experentia* **1967**, *23*, 85; b) L. G. Gordon, D. A. Haydon, *Biochim. Biophys. Acta* **1972**, *255*, 1014. Selected reviews: c) D. S. Cafiso, *Annu. Rev. Biophys. Biomol. Struct.* **1994**, *23*, 141; d) M. S. P. Sansom *Q. Rev. Biophys.* **1993**, *26*, 365; e) B. Leitgeb, A. Szekeres, L. Manczinger, C. Vágvölgyi, L. Kredics, *Chem. Biodivers*. **2007**, *4*, 1027; f) G. A. Woolley, B. A. Wallace, *J. Membr. Biol*. **1992**, *129*, 109.

[4] L. Whitmore, B. A. Wallace, *Eur. Biophys. J.* **2004**, *33*, 233.

[5] Several structures have been proposed: a) R. O. Fox, F. M. Richards, *Nature* **1982**, *300*, 325; b) M. K. Mathew, P. Balaram, *FEBS lett*. **1983**, *157*, 1; c) M. Bak, R. P. Bywater, M. Hohwy, J. K. Thomsen, K. Adelhorst, H. J. Jakobsen, O. W. Sørensen, N. C. Nielsen, *Biophys. J.* **2001**, *81*, 1684; d) J. Breed, P. C. Biggins, I. D. Kerr, O. S. Smart, M. S. P. Sansom, *Biochim. Biophys. Acta* **1997**, *1325*, 235; e) D. P. Tieleman, B. Hess, M. S. P. Sansom, *Biophys. J.* **2002**, *83*, 2393; f) D.

Constantin, G. Brotons, A. Jarre, C. Li, T. Salditt, *Biophys. J.* **2007**, *92*, 3978; g) J. E. Hall, I. Vodyanoy, T. M. Balasubramanian, G. R. Marshall, *Biophys. J.* **1984**, *45*, 233; h) K. He, S. J. Ludtke, D. L. Worchester, H. W. Huang, *Biophys. J.* **1996**, *70*, 2659; i) J. Pan, S. Trastram-Nagle, J. F. Nagle, *J. Membr. Biol.* **2009**, *231*, 11; j) L. Thøgersen, B. Schiøtt, T. Vosegaard, N. C. Nielsen, E. Tajkjorshid, *Biophys. J.* **2008**, *95*, 4337; k) E. S. Salnikov, M. De Zotti, F. Formaggio, X. Li, C. Toniolo, J. D. J. O'Neil, J. Raap, S. A. Dzuba, B. Bechinger, *J. Phys. Chem. B* **2009**, *113*, 3034.

[6] a) H. Duclohier, H. Wroblewski, *J. Membr. Biol.* **2001**, *184*, 1; b) D. O. Mak, W. W. Web, *Biophys. J.* **1995**, *69*, 2323; c) T. Vosegaard, K. Bertelsen, J. M. Pedersen, L. Thøgersen, B. Schiøtt, E. Tajkhorshid, T. Skrydstrup, N. C. Nielsen, *J. Am. Chem. Soc.* **2008**, *130*, 5028; d) K. Bertelsen, B. Paaske, L. Thøgersen, E. Tajkhorshid, B. Schiøtt, T. Skrydstrup, N. C. Nielsen, T. Vosegaard, *J. Am. Chem. Soc.* (*in press*); e) J. Dittmer, L. Thøgersen, J. Underhaug, K. Bertelsen, T. Vosegaard, J. M. Pedersen, B. Schiøtt, E. Tajkhorshid, T. Skrydstrup, N. C. Nielsen, *J. Phys. Chem. B* **2009**, *113*, 6928;

[7] Reviewed in: G. A. Woolley, *Chem. Biodivers.* **2007**, *4*, 1323.

[8] a) H. Duclohier, G. Alder, K. Kociolek, M. T. Leplawy, *J. Pept. Sci.* **2003**, *9*, 776; b) A. Matsubara, K. Asami, A. Akagi, N. Nishino, *Chem. Commun.* **1996**, 2069; c) A. J. Wassner, J. A. Hurt, J. D. Lear, K. S. Åkerfeldt, *Org. Lett.* **2002**, *4*, 1647.

[9] a) C. W. Tornøe, C. Christensen, M. Meldal, *J. Org. Chem.* **2002**, *67*, 3057; b) V. V. Rostovtsev, L. G. Green, V. V. Fokin, K. B. Sharpless, *Angew. Chem. Int. Ed.* **2002**, *41*, 2596; c) F. Himo, T. Lovell, R. Hilgraf, V. V. Rostovtsev, L. Noodleman, K. B. Sharpless, V. V. Fokin, *J. Am. Chem. Soc.* **2005**, *127*, 210; d) V. D. Bock, H. Hiemstra, J. H. van Maarseveen, *Eur. J. Org. Chem.* **2006**, 51; e) M. Meldal, C. W. Tornøe, *Chem. Rev.* **2008**, *108*, 2952.

[10] A. R. Khan, P. Forgo, K. J. Stine, V. T. D'Souza, *Chem. Rev.* **1998,** *98,* 1977.

[11] a) A. Gadelle, J. Defaye, *Angew. Chem. Int. Ed.* **1991**, *30*, 78; b) P. R. Ashton, R. Königer, J. F. Stoddart, *J. Org. Chem.* **1996**, *61*, 903; c) S. Srinivasachari, K. M. Fichter, T. M. Reineke, *J. Am. Chem. Soc.* **2008**, *130*, 2046.

[12] C. U. Hjørringgaard, J. M. Pedersen, T. Vosegaard, N. C. Nielsen, T. Skrydstrup, *J. Org. Chem.* **2009**, *74*, 1329.

[13] The purity of the conjugates was estimated on the peak areas in the MALDI-TOF MS spectra. The four conjugates had a purity > 80%.

[14] a) J. F. Hunt, P. Rath, K. J. Rothschild, D. M. Engelman, *Biochemistry* **1997**, *36*, 15177; b) P. W. Winston, D. H. Bates, *Ecology*, **1960**, *41*, 232.

[15] Y. Wu, H. W. Huang, G. A. Olah, *Biophys. J.* **1990**, *57*, 797.

[16] T. M. Allen, L. G. Cleland, *Biochim. Biophys Acta* **1980**, *597*, 418.

[17] The [Peptide]/[Lipid] ratio needed to obtain 50% calcein release: Alamethicin: 1/100. AlmCαCD and AlmCβCD: 1/1000. AlmNαCD and AlmNβCD: 1/10000.
[Peptide] is the concentration of alamethicin units, meaning that AlmCαCD and AlmNαCD contain 6 alm-units and AlmCβCD and AlmNβCD contain 7 alm-units.

[18] B. S. Vad, L. A. Thomsen, K. Bertelsen, M. Franzmann, J. M. Pedersen, S. B. Nielsen, T. Voesgaard, Z. Valnickova, T. Skrydstrup, J. J. Enghild, R. Wimmer, N. C. Nielsen, D. E. Otzen, *Biochim, Biophys. Acta,* Manuscript accepted for publication.

Channel-forming peptides

Claudia U. Hjørringgaard, Brian S. Vad, Søren B. Nielsen, Thomas Vosegaard, Niels Chr. Nielsen, Daniel E. Otzen* and Troels Skrydstrup* _____ **Page – Page**

Cyclodextrin-Scaffolded Alamethicin with Efficient Membrane Permeabilizing Properties

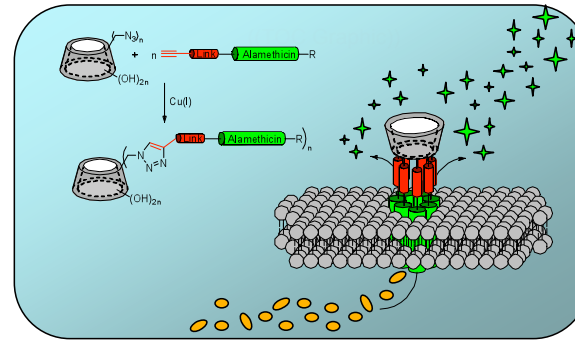

Bound is better than free. Alamethicin:cyclodextrin conjugates reveal an impressive 100-fold increase in the membrane permeabilizing abilities compared to the free antimicrobial peptide.

Supporting information for this article is available on the WWW under http://www.angewandte.org or from the author.

Supporting information for this article is available on the WWW under http://www.angewandte.org or from the author.

Cyclodextrin-Scaffolded Alamethicin with Efficient Permeabilizing Properties

Claudia U. Hjørringgaard, Brian S. Vad, Søren B. Nielsen, Thomas Vosegaard, Niels Chr. Nielsen, Daniel Otzen and Troels Skrydstrup.

Department of Chemistry, Center for Insoluble Protein Structures and Interdisciplinary Nanoscience Center,Aarhus University, Langelandsgade 140, DK-8000 Aarhus C, Denmark. Department of Molecular Biology, Aarhus University, Gustav Wieds Vej 10C, 8000 Aarhus C, Denmark.

Table of Contents

1. General experimental

Unless otherwise noted all reactions were carried out under inert atmosphere. Reactions were monitored by thin-layer chromatography (TLC) analysis. Flash chromatography was carried out on Fluka silica gel 60 (230-400 mesh).
All solvents and reagents were obtained commercially and were used without further purification with the exception of CH_2Cl_2, which was freshly distilled from CaH_2 prior to use.

NMR spectra were recorded on a Varian Gemini 400 spectrometer. ^{1}H-NMR at 400 MHz, ^{13}C NMR at 100 MHz and ^{19}F-NMR at 377 MHz. The chemical shifts are reported in ppm relative to solvent residual peak[1]. The following abbreviations are used to indicate multiplicity: s, singlet; d, doublet, dd, double doublet; t, triplet; dt, double triplet; dq, double quartet; m, multiplet.

MS spectra were recorded on a Micromass LC-TOF (ES) apparatus.
MALDI-TOF MS were recorded on a Bruker Daltonics autoflex mass spectrometer using α-cyano-4-hydroxycinnamic acid matrix.

SPPS was performed on a CEM Liberty microwave assisted peptide synthesizer on a 0.10 mmole scale unless otherwise noted. All SPPS resins, reagents and amino acids (excluding acid fluorides) were purchased from Iris Biotech, Germany. Amino acids and reagents are solutions in DMF unless otherwise noted.

A profound description of the different coupling cycles used for the SPPS can be seen in the supporting information to the note *An Automated Solid-phase Synthesis of Peptaibols*.[2] The peptides are synthesized using either Method A (single coupling of all amino acids) or Method B (double coupling of amino acids positioned after an α,α-dialkylated amino acid).

Analytical RP-HPLC was performed using an Agilent 1100 system with a Vydac nukleosil 100-5 column (C18, 4.6 mm ID x 250 mm, 5 μm particle diameter) or an Agilent Zorbax SB300-C18 (4.6 mm x 250 mm) operated at a flow rate of 1 mL/min at rt. Semi-preparative RP-HPLC purification was performed on an Agilent 1200 system with a Vydac 208TP510 column (C8, 10 mm ID x 250 mm, 5 μm particle diameter) or an Agilent Zorbax SB-C18 (9.4 mm x 250 mm) operated at a flow rate of 5 mL/min at rt. The solvent system: A = 0.1% TFA in H_2O, B = 0.1% TFA in MeCN. Absorbance was monitored at 215 nm and product percentages are given by peak areas at 215 nm.

Gel filtration was performed on an Agilent 1200 system using a Superdex^{TM} 200 10/300 column operated at a flow rate of 0.5 mL/min. The eluting solvent: 20% MeCN in NH_3(aq, 2.5%).

[1] Gottlieb, H. E.; Kotlyar, V.; Nudelman, A. *J. Org. Chem*. 1997, ***62***, 7512-7515.
[2] Hjørringgaard, C. U.; Pedersen, J. M.; Vosegaard, T.; Nielsen, N. C.; Skrydstrup, T. *J. Org. Chem*. **2009**, *74*, 1329-1332.

2. Modifications of Cyclodextrin[3]

Per-6-iodo-β-cyclodextrin, 1

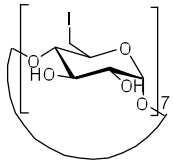

To a stirred solution of PPh_3 10.59 g, 40.37 mmol) in dry DMF (40 mL) was added I_2 (10.56 g, 41.72 mmol) over 10 min. Dry β-cyclodextrin (3.05 g, 2.69 mmol) was added and the temperature raised to 70˚c. The solution was stirred at this temperature for 20 h, after which it was reduced to approximately 15 mL under reduced pressure. NaOMe in MeOH (3 M, 18 mL) was added and the mixture was cooled to 0˚c and stirred for 30 min. The reaction mixture was poured into MeOH (400 mL) to form a precipitate, which was washed with MeOH, filtered and dried. The brownish precipitate was then Soxhlet extracted with MeOH for 24 h and dried under vacuum to give the pure product (3.79 g, 74%) as a white powder. ^{1}H-NMR (400 MHz, DMSO-d_6) δ (ppm) 3.29 (t, J = 9.4 Hz, 7H), 3.31 (H_2O), 3.35-3.47 (m, 14H), 3.57-3.67 (m, 14H), 3.80 (d, J = 9.4 Hz, 7H), 4.99 (d, J = 2.8 Hz, 7H), 5.92 (s, 7H), 6.02 (d, J = 6.4 Hz, 7H). ^{13}C-NMR (100 MHz, DMSO-d_6) δ (ppm) 9.5, 70.9, 71.9, 72.2, 85.9, 102.1. MALDI-TOF MS: $C_{42}H_{63}I_7O_{28}$ [M+Na+]; calculated 1926.6717, found 1925.9270.

Per-6-iodo-α-cyclodextrin, 2

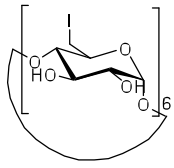

Same procedure as for per-6-iodo-β-cyclodextrin. Product (4.02 g, 80 %) as a white powder. ^{1}H-NMR (400 MHz, DMSO-d_6) δ (ppm) 3.31 (H_2O), 3.32-3.38 (m, 12H), 3.48-3.52 (m, 6H), 3.58-3.62 (m, 6H), 3.73 (d, J = 8.9 Hz, 6H), 3.80 (dt, J = 8.9 Hz, J = 2.4 Hz, 6H), 4.95 (d, J = 3.6 Hz, 6H), 5.63 (d, J = 2.4 Hz, 6H), 5.78 (d, J = 6.8 Hz, 6H). ^{13}C-NMR (100 MHz, DMSO-d_6) δ (ppm) 9.7, 70.7, 71.7, 72.2, 86.3, 101.8. MALDI-TOF MS: $C_{36}H_{54}I_6O_{24}$ [M+Na+]; calculated 1654.7171, 1654.2162.

Per-6-azido-β-cyclodextrin, 3

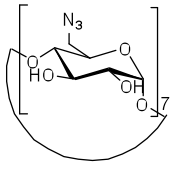

To a solution of per-6-iodo-β-cyclodextrin (1.00 g, 0.53 mmol) in dry DMF (15 mL) was added NaN_3 (0.34 g, 5.2 mmol). The suspension was stirred at 80˚c for 24 h and then poured into ice-cold water (400 mL) to form a precipitate. The precipitate was filtered and dried under vacuum to give the pure product (0.58 g, 84%) as a white powder.
^{1}H-NMR (400 MHz, DMSO-d_6) δ (ppm) 3.30 (H_2O), 3.32-3.38 (m, 14H), 3.55-3.61 (m, 14H), 3.69-3.77 (m, 14H), 4.89 (d, J = 3.6 Hz, 7H), 5.73 (d, J = 2.0 Hz, 7H), 5.87 (d, J = 6.8 Hz, 7H). ^{13}C-NMR (100 MHz, DMSO-d_6) δ (ppm) 51.3, 70.3, 72.0, 72.6, 83.2, 102.1. MALDI-TOF MS: $C_{42}H_{63}N_{21}O_{28}$ [M+Na+]; calculated 1332.4049, found 1332.0047.

[3] Srinivasachari, S.; Fichter, K. M.; Reineke, T. M. *J. Am. Chem. Soc*. **2008**, *130*, 4618-4627.

Per-6-azido-α-cyclodextrin, 4

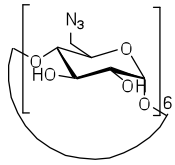

Same procedure as for per-6-azido-β-cyclodextrin. Product (1.31 g, 81%) as a white powder. ^{1}H-NMR (400 MHz, DMSO-d_6) δ (ppm) 3.31 (H_2O), 3.33-3.40 (m, 12H), 3.56-3.61 (dd, *J* = 13.2 Hz, *J* = 6.8 Hz, 6H), 3.72-3.82 (m, 18H), 4.88 (d, *J* = 3.6 Hz, 6H), 5.47 (d, *J* = 2.4 Hz, 6H), 5.64 (d, *J* = 6.8 Hz, 6H). ^{13}C-NMR (100 MHz, DMSO-d_6) δ (ppm) 51.4, 70.4, 71.6, 72.7, 83.4, 101.8. MALDI-TOF MS: $C_{36}H_{54}N_{18}O_{24}$ [M+Na+]; calculated 1145.3456, found 1145.1822.

3. Peptide synthesis

2,5-dioxopyrrolidin-1-yl pen-4-ynoate, 15[4]

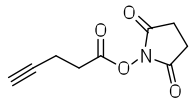

To a stirred solution of 4-pentynoic acid (1.00 g, 10.2 mmol) and N-hydroxysuccinimide (1.17 g, 10.2 mmol) in CH_2Cl_2/DMF (9:1, 5 mL) was added EDC (1.95 g, 10.2 mmol). The solution was stirred at rt overnight. The reaction mixture was diluted with CH_2Cl_2 (10 mL) and washed with 1M HCl, $NaHCO_3$ (sat.) and brine. The organic phase was dried with Na_2SO_4, filtered and evaporated *in vacuo*. The pure product was obtained by column chromatography (1:1 pentane/EtOAc as eluent) giving the product (1.48 g, 74%) as a white solid. ^{1}H-NMR (400 MHz, $CDCl_3$) δ (ppm) 2.05 (t, *J* = 2.8 Hz, 1H), 2.59-2.63 (m, 2H), 2.83-2.89 (m, 6H). ^{13}C-NMR (100 MHz, $CDCl_3$) δ (ppm) 14.3, 25.8, 30.5, 70.3, 81.1, 167.2, 169.1. HRMS $C_9H_9NO_4$ [M+Na+]; calculated 218.0430, found 218.0442.

Alamethicin[15-19]F-linker, Ac-VUUEQF-linker, 5

Synthesized by method B on a trityl resin preloaded with bis-(aminoethyl)ethylene glycol (0.25 mmol).
N-terminal acetylation was performed by treating the resin with Ac_2O (1.75 mmol) and DIPEA (3.50 mmol) in DMF (2 mL) for 45 min. Cleavage and deprotection of the peptide was performed by treating the resin with 5 mL TFA/CH_2Cl_2/H_2O/TIPS 47:47:4:2 (v/v) for 50 min. The cleavage mixture was concentrated to approximately 1 mL under reduced pressure, followed by precipitation in cold *t*-butyl methyl ether. Repeated centrifugation, decantation and trituration (3 times) followed by lyophilization gave the crude peptide (147.5 mg). To the crude peptide was added $NaHCO_3$ (aq) (2 mL of a solution of 53 mg $NaHCO_3$ in 3 mL H_2O) and 2,5-dioxopyrrolidin-1-yl pen-4-ynoate (63 mg, 0.325 mmol) dissolved in 0.5 mL DMF. The reaction mixture was shaken for 1 h, after which the last $NaHCO_3$ (aq) (1 mL) was added. The mixture was shaken over night. 1 eq. 2,5-dioxopyrrolidin-1-yl pen-4-ynoate and 2.5 eq. $NaHCO_3$ was added and the mixture was stirred for another day. The mixture was lyophilized, which gave the crude peptide-linker (365 mg). The crude was purified by semi-preparative HPLC-purification on a C8 column using a linear gradient from 5 to 40 % B in A over 20 min with a flow rate of 5 mL/min, giving pure alamethicin[15-19]F-linker (46.4 mg, 20% yield, 99.6% purity). MALDI-TOF MS: $C_{45}H_{69}N_9O_{13}$ [M+Na^+]; calculated 966.4913, found 966.3637.

[4] Wan, Q.; Chen, J.; Chen, G.; Danishefsky, S. J. *J. Org. Chem.* **2006**, *71*, 8244-8249,

Alamethicin[11-19]F-linker Ac-GLUPVUUEQF-linker, 6

Synthesized by method B on a trityl resin preloaded with bis-(aminoethyl)ethylene glycol (0.25 mmol).
N-terminal acetylation was performed by treating the resin with Ac_2O (1.75 mmol) and DIPEA (3.50 mmol) in DMF (2 mL) for 45 min. Cleavage and deprotection of the peptide was performed by treating the resin with 5 mL TFA/CH_2Cl_2/H_2O/TIPS 47:47:4:2 (v/v) for 50 min. The cleavage mixture was concentrated to approximately 1 mL under reduced pressure, followed by precipitation in cold *t*-butyl methyl ether. Repeated centrifugation, decantation and trituration (3 times) followed by lyophilization gave the crude peptide (376 mg). To the crude peptide was added $NaHCO_3$ (aq) (3 mL of a solution of 212 mg $NaHCO_3$ in 4 mL H_2O) and 2,5-dioxopyrrolidin-1-yl pen-4-ynoate (98 mg, 0.50 mmol) dissolved in 0.5 mL DMF. The reaction mixture was shaken for 1 h, after which the last $NaHCO_3$ (aq) (1 mL) was added. The mixture was shaken over night. 2,5-dioxopyrrolidin-1-yl pen-4-ynoate (30 mg, 0.154 mmol) and $NaHCO_3$ (100 mg) was added and the mixture was stirred for 4 h. The mixture was lyophilized, which gave the crude peptide-linker (885 mg). The crude was purified by semi-preparative HPLC-purification on a C8 column using a linear gradient from 20 to 50 % B in A over 20 min with a flow rate of 5 mL/min, giving pure alamethicin[11-19]F-linker (118 mg, 39% yield, 94% purity). MALDI-TOF MS: $C_{62}H_{97}N_{13}O_{17}$ [M+Na^+]; calculated 1318.7023, found 1318.4678.

Alamethicin[1-19]F-linker Ac-UPUAUAQUVUGLUPVUUEQF-linker, 7

Synthesized by method B on a trityl resin preloaded with bis-(aminoethyl)ethylene glycol (0.10 mmol).
N-terminal acetylation was performed by treating the resin with Ac_2O (1.75 mmol) and DIPEA (3.50 mmol) in DMF (2 mL) for 45 min. Cleavage and deprotection of the peptide was performed by treating the resin with 5 mL TFA/CH_2Cl_2/H_2O/TIPS 47:47:4:2 (v/v) for 50 min. The cleavage mixture was concentrated to approximately 1 mL under reduced pressure, followed by precipitation in cold *t*-butyl methyl ether. Repeated centrifugation, decantation and trituration (3 times) followed by lyophilization gave the crude peptide (227.2 mg). To the crude peptide was added $NaHCO_3$ (aq) (2 mL of a solution of 23 mg $NaHCO_3$ in 3 mL H_2O) and 2,5-dioxopyrrolidin-1-yl pen-4-ynoate (23 mg, 0.325 mmol) dissolved in 0.5 mL DMF. The reaction mixture was shaken for 1 h, after which the last $NaHCO_3$ (aq) (1 mL) was added. The mixture was shaken over night. 1 eq. 2,5-dioxopyrrolidin-1-yl pen-4-ynoate and 2.5 eq. $NaHCO_3$ was added and the mixture was stirred for another day. The mixture was lyophilized, which gave the crude peptide-linker (368 mg). The crude was purified by semi-preparative HPLC-purification using a C18 column and a linear gradient from 50 to 90 % B in A over 20 min with a flow rate of 5 mL/min, giving pure alamethicin[1-19]F-linker (58.0 mg, 27% yield, 96% purity). MALDI-TOF MS: $C_{103}H_{166}N_{24}O_{28}$ [M+Na^+]; calculated 2210.2201, found 2210.7297.

Linker-Alamethicin[1-20] Linker-UPUAUAQUVUGLUPVUUEQ-Phol, 8

Synthesized by method B on a trityl resin preloaded with phenylalaninol (0.10 mmol). 8-(9-Fluorenylmethyloxycarbonyl-amino)-3,6-dioxaoctanoic acid was double coupled onto the peptyl-resin using standard coupling conditions. Pentynoic acid was coupled onto the peptidyl-resin using standard coupling conditions. Cleavage and deprotection of the peptide was performed by treating the resin with 5 mL TFA/CH_2Cl_2/H_2O/TIPS 47:47:4:2 (v/v) for 50 min. The cleavage mixture was concentrated to approximately 1 mL under reduced pressure, followed by precipitation in cold *t*-butyl methyl ether. Repeated centrifugation, decantation and trituration (3 times) followed by lyophilization gave the crude peptide (180 mg). The crude was purified by semi-preparative HPLC-purification using a C18 column and a linear gradient from 50 to 90 % B in A over 20 min with a flow rate of 5 mL/min, giving pure Linker-Alamethicin[1-20] (26 mg, 12% yield, 100% purity). MALDI-TOF MS: $C_{101}H_{163}N_{23}O_{28}$ [M+Na^+]; calculated 2169.1936, found 2169.0523.

4. Peptide characterization

Compound 5

HPLC trace

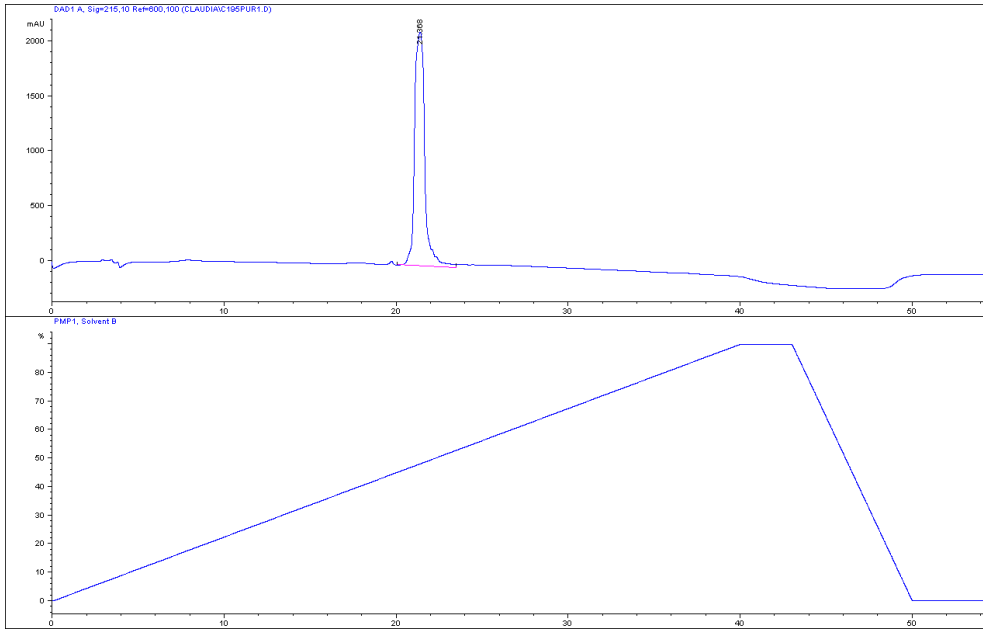

MALDI-MS

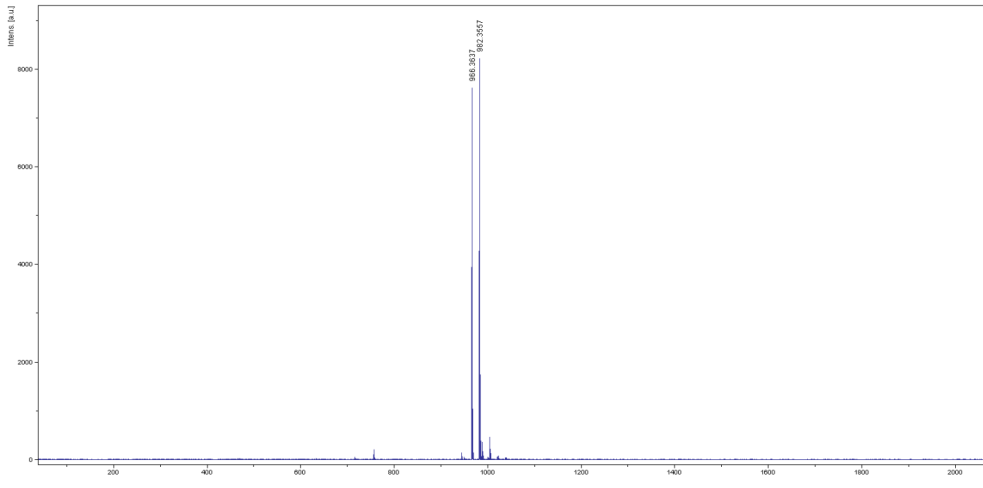

Compound 6

HPLC trace

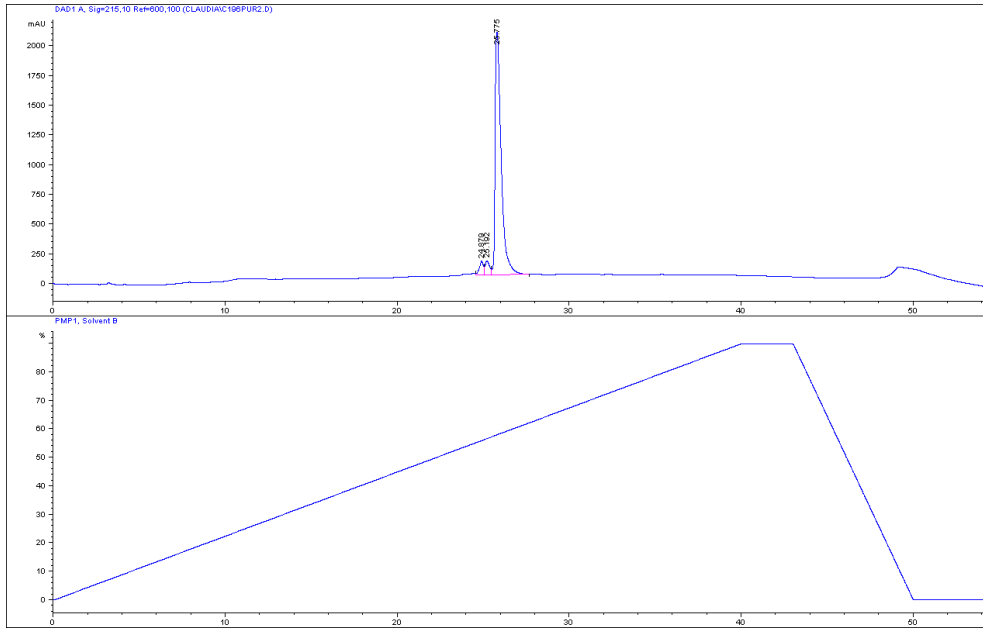

MALDI-MS

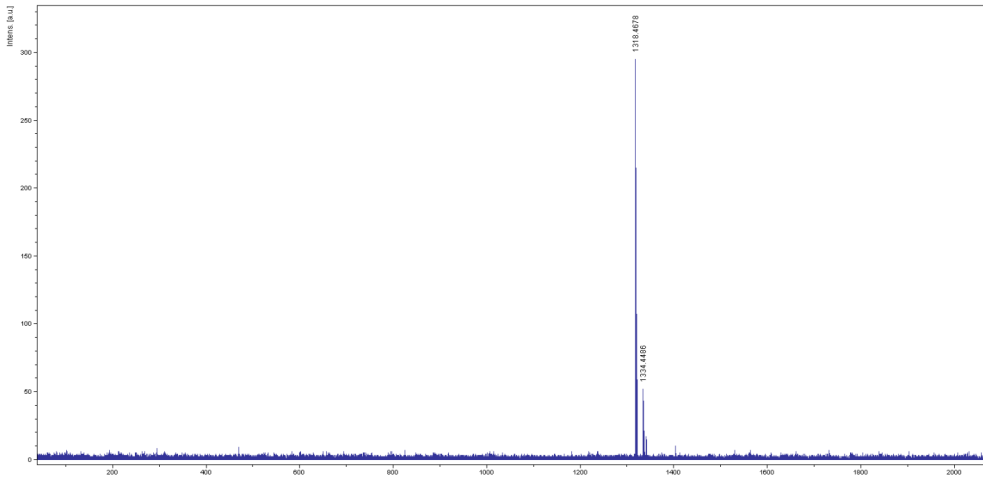

Compound 7

HPLC trace

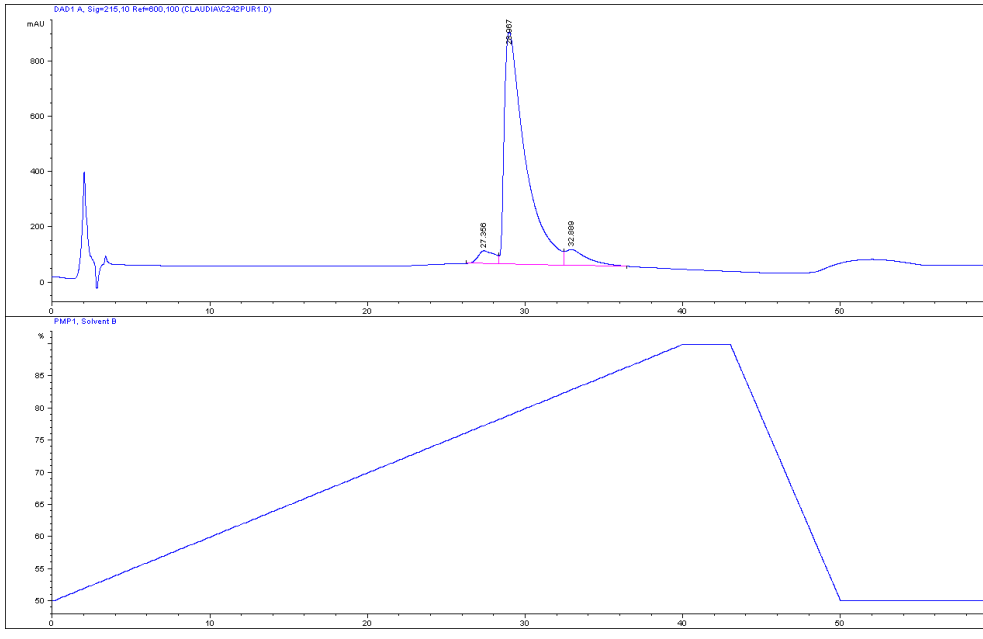

MALDI-MS

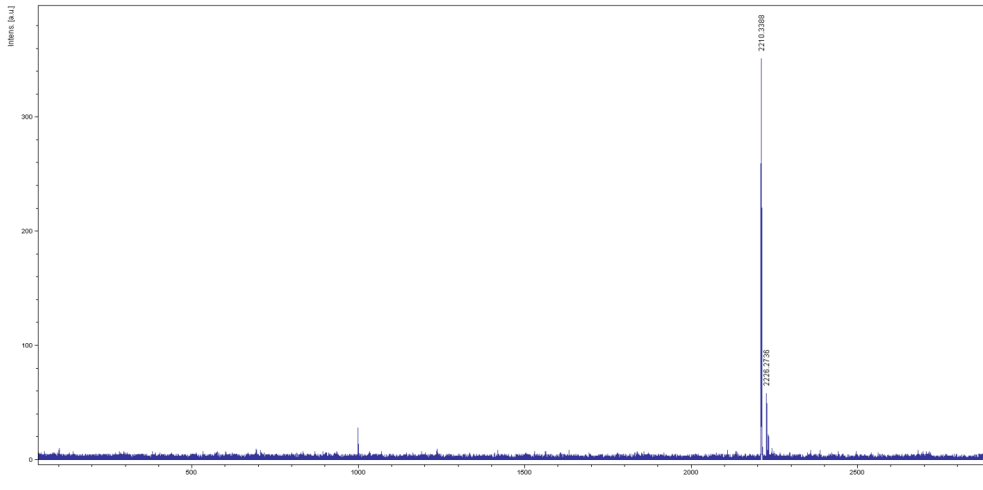

Compound 8

HPLC trace

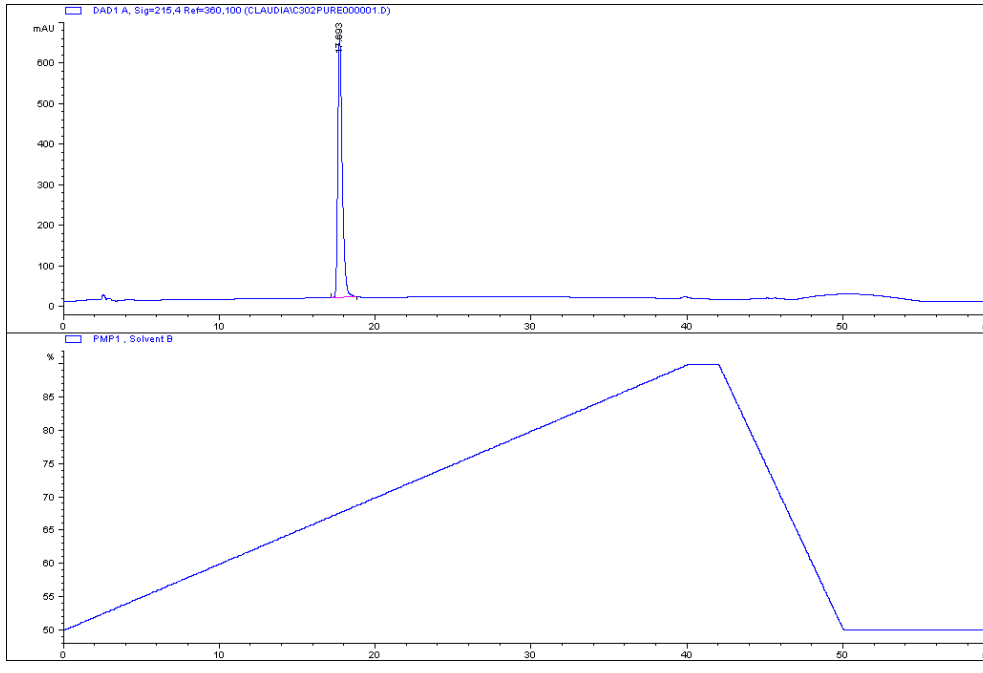

MALDI-MS

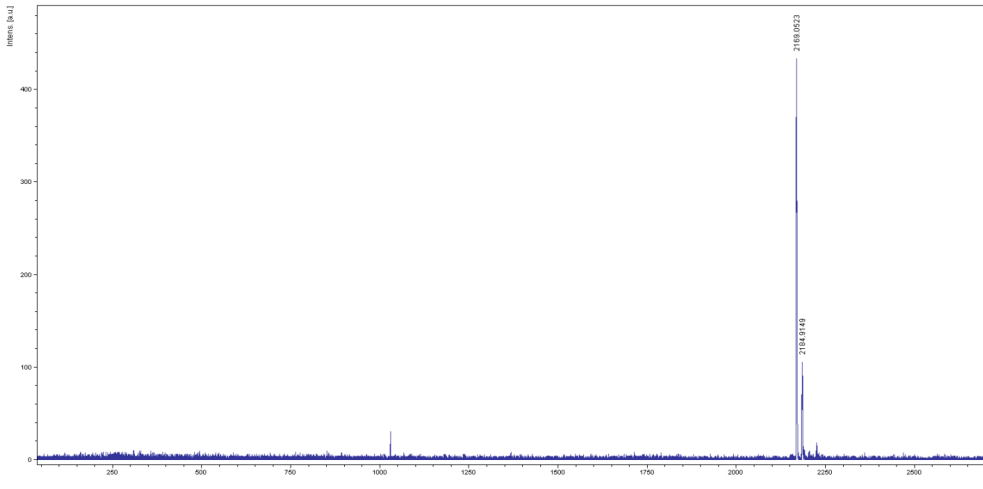

5.Click chemistry

General procedure for the CuAAC using the optimized conditions

The azide was dissolved in dry DMF (0.01 M) under an atmosphere of argon. The alkyne (1.1 eq. pr. azide) and Et_3N (20 eq.) were added and the reaction mixture was deoxygenated by bubbling through with argon for 15 min. CuI (20 mol% according to the alkyne) was added and the reaction mixture was heated to 70˚C and stirred for X h.
Quadrapure™ IDA resins (0.16 mmol/g) were added and shaken over night. The resins were filtered off and the reaction mixture evaporated *in vacuo*.

Per-6-(4-(*N*-(2-(2-(2-Alm[15-19]F-aminoethoxy)ethoxy)ethyl)pent-4-ylamide)-1*H*-1,2,3-triazol-1-yl)-β-cyclodextrin, 9

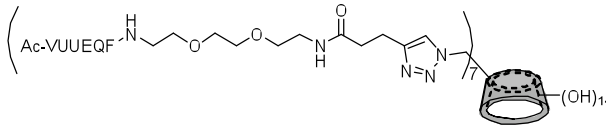

Reaction mixture was stirred for 4 h.
The crude product was dissolved in MeCN/H_2O, lyophilized and purified by semi-preparative HPLC-purification on a C8 column using a linear gradient from 20 to 50 % B in A over 20 min with a flow rate of 5 mL/min, giving pure product (5.7 mg, 51% yield, 97% purity). MALDI-TOF MS: $C_{357}H_{546}N_{84}O_{119}$ [M+Na^+]; calculated 7936.9153, found 7940.0840.

Per-6-(4-(*N*-(2-(2-(2-Alm[11-19]F-aminoethoxy)ethoxy)ethyl)pent-4-ylamide)-1*H*-1,2,3-triazol-1-yl)-β-cyclodextrin, 10

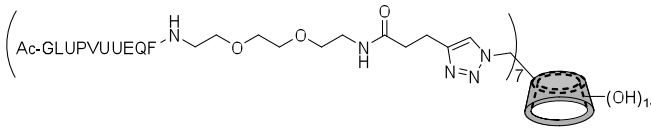

The reaction mixture was stirred for 4 h.
The crude product was dissolved in MeCN/H_2O and lyophilized. The crude product was purified by semi-preparative HPLC-purification on a C8 column using a linear gradient from 5 to 95 % B in A over 30 min with a flow rate of 5 mL/min, giving pure product (10.4 mg, 46% yield, 90% purity). MALDI-TOF MS $C_{476}H_{742}N_{112}O_{147}$ [M+Na^+]; calculated 10402.3927, [M+K^+]; calculated 10418.3666, found 10407.0711.

Per-6-(4-(*N*-(2-(2-(2-Alm[1-19]F-aminoethoxy)ethoxy)ethyl)pent-4-ylamide)-1*H*-1,2,3-triazol-1-yl)-β-cyclodextrin, 11

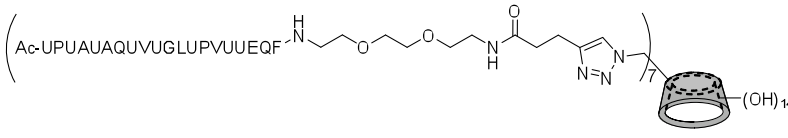

The reacton mixture was stirred over night.
The crude product was dissolved in MeCN/H_2O and lyophilized. The crude product was purified by gel filtration using a Superdex^{TM} 200 10/300 column with 20% MeCN in 2.5% NH_3(aq) as the eluent. The flow rate was 0.5 mL/min. The product was isolated as a white solid (7.4 mg, 49%). MALDI-TOF MS $C_{763}H_{1225}N_{189}O_{224}$[M+$K^+$+2*$Cu^{2+}$-4*$H^+$]; calculated 16780.8192, found 16780.7782.

Per-6-(4-(*N*-(2-(2-(2-Alm[1-19]F-aminoethoxy)ethoxy)ethyl)pent-4-ylamide)-1*H*-1,2,3-triazol-1-yl)-α-cyclodextrin, 12

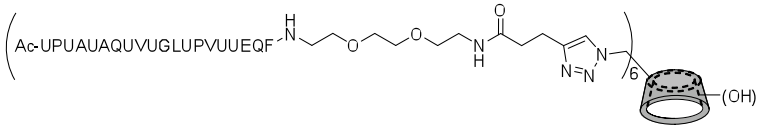

The reaction mixture was stirred over night.
The crude product was dissolved in MeCN/H_2O and lyophilized. The crude product was purified by gel filtration using a Superdex^{TM} 200 10/300 column with 20% MeCN in 2.5% NH_3(aq) as the eluent. The flow rate was 0.5 mL/min. The product was isolated as a white solid (9.3 mg, 60%).

MALDI-TOF MS $C_{652}H_{1046}N_{162}O_{191}$ [M+Cu^{2+}+5*Na^{+}-6*H^{+}]; calculated 14373.5435, found 14374.1156.

Per-6-(4-(*N*-(2-(2-(Alm[1-20]aminomethoxy)ethoxy)ethyl)pent-4-ylamide)-1*H*-1,2,3-triazol-1-yl)-β-cyclodextrin, 13

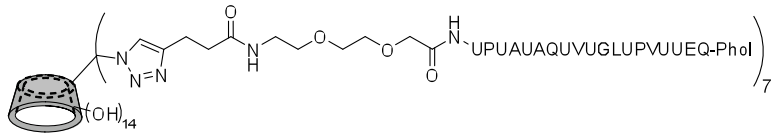

The reacton mixture was stirred for 20 h.
The crude product was dissolved in MeCN/NH_3(aq,2.5%) and lyophilized. The crude product was purified by gel filtration using a Superdex^{TM} 200 10/300 column with 20% MeCN in 2.5% NH_3(aq) as the eluent. The flow rate was 0.5 mL/min. The product was isolated as a light blue solid (8.9 mg, 89%). MALDI-TOF MS $C_{749}H_{1204}N_{182}O_{224}$[M+3*$Na^{+}$+3*$Cu^{2+}$-8*$H^{+}$]; calculated 16582.537592, found 16581.1387.

Per-6-(4-(*N*-(2-(2-(Alm[1-20]aminomethoxy)ethoxy)ethyl)pent-4-ylamide)-1*H*-1,2,3-triazol-1-yl)-α-cyclodextrin, 14

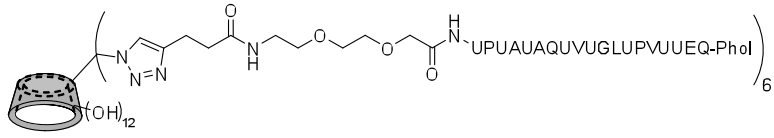

The reacton mixture was stirred for 20 h.
The crude product was dissolved in MeCN/NH_3(aq,2.5%) and lyophilized. The crude product was purified by gel filtration using a Superdex^{TM} 200 10/300 column with 20% MeCN in 2.5% NH_3(aq) as the eluent. The flow rate was 0.5 mL/min. The product was isolated as a light blue solid (8.5 mg, 86%). MALDI-TOF MS $C_{640}H_{1030}N_{156}O_{156}$[M+$Na^{+}$+3*$Cu^{2+}$-6*$H^{+}$]; calculated 14149.3206, found 14149.4697.

6. Characterization of the cyclodextrin peptide conjugates:

Compound **9**

HPLC trace

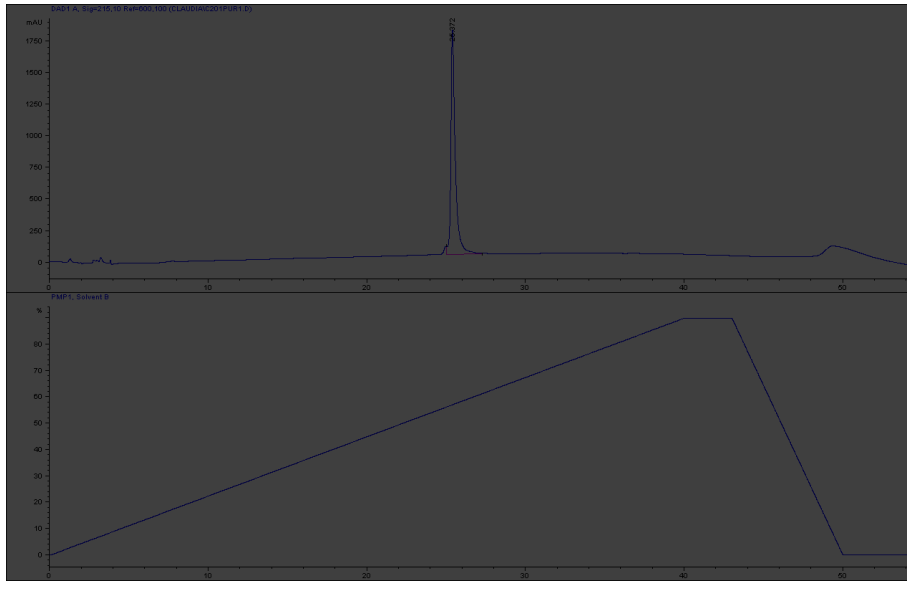

MALDI-TOF MS

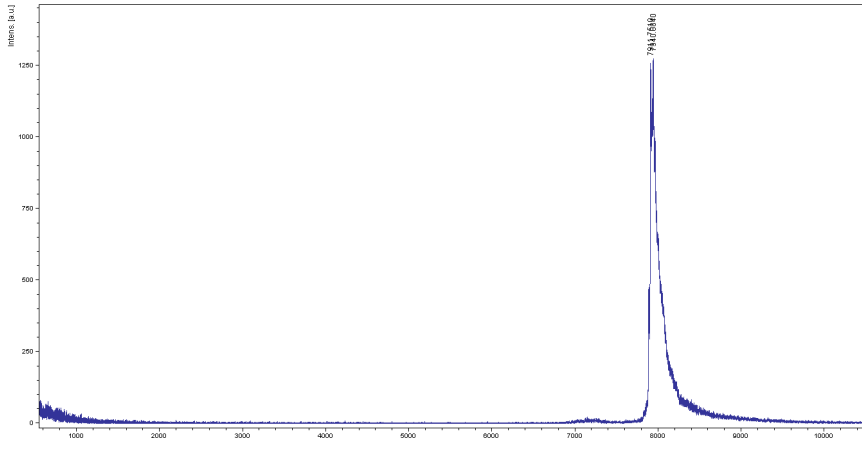

Compound **10**

HPLC trace

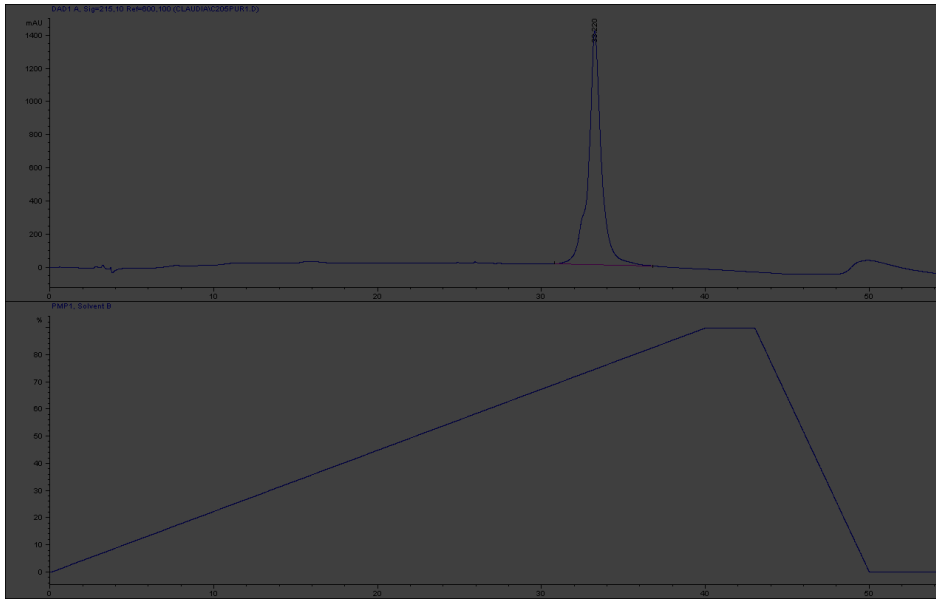

MALDI-TOF MS

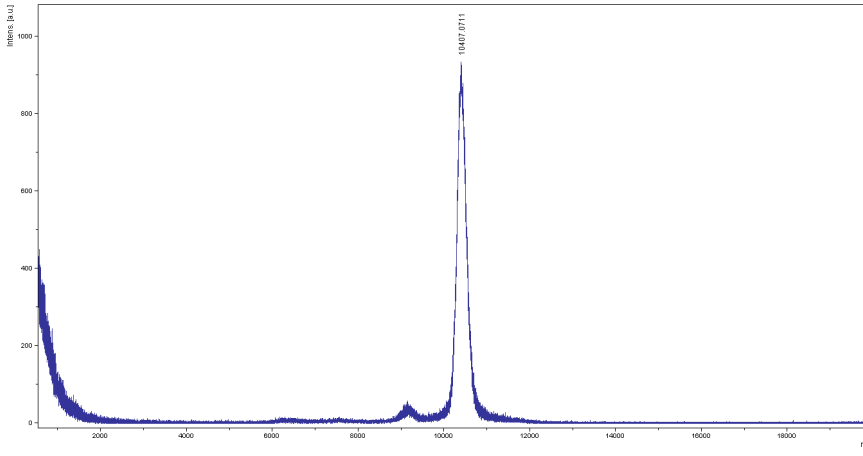

Compound **11**

GFC trace

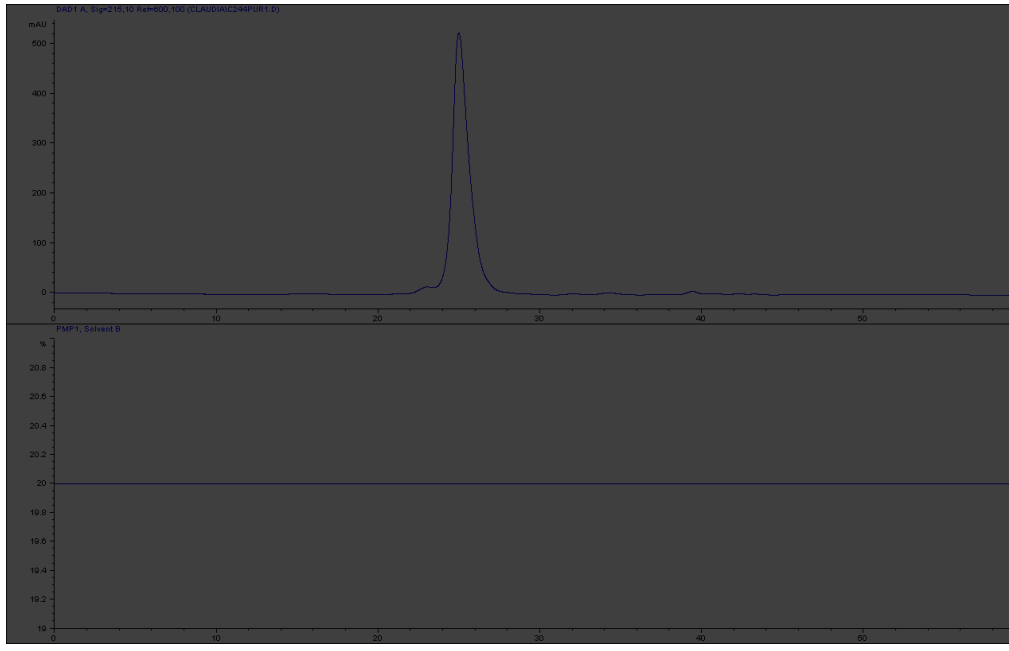

MALDI-TOF MS

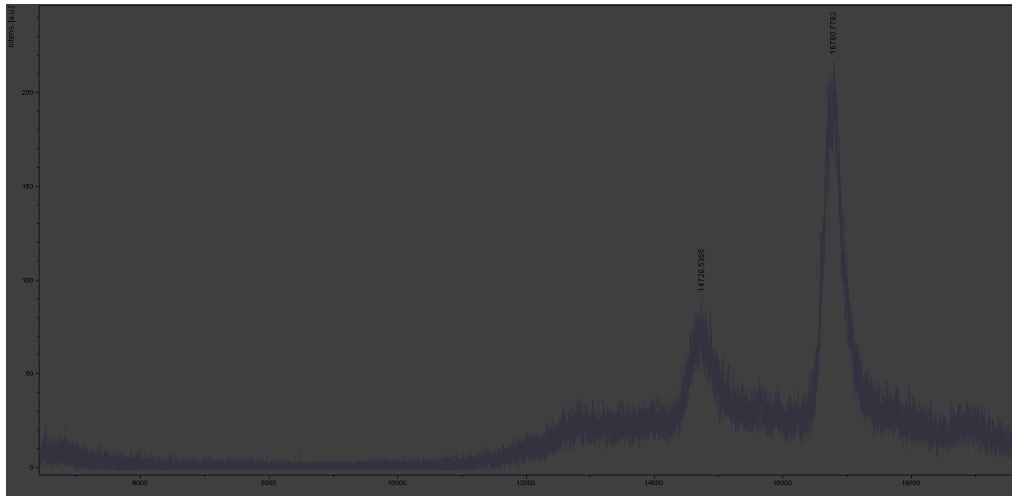

Compound **12**

GFC trace

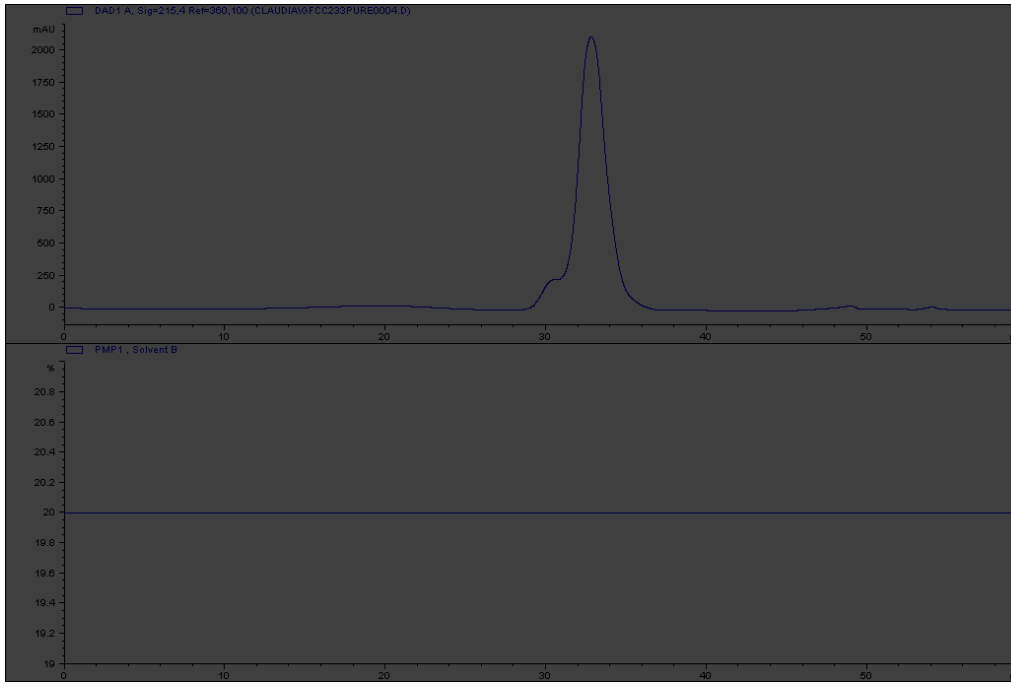

MALDI-TOF MS

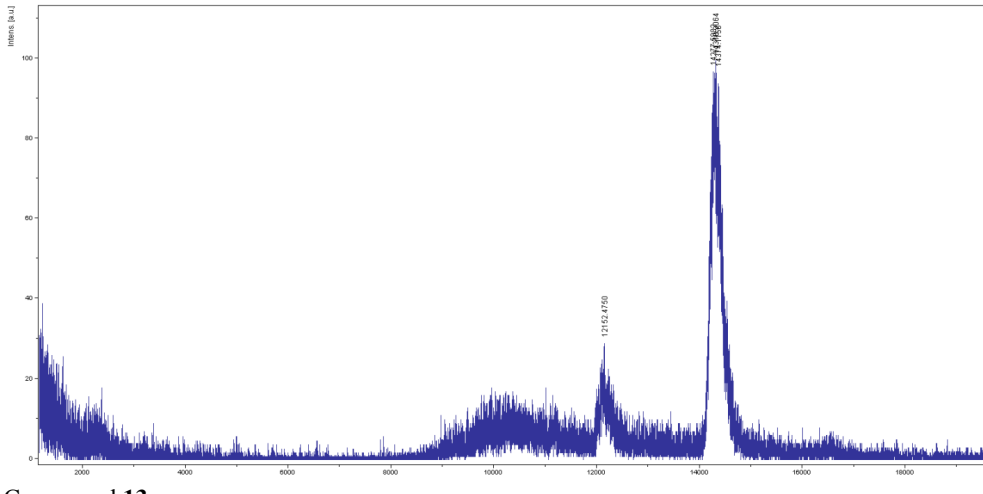

Compound **13**

GFC trace

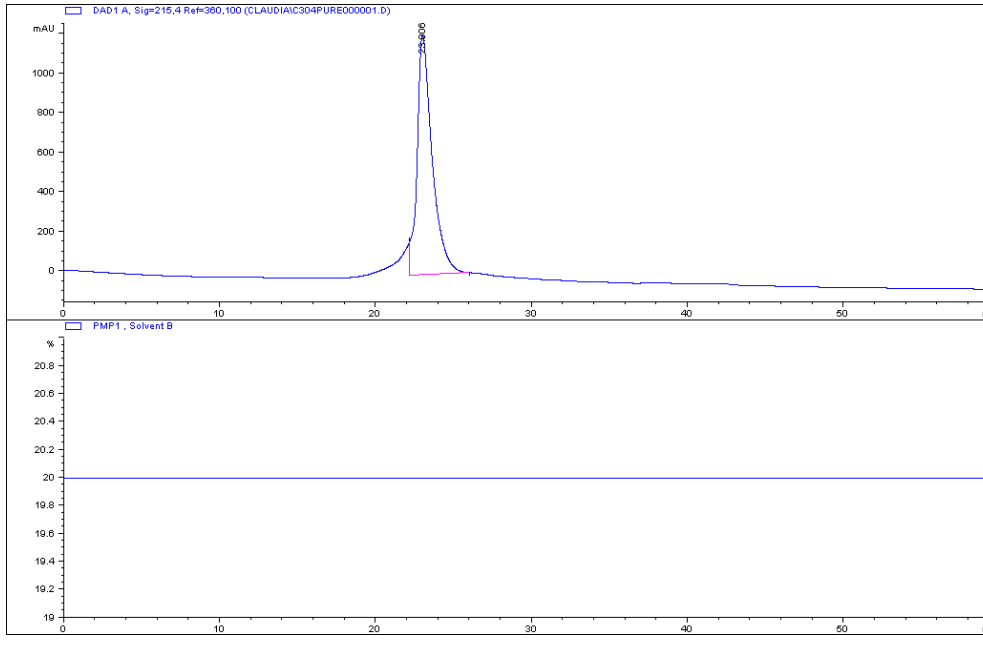

MALDI-TOF MS

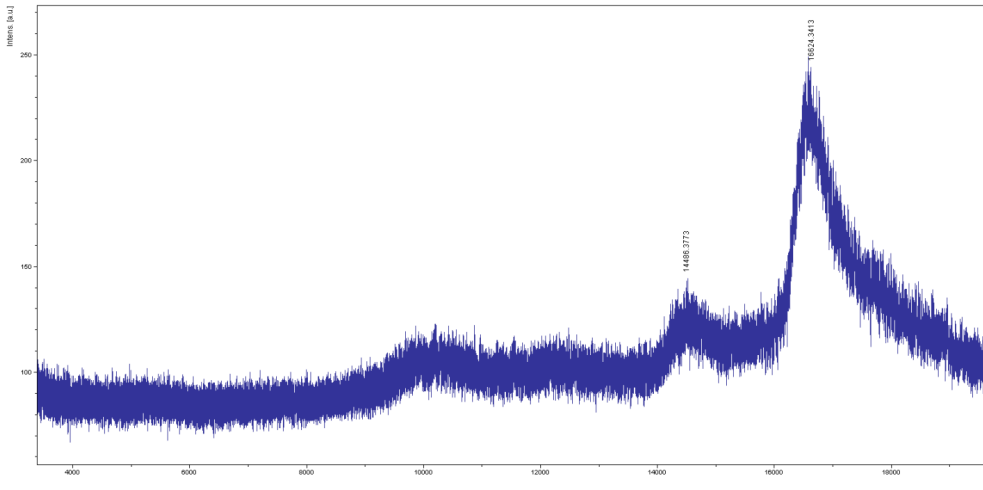

Compound **14**

GFC trace

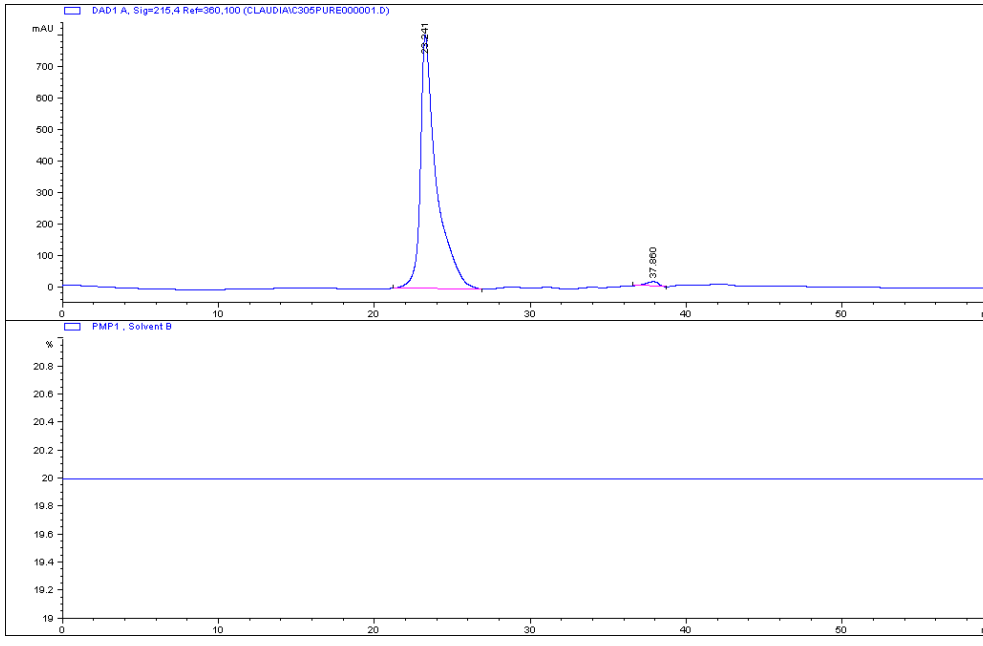

MALDI-TOF MS

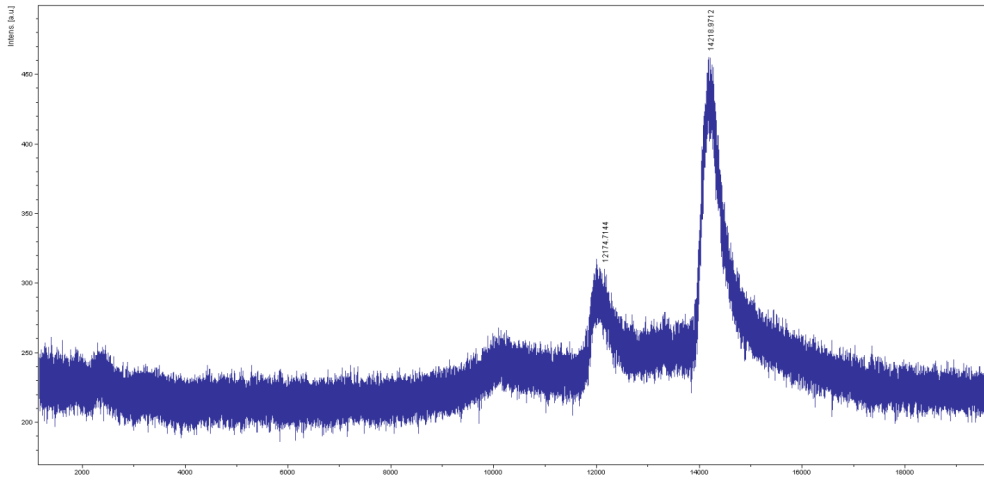
Intens. [a.u.]
450
400
350
300
250
200
12174.7144
14218.9712
2000
4000
6000
8000
10000
12000
14000
16000
18000
m/z

Paper IV:

The interaction of equine lysozyme:oleic acid complexes with lipid membranes suggests a cargo off-loading mechanism

Søren B. Nielsen, Kristina Wilhelm, Brian Vad, Ludmilla Morozova-Roche and Daniel Otzen
Manuscript submitted

The interaction of equine lysozyme:oleic acid complexes with lipid membranes suggests a cargo off-loading mechanism

Søren B. Nielsen[1,2], Kristina Wilhelm[3], Brian Vad[1], Jürgen Schleucher[3], Ludmilla Morozova-Roche[3], Daniel Otzen[1*]

[1] Interdisciplinary Nanoscience Center (iNANO), Department of Molecular Biology, University of Aarhus, Gustav Wieds Vej 10C, DK – 8000 Aarhus C

[2] Department of Food Science, Faculty of Agricultural Sciences, University of Aarhus, Blichers Allé, DK - 8830 Tjele

[3] Medical Biochemistry and Biophysics, Umeå University, SE-901 87 Umeå, Sweden

* To whom correspondence should be addressed: Tel: +45 89425046, e-mail dao@inano.au.dk

Running Title: ELOA-membrane interactions

Keywords: confocal laser scanning microscopy; equine lysozyme; oleic acid; supported lipid bilayers; quartz crystal microbalance with dissipation

Abbreviations: QCM-D, Quartz crystal microbalance with dissipation; CD, Circular dichroism; EL, equine lysozyme; ELOA, EL complex with oleic acid; OA, oleic acid, CSLM, Confocal scanning laser microscopy, Df, dissipation-frequency

ABSTRACT

The normal function of equine lysozyme (EL) is the hydrolysis of peptidoglycan residues of bacterial cell walls. EL is closely related to α-lactalbumins with respect to sequence and structure and further possesses the calcium binding site of α-lactalbumins. Recently, EL multimeric complexes with oleic acids (ELOA) were shown to possess tinctorial and morphological properties, similar to amyloidal aggregates, and to be cytotoxic. ELOA's interactions with phospholipid membranes appears to be central to its biological action, similar to human α-lactalbumin made lethal to tumor cells (HAMLET). Here, we describe the interaction of ELOA with phospholipid membranes. Confocal scanning laser microscopy shows that ELOA, but not native EL, accumulates on the surface of giant unilamellar vesicles, without inducing significant membrane permeability. Quartz crystal microbalance with dissipation (QCM-D) data indicated an essentially non-disruptive binding of ELOA to supported lipid bilayers, leading to formation of highly dissipative and "soft" lipid membrane; at higher concentrations of ELOA, the lipid membrane desorbs from the surface probably as bilayer sheets of vesicles. This membrane rearrangement occurred to a similar extent when free oleic acid (OA) was added, but not when free OA was removed from ELOA by prior incubation with BSA, emphasizing the role of OA in this process. NMR data indicated an equilibrium between free and bound OA which shifts towards free OA as ELOA is progressively diluted indicating that OA is relatively loosely bound. Activity measurements together with fluorescence spectroscopy and circular dichroism suggested a conversion of ELOA toward a more native-like state on interaction with lipid membranes, although complete refolding was not observed. Altogether, these results suggest that ELOA may act as an OA carrier and facilitate OA transfer to the membrane. ELOA's properties illustrate that protein folding variants may possess specific functional properties distinct from the native protein.

INTRODUCTION

Insoluble β-sheet rich protein aggregates termed amyloids figure in numerous ailments such as Alzheimer's, Parkinson's, type II diabetes, localized and systemic amyloidoses etc.[1]. However, it is increasingly recognized that the cytotoxic species in these aggregation diseases are not the mature amyloids, but rather prefibrillar protein aggregates designated oligomers[2]. The oligomers tend to accumulate at the early stages of the aggregation process although their exact mechanistic relation to the mature amyloids is complex[3]. The oligomers can also self-assemble spontaneously during storage and application of non-disease-related proteinaceous materials in biopharmaceutical and other industrial processes and cause serious side-effects[4; 5]. In some cases, however, oligomer cytotoxicity can be very useful: the proteinaceous complexes known as HAMLET and BAMLET (human and bovine α-lactalbumin made lethal to tumor cells) induce cell death specifically in harmful tumor cells and spare healthy cells[6]. These complexes are found in milk and can be produced *in vitro* by complexing proteins with OA molecules[7; 8; 9]. The mechanisms of interactions of protein oligomers with cell membranes and their penetration into cells are central for understanding their toxicity and specificity towards cancer cells. Protein oligomers in neurodegenerative diseases are thought to exert cytotoxicity by permeabilizing neurons[10]. Similar mechanisms may be at play for HAMLET and BAMLET, which irreversibly bind to unilamellar DPPC vesicles and plasma membrane, causing nonselective permeability of the membrane[11], while OA and proteins taken separately do not induce similar effects.

The complex between the 123-residual equine lysozyme (EL) and OA (termed ELOA) exerts cytotoxic properties similar to HAMLET[12]. ELOA is an attractive model system as it is stable, well populated and can be produced in a controlled manner by partial unfolding of EL on an anion exchange matrix

within the column preloaded with OA and followed by salt gradient elution[12] – a process similar to the formation of HAMLET[12; 13]. EL is a close structural homologue of human and bovine α-lactalbumin and has been described as an evolutionary link between lysozymes and α-lactalbumins. Like lysozymes, it hydrolyzes linkages within peptidoglucan in bacterial cell walls, but like α-lactalbumins it binds calcium[14]. ELs folding behavior has been intensively studied (reviewed by Morozova-Roche (2007)[14]). EL forms numerous partially folded states under mild denaturing conditions, which closely resemble kinetic intermediates populated during EL refolding[15; 16; 17]. Under acidic conditions EL forms a molten globular state and self-assembles into amyloid oligomers and fibrils during prolonged incubation[18; 19]. In ELOA EL is present in a partially unfolded state due to its interaction with OA[12]. ELOA displays properties similar to EL amyloid oligomers such as the affinity to amyloid specific Thioflavin T and Congo red dyes as well as ability to associate into ring-shaped structures described for the EL amyloid assemblies[19].

ELOA's properties make it very relevant to focus on its interactions with phospholipid membranes. The purpose of the present study is to gain insights into the structural rearrangements occurring in both ELOA and the membrane during this process. By using quartz crystal microbalance with dissipation (QCM-D), confocal laser scanning microscopy (CSLM), fluorescence of calcein dye loaded into synthetic vesicles, NMR, spectroscopic methods and biochemical techniques we provide a detailed picture of these rearrangements. This leads us to propose a model for ELOA incorporation into lipid membranes in which EL functions as a carrier for OA which facilitates its transfer into the membrane, followed by protein release and (partial) renaturation.

RESULTS

OA exists in a reversible equilibrium with EL in the ELOA complex

To determine the stability of the ELOA complex, we used ^{1}H NMR spectroscopy to analyze the equilibrium between free and bound OA in ELOA. Figure 1A shows that the olefinic region of the NMR spectrum changes with ELOA concentration. In addition to the signal for bound OA at 5.2 ppm, a second signal appears at 5.4 ppm and becomes increasingly predominant at lower ELOA concentrations. Close inspection of the signals shows that with decreasing ELOA concentration, the line width of the new peak decreases while the line width of the bound peak increases. For example, the bound OA signal at 40 μM is at half height more narrow than the resolved tip of the bound OA signal at 1.6 μM, although less than half the height of the latter is exposed. For two molecular species undergoing chemical exchange, these linewidth trends are expected as the ratio between both species shifts, because chemical exchange mainly broadens the signal of the minor species. Thus, the increasing fraction of the new signal, and the changes in line widths, suggest an equilibrium between OA in the bound state and a second state. The chemical shift of the new signal agrees with the chemical shift of the olefinic protons of free OA, indicating that the second state is free OA.

These results indicate that with decreasing concentration of ELOA, an increasing fraction of OA dissociates from the complex. This is confirmed by 2D NMR exchange spectroscopy, which shows that both olefinic signals belong to the same molecular species in chemical exchange (data not shown). OA dissociation from ELOA at low concentrations is expected for reversible binding of OA to EL. Consistent with this, the fraction of bound OA versus total ELOA concentration has the shape of a hyperbolic binding curve (Fig. 1B).

ELOA accumulates on phospholipid membranes

ELOA has been shown to induce rupture of PC12 cells after incubation with ELOA for more than 50 minutes[12]. We therefore examined the binding of ELOA to lipid membranes of giant unilamellar vesicles (GUVs) to elucidate whether the interaction led to membrane collapse. GUVs containing entrapped Alexa Fluor 633 dye were incubated with NBD-labeled ELOA and the fluorescence of the dyes was visualized by confocal scanning laser microscopy (CSLM) (Fig. 2). While NBD-ELOA clearly accumulated on the surface of GUVs in a similar fashion as described for PC12 cells prior to rupture[12], we did not observe any ruptured vesicles, which would manifested in release of Alexa Fluor 633 dye, even after exposure for 24 hours. We further found that NBD labeled EL did not accumulate on membranes (data not shown), suggesting that complexation with OA is a prerequisite for membrane interaction.

To evaluate the ability of ELOA to facilitate membrane permeabilization by small molecules, we carried out calcein dye leakage experiments using ratios of 7 to 110 lipid molecules per EL monomer in ELOA (Fig 3). Under these conditions, we observed only small degree of vesicle permeabilization with leakage levels of 3-6%, measured by increasing fluorescence of released calcium dye (Fig. 3). The leakage occurs at ELOA:lipid molar ratios of 1:7 - 1:22, corresponding to OA:phospholipid molar ratios of ~ 4.5:1 to 1.5:1, respectively. This is very inefficient compared to the complete permeabilization of membranes by *e.g.* antimicrobial peptides at P:L ratios of 1:500 and less[20]. Together with the CSLM data, these results indicate a small increase in vesicle permeability rather than complete vesicle rupture and also show that unrealistically high concentrations of ELOA are needed to increase the permeability of small molecules.

Phospholipid bilayers are converted to highly hydrated film on interaction with ELOA

Interactions between ELOA and lipid membranes were investigated further using the QCM-D technique. QCM-D monitors changes in resonance frequency (Δf) and energy dissipation (ΔD) at the solid-liquid interface. This in turn provides information on changes in the viscoelastic properties of films on a surface[21]. QCM-D measures are sensitive to the acoustic mass coupled to the oscillation of the crystal, in contrast to optical techniques such as surface plasmon resonance and dual polarization interferometry which identify the optical mass of adsorbed molecules only. This makes the QCM-D technique especially suited for the analysis of films in which rearrangements may lead to changes in the amount of bound water molecules, which consequently lead to an amplification of the measured signal. We note, however, that it is not possible to distinguish between contributions from the bilayer, protein and water moieties coupled to the oscillation of the sensor crystal.

To probe the interaction between ELOA and membranes using the QCM-D technique, supported lipid bilayers made of 80:20 DOPC:DOPG were formed by spontaneous vesicles collapse as previously described[22]. Successful formation of lipid bilayers was shown by a characteristic two-step process in which liposomes accumulate until a critical surface coverage is achieved, after which the vesicles collapse into supported lipid bilayers (Fig. 4A-B). This is clearly shown by the initial decrease in resonance frequency (liposome binding) which after passing the local minimum corresponding to the critical surface coverage increases to ~ -26 Hz with low dissipation values, characteristic for lipid bilayers[23]. Injection of 0.3µM ELOA, the lowest concentration employed in this study, did not lead to detectable changes in resonance frequency or dissipation values (Fig 4A-B). However, on injection of 1µM ELOA we observed a decrease in resonance frequency to ~ -50Hz and an increase in ΔD to ~3.5×10^{-6}, suggesting binding of the complex and the formation of a softer film ($\Delta D/\Delta f \sim 0.07 \times 10^{-6}$

compared to $\Delta D/\Delta f$~ 0.01 x10^{-6} for a bilayer). The injection of 3-10µM led to more complex changes in Δf, as shown by an initial decrease, followed by an increase, in Δf values with minima between ~ -44 and -56 Hz. This indicates that the bilayer and/or protein complex rearrange after initial adsorption. The increase in Δf rapidly reached a plateau at ~ -30 Hz during exposure to 3µM ELOA, whereas a continuous (but abating) increase in resonance frequency was observed during the entire course of the interaction on exposure to 10µM ELOA. We further observed that an increase in the ELOA concentration led to further increases in energy dissipation, indicating the formation of a softer film as indicated by the ratio of $\Delta D/\Delta f$ describing the softness per mass unit (Table 1). The $\Delta D/\Delta f$ ratio upon addition of 10µM ELOA was ~ 2-3.5 times higher than that observed for a layer of 120nm vesicles tethered to supported membrane[24] and for the outgrowth of lipid structures on exposure of membranes to 200µM docosahexanoic acid[25]. This further emphasizes the conversion of the rigid bilayer to a complex, highly dissipative film on interaction with ELOA. Injection of 320µM OA (corresponding approximately to the amount of bound OA in 10µM ELOA, cfr. Fig. 1B) caused similar changes in ΔD as the addition of 3 µM ELOA. However, the changes of Δf were smaller in amplitude, probably reflecting the smaller mass contribution of OA compared to the ELOA complex.

Fig 4A-B and Table 1 shows the effect of rinsing after allowing ELOA or OA to interact with the supported membranes for ~ 2 hours. While injection of 1µM ELOA does not lead to significant changes in Δf and ΔD, rinsing of samples incubated with 3-10µM ELOA or 320µM OA (corresponding to 10µM ELOA) led to an increase in Δf and decrease in ΔD which indicates mass removal. Since calcein dye leakage and CLSM experiments indicate that the lipid film is not broken, we interpret it as a release of the lipid film from the surface.

A plot of ΔD versus Δf relates changes observed in ΔD to changes in Δf and eliminates the time parameter (Fig 5). Generally, a given point in the dissipation-frequency (Df) landscape corresponds to a certain state of the surface and ΔD-Δf plots may thus reveal differences in the adsorption process or secondary processes such as structural rearrangements of the adsorbed film, irrespective of time[26].

We observed a similar initial adsorption behavior at ELOA concentrations of 1, 3, 5 and 10µM, leading to maximum shifts in ΔD and Δf to ~ 3.5-4.5 units and -42 to -50 Hz, respectively. Fig. 5 allows us to deduce that the system passes through approximately the same states during the initial adsorption of ELOA, clearly indicating the adsorption of the protein complex on the bilayer surface in a similar manner regardless of protein concentration. While the 1µM injection does not appear to cause significant rearrangements of the film after adsorption, the injection of 3-10µM ELOA complex displays a much more complex course. After initial adsorption, we observe a turn toward a more dissipative film with a small (10µM) or larger (3µM) decrease in the resonance frequency, followed by an almost vertical regime in which the associated film becomes even more dissipative. The remarkably large dissipation shift with small or non-existing frequency shifts observed on exposure of the bilayer to 3-10µM ELOA indicates a softening of the film. Subsequently, we observed desorption of material from the surface, leading to a reduction of Δf less the -26 Hz level of an unmodified bilayer. This is good evidence that membrane integrity is lost and material desorbs from the surface, leaving a highly dissipative film on the surface. Since the trajectory on injection of 3µM ELOA resembles the reverse of the initial vesicle collapse, we speculate that the lipid film detaches from the surface in the form of bilayer sheets of vesicles.

We note that the trajectory observed at these concentrations is similar to those obtained for OA (320µM, see Fig. 5) although ELOA signal amplitudes are greater and thus extend further out into the *Df* landscape. We attribute this to the significant mass contribution of EL in complex with OA.

To further evaluate the importance of OA in the interaction with lipid bilayers, we evaluated the ability of 320 µM OA and 3 µM ELOA to bind after exposure to fat-free BSA. We found that the interaction was eliminated by the presence of 10mg/ml (130 µM) BSA. Each BSA contains at least 5 binding sites for OA, so there is clearly sufficient binding capacity to mop up all OA[27]. Further, no binding was observed using native EL, in agreement with CSLM experiments (data not shown). These observations clearly suggest that OA mediates the interaction with the membrane.

Conformational changes of ELOA upon interaction with lipids

Equine lysozyme undergoes partial unfolding into a molten globular state during complexation with OA[12]. We examined the conformation changes occurring in ELOA upon interaction with lipids by circular dichroism and fluorescence spectroscopy. Tryptophan emission spectra (Fig. 6, insert) were recorded during titration with 80:20 DOPC:DOPG LUVs. These spectra provide information about conformational changes in the vicinity of the 5 Trp residues of ELOA. The large number of Trp residues results in a broad spectrum with a maximum at ca. 345 nm in the native state, which blue-shifts by 2-3 nm in ELOA. We used the ratio of fluorescence intensities at 350 and 330 nm (I_{350}/I_{330}) as a measure of the spectral shift upon each addition of LUVs. There were no changes in the spectral maximum or fluorescence intensity upon titration of holo EL with LUVs and the ratio of I_{350}/I_{330} remained constant (Fig 6). However, we observed an increase of I_{350}/I_{330} upon titration of ELOA with LUVs from ca. 1.17 to 1.43, which brings it close to that of holo EL.

The CD spectrum of native EL in PBS (Fig. 7) is characterized by minima at ~206 and 227nm, in agreement with previous reports[15; 16]. By contrast in ELOA the minimum at ~227nm is diminished to a shoulder and the CD spectrum displays a spectral shape similar to the molten globule state of EL[12; 16]. Increasing amounts of 80:20 DOPC:DOPG vesicles were added to the complex while monitoring the development in CD after each addition. Addition of LUVs to ELOA resulted in an increase of the absolute value of the ellipticity at 227 nm, counterbalanced by a decrease of the signal saround 220 and 206 nm. These changes move the shape of the spectrum partially towards that of the native state, just as observed for the fluorescence spectra, although the spectra remain lower in amplitude.

A more sensitive test for the recovery of the native state is to measure enzymatic activity. We carried out these assays using *Micrococcus lysodeikticus.* Hydrolysis of this Gram-positive bacterium's cell walls by lysozyme leads to a decrease in light scattering which provides a convenient and simple activity assay. As enzymes we used EL, ELOA and ELOA pretreated by incubation with 25 fold molar excess of lipids. Fig. 8A clearly shows that addition of lipids to ELOA leads to a lysozyme activity of 0.388±0.003 A_{450} $min^{-1}mg^{-1}$, which is 22% of the activity for native EL (1.77±0.06 A_{450} $min^{-1}mg^{-1}$). In contrast, ELOA in the absence of lipids shows an activity of 0.185±0.001 A_{450} $min^{-1}mg^{-1}$ (10% of native EL). Since the ELOA complex may interact with lipid components of the *Micrococcus* membrane, we attribute this residual activity to partial refolding occurring as a result of this interaction. Incubation of *Micrococcus lysodeikticus* with lipids alone did not result in changes in absorbance (data not shown). Our data are thus consistent with a partial refolding of ELOA upon lipid interaction.

Proteolysis experiments on the same samples further showed increased resistance of ELOA preincubated with lipids toward proteolytic digestion by trypsin (Fig 8B). This indicates that ELOA preincubated with lipids is in a more compact state than ELOA alone, although still more susceptible to

proteolytic attack than native EL. Together, proteolysis and activity data support a partial refolding of ELOA toward a native-like conformation.

DISCUSSION

Complexation with OA is central to the binding of ELOA to, and effect on, membranes

The interaction of ELOA with lipid vesicles and supported lipid bilayers depends on the ELOA concentration and requires complexation with OA. At low concentrations (~1µM) such as those employed in CSLM (Fig 1), the complex accumulates at the surface of both GUVs and SPBs (Fig 4A-B). Exposure of membranes to larger concentrations of ELOA leads to more complex behavior of ELOA as shown by QCM-D results (Fig. 4-5). First, the complex binds to lipid membranes. Subsequently, rearrangements of the film through multiple steps (Fig. 4) lead to the formation of a highly dissipative film followed by apparent removal of material from the surface.

The ELOA complex used in this study contains ~ 32 OA molecules per lysozyme molecule and the OA content of the highest ELOA concentration of 10µM employed in these studies thus corresponds to ~ 320µM OA. We note, however, that the amplitude of signals of ELOA at 3-10µM was much larger than the amplitude of 320µM OA alone and that control experiments in which ELOA (and free OA) samples were incubated with excess BSA showed no binding to membranes. Further, NMR data indicate an equilibrium between free and bound OA in ELOA which progressively shift toward free OA on dilution. The dissociation of OA occurs in the same concentration range of ELOA as used in our QCM-D experiments. Our CSLM and NMR data (Figs. 1 and 2) nicely complement the QCM-D observations. The complex exploration mode of the *Df* landscape (Fig 5) is observed only in the 3-10µM range of ELOA at which OA is preferentially associated in the ELOA complex (~ 70-90% bound), whereas an apparent simple binding to the membrane is observed at 1µM where ~ 30% OA is bound in ELOA. This clearly indicates that complexation of EL with OA is necessary for membrane

interactions. Furthermore, the similarity of the interaction (in spite of the difference in amplitude) of free OA and ELOA with lipid membranes supports the same conclusion.

ELOA as a possible membrane-targeting OA transporter without translocation

We have found that ELOA itself also undergoes significant conformational changes upon interaction with lipid membranes. Intrinsic fluorescence measurements indicate a noticeable red shift of the fluorescence emission spectrum of ELOA in the presence of LUVs (Fig 6), which reflects the change in the local environment of tryptophan residues of EL and an increase in solvent accessibility of some of them. The spectral maximum of ELOA in the presence of excess of LUVs approaches that of native EL. In ELOA, EL is present in a molten globule type conformation[12]. The intrinsic fluorescence spectrum of EL molten globule in general, and in particular the spectrum of buried tryptophan residues probed by external quenchers[16], are characterized by a blue shift of spectral maximum compared to these of the native state, indicating that some internal tryptophan residues are constrained within the molten globule. Moreover, within ELOA some aromatic residues are in contact with OA molecules as shown previously by the presence of cross-peaks between proton resonances of aromatic residues and OA in a NOESY spectrum[12]. The interaction of ELOA with phospholipid vesicles may disrupt these interactions and remove constraints in the tryptophan environment, bringing some of them towards a native-like conformation.

Consistent with this, we have observed changes in the far UV CD spectrum of ELOA upon increasing lipid concentration, which resemble a shift from the molten globule towards the native-like conformation (Fig 7). In a previous study the perturbations of the CD spectra both in the near and far-UV regions observed on conversion of EL from the native to molten globule state were interpreted as

the rearrangement and burial of a number of aromatic side-chains, particularly indole groups[16; 28]. Therefore ELOA's interaction with lipids promotes the conformational transition of EL towards a more native-like state. This was further confirmed by partial recovery of lysozyme activity upon interaction with lipids and decrease of protein resistance towards proteolytic degradation (Fig 8).

The interaction of proteins with lipid membranes has been shown previously to modulate the structure and function of many proteins. Some proteins undergo partial unfolding and acquire a molten globule conformation upon interaction with lipids, particularly under mildly acidic conditions, as shown for bovine α-lactalbumin in the presence of small unilamellar vesicles[29]. The fact that EL displays some native-like characteristics upon interaction of the ELOA complex with lipid membranes indicates that ELOA may dissociate, leading to EL release from the complex. Consequently EL does not appear to translocate across lipid membranes as described for HAMLET[30]. We note that Helix C of bovine α-lactalbumin in the molten globular state has been shown to be involved in the interaction with lipid membranes owing to its amphiphatic structure[31]. The sequence of helix C in EL is very similar to that of bovine α-lactalbumin, suggesting that this particular part of the protein may be involved in the binding of ELOA to membranes. This begs the question is to why HAMLET, but not ELOA, is translocated. Translocation of HAMLET has been suggested to be induced by a combination of the oleic acid cofactor and a specific phospholipid composition of the membrane[31]. OA is a known penetration enhancer which increases skin permeability by imposing an increased conformational freedom and flexibility of membrane lipids[32; 33]. Increased flexibility may promote translocation of HAMLET whereas other parameters appear to hinder translocation of ELOA. All this suggests that ELOA may instead function as a carrier for OA by enhancing its solubility in an aqueous environment while at the same time directing it towards the membrane. Furthermore, we speculate that the release of

a large number of OA molecules in a small region may exert a stronger effect than a more diffuse uptake of free OA from solution.

MATERIALS AND METHODS

Materials: 1,2-dioleoylphosphatidylcholine (DOPC) and 1,2-dioleoylphosphatidylcholine (DOPG) lipids were from Avanti Polar Lipids (Alabaster, AL, USA) supplied as dry powder. Chloroform (Sigma, St. Louis, MO, USA) and methanol (Sigma, Steinheim, Germany) were of 99% purity or higher. Sucrose 99.5% and D(+)-Glucose 99.5% purity, TCPK-treated trypsin from bovine pancreas and lyophilized *Micrococcus lysodeikticus* cells were from Sigma (St. Louis, MO, USA). Alexa 633 and NBD-X SE (Succinimidyl 6-(N-(7-nitrobenz-2-oxa-1,3-diazol-4-yl)amino)hexanoate) were from Invitrogen (Carlsbad, CA, USA). Triton X-100 and Calcein disodium salt were from Fluka (Buchs, Switzerland). ELOA concentrations were estimated using native EL's extinction coefficient $E_{280nm}^{1\%}$=23.5[19].

Preparation of ELOA complexes: The ELOA complex containing 32 OAs per EL monomer was produced on an ion exchange column as previously described[12]. In brief, the anion exchange matrix was conditioned with OA followed by loading of EL in 10mM Tris-Cl pH 9.0 to the column. The ELOA complex with OA was eluted by a continous gradient of NaCl from 0 to 1.5M in the same buffer followed by dialysis and lyophilization. The concentration of dissolved ELOA was estimated by absorption spectroscopy using EL's extinction coefficient. The concentration of bound OA was determined by ^{1}H-NMR (see below).

NMR spectroscopy: ^{1}H NMR spectra of ELOA were acquired at 25°C on a DRX 600 spectrometer (Bruker, Fällanden, Switzerland) equipped with a cryogenically cooled ^{1}H observe probe. 0.5 mg ELOA were dissolved in 500 µl 10mM Tris buffer in D_2O to make a 40 µM ELOA sample. Sample aliquots were directly transferred into other NMR tubes and buffer added to 500 µl to achieve the

desired dilutions. With decreasing ELOA concentrations, an increasing number of scans were collected. Spectra were processed with 10 Hz line broadening and polynomial baseline correction. The stoichiometry between EL and OA was determined by comparing the integrals of the aromatic resonances of EL with the signal of the olefinic protons of OA.

Preparation of phospholipid vesicles: A 10mg/ml stock solution of 80% DOPC and 20% DOPG by weight was prepared in chloroform by weighing off lipids. Giant unilamellar vesicles (GUVs) were prepared by electroformation [11]. 10-15µl lipid stock was applied to platinum electrodes and dried in vacuum. The chamber was filled with 500µl 200mM sucrose including 10µg/ml Alexa fluor 633 fluorescent dye and vesicles were formed by applying a sine curve of 10 Hz at 1.5V for 1 hour in the dark at RT. GUVs were released from electrodes by applying a 1 Hz sine curve at 3V for 30 minutes. A PD-10 column desalting column was equilibrated in 200mM glucose and the exterior of vesicles were replaced by passage through the column while capturing the flow-through.

Large unilamellar vesicles (LUVs) were prepared by extrusion. A 5mg dry lipid film was formed by evaporation of chloroform and the lipids were rehydrated in (A) 1ml 10mM PBS pH 7.4 or (B) 20mM HEPES-KOH, 150mM NaCl, 2mM $CaCl_2$ to obtain 5mg/ml lipid. Vesicles were subjected to 5 cycles of freeze-thawing using liquid nitrogen and a 25°C water bath and extruded through 100-nm polycarbonate membranes 15 times using a MiniExtruder (Avanti Polar Lipids, Alabaster, AL, USA) at room temperature. Vesicles for calcein release were prepared similarly in buffer A, except that 70mM calcein was included in the rehydration buffer. Extruded calcein-containing vesicles were further purified on a PD-10 desalting column to remove non-encapsulated calcein and diluted 500x prior to use.

Fluorescence spectroscopy: Fluorescence spectroscopy was done using a Perkin-Elmer LS55 fluorescence spectrophotometer (PerkinElmer A/S, Hvidovre, Denmark) with the cuvette holder thermostatted at 25°C using a water bath. Excitation and emission wavelengths were 295 and 310-400nm, respectively, using 5nm slits, a scan speed of 200nm/min and accumulation of 3 spectra. 2µM ELOA or EL were dissolved in 10mM PBS pH 7.4 and titrated with 80:20 DOPC:DOPG LUVs. The emission intensity was normalized according to dilution of the protein sample.

Confocal laser scanning microscopy: Confocal laser scanning microscopy was done on a LSM 50 meta scanning confocal microscopy from Zeiss GmbH (Jena, Germany) using a 40x water immersion objective (Carl Zeiss, C-Apochromat 40x/1.2W correction collar). The excitation wavelengths of Alexa 633 was set at 633 nm and NBD-labeled ELOA at 458nm using Argon and HeNe laser beams, respectively. Fluorescence emission of Alexa 633 and the NBD-X label was recorded using LP650 and BP505-550 filters, respectively. ELOA and EL were labeled with NBD-X SE by mixing 0.1ml 1M sodium bicarbonate pH 8.3 with 0.4ml 40µM (~1mg/ml) protein solution in PBS pH 7.4 and 25µl 10mg/ml NBD-X SE in DMSO followed by incubation for 1 hour at room temperature. Unreacted NBD was removed by a desalting step in a PD-10 column. 500µl GUV suspension was transferred to an eight-well microscopy chamber (Lab-Tek Brand Products, Naperville, IL) and mixed with 50µl NBD-labeled ELOA or 50µl NBD-labeled EL to obtain ~ 1µM protein in the microscopy chamber. Recording of images was started immediately afterwards for every 15 s.

Quartz crystal microbalance with dissipation (QCM-D): QCM-D data were recorded using a Q-sense E4 (Q-sense AB, Västra Frölunda, Sweden) system with 5 MHz AT-cut SiO_2 coated sensors (QSX 303). Sensors were cleaned by immersion for 30 minutes in 2% SDS followed by UV/Ozone treatment for 10 minutes with washing in MilliQ water between. Equilibration was done in 10mM PBS pH 7.4

(baseline) at 25°C followed by deposition of SUVs (100µg/ml lipid) in 20mM HEPES-KOH pH 7.4, 150mM NaCl, 2mM $CaCl_2$ and finally the buffer was replaced with 10mM PBS before sample injection. Washing and lipid deposition was done at a flow rate of 200µl/min while injections of ELOA in 10mM PBS pH 7.4 was done in stagnant flow mode by injection of 350µl at 200µl/min. OA solutions were prepared in 10mM PBS pH 7.5, 0.5% ethanol. The 7^{th} overtone is reported unless otherwise stated.

Calcein dye leakage: Calcein release was investigated using a Varian Cary Eclipse spectrofluorimeter (Varian, Palo Alto, CA, USA) equipped with a thermostated (25°C) cuvette holder with stirring. Excitation and emission wavelengths of 490nm and 515nm and slit widths of 2.5nm were used, respectively. 750µl calcein vesicle suspension was transferred to the cuvette and the baseline fluorescence was recorded (F_0). Aliquots of 10µl ELOA complex was added to monitor vesicle permeability, leading to the calcein fluorescence intensity F. Subsequent addition of 10µl 2% Triton X-100 lead to maximum calcein dye leakage with the fluorescence intensity F_{max}. The degree of calcein dye leakage was subsequently calculated using eq. 1:

$$\text{Dye leakage} = (F-F_0)/(F_{max}-F_0)*100\% \quad (1)$$

Lysozyme activity assays: ELOA was incubated with and without 25-fold molar excess of 80:20 w/w% DOPC:DOPG in the form of LUVs for 30 minutes at RT to analyse the stability and activity of the complex after exposure to lipids. Lysozyme activity was evaluated by the decrease in turbidity of 0.15mg/ml *Micrococcus lysodeikticus* substrate measured by the change in absorbance at 450 nm using an Amersham Biosciences Ultrospec 3100 pro UV/VIS spectrophotometer and 1cm cuvettes. 960µl

substrate was mixed with 40µl ELOA ± lipid or native EL as reference. Results are mean values of quadruple measurements ± standard error of mean.

Proteolysis resistance: To evaluate the resistance to proteolytic digestion, aliquots of trypsin were added to aliquots of the samples to obtain 10, 1, 0.1 and 0.01 weight-% trypsin relative to EL followed by incubation at RT for 30 minutes. The reaction was stopped by the addition of reducing SDS-PAGE sample buffer followed by heating to 95°C for 5 minutes. Protein bands were separated by SDS-PAGE using 15% Bis-Tricine gel electrophoresis and 140V for 45 minutes and stained using Coomassie Blue G-250.

REFERENCES

1. Chiti, F. & Dobson, C. M. (2006). Protein misfolding, functional amyloid, and human disease. *Ann. Rev. Biochem.* 75, 333-366.
2. Lambert, M. P., Barlow, A. K., Chromy, B. A., Edwards, C., Freed, R., Liosatos, M., Morgan, T. E., Rozovsky, I., Trommer, B., Viola, K. L., Wals, P., Zhang, C., FInch, C. E., Krafft, G. A. & Klein, W. L. (1998). Diffusible, nonfibrillar ligands derived from Abeta1-42 are potent central nervous system neurotoxins. *Proc. Natl. Acad. Sci. U.S.A.* 95, 6448-6453.
3. Morris, A. M., Watzky, M. A. & Finke, R. G. (2009). Protein aggregation kinetics, mechanism, and curve-fitting: a review of the literature. *Biochim. Biophys. Acta* 1794, 375-397.
4. Frokjaer, S. & Otzen, D. E. (2005). Protein drug stability - a formulation challenge. *Nat. Rev. Drug. Delivery* 4, 298-306.
5. Morozova-Roche, L. & Malisauskas, M. (2007). A false paradise-mixed blessings in the protein universe: the amyloid as a new challenge in drug development. *Current medicinal chemistry* 14, 1221-1230.
6. Svanborg, C., Ågerstam, H., Düringer, C., Fischer, W., Gustafsson, L., Hallgren, O., Leijonhuvud, I., Linse, S., Mossberg, A.-K., Nilsson, H., Pettersson, J., Svensson, M., Aronson, A. & Bjerkvig, R. (2003). HAMLET kills tumor cells by apoptosis - cellular, molecular and therapeutic aspects. *Adv. Cancer Res.* 88, 1-29.
7. Svensson, M., Sabharwal, H., Håkansson, A., Mossberg, A.-K., Lipniunas, P., Leffler, H., Svanborg, C. & Linse, S. (1999). Molecular characterization of alpha-lactalbumin folding variants that induce apoptosis in tumor cells. *J. Biol. Chem.* 274, 6388-6396.
8. Svensson, M., Håkansson, A., Mossberg, A.-K., Linse, S. & Svanborg, C. (2000). Conversion of alpha-lactalbumin to a protein inducing apoptosis. *Proc. Natl. Acad. Sci. U.S.A.* 97, 4221-4226.
9. Mok, K. H., Pettersson, J., Orrenius, S. & Svanborg, C. (2007). HAMLET, protein folding, and tumor cell death. *Biochem. Biophys. Res. Comm.* 354, 1-7.
10. Volles, M. J. & Lansbury, P. T. (2003). Zeroing in on the pathogenic form of alpha-synuclein and its mechanism of neurotoxicity in Parkinson's Disease. *Biochemistry* 42, 7871-7878.
11. Zherelova, O., Kataev, A., Grishchenko, V., Knyazeva, E., Permyakov, S. & Permyakov, E. (2009). Interaction of antitumor α-lactalbumin—oleic acid complexes with artificial and natural membranes. *Journal of Bioenergetics and Biomembranes* 41, 229-237.
12. Wilhelm, K., Darinskas, A., Noppe, W., Duchardt, E., Hun Mok, K., Vukojevi, V., Schleucher, J. & Morozova-Roche, L., A. (2009). Protein oligomerization induced by oleic acid at the solid/liquid interface - equine lysozyme cytotoxic complexes. *FEBS Journal* 276, 3975-3989.
13. Hakansson, A., Zhivotovsky, B., Orrenius, S., Sabharwal, H. & Svanborg, C. (1995). Apoptosis Induced by a Human Milk Protein. *Proceedings of the National Academy of Sciences* 92, 8064-8068.
14. Morozova-Roche, L. A. (2007). Equine lysozyme: The molecular basis of folding, self-assembly and innate amyloid toxicity. *FEBS letters* 581, 2587-2592.
15. Van Dael, H., Haezebrouck, P., Morozova, L., Arico-Muendel, C. & Dobson, C. M. (1993). Partially folded states of equine lysozyme. Structural characterization and significance for protein folding. *Biochemistry* 32, 11886-11894.

16. Morozova-Roche, L. A., Arico-Muendel, C. C., Haynie, D. T., Emelyanenko, V. I., Van Dael, H. & Dobson, C. M. (1997). Structural characterisation and comparison of the native and A-states of equine lysozyme. *Journal of Molecular Biology* 268, 903-921.
17. Morozova-Roche, L. A., Jones, J. A., Noppe, W. & Dobson, C. M. (1999). Independent Nucleation and Heterogeneous Assembly of Structure During Folding of Equine Lysozyme. *Journal of Molecular Biology* 289, 1055-1073.
18. Morozova, L. A., Haynie, D. T., Arico-Muendel, C., Dael, H. V. & Dobson, C. M. (1995). Structural basis of the stability of a lysozyme molten globule. *Nature Structural Biology* 2, 871-875.
19. Malisauskas, M., Zamotin, V., Jass, J., Noppe, W., Dobson, C. M. & Morozova-Roche, L. A. (2003). Amyloid protofilaments from the calcium-binding protein equine lysozyme: formation of ring and linear structures depends on pH and metal ion concentration. *Journal of molecular biology* 330, 879-890.
20. Shai, Y. (2002). Mode of action of membrane active antimicrobial peptides. *Biopolymers* 66, 236-248.
21. Justesen, P. H., Kristensen, T., Ebdrup, T. & Otzen, D. E. (2004). Investigating phospholipase action on vesicles and supported planar bilayers using a quartz crystal microbalance. *J. Coll. Int. Sci.* 279, 399–409.
22. Keller, C. A. & Kasemo, B. (1998). Surface specific kinetics of lipid vesicle adsorption measured with a quartz crystal microbalance. *Biophys. J.* 75, 1397-1402.
23. Keller, C. A. & Kasemo, B. (1998). Surface specific kinetics of lipid vesicle adsorption measured with a quartz crystal microbalance. *Biophys.J.* 75, 1397-1402.
24. Patel, A. R. & Frank, C. W. (2006). Quantitative analysis of tethered vesicle assemblies by quartz crystal microbalance with dissipation monitoring: Binding dynamics and bound water content. *Langmuir* 22, 7587-7599.
25. Thid, D., Benkoski, J. J., Svedhem, S., Kasemo, B. & Gold, J. (2007). DHA-Induced Changes of Supported Lipid Membrane Morphology. *Langmuir* 23, 5878-5881.
26. Höök, F., Rodahl, M., Kasemo, B. & Brzezinski, P. (1998). Structural changes in hemoglobin during adsorption to solid surfaces: Effects of pH, ionic strength, and ligand binding. *Proceedings of the National Academy of Sciences of the United States of America* 95, 12271.
27. Hamilton, J. A. (1992). Binding of fatty acids to albumin: a case study of lipid-protein interactions. *Physiology* 7, 264-270.
28. Morozova, L., Haezebrouck, P. & Van Cauwelaert, F. (1991). Stability of equine lysozyme. I. Thermal unfolding behaviour. *Biophysical chemistry* 41, 185.
29. Chenal, A., Vernier, G., Savarin, P., Bushmarina, N. A., Gèze, A., Guillain, F., Gillet, D. & Forge, V. (2005). Conformational states and thermodynamics of α-lactalbumin bound to membranes: a case study of the effects of pH, calcium, lipid membrane curvature and charge. *Journal of molecular biology* 349, 890-905.
30. Håkansson, A., Andréasson, J., Zhivotovsky, B., Karpman, D., Orrenius, S. & Svanborg, C. (1999). Multimeric a-lactalbumin from human milk induces apoptosis through a direct effect on cell nuclei. *Experimental cell research* 246, 451-460.
31. Agasøster, A. V., Halskau, Ø., Fuglebakk, E., Frøystein, N., Muga, A., Holmsen, H. & Martínez, A. (2003). The Interaction of Peripheral Proteins and Membranes Studied with -

Lactalbumin and Phospholipid Bilayers of Various Compositions. *Journal of Biological Chemistry* 278, 21790-21797.

32. Turunen, T. M., Urtti, A., Paronen, P., Audus, K. L. & Rytting, J. H. (1994). Effect of some penetration enhancers on epithelial membrane lipid domains: evidence from fluorescence spectroscopy studies. *Pharmaceutical research* 11, 288-294.
33. Ongpipattanakul, B., Burnette, R. R., Potts, R. O. & Francoeur, M. L. (1991). Evidence that oleic acid exists in a separate phase within stratum corneum lipids. *Pharmaceutical research* 8, 350-354.

FIGURE LEGENDS

Figure 1: NMR analysis of the degree of OA binding to ELOA. (A) ^{1}H NMR spectra of ELOA, as function of EL concentration. (B) Number of OA molecules bound to EL as function of EL concentration. The dashed binding curve is added to guide the eye.

Figure 2: Confocal laser scanning microscopy shows time dependent accumulation of ELOA on 80:20 DOPC:DOPG membranes. NBD-labelled ELOA was incubated with GUVs containing Alexa Fluor 633 dye.

Figure 3: Calcein dye leakage from lipid vesicles induced by ELOA. Fluorescence of calcien released from vesicles upon ELOA interactions was compared with the fluorescence intensity at 100% release of calcein induced by addition of Triton X-100.

Figure 4: Quartz crystal microbalance with dissipation monitoring and analysis of ELOA and OA interaction with 80;20 DOPC:DOPG supported lipid bilayers. ELOA or OA were injected onto preformed bilayers (characterized by a frequency drop Δf of -26Hz and a low dissipation ΔD). The process was monitored through (A) Δf and (B) ΔD.

Figure 5: Dissipation-frequency (D-f) plot of QCM-D data during bilayer formation and ELOA or OA interaction. The insert shows closeups for 0.3µM ELOA and 3µM ELOA in the presence of 10mg/ml BSA.

Figure 6: The effect of 100nm 80:20 DOPC:DOPG LUV on the intrinsic tryptophan fluorescence of ELOA (■) and EL (□). The insert shows the development in the fluorescence emission spectrum of ELOA during titration as denoted by the arrow.

Figure 7: Changes in secondary structure of ELOA on interaction with 100nm 80:20 DOPC:DOPG LUVs determined by circular dichroism. The arrows indicate the development in the CD on increasing lipid concentration (1:12.5, 1:50, 1:125 and 1:250 ratios of EL to lipid monomers).

Figure 8: Proteolytic resistance and lysozyme activity of ELOA. ELOA, EL and ELOA incubated with 25 fold excess of lipids (LUVs) were examined on (A) the lysozyme activity on *Micrococcus lysodeikticus* substrate and (B) proteolytic resistance toward trypsin analysed by SDS-PAGE. 10-fold dilutions from 10-0.01 weight-% of EL content are indicated by the slopes above gels. M denotes the molecular weight marker band at 15kDa.

Table 1

Summary of QCM-D data for interaction of ELOA with supported lipid bilayers of 80:20 DOPC:DOPG.

Sample	$-\Delta D$ (x 10^6)/Δf after addition of ELOA	$-\Delta D$ (x 10^6)/Δf after rinsing with buffer
Untreated bilayer	0.01	0.01
0.3μM ELOA	0.01	0.01
1μM ELOA	0.07	0.07
3μM ELOA	0.11	0.24
10μM ELOA	0.46[a]	0.30
320μM OA[b]	0.25	0.39

Notes:
[a] ΔD and Δf values determined at endpoint before washing.
[b] 320μM OA corresponds to the approximate amount of OA in 10μM ELOA complex.

Figure

Nielsen et al. Figure 1

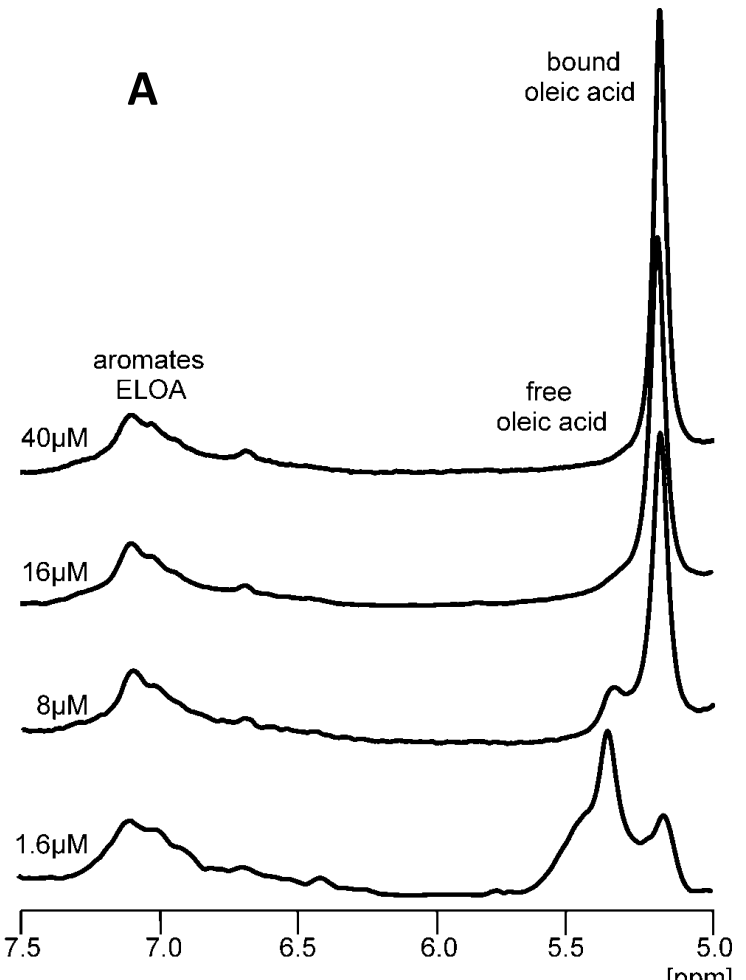

Nielsen et al. Figure 1

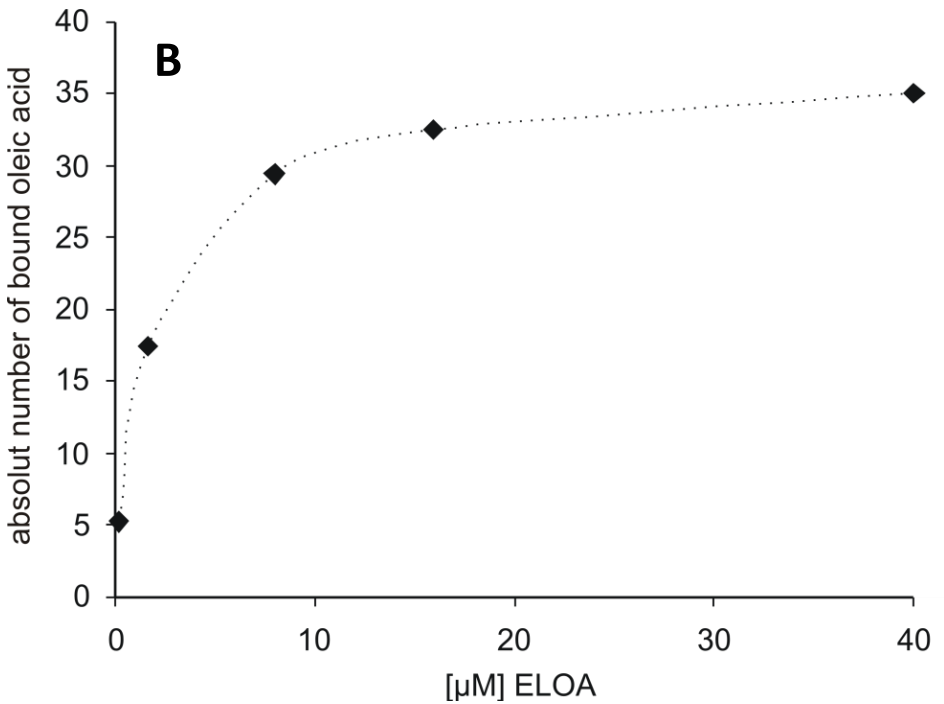

Nielsen et al. Figure 2

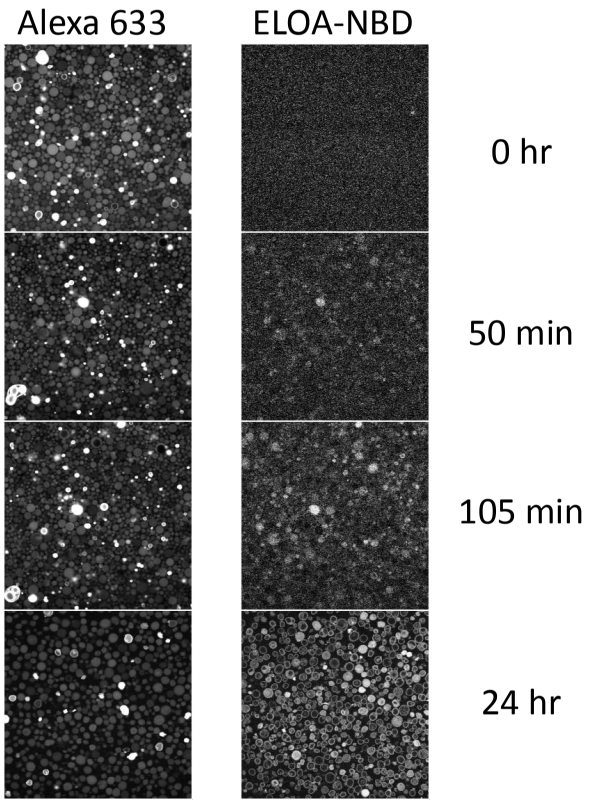

Nielsen et al. Figure 3

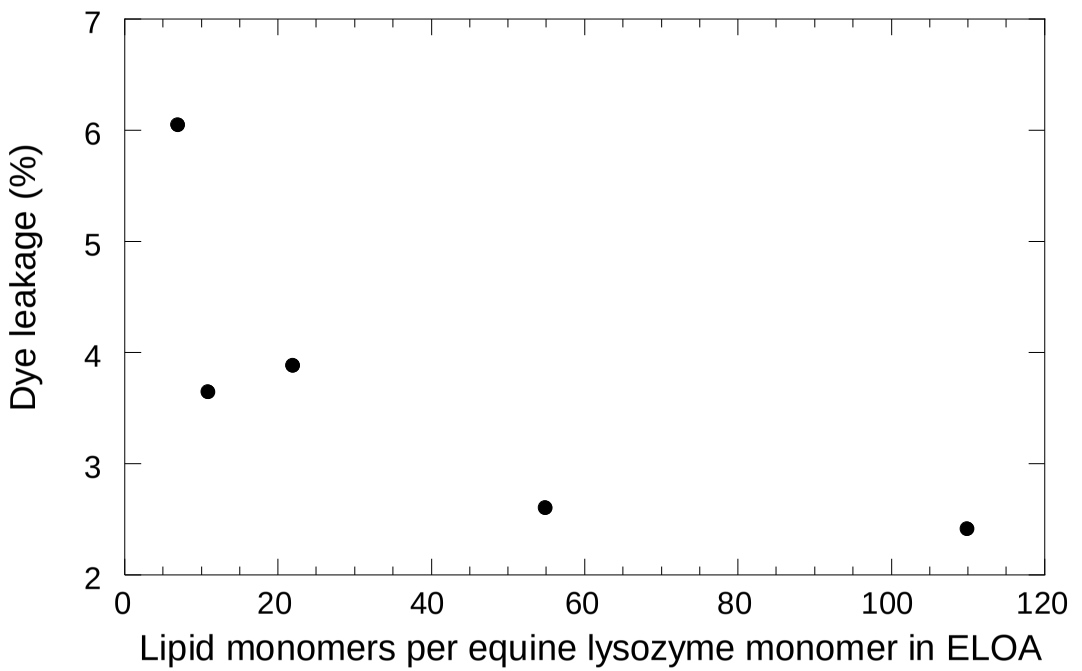

Nielsen et al. Figure 4

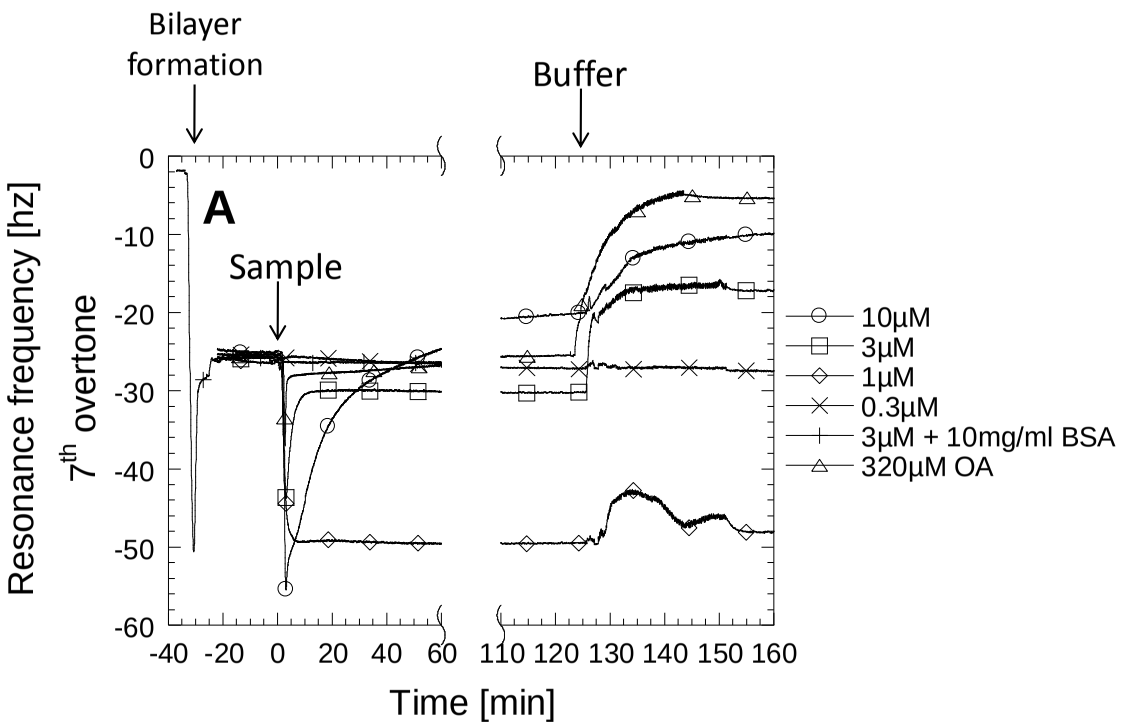

Nielsen et al. Figure 4

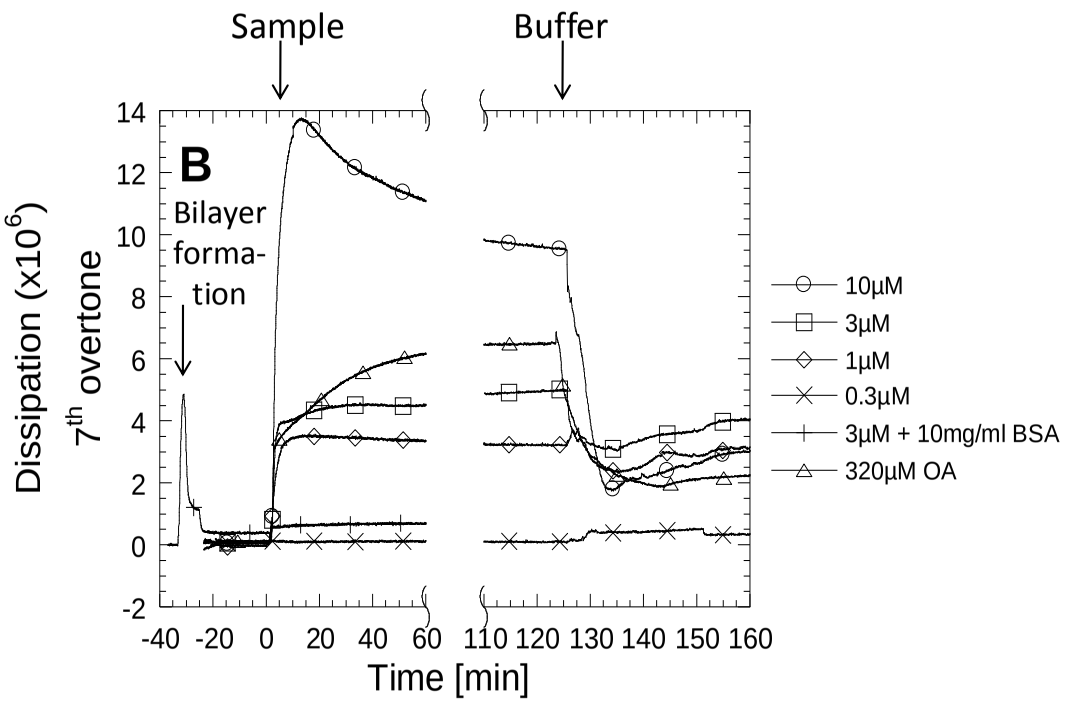

Nielsen et al. Figure 5

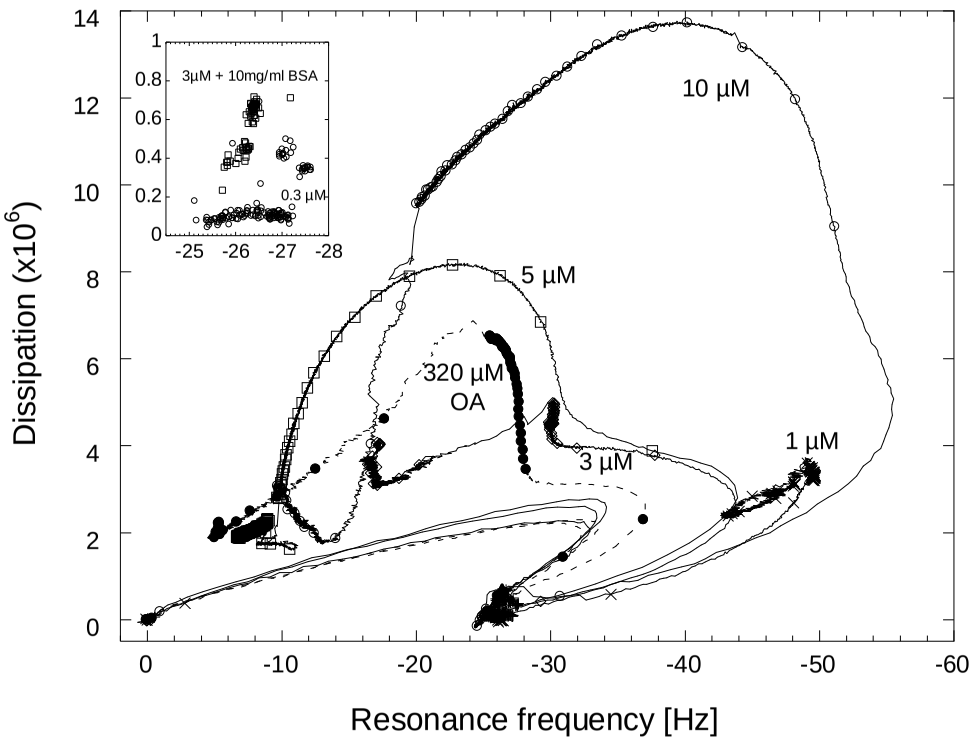

Nielsen et al. Figure 6

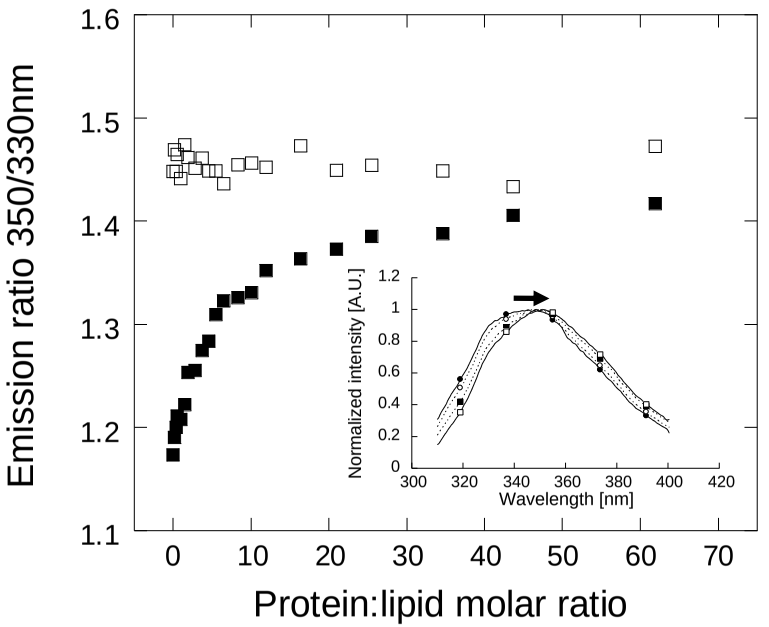

Nielsen et al. Figure 7

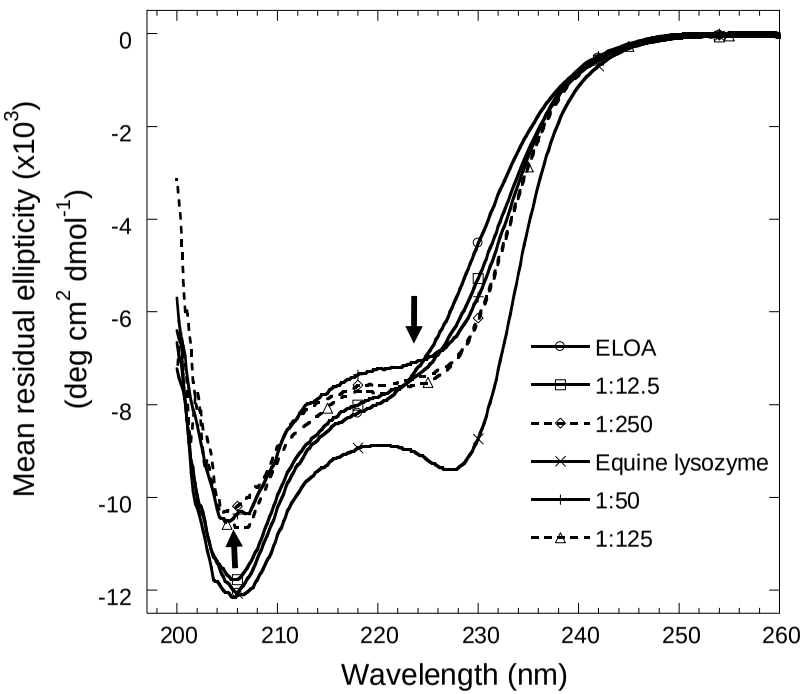

Nielsen et al. Figure 8

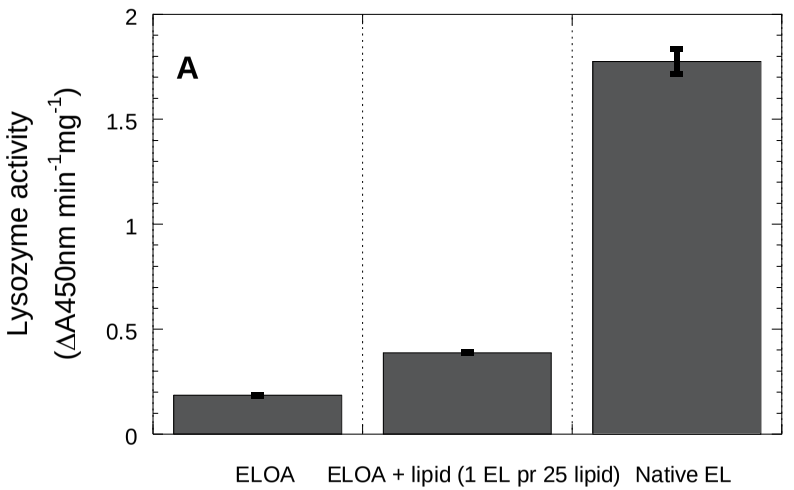

Nielsen et al. Figure 8

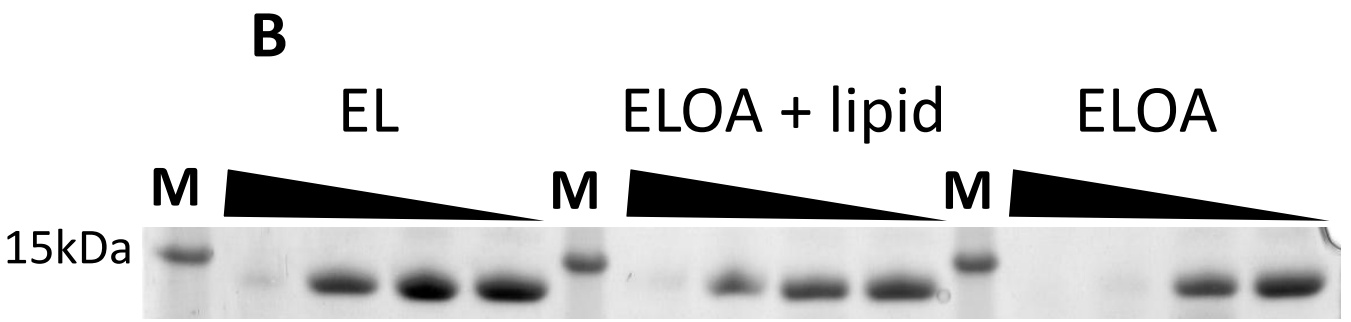

Paper V:

β-sheet aggregation of kisspeptin is stimulated by heparin but inhibited by amphiphiles

Søren B. Nielsen, Magnus Franzmann, Rajiv V. Basaiawmoit, Reinhard Wimmer, Jens D. Mikkelsen and Daniel E. Otzen

Manuscript submitted

β-sheet aggregation of kisspeptin-10 is stimulated by heparin but inhibited by amphiphiles

Søren B. Nielsen[1,2], Magnus Franzmann[3], Rajiv V. Basaiawmoit[1], Reinhard Wimmer[3], Jens D. Mikkelsen[4] and Daniel E. Otzen[1,5]

[1] Interdisciplinary Nanoscience Center (iNANO), Department of Molecular Biology, University of Aarhus, Gustav Wieds Vej 10C, DK – 8000 Aarhus C

[2] Department of Food Science, Faculty of Agricultural Sciences, University of Aarhus, Blichers Allé, DK - 8830 Tjele

[3] Department of Life Sciences, Aalborg University, Sohngaardsholmsvej 49, DK – 9000 Aalborg

[4] Neurobiology Research Unit, Juliane Maries Vej 24, Rigshospitalet, Copenhagen University Hospitalet, DK – 2100 Copenhagen Denmark

[5] To whom correspondence should be addressed. Tel. + 45 89 42 50 46, fax + 45 86 12 31 78, e-mail dao@inano.dk

Key words: peptide hormone, amyloid, random coil, heparin.

Running title: Fibrillation of kisspeptin-10 at pH 5.2 and 7.0

SUMMARY

The murine 10-residue neurohormone kisspeptin is an important regulator of reproductive behavior and gonadotrophin secretion. It is known to form a random coil in solution, but undergoes a structural change in the presence of membranes although the nature of this change is not fully determined. The peptide's conformational versatility raises the question whether it is also able to form ordered aggregates under physiological conditions, which might be relevant as a storage mechanism. Here we show that heparin induces kisspeptin to form β-sheet rich amyloid aggregates both at neutral (pH 7.0) and slightly acidic (pH 5.2) conditions. Heparin is not required for the initial pre-fibrillar steps but only for the final rate-limiting fibrillation step. Aggregation is completely inhibited by sub-micellar concentrations of zwitterionic and anionic surfactants. Unlike previous reports, our NMR data do not indicate persistent structure in the presence of zwitterionic surfactant micelles. Thus kisspeptin can aggregate under physiologically relevant conditions provided heparin is present, but the process is highly sensitive to the presence of amphiphiles, highlighting the very dynamic nature of the peptide conformation and suggesting that kisspeptin aggregation is a biologically regulatable process.

INTRODUCTION

The peptides derived from the metastasis suppressor gene transcript *Kiss1* are involved in regulation of gonadotrophins in vertebrates [1-3]. Numerous structurally related peptides named kisspeptins have been identified in several species, and their actions are mediated via the G-protein coupled receptor Kiss1R (also termed GPR54, AXOR12 or hOT7T175) [4-6]. It has been proposed that kisspeptin/Kiss1R is primarily located in the hypothalamus, where kisspeptins operate as essential transmitters for the activation of GnRH neurons at puberty and the kisspeptin/Kiss1R neurons are regulated by gonadal and metabolic signals [7-9]. The human *Kiss1* gene encodes a 145 amino acid precursor peptide that is likely cleaved into an C-terminal 54 amino acid product known as human kisspeptin-54 (also named metastin) [10]. In rodents, the kisspeptin precursor is post-translationally spliced into a 52 amino-acid peptide (murine kisspeptin-52), which shows several sequence differences to the human kisspeptin-54 sequence, including a putative disulfide bridge between position 4 and 16 [11]. Further, the C-terminal amino acid residue differs in that the C-terminal residue is Tyr in rodents but Phe in man. The biological activity of kisspeptins is determined by the C-terminal end of the peptide, because shorter fragments such as kisspeptin-10, also bind to Kiss1R with the same affinity as the longer forms [11-13].

Very little is known about the structure and sequence of naturally occurring kisspeptins in blood or in extracellular spaces and nothing is known about their structure in cells. The structure appears to be mainly random coil in aqueous buffer at neutral pH, but undergoes structural changes in the presence of lipid vesicles and membrane-mimicking micelles [14], but the available data do not suggest regular secondary structure. There have been no reports of the ability of kisspeptins to aggregate to form cross-β sheet structures

called amyloids. Nevertheless, such an amyloidogenic property might be expected. It has been proposed that the ability of proteins and peptides to form amyloidal aggregates is an intrinsic property of the polypeptide chain [15], and this propensity can be encouraged by allowing the protein to adopt a more dynamic structure through *e.g.* partial denaturation. Kisspeptin's random coil structure provides ready access to a number of different conformations. By analogy, the peptide hormone glucagon, which is natively unfolded, fibrillates easily in solution [16,17] although its low solubility and low physiological concentration at neutral pH renders this physiologically somewhat irrelevant. However, for peptides with higher solubility at neutral pH, access to the amyloid state may provide a convenient and pH-sensitive storage mechanism. A large number of peptide hormones can form β-sheet structures under physiological conditions, particularly in the presence of the highly sulphonated, naturally occurring glucosaminoglycan heparin, and this may function as a physiological storage mechaism [18]. Indeed, a recent report proposed the use of amyloidal aggregates in pharmaceutical applications for controlled long-term release of GnRH hormone analogs at the appropriate target location [19]. Commensurate with this, long-acting GnRH analogs, but not the short-term acting versions, were able to form fibrils under physiological conditions [19].

Here we examine the propensity of murine kisspeptin-10 (mKp-10) to aggregate at pH 5.2 and 7.0, which correspond to the pH conditions within neuroendocrine secretory granules [20] and the synaptic space [21], respectively. mKp-10 only differs from its human analog in the C-terminal residue, which is Tyr in mice and Phe in humans. These two residues are known to have comparable abilities to stabilize amyloid aggregates [22,23] and therefore we do not expect human kisspeptin to differ significantly from mKp-10 in this

aspect . Further, we evaluate the effect of sodium chloride, divalent cations and heparin on mKp-10 aggregation. In addition to its role in inducing fibrils in peptide hormones [18,19], heparin is present in, and induces formation of, many other natural amyloid deposits [24]. We show that although mKp-10 does not aggregate in buffer alone, heparin encourages fibrillation at both pH values. However, amphiphiles strongly inhibit the reaction at surfactant concentrations well below those where detectable structural changes occur. Furthermore, although structural changes do occur at higher surfactant concentrations, they do not lead to persistent secondary structure, but most likely a highly fluctuating state. Our results indicate that mKp-10 aggregation is a highly regulatable process.

RESULTS

Formation of mKp-10 aggregates in the presence of heparin

We investigated whether mKp-10 could be induced to aggregate under physiologically relevant conditions, as recently shown for several GnHR analogs [19]. mKp-10 was incubated in a plate reader with shaking at 37°C in the presence of the dye Thioflavin T (ThT), whose fluorescence emission intensity increases upon binding to fibrils [25]. No significant changes in ThT fluorescence were observed over 70 hours at neutral (7.0) and slightly acidic (5.2) pH, indicating that mKp-10 did not fibrillate into amyloid aggregates in simple buffer systems (Fig. 1). However, when we repeated the fibrillation experiment in the presence of a weight-equivalent amount of heparin, we observe a doubling in the ThT fluorescence emission intensity at both pH-values after a lag phase of (Fig. 1). The baseline from which this doubling occurs is significantly higher than the baseline ThT fluorescence in the absence of heparin. ThT is known to bind to biopolymers such as cellulose [26] and DNA [27]. Nevertheless, heparin alone does not lead to increased ThT fluorescence intensities (data not shown). We interpret this to mean that mKp-10 rapidly forms initial aggregates in the presence of heparin (to which ThT binds), followed by a slow progression to another type of aggregate.

Clearly heparin is required for the formation of both the early and late-stage aggregates. The question is whether the early-stage aggregates are precursors to the late-stage aggregates and whether heparin is required to facilitate this process; alternatively, it may be that mKp-10 can by itself undergo initial changes at an early stage of the aggregation process so that heparin merely helps the incipient aggregate over a critical

barrier before the actual fibrils form. We may resolve this by addressing the nature of the lag phase. A lag phase prior to a rise is often interpreted as a series of molecular rearrangements leading to a fibrillation nucleus, whose formation is rate-limiting for fibrillation [28]. Another view is that the lag phase corresponds to the early stage of an exponential growth curve in which fibrils grow by secondary nucleation, leading to a cascade of growth which eventually emerges as a steep increase in fluorescence [29]. Given that aggregation can be controlled by the presence of heparin, it is possible for us to distinguish these two scenarios by only adding heparin towards the end of the period corresponding to the lag phase. If the addition of heparin at this stage induces the immediate growth of fibrils, that indicates that mKp-10 is poised to form fibrils at this stage, only needs a catalyst to overcome the final hurdle and therefore aggregates by the formation of a high-energy nucleus that has to be stabilized. Secondary nucleation can be ruled out in this case, because even if heparin were to stabilize the initial steps in such a mechanism, it would still be necessary for the peptide to go through a pre-growth phase in order to accumulate enough aggregate that can bind ThT; in secondary nucleation, all the aggregative species are present from the very early stages of the process, albeit only at low concentrations. If on the other hand the aggregation only sets in after a period corresponding to a whole lag phase, that suggests that mKp-10 cannot even undertake the initial pre-fibrillar aggregation steps by itself but needs heparin to set the whole process in motion (but whether this occurs by a rate-limiting nucleus or by secondary nucleation cannot then be determined).

The results are unequivocal: when we preincubate mKp-10 with shaking at 37^{o}C in the absence of heparin and then add heparin after 70 hrs, we observe an immediate jump in fluorescence at pH 5.2, reaching approximately the baseline observed in the presence of

heparin; subsequently there is a rise in fluorescence which is very similar to that observed for samples incubated with heparin from time zero (Fig. 1). No such effect is observed when buffer is added instead of heparin (data not shown). The effect is similar at pH 7.0, with the important difference that there is no “burst phase” jump in fluorescence but just a steady rise in the ThT fluorescence from ase level. From these results, we conclude that mKp-10 aggregates through a rate-limiting nucleus whose formation determines the length of the lag phase, and that the presence of heparin is only required to facilitate the final step leading to formation of ThT-binding aggregates. Furthermore, the burst phase upon addition of heparin at pH 5.2 suggests that the initial aggregates described above may still form at this pH but do not play a role in the subsequent formation of the later-stage aggregates. Consistent with this, at pH 7.0 there is no burst phase at all, indicating that these initial aggregates cannot form at pH 7.0 when mKp-10 has had time to form the prefibrillar structures that subsequently lead to aggregates.

In contrast to the immediate effect of heparin on aggregation in salt-free samples, lag phases of 10-20 hrs were observed for both pH 5.2 and pH 7.0 samples containing 150mM NaCl, and the end-ThT emission levels are reduced by a factor ~2 (data not shown). This suggests that binding of mKp-10 to the polyanion heparin, which is a prerequisite for amyloid formation, is mediated by electrostatic forces and therefore reduced when the ionic strength is increased. This agrees with mKp-10’s peptide charge. With 1 Arg, 2 Tyr and no acidic residues, mKp-10 retains a net charge of +1 in the pH interval 5-7 and only becomes electrically neutral above pH 9, so it is likely to be strongly attracted to the polyanion heparin at neutral pH.

Aggregation of mkp-10 is accompanied by development of β-sheet structure

CD and FTIR spectroscopy methods were applied to investigate conformational changes associated with aggregation of mKp-10 in the presence of heparin. The CD spectra of mKp-10 incubated for several days at pH 5.2 and 7.0 in the absence of heparin show a distinct maximum at 226nm after incubation for several days, resembling the spectrum of mKp-10 in MilliQ water (Fig. 2). The positive band closely resembles those observed for alanine scanning analogs of human Kisspeptin analogues [14]. mKp-10 and its human homolog are unusually rich in aromatic residues which make up 50% of the 10-residue sequence, and this is reflected in the CD spectrum with maxima at 226, 220 and 224 nm, respectively [30]. The spectra thus do not show any signs of β-sheet or α-helical conformations and retain random coil structure as expected *a priori* from the ThT binding profiles.

However, the addition of an equivalent weight amount of heparin to mKp-10 samples greatly changes the CD spectrum compared to mKp-10 in H_2O as shown by a clear minimum at 220nm at pH 7.0 (Fig. 2), which is very close to the 215-218 nm assigned to β-sheets [31]. The minimum at 217nm present at pH 5.2, although smaller in intensity, clearly demonstrates the formation of β-sheet structure in the presence of heparin. The additional negative band at approximately 235nm has been ascribed to the formation of turn structures in assembled aggregates [32].

To investigate the structural changes further, ATR-FTIR spectra of the samples were obtained of mKp-10 fibrils (Fig. 3). We observe two major peaks with maxima at approximately 1604 and 1631cm^{-1} for aggregates at pH 5.2 aggregates, and at 1605 and 1633cm^{-1} for pH 7.0 aggregates. The major peaks at 1631 and 1633 cm^{-1} in pH 5.2 and pH 7.0 samples, respectively, may be assigned to extended β-sheet structures. An

additional band at approximately 1624cm^{-1} was observed at for heparin-containing samples at pH 7.0. This value is within the 1611cm^{-1} to 1630cm^{-1} range expected for amyloid fibrils [33].

The vibrations observed at approximately 1604-1605cm^{-1} cannot be assigned to distinct secondary structure elements. However, such bands may arise due to ring vibrations of tyrosine residues, which make up two out of mkp10's ten amino acid residues. Tyrosine ring vibration is further supported by the presence of additional vibrational bands in the amide II region at approximately 1502 and 1517cm^{-1}, respectively [34].

Atomic Force Microscopy reveals fibrillar structures

Atomic force microscopy was applied to characterize the morphology of the aggregated mKp-10 samples. In agreement with CD measurements, no aggregates were observed in the samples before addition of heparin (data not shown). However, heparin-containing samples at pH 5.2 and 7.0 both showed fibrillar morphology (Fig. 4A and 4B). mKp-10 in sodium acetate buffer at pH 5.2 showed a mass of very thin bundled fibres (Fig. 4A) spread out over a large area. The fibres were about 50nm in width and about 7nm in height, as seen from the cross-section of an individual fibril (Fig. 4A') at the edge of the mass. Though very similar in morphology to the pH 5.2 sample, the mKp-10 fibres formed in phosphate buffer pH 7.0 were only around 1.5 nm in height (Fig. 4B') and showed a more twisted morphology than fibrils formed at pH 5.2. Thus CD, FTIR and AFM consistently show that the aggregates formed at the two pH-values are both rich in β-sheets but show distinct differences. This also agrees nicely with the plate-reader data

in which the prefibrillar aggregates formed in the absence of heparin prevent the formation of early stage aggregates when heparin is added at pH 7.0, but not at pH 5.2.

mKp-10 interaction with amphiphiles prevents aggregation at sub-micellar concentrations

Given that both aggregation and membrane interactions may be biologically relevant for mKp-10's function, we decided to investigate the impact of amphiphiles on mKp-10 aggregation. We started out by reproducing the CD spectra by Lee at al. [35] and showed that DPC only induced significant changes in mKp-10 structure at concentrations above the cmc (Fig. 5A). This suggests an interaction, and hence a structural change in the peptide, only upon micelle formation. However, as reported by Lee, the CD spectra do not indicate any classical α-helix or β-strand structure in the presence of micelles.

In contrast to the CD data, there was clear evidence for interactions with DPC below the cmc when we investigated aggregation of mKp-10 in the presence of different concentrations of DPC. As little as 0.01 mM DPC was sufficient to completely block the increase in ThT fluorescence within the 4-day measurement period (Fig. 5B), and only as we approach the cmc do we see a rise in fluorescence over time, which becomes very rapid at 3 mM DPC. However, the fluorescence rise at this concentration is unlikely to be related to aggregation, since we are unable to pellet mKp-10 aggregated at micellar DPC concentrations. We summarize these data by plotting the endpoint ThT emission intensity versus DPC concentration (Fig. 5C). They clearly show the decline in ThT fluorescence with increase in DPC concentration up to around 1 mM DPC, after

which ThT emission starts to rise again due to micelle-liked but non-aggregative phenomena.

Similar experiments conducted in the presence of SDS at both pH-values show a simpler pattern. Just as DPC, SDS (whose cmc is around 3 mM under the present buffer conditions according to pyrene measurements [36]) inhibits the rise in ThT emission at concentrations as low as 0.01 mM, but unlike DPC there is no compensatory rise in ThT fluorescence emission above the cmc (Fig. 5C). Addition of DPC and SDS to final concentrations of 10μM-10mM and 10-100μM, respectively, to preformed aggregates did not result in changes in ThT fluorescence, indicating that the surfactants interact with mKp-10 prior to aggregation and not the aggregate itself. In contrast, 1 and 10mM SDS concentrations lead to partial and complete solubilization of the aggregates, respectively, as indicated by a decrease in ThT fluorescence (data not shown).

Thus there is clearly a discrepancy between the CD data, which suggest interactions only with micellar DPC, and the aggregation data, which indicate interactions with sub-micellar DPC.

In contrast to the surfactants DPC and SDS, simple phospholipid vesicles composed entirely of the zwitterionic lipid di-oleoyl-phosphatidyl choline (DOPC) or containing 80% DOPC and 20% of the anionic lipid di-oleoyl-phosphatidyl glycerol failed to have any impact on the fibrillation of kisspeptin in the presence of heparin at either pH 5.2 or pH 7.0 (data not shown).

We turned to NMR to ascertain independently whether mKp-10 interacts with micelles. Diffusion measurements of mKp-10 show a significant decrease in the diffusion constant upon addition of DPC in the range of 0 to 10 mM. At 10 mM DPC, the observed diffusion constant of mKp-10 is very close to that of the DPC micelle (Fig. 6).

Addition of more DPC does not lead to a further decrease in diffusion constant. This is a clear indication that the peptide is strongly bound to the micelles.

The far-UV CD spectrum did not reveal any regular secondary structure elements. This is corroborated by NMR data. We assigned the NMR signals of mKp-10 in the presence of DPC micelles. Despite a complete assignment of the resonances, we did not find any sequential dNN(i,i+1) or medium range dαN(i,i+3) NOEs which are typical signs of α-helix secondary structure. The lack of these signals clearly indicates that the peptide is unstructured in the presence of DPC. This is further supported by the observation of exchange cross-peaks between every single observable H^N atom and water, which reflects the exposure of the amide protons towards the solvent. Clearly none of these atoms are buried in the micelles and none of them are involved in stable hydrogen bonds, as would be expected in secondary structure elements. Thus we conclude that mKp-10 must bind to DPC micelles in a conformation which is different from the random coil structure adopted in solution but nevertheless remains highly flexible and solvent-exposed.

DISCUSSION

Aggregation of kisspeptin by heparin: a storage and release mechanism?

We have shown that the 10-residue peptide kisspeptin-10 can form amyloid structures under physiological conditions, provided heparin is present. The existence of amyloids is corroborated by ThT binding, formation of β-rich structures according to CD and FTIR (including the amyloid-specific band around 1627 cm^{-1}) and fibrillar morphology according to AFM. While the reason for heparin's ability to induce amyloids is unclear, it is possible that the β-sheet conformation provides the best binding mode for mKp-10-heparin interactions. In combination with heparin's linear repeat structure, this may provide a nucleation point for subsequent amyloid formation and growth. Interactions are clearly mediated by electrostatics, in view of the reduction in the degree of ThT emission intensity induced by the presence of salt. Our experiments with delayed addition of heparin suggest that heparin is not required for the very early stages of pre-fibrillar assembly but simply stabilizes the peptide in the rate-limiting step prior to the formation of fibrils. This indicates that mKp-10 is able to undergo a certain degree of self-assembly by itself.

Our observations are consistent with the observation by Riek and co-workers on the wide-spread aggregation of peptide hormones, particularly in the presence of heparin and other glucosaminoglycans [18] and their proposal that this state may be used as a natural storage mechanism for at least some hormones, including mKp-10. Physiologically, mKp-10 is believed to be stored in dense-cored granula and released to the synaptic cleft and the proximal extracellular space, or into the blood stream. The peptide products of the intracellular processing of the kisspeptin precursor are at present

unknown. However, dibasic cleavage gives rise to a 52 amino-long peptide in mice, and as there are two Cys residues in this sequence, an S-S bridge is likely to be established. The C-terminal peptide has been shown to be present as a cleavage product from placenta [13], but to what extent it is present in extracellular spaces or within the granula is unresolved. Our data indicate that mKp-10 is able to form amyloid with comparable ease at pH 5.2 and 7.0 although the architecture of the fibrils differ slightly, so changes in pH are not likely to affect release.

Amphiphiles strongly affect heparin aggregation propensity through subtle interactions that can only be detected indirectly

The observations on the stimulation of mKp-10 aggregation by heparin confirm existing reports on the aggregation of peptide hormones by glucosaminoglycans [18]. However, a novel observation in our view is the profound inhibitory effect of sub-micellar concentrations of amphiphiles on kisspeptin aggregation. We do not believe that these observations are of direct relevance for a discussion of mKp-10's interaction with the cellular membrane, as zwitterionic and partially anionic lipids did not affect the aggregation ThT profile. Rather, they provide more insight into the highly flexible conformation that mKp-10 adopts in solution and the delicate network of interactions required to form the aggregate structures that eventually lead to fibrils. Our data indicate that interactions with sub-micellar concentrations of surfactants, which are undetectable by CD or NMR, are sufficient to inhibit formation of the aggregates. These interactions must only have very subtle effects on the mKp-10 conformation since even the presence of DPC micelles – which induces marked changes in the CD spectrum - leads to a structure which lacks persistent hydrogen-bonding and regular secondary structure. It is

possible that the micelle-bound structure contains nascent structure which on average provides a certain degree of organized structure but is too dynamic and flickering to form stable hydrogen-bonds and measurable shielding from solvent-exposure. In this sense, the structure of micelle-bound mKp-10 corresponds to the very early stages of folding of globular proteins where some structure may be detectable by UV-Vis spectroscopy but not by protection against hydrogen-deuterium exchange [37].

It has been suggested that the lack of structure of mKp-10 and its precursor KP-54 may confer advantages in its ability to recognize and bind a wide range of target proteins [38]. It is definitely clear that changes in the solvent conditions can easily displace the peptide's conformational preferences, which suggests that mK-10 aggregation can be regulated biologically, *e.g.* by binding to other proteins or by low concentrations of naturally occurring amphiphiles such as lipids. Somehow the sub-micellar surfactant interactions displace the ensemble structure of mKp-10 towards a state that is less prone to aggregation while heparin has the opposite effect. Sub-micellar concentrations of SDS are known to induce aggregation of many larger proteins [39-44]. Recent Small Angle X-ray Scattering data suggest that this aggregation occurs by the formation of micelles bridging different proteins [45](Giehm, D.E.O., unpublished observations). This immediately suggests a simple explanation for the inability of SDS to stimulate mKp-10 aggregation: the peptide is too small to stabilize and link micellar clusters bridging different peptide molecules.

The NMR structure of kisspeptin is inconsistent with regular secondary structure

The binding of mKp-10 analogues to different amphiphiles has previously been investigated to determine whether receptor-binding could be preceded by mKp-10's partitioning into the membrane. A 13-residue extension of mKp-10 (mKp-13) is reported to adopt a helical structure in SDS at pH 5.5, consistent with SDS' potent α-helix inducing properties [46], while mKp-10 in SDS gave poor NMR spectra [47]. DPC has been shown to induce a non-helical structure in the mKp-10 mutant S5A characterized by several tight turns at pH 3.5 [35], whereas the F10A mutant did not adopt any regular structure with DPC. In this study, DPC was shown to induce this structure only at concentrations at and above its critical micelle concentration (1.1 mM), cfr. Fig. 2 in [35] where structural changes only occur at peptide:DPC ratios of 1:25 and above at a mKp-10 concentration of 0.15 mM. This is consistent with our own observations.

A recent publication reports a mixed α-helix/3_{10}-helix structure for mKp10 and both F6A and F10A mutants [48]. In this study the authors report (slightly different) helicoidal structures for mKp-10, F6A-mKp-10 and F10A-mKp-10 in DPC but the pH value at which these are measured are not reported in the article.

The reported structures in literature are thus somewhat self-contradicting. A proper comparison is difficult, since different mutants, different pH values and different detergents were used. The structures reported in [47] and [35] were calculated based on relatively few medium-range NOEs, as can be seen on the sequence plots shown in both papers. No sequence plot is given in [48] that allows an evaluation of the structure determination.

We observe that although mKp-10 undergoes structural changes in the presence of DPC micelles according to CD spectra, the peptide remains in a highly solvent-exposed conformation which allows rapid hydrogen exchange. We are aware that these findings

do not agree with the results reported by Gutierrez-Pascual et al. [48] who, based on their own NMR data, proposed that mKp-10 adopts a mixture of α-helical and 3_{10} structure. At present the reason for this discrepancy is unclear, but it is possible that experimental differences may play a role, since it is obvious that even small changes in the solvent conditions may affect the kisspeptin structure.

MATERIALS AND METHODS

Chemicals: Heparin ammonium salt from porcine intestinal mucosa was a product of Fluka (Buchs, Switzerland). Thioflavin T (Sigma prod. No T3516) dissolved in 96% ethanol and the concentration was determined using ε_{412nm} of $36000M^{-1}$ [49]. Dodecylphosphocholine (DPC) was purchased from Avanti Polar Lipids (Alabaster, AL) and DPC-d_{38} from Cambridge Isotope Laboratories Inc. (Andover, MA). Murine Kisspeptin-10 (YNWNSFGLRY-amide, mKp-10) was synthesized by Caslo Aps (Lyngby, Denmark).

Preparation of mKp-10 aggregates: mKp-10 was dissolved in MilliQ water [50] due to its low solubility in buffered solution, and the peptide concentration was measured by UV absorbance at 280nm using a Nanodrop ND-1000 UV/Vis spectrophotometer (NanoDrop Products, Wilmington, USA) and a calculated extinction coefficient (1 Trp, 2 Tyr) of $8480M^{-1}cm^{-1}$ [51]. Peptide was added to a final concentration of 0.5mg/ml in 200µl sample volume also containing 40µM Thioflavin T (ThT) in a 96 well clear bottom microtiter plate (Nunc International, New York, USA) covered with a clear film to avoid evaporation. Buffers employed were 20mM sodium acetate pH 5.2 and 20mM sodium phosphate pH 7.0. The plate was incubated for several days at 37°C in cycles of 10 minutes orbital shaking at 100rpm and 10 minutes rest in a Tecan Genios Pro platereader (Tecan Group Ltd, Männedorf, Germany). The settings employed in the plate reader were an excitation wavelength of 448nm and emission wavelength of 485nm. The gain was set to manual with a value of 45 units. For experiments in the presence of heparin, we included heparin at a concentration of 0.5 mg/ml from a stock of 5 mg/ml. To evaluate the effect of heparin on mKp-10 aggregation after pre-incubation, 20µl 5mg/ml heparin (20µl appropriate buffer to control samples) was

added to sample wells at 70 hours of incubation. 20 µl buffer was added to control samples. The samples were removed from the plate reader for less than 5 minutes during this procedure.

Circular dichroism: Far-UV CD spectra were recorded on a Jasco J-810 spectropolarimeter (Jasco Spectroscopic Co. Ltd., Hachioji City, Japan) thermostatted at 25°C and using a 1mm quartz cuvette. The ellipticities were recorded in the 205-250 nm wavelength range. mKp-10 concentrations were 0.25mg/ml (250 µM) for aggregate studies and 0.13 mg/ml (130 µM) in the presence of varying concentrations of DPC (0 mM, 0.01 mM, 0.1 mM, 1 mM, 3 mM or 50 mM). All samples contained 20 mM sodium phosphate (pH 7.0).

Fourier transform infrared spectroscopy: ATR-FTIR measurements were performed on a Bruker Tensor 27 instrument (Bruker, Karlsruhe, Germany) equipped with a Specac Golden Gate single-reflection diamond attenuated total reflectance (ATR) cell (Specac Ltd., Orpington, United Kingdom). MKp-10 aggregates were washed in 2x1ml MilliQ H_2O by centrifugation at 13000 rpm for 5 minutes to remove potentially interfering buffer signals. After the second wash, the supernatant was removed and the aggregates were suspended in minimal volume by gentle pipetting. Aliquots of sample were applied to the crystal and dried in a stream of nitrogen gas until the water signal had stabilized. Sample was added until the intensity of the primary amide I band reached at least 0.1 absorbance units. The absorption spectrum was recorded in the interval 1000-4000 cm^{-1} using a nominal resolution of 2 cm^{-1} and 64 accumulations. The obtained data were processed by applying atmospheric compensation and baseline corrections and finally peaks were fitted to Lorentzian line shapes to obtain estimates of vibrational bands using OPUS version 5.5 (Bruker, Karlsruhe, Germany).

Atomic force microscopy: Samples for AFM analysis were withdrawn from the 96-well plate after the fibrillation kinetics had reached a plateau. To reduce drying artifacts, the samples were withdrawn by a pipette after making a small perforation of the cover film and stored in an eppendorf tube. 2 µL was transferred to freshly cleaved mica and blow-dried immediately. To wash out any salts, the mica surface was rinsed with MilliQ H_2O. The samples were imaged on an Agilent 5100 AFM/SPM microscope (Agilent Technologies, Santa Clara, CA, USA). To ensure high resolution imaging and minimal sample distortion by tip compression, AFM imaging was performed in the tapping mode at scan frequencies of 1–2 Hz. The cantilevers used were silicon nitride cantilevers. All AFM images were globally flattened and visualized using the commercial Scanning Probe Image Processor software (SPIP™, Image Metrology ApS, Version 4.2, Lyngby, Denmark).

Nuclear Magnetic Resonance: All NMR spectra were recorded at 310 K on a BRUKER DRX600 spectrometer operating at a field strength of 14.1 T, equipped with a TXI(H/C/N) probe with triple-axis gradients. 1 mM mKp-10 were dissolved in 90 mM DPC-d_{38}, 20 mM phosphate buffer, 0.05% sodium azide, 5% D_2O, pH 7.0 to a final volume of 500 µL. A 2D NOESY spectrum with 80 ms mixing time was recorded with a WATERGATE water suppression [52]. [^{1}H, ^{1}H]-TOCSY spectra with 50 ms mixing time were recorded using a clean-TOCSY pulse sequence with a 15 kHz spin-lock and excitation sculpting water suppression[53,54]. 2QF-COSY and [^{1}H-^{13}C]-HSQC were recorded using standard sequences taken from the Bruker Topspin pulse sequence library. All spectra were processed using Topspin version 1.3. Assignment of all NMR spectra were performed using the program CARA version 1.5.5 [55]. For diffusion measurements, a sample containing 1 mM mKp-10, 20 mM phosphate buffer, 0.05%

sodium azide, pH 7.0 dissolved in 100% D_2O was stepwise mixed with a sample containing 1 mM mKp-10, 1 M DPC, 20 mM phosphate buffer, 0.05% sodium azide, pH 7.0 dissolved in 100% D_2O to give DPC concentrations of 0, 5, 10, 20, 50 and 100 mM. Diffusion coefficients were determined for mKp-10 signals at all DPC concentrations using a double stimulated echo pulse sequence [56-58] applied with an off-resonance E-BURP1 [59] selective pulse of 1.88 ms length centered at 7.93 ppm for selective excitation of the aromatic mKp-10 signals. 16 spectra were recorded with increasing gradient strengths ranging from 9 to 36 Gcm^{-1}. DPC diffusion coefficients were measured in the same way, but without a selective readout pulse. mKp-10 and DPC signals were integrated at each gradient strength and diffusion constants were fitted using Bruker TopSpin version 1.3

FIGURES

Figure 1

Aggregation of 0.5mg/ml mKp-10 at pH 5.2 and 7.0 at 37°C over time monitored by Thioflavin T fluorescence. Two samples ("pH 7.0" and "pH 5.2") were incubated without heparin while two samples (indicated by "heparin" in the graph legend) were incubated with 0.5 mg/ml heparin for the whole incubation period. For two of the samples ("heparin added"), heparin was added after 70 hrs (indicated by the arrow) to a final concentration of 0.5mg/ml.

Figure 2

Far-UV circular dichroism spectra of mKp-10 samples before and after incubation at 0.5mg/ml in 20mM NaOAc pH 5.2 and 20mM sodium phosphate pH 7.0 with 1:1 w/w % heparin.

Figure 3

Fourier transform infrared spectroscopy spectra of mKp-10 aggregates in (A) 20mM NaOAc pH 5.2 and (B) 20mM sodium phosphate pH 7.0 prepared as in Fig. 2. Curve fitting was performed with Lorentzian line shapes.

Figure 4

AFM imaging of fibrillar mKp-10 aggregates after incubation at 37°C in the presence of 1:1 w/w heparin in (A) 20mM NaOAc pH 5.2 and (B) 20mM sodium phosphate pH 7.0.

Figure 5

(A) Far-UV CD spectra of mKp-10 at pH 7.0 recorded in 0-10 mM DPC.

(B) Time course of ThT fluorescence for 0.5 mg/ml mKp-10 incubated with 0.5 mg/ml heparin in 0-10 mM DPC.

(C) End-point ThT fluorescence emission intensities for mKp-10 incubated at pH 7.0 and 5.2 in 0-10 mM DPC and SDS. Intensities were determined by linear fitting of the intensity data within the last 20 hours of the measurements and interpolation to 160 hrs. Background intensities of ThT in DPC and SDS have been subtracted.

Figure 6

(○) Diffusion constant measurements of mKp-10 in the presence of increasing amounts of DPC. (◊) Observed diffusion constants of DPC at various concentrations; this represents a combined contribution from both monomeric and micellar DPC molecules. ( ) Calculated diffusion constant for micelle bound DPC.

ACKNOWLEDGEMENTS

S.B.N. is supported by a grant from the Danish Committee for Food and Health (FøSu). R.V.B. is supported by a postdoctoral stipend from the Carlsberg Foundation. M. F. is supported by the Villum Kann Rasmussen Foundation (BioNET) and the Danish Research Council. The NMR laboratory at Aalborg University is supported by the Obel Foundation. D.E.O. is supported by the Danish Research Foundation (inSPIN) and by BioNET.

REFERENCES

1. de Roux, N.; Genin, E.; Carel, J. C.; Matsuda, F.; Chaussain, J. L.; Milgrom, E. Proc Natl Acad Sci U S A 2003, 100, 10972-10976.

2. Funes, S.; Hedrick, J. A.; Vassileva, G.; Markowitz, L.; Abbondanzo, S.; Golovko, A.; Yang, S.; Monsma, F. J.; Gustafson, E. L. Biochem Biophys Res Commun 2003, 312, 1357-1363.

3. Seminara, S. B.; Messager, S.; Chatzidaki, E. E.; Thresher, R. R.; Acierno, J. S., Jr.; Shagoury, J. K.; Bo-Abbas, Y.; Kuohung, W.; Schwinof, K. M.; Hendrick, A. G.; Zahn, D.; Dixon, J.; Kaiser, U. B.; Slaugenhaupt, S. A.; Gusella, J. F.; O'Rahilly, S.; Carlton, M. B.; Crowley, W. F., Jr.; Aparicio, S. A.; Colledge, W. H. N Engl J Med 2003, 349, 1614-1627.

4. Seminara, S. B.; Kaiser, U. B. Endocrinology 2005, 146, 1686-1688.

5. Smith, J. T.; Clifton, D. K.; Steiner, R. A. Reproduction 2006, 131, 623-630.

6. Tena-Sempere, M. Neuroendocrinology 2006.

7. Castellano, J. M.; Navarro, V. M.; Fernandez-Fernandez, R.; Nogueiras, R.; Tovar, S.; Roa, J.; Vazquez, M. J.; Vigo, E.; Casanueva, F. F.; Aguilar, E.; Pinilla, L.; Dieguez, C.; Tena-Sempere, M. Endocrinology 2005, 146, 3917-3925.

8. Dungan, H. M.; Clifton, D. K.; Steiner, R. A. Endocrinology 2006, 147, 1154-1158.

9. Shahab, M.; Mastronardi, C.; Seminara, S. B.; Crowley, W. F.; Ojeda, S. R.; Plant, T. M. Proc Natl Acad Sci U S A 2005, 102, 2129-2134.

10. Aparicio, S. A. Cell Metab 2005, 1, 293-296.

11. Ohtaki, T.; Shintani, Y.; Honda, S.; Matsumoto, H.; Hori, A.; Kanehashi, K.; Terao, Y.; Kumano, S.; Takatsu, Y.; Masuda, Y.; Ishibashi, Y.; Watanabe, T.; Asada, M.;

Yamada, T.; Suenaga, M.; Kitada, C.; Usuki, S.; Kurokawa, T.; Onda, H.; Nishimura, O.; Fujino, M. Nature 2001, 411, 613-617.

12. Kotani, M.; Detheux, M.; Vandenbogaerde, A.; Communi, D.; Vanderwinden, J. M.; Le Poul, E.; Brezillon, S.; Tyldesley, R.; Suarez-Huerta, N.; Vandeput, F.; Blanpain, C.; Schiffmann, S. N.; Vassart, G.; Parmentier, M. J Biol Chem 2001, 276, 34631-34636.

13. Muir, A. I.; Chamberlain, L.; Elshourbagy, N. A.; Michalovich, D.; Moore, D. J.; Calamari, A.; Szekeres, P. G.; Sarau, H. M.; Chambers, J. K.; Murdock, P.; Steplewski, K.; Shabon, U.; Miller, J. E.; Middleton, S. E.; Darker, J. G.; Larminie, C. G.; Wilson, S.; Bergsma, D. J.; Emson, P.; Faull, R.; Philpott, K. L.; Harrison, D. C. J Biol Chem 2001, 276, 28969-28975.

14. Lee, J. Y.; Moon, J. S.; Eu, Y. J.; Lee, C. W.; Yang, S. T.; Lee, S. K.; Jung, H. H.; Kim, H. H.; Rhim, H.; Seong, J. Y. Archives of biochemistry and biophysics 2009.

15. Dobson, C. M. Philosophical Transactions of the Royal Society B: Biological Sciences 2001, 356, 133-145.

16. Pedersen, J. S.; Dikov, D.; Flink, J. L.; Hjuler, H. A.; Christiansen, G.; Otzen, D. E. J Mol Biol 2006, 355, 501-523.

17. Pedersen, J. S.; Dikov, D.; Flink, J. L.; Otzen, D. E. Biophys J 2006, 90, 4181-4194.

18. Maji, S. K.; Perrin, M. H.; Sawaya, M. R.; Jessberger, S.; Vadodaria, K.; Rissman, R. A.; Singru, P. S.; Nilsson, K. P. R.; Simon, R.; Schubert, D.; Eisenberg, D.; Rivier, J.; Sawchenko, P.; Vale, W.; Riek, R. Science 2009, 325, 328-332.

19. Maji, S. K.; Schubert, D.; Rivier, C.; Lee, S.; Rivier, J. E.; Riek, R. PLoS Biol 2008, 6, e17.

20. Gerdes, H. H.; Rosa, P.; Phillips, E.; Baeuerle, P. A.; Frank, R.; Argos, P.; Huttner, W. B. Journal of Biological Chemistry 1989, 264, 12009-12015.

21. Chen, J. C. T.; Chesler, M. Proceedings of the National Academy of Sciences 1992, 89, 7786-7790.

22. Chiti, F.; Stefani, M.; Taddei, N.; Ramponi, G.; Dobson, C. M. Nature 2003, 424, 805-808.

23. Fernandez-Escamilla, A. M.; Rousseau, F.; Schymkowitz, J.; Serrano, L. Nat Biotechnol 2004, 22, 1302-1306.

24. Watson, D. J.; Lander, A. D.; Selkoe, D. J. J Biol Chem 1997, 272, 31617-31624.

25. Levine, H. I. Meth Enzymol 1999, 309, 274-284.

26. Raj, C. R.; Ramaraj, R. Photochem Photobiol 2001, 74, 752-759.

27. Ilanchelian, M.; Ramaraj, R. J Photochem Photobiol A 2004, 162, 129-137.

28. Harper, J. D.; Lansbury, P. T. J. Ann Rev Biochem 1997, 66, 385-407.

29. Ferrone, F. Meth Enzymol 1999, 309, 256-274.

30. Krittanai, C.; Johnson, W. C. Analytical biochemistry 1997, 253, 57-64.

31. Greenfield, N. J. Nature Protocols 2007, 1, 2876-2890.

32. MacPhee, C. E.; Dobson, C. M. J Am Chem Soc 2000, 122, 12707-12713.

33. Zandomeneghi, G.; Krebs, M. R. H.; McCammon, M. G.; Fandrich, M. Protein Science 2004, 13, 3314-3321.

34. Venyaminov, S. Y.; Kalnin, N. N. Biopolymers 1990, 30.

35. Lee, J. Y.; Moon, J. S.; Eu, Y.-J.; Lee, C. W.; Yang, S.-T.; Lee, S. K.; Jung, H. H.; Kim, H. H.; Rhim, H.; Seong, J. Y.; Kim, J. I. Arch Biochem Biophys 2009, 485, 109-114.

36. Andersen, K.; Westh, P.; Otzen, D. E. Langmuir 2008, 15, 399-407.

37. Guijarro, J. I.; Jackson, M.; Chaffotte, A. F.; Delepierre, M.; Mantsch, H. H.; Goldberg, M. E. Biochemistry 1995, 34, 2998-3008.

38. Shin, R.; Welch, D. R.; Nishra, V. K.; Nash, K. T.; Hurst, D. R.; Krishna, N. R. Clinical & Experimental Metastasis 200X.

39. Otzen, D. E.; Nesgaard, L.; Andersen, K. K.; Hansen, J. H.; Christiansen, G.; Doe, H.; Sehgal, P. Biochim Biophys Acta 2008, 1784, 400-414.

40. Yamamoto, S.; Kasegawa, K.; Yamaguchi, I.; Tsutsumi, S.; Kardos, J.; Goto, Y.; Gejyo, F.; Naiki, H. Biochemistry 2004, 43, 11075-11082.

41. Dombi, G. W.; Halsall, H. B. Biochem J 1985, 228, 551-556.

42. Pertinhez, T. A.; Bouchard, M.; Smith, R. A. G.; Dobson, C. M.; Smith, L. J. FEBS Lett 2002, 529, 193-197.

43. Moosavi-Movahedi, A. A.; Pirzadeh, P.; Hashemnia, S.; Ahmadian, S.; Hemmateenejad, B.; Amani, M.; Saboury, A. A.; Ahmad, F.; Shamsipur, M.; Hakimelahi, G. H.; F.Y., T.; Alijanvand, H. H.; Yousefi, R. Colloids Surf B Biointerfaces 2007, 60, 55-61.

44. Necula, M.; Chirita, C. N.; Kuret, J. J Biol Chem 2003, 278, 46674-36680.

45. Andersen, K. K.; Oliveira, C. L. P.; Larsen, K. L.; Poulsen, F. M.; Callisen, T. H.; Westh, P.; Pedersen, J. S.; Otzen, D. E. J Mol Biol 2009, 391, 207-226.

46. Jirgensons, B. J Biol Chem 1967, 242, 912-918.

47. Orsini, M. J.; Klein, M. A.; Beavers, M. P.; Connolly, P. J.; Middleton, S. A.; Mayo, K. H. J Med Chem 2007, 50, 462-471.

48. Gutierrez-Pascual, E.; Leprince, J.; Martinez-Fuentes, A. J.; Segalas-Milazzo, I.; Pineda, R.; Roa, J.; Duran-Prado, M.; Guilhaudis, L.; Desperrois, E.; Lebreton, A.; Pinilla, L.; Tonon, M. C.; Malagon, M. M.; Vaudry, H.; Tena-Sempere, M.; Castano, J. P. Mol Pharmacol 2009, 76, 58-67. Epub 2009 Apr 2023.

49. Johnson, J. L.; Cusack, B.; Davies, M. P.; Fauq, A.; Rosenberry, T. L. Biochemistry 2003, 42, 5438-5452.

50. Song, J. FEBS Lett 2009, 583, 953-959.

51. Gasteiger, E.; Hoogland, C.; Gattiker, A.; Duvaud, S.; Wilkins, M. R.; Appel, R. D.; Bairoch, A. The proteomics protocols handbook 2005, 571–607.

52. Piotto, M.; Saudek, V.; Sklenár, V. J Biomol NMR 1992, 2, 661-665.

53. Hwang, T. L.; Shaka, A. J. J Magn Reson 1995, 112, 275 - 279.

54. Griesinger, C.; Otting, G.; Wuethrich, K.; Ernst, R. J Am Chem Soc 1988, 110, 7870 - 7872.

55. Keller, R. wwwnmrch 2009.

56. Jerschow, A.; Muller, N. J Magn Reson 1997, 125 372-375.

57. Jerschow, A.; Müller, N. J Magn Reson 1998, 132, 13-18.

58. Wüthrich, K. NMR of Proteins and Nucleic Acids, Wiley, New York 1986.

59. Geen, H.; Freeman, R. J Magn Reson 1991, 93, 93 - 141.

Nielsen et al. Fig. 1

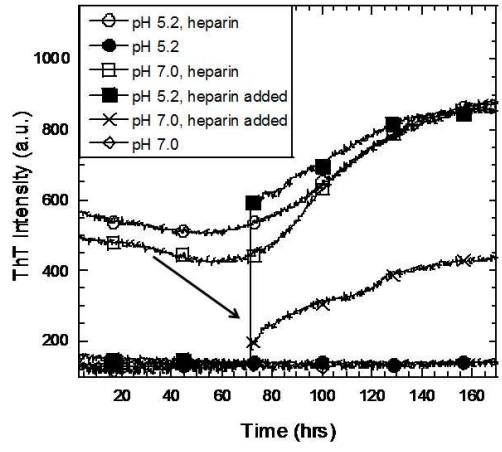

Figure 1
254x190mm (96 x 96 DPI)

Nielsen et al. Fig. 2

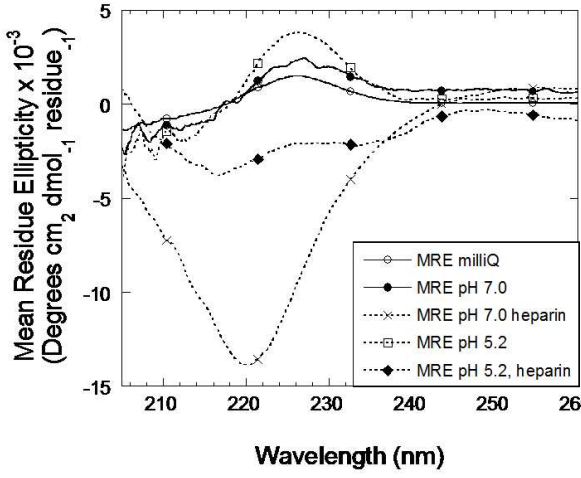

Figure 2
254x190mm (96 x 96 DPI)

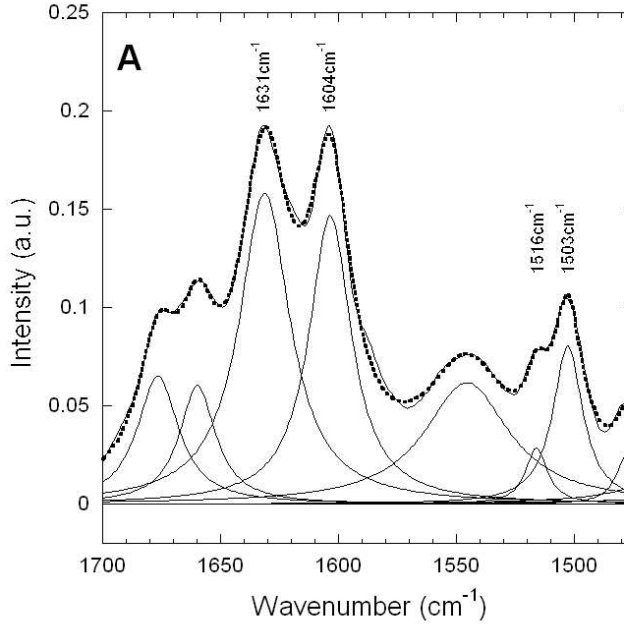

Figure 3A
285x285mm (72 x 72 DPI)

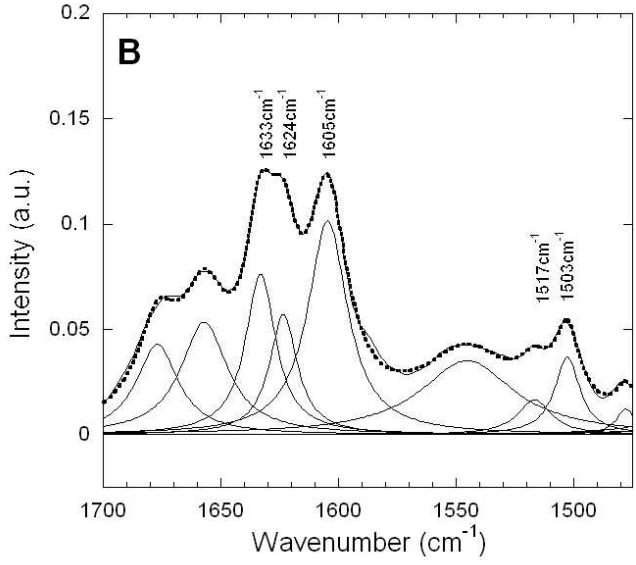

Figure 3B
285x255mm (72 x 72 DPI)

Nielsen et al. Fig. 4A

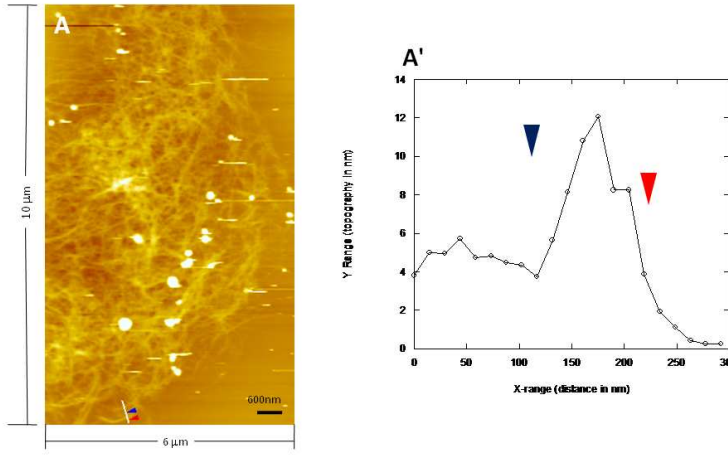

Figure 4A
254x190mm (96 x 96 DPI)

Nielsen et al. Fig. 4B

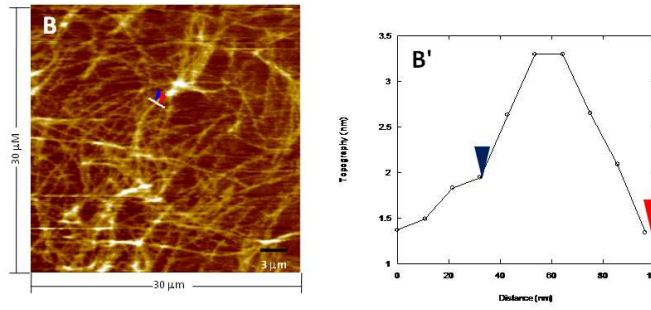

Figure 4B
254x190mm (96 x 96 DPI)

Nielsen et al. Fig. 5A

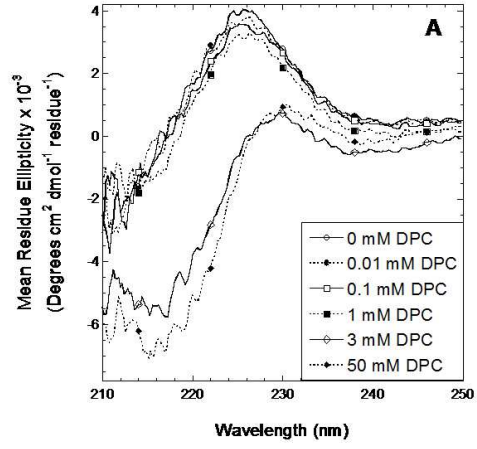

Figure 5A
254x190mm (96 x 96 DPI)

Nielsen et al. Fig. 5B

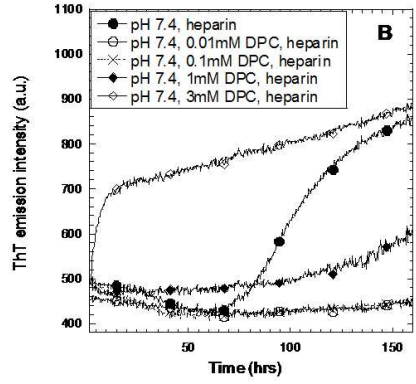

Figure 5B
254x190mm (96 x 96 DPI)

Nielsen et al. Fig. 5C

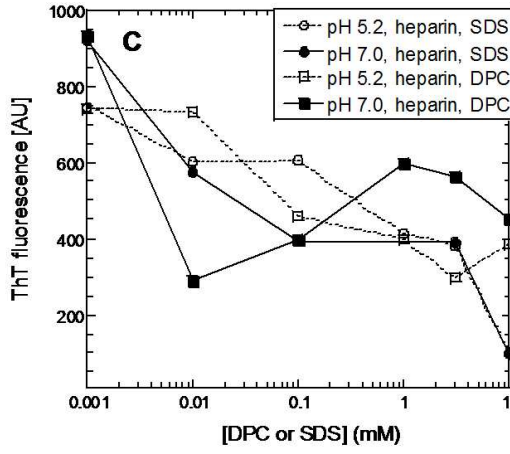

Figure 5C
254x190mm (96 x 96 DPI)

Nielsen et al. Fig. 6

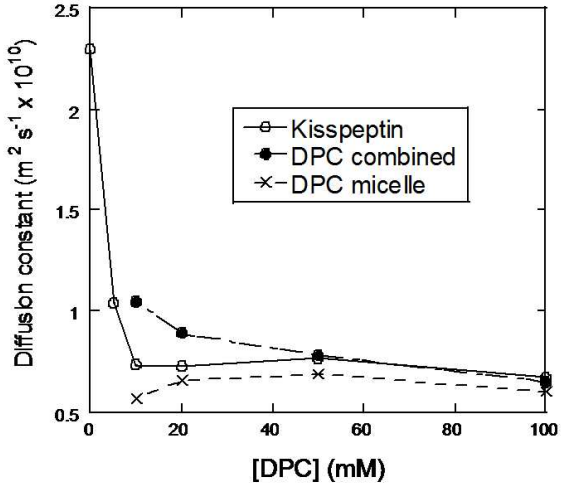

Figure 6
254x190mm (96 x 96 DPI)

Paper VI:

Modulation of cutinase stability and structure by phospholipid detergents

Pankaj Sehgal, Søren Bang Nielsen, Shona Pedersen, Reinhard Wimmer, Daniel E. Otzen
Published in Biochim Biophys Acta (2007) 1774, pages 1544-1554

Available online at www.sciencedirect.com
ScienceDirect
Biochimica et Biophysica Acta 1774 (2007) 1544–1554
Biochimica et Biophysica Acta
BBA
www.elsevier.com/locate/bbapap

Modulation of cutinase stability and structure by phospholipid detergents

Pankaj Sehgal [1,2], Søren Bang Nielsen [1], Shona Pedersen [3], Reinhard Wimmer, Daniel E. Otzen *

Center for Insoluble Protein Structures (inSPIN), Department of Life Sciences, Aalborg University, Sohngaardsholmsvej 49, DK-9000 Aalborg, Denmark

Received 26 April 2007; received in revised form 18 September 2007; accepted 19 September 2007
Available online 4 October 2007

Abstract

Fusarium solani pisi cutinase hydrolyses triglycerides of different lengths. Here we show that micelle-forming short-chain (C6–C9) phospholipids significantly reduce cutinase stability (both below and above the critical micelle concentration cmc) and rates of folding (only above cmc), trapping cutinase in an inactive state which only regains activity over hours to days, rather than the few seconds required for refolding in the absence of detergent. Destabilization decreases with increasing chain length, and increases with cmc, indicating that monomers and micelles cooperate in destabilizing cutinase. Detergents have little effect on enzymatic activity and confer no changes in secondary structure. Some changes in chemical shift occur around the enzyme active site, although distant regions are also affected. To our knowledge, this is the first example of marked destabilization of a water-soluble protein by zwitterionic detergents, highlighting the multitude of different detergent interactions with enzymes that target amphiphilic substrates and providing means of trapping a protein in a metastable state. We propose a model for destabilization where monomers via various binding sites on the native state prime it for interacting with micelles in a destabilizing fashion, whereas only micelles halt refolding due to the absence of these monomer-binding sites in the denatured state.

Keywords: Cutinase; Detergent; Phosphocholine; Stability; Activity

1. Introduction

Cutinases are small lipolytic enzymes capable of hydrolysing both soluble esters and water-insoluble lipids such as triglycerides. Unlike lipases, they show no interfacial activation in the presence of an organized amphiphilic environment such as detergent micelles or lipid membranes, and are therefore placed as intermediates between lipases and esterases [1–3]. Cutinase from *Fusarium solani pisi* (EC 3.1.1.74) is a oblate-formed one-domain 199-residue globular enzyme whose crystal structure at 1 Å resolution [4] reveals a central, five-stranded, parallel β-sheet surrounded by helices. The enzyme's active site is situated on the surface and consists of the catalytic triad Ser 120, His 188 and Asp 175. The placement of the active site serine on the surface of cutinase could explain the lack of interfacial activation [5]. The active site pocket is flanked by two loops. There is no consensus between various investigations [5–8] as to which residues are involved in these loops, however, all include at least residues 80–87 and residues 180–188.

Much work has focused on the interaction of cutinase with lipid substrates. Apart from numerous studies concerning the enzymatic activity of cutinase towards several substrates, more structurally minded investigations have appeared including a crystal structure of the protein inhibited by a substrate analogue [7], and investigations of the intramolecular dynamics of cutinase with and without a phosphonate inhibitor [8,9]. A recent study on the interaction of cutinase with a spin-labelled micellar monoglyceride (a non-covalently bound substrate) revealed that substrate binding altered the chemical shifts and intramolecular mobility of the loops surrounding the active site [10]. The study also identified hydrophobic residues in the loops in contact with the substrate's hydrophobic chain.

Detergents have been used in many studies to shed further light on the mechanisms involved in protein denaturation [11]

* Corresponding author. Present address: Center for Insoluble Protein Structures (inSPIN), Interdisciplinary Nanoscience Center, Department of Molecular Biology, Gustav Wieds Vej 10C, Aarhus University, DK-8000 Aarhus C, Denmark. Fax: +45 86 12 31 78.
E-mail address: dao@inano.dk (D.E. Otzen).
[1] These two authors contributed equally to this work.
[2] Present address: Department of Chemistry, Graduate School of Science, Osaka City University, 3-3-138 Sugimoto Cho, Sumiyoshi-ku, Osaka 558-8585, Japan.
[3] Present address: Department of Clinical Biochemistry, Aalborg University Hospital, DK-9100 Aalborg, Denmark.

1570-9639/$ - see front matter © 2007 Elsevier B.V. All rights reserved.
doi:10.1016/j.bbapap.2007.09.011

and as water-soluble lipid mimetics. They occupy a special position in lipase research due to their combination of interfacial activity and substrate similarity. We have previously shown that non-ionic and zwitterionic detergents can strongly activate the lipase from *Thermomyces lanuginosus* [12] below the cmc, indicating that detergent monomers can bind strongly to lipase, presumably in the vicinity of the active site. However, activation does not destabilize lipases: non-ionic and zwitterionic detergents (monomers or micelles) had no effect on the thermal stability of the protein, unlike the anionic SDS which both activated and destabilized the protein, both as monomer and micelle. The destabilizing effect of anionic detergents is coupled to the negative charge which, particularly in the micellar state, rips protein structures apart due to strong repulsive electrostatic forces. Thus, SDS has been shown to lead to both rapid partial unfolding and slow irreversible inactivation of cutinase [13], while taurodeoxycholate reduces cutinase's melting temperature but makes thermal unfolding reversible [14] and AOT (bis(2-ethylhexyl) sodium sulfosuccinate) denatures cutinase in a titratable manner [15]. Electrostatic repulsion is lacking in non-ionic and zwitterionic detergent micelles, although they are useful for shielding hydrophobic patches on the protein surface against aggregation. This is exemplified by the ability of non-ionic detergent micelles to partially suppress thermally induced cutinase aggregation [16] as well as aggregation-inhibition by zwitterionics such as zwittergent 3–12 [17] and CHAPS [18]. There is no precedence for the destabilization of water-soluble proteins by zwitterionics, although dimethyldodecyl-ammonio-propane sulfonate (DPS) is destabilizing towards the β-barrel membrane protein AIDA [19]. In the present study, we report that zwitterionic phospholipids detergents have a very unexpected influence on cutinase below and above cmc, which is the reverse of their affect on lipase: they destabilize it considerably without affecting activity. Furthermore, destabilization occurs to a greater extent with short-chain phospholipids, and shows an excellent correlation with cmc. This suggests that the monomeric state is involved in destabilization. When cutinase refolds from the pH-denatured state in the presence of zwitterionic detergent, activity is only regained partially and at a very slow rate, although the native state is not unfolded by detergent under these conditions. This indicates that detergents can trap cutinase in a non-native state. However, trapping of cutinase occurs above the cmc, indicating that micelles are the only active species inhibiting refolding. We interpret our results to mean that monomers via various binding sites on the native state of cutinase prime the protein for interacting with micelles in a destabilizing fashion, whereas only micelles halt refolding due to the absence of these monomer-binding sites in the denatured state. The sensitivity of cutinase to zwitterionic detergents reveals that different classes of lipolytic enzymes may respond to amphiphilic environments in a variety of ways.

2. Materials and methods

2.1. Materials

1,2-dihexanoyl-*sn*-glycero-3-phosphocholine (C_6PC), 1,2-diheptanoyl-*sn*-glycero-3-phosphocholine (C_7PC), 1,2-dioctanoyl-*sn*-glycero-3-phosphocholine (C_8PC), 1,2-dinonoyl-*sn*-glycero-3-phosphocholine (C_9PC), 1,2-dioleoyl-*sn*-glycero-3-phosphocholine (DOPC), dodecylphosphocholine (DPC) were from Avanti Polar Lipids (Alabaster, AL); n-dodecyl-β-D-maltoside (DM) was from Calbiochem, Canada; dimethyl-dodecylammoniopropanesulfonate (DPS) was from Fluka, and lauroyltrimethylammonium chloride (LTAC) was from Lancaster, England. The purity of all chemicals was >99%.

2.2. Protein production

Cutinase from *Fusarium solani pisi* (SwissProt entry P00590) was cloned and expressed in *Escherichia coli* WK-6 strain, a kind gift from Corvas International N.V. (Gent, Belgium). This variant of the enzyme contains a 15-residue propeptide which remains after cleavage of the PhoA signal sequence [20], so that the enzyme under investigation consists of 214 amino acids. The recombinant enzyme was produced and purified to >95% purity as described [21], dialyzed extensively against water and lyophilized. Production and purification of ^{15}N-labelled cutinase from the expression vector pFCEX1 in *E. coli* BL21(DE3) were carried out as described [22], using minimal medium (M9) with ^{15}N ammonium sulphate (99%, Spectra Stable Isotopes).

2.3. Stopped-flow experiments

These were performed on an Applied Photophysics (Leatherhead, UK) SX18MV stopped-flow apparatus. The protein solution and the detergent solutions were mixed in a 1:10 ratio to give a final protein concentration of 2 μM and the desired detergent concentrations. Refolding was initiated from the pH-denatured state (pH 1.5 in HCl) and cutinase refolded by mixing 1:10 with detergent at pH 4.5 (the final pH was within 0.1 pH unit of 4.5). Time courses were fitted to a double-exponential decay as described, in which the rate constant of the major rapid relaxation phase represents the dominant folding process [28].

2.4. Activity measurements

These were carried out at pH 8.0 in 20 mM Tris pH 8.0 at 20 °C in the presence of different concentrations of C_7PC, using *p*-nitrophenol butyrate as substrate [16]. Since the *p*-nitrophenolate ion titrates with a pK_a of 6.7, the low extinction coefficient of the protonated *p*-nitrophenol ion made it unfeasible to measure activity at pH 4.5. Cutinase was handled as described in the text prior to the activity measurement.

2.5. Thermal denaturation of cutinase

Thermal scans of 4 μM protein were performed in 10 mm quartz cuvettes on an Eclipse fluorimeter (Cary-Varian) with a scan rate of 90 °C/hr between 15 and 75 °C using excitation and emission wavelengths of 295 nm and 350 nm, respectively, 1 second acquisition times and 10 nm slits widths. All thermal scans were made in 25 mM sodium acetate pH 4.5 unless otherwise indicated. For scans at other pH-values, the following buffers were used: 25 mM sodium acetate pH 6, 25 mM Tris pH 7.5 and 25 mM Tris pH 9. Raw fluorescence data were fitted in KaleidaGraph 4.0 (Synergy Software, Reading PA) to the following equation [23]:

$$\theta = \frac{\alpha_N + \beta_N T + (\alpha_D + \beta_D T) * e^{-\left(\Delta H_{Tm}\left(1-\frac{T}{T_m}\right)\right)/RT}}{1 + e^{-\left(\Delta H_{Tm}\left(1-\frac{T}{T_m}\right)\right)/RT}} \quad (1)$$

where θ is the measured fluorescence intensity, α_N and α_D are the fluorescence intensity-values for the folded and denatured states, respectively, at 298 K, β_N and β_D are the slopes of the baselines of the native and denatured states, respectively, and ΔH_{Tm} is the enthalpy of unfolding at the midpoint of denaturation, T_m. Note that this equation is formally only applicable to a reversible two-state unfolding process and not to an irreversible process. However, in practice the unfolding scans fit very satisfactorily to Eq. (1). In any case, the T_m-values are used for comparative purposes. T_m-values (Kelvin) are subsequently converted to t_m-values (°C). Fluorescence scans yielded the same melting temperatures as CD (cfr. [16]), required less material and could be recorded for 4 solutions in parallel.

2.6. CD spectroscopy

Scans were recorded on a Jasco J-810 spectropolarimeter (Jasco spectroscopic Co. Ltd., Hachioji City, Japan). For far-UV scans we used 5 μM protein in a 1-mm quartz cuvette, while near-UV scans required 50 μM protein in a 10-mm cuvette. In both cases, spectra were recorded at a band width of 2 nm, using steps of 0.2 nm and a scan speed of 50 nm/ min. Five accumulations were averaged to yield a final spectrum. Buffer spectra were subtracted.

2.7. Pyrene experiments

A saturated solution of pyrene in buffer (ca. 1 μM) was prepared by shaking pyrene powder with buffer on a shaking table for at least 15 min, followed by centrifugation to discard the pellet. This solution was then diluted 1:1 into buffer containing different concentrations of C_7PC with or without 2 μM cutinase. The solution was excited at 335 nm, and fluorescence emission spectra (350–420 nm) were recorded at 25 °C on a PerkinElmer LS55 spectrometer (PerkinElmer A/S, Hvidovre, Denmark) using 10 nm excitation and emission slit widths. The ratio of the intensities of the third (I_3 at 372.5 nm) and first (I_1 at 382.5 nm) emission bands, I_3/I_1, was used as a measure of the polarity of the probe's environment [24].

2.8. Cmc measurements

These were determined at 25 °C in 25 mM sodium acetate pH 4.5 using the dye NPN as described [12]. There was no significant deviation from available literature values (data not shown).

2.9. NMR measurements

All NMR measurements were carried out using a Bruker DRX600 NMR spectrometer with a triple-axis gradient TXI (H/C/N) probe at 298 K. Data were processed using XwinNMR3.6 and analysed with the NEASY [25] tool of CARA [26]. [^{15}N–^{1}H]-HSQC spectra [27] were recorded with a resolution of 1.9 Hz/Pt in the direct (^{1}H) and 9.5 Hz/Pt in the indirect (^{15}N) dimension. Freeze-dried cutinase was dissolved to a final concentration of 0.7 mM in 20 mM phosphate buffer pH 7.0 containing 5% D_2O. Small aliquots of a 882 mM solution of C_6PC in H_2O were added to the cutinase solution to yield concentrations of 4.4 mM and 30.8 mM C_6PC. HSQC spectra were recorded at each concentration. After a week at room temperature, the NMR sample of cutinase at 30.8 mM C_6PC showed signs of degradation and was not used any further. Chemical shift changes in HSQC spectra were quantified by calculation of an absolute change in chemical shift as:

$$\Delta_{HSQC} = \sqrt{\Delta\nu_H^2 + 3*\Delta\nu_N^2} \quad (2)$$

where $\Delta\nu_H$ is the chemical shift change of H^N atoms expressed in Hz, and $\Delta\nu_H$ is the chemical shift change of N atoms expressed in Hz.

3. Results

3.1. Refolding of cutinase is markedly slowed down in the presence of phospholipids detergents

Our initial motivation for working with cutinase and phospholipids was to investigate whether amphiphilic substances could modulate the enzyme's folding pathway and allow partially folded states to accumulate *en route* to the native state. Short chain phospholipids represent one such class of amphiphiles. Despite their similarity to the natural substrates of cutinase (triglycerides), cutinase is not known to hydrolyse phospholipids, and we have not been able to demonstrate any activity using either a pH-indicator-based plate assay or direct monitoring by NMR (E.M. Petersen and R.W., unpublished results). In the absence of detergents, cutinase has been shown to transiently accumulate an off-pathway folding intermediate when folding at low denaturant concentrations at pH 4.5 [28,29]. We initiated folding of cutinase from the pH-denatured state (pH 1.5) by rapid transfer to a pH 4.5 buffer using a stopped-flow apparatus, following the reaction by changes in Trp fluorescence [28,29] to obtain the refolding rate constant k_f:. When we followed the folding kinetics of cutinase under conditions where we include different amounts of diacyl phospholipids of chain length 6–8 or the phospholipid analogue dodecyl phosphocholine in the pH 4.5 buffer, k_f: was found to vary in a characteristic manner: at concentrations up to 50% of the detergent's critical micelle concentration, folding kinetics are not affected, but close to the cmc, k_f plunges dramatically to very low values, following a linear relationship in a log–log plot (Fig. 1A). The marked decline in refolding kinetics with increasing concentration of detergent is reminiscent of the effect of denaturants [30], with the important difference that the log of the microscopic rate constants show a dependence on (non-logarithmic) denaturant concentration.

Cutinase folding is influenced by the nature of the denatured state and occurs faster from the GdmCl-denatured state than from the pH-denatured state, possibly due to transient oligomeric interactions in the deadtime of folding [29]; however, irrespective of the denatured state (pH 1.5, 2.2 M GdmCl or 6.6 M GdmCl), we observe the same general behaviour and an abrupt drop in k_f around the same detergent concentration (Fig. 1A). The inflection point (the detergent concentration at which the drop occurs) can be estimated by determining the intersection of the two linear sections of the plot. There is a clear correspondence between the inflection point and the cmc (Fig. 1B), yielding a slope of 0.98± 0.14 and an intercept of −0.12±0.09. Thus the inflection point corresponds to the cmc and the onset of micellar structure. There is a slight shift in the inflection point towards higher detergent concentrations in the presence of increasing concentrations of GdmCl, but this is probably related to the competition between GdmCl and detergent for binding to cutinase.

The precipitous decline in the refolding rate at increasing detergent concentrations suggested that the detergent micelles might trap cutinase in specific non-native conformations. To clarify this, we measured the hydrolytic activity of cutinase towards *p*-nitrophenolbutyrate in the presence of different detergents. The actual activity assays had to be done at pH 8.0 rather than at pH 4.5 because of the low absorption of the nitrophenol group (pK_a 6.7) at pH 4.5. When cutinase in the native state (either at pH 4.5 or 8.0) is mixed with detergent at the concentrations corresponding to those in Fig. 1A and then transferred to pH 8.0 to measure activity, the detergent does not significantly affect activity for either C_6PC, C_7PC or C_9PC (Fig. 2A and B). However, if cutinase is first denatured at pH 1.5 (in the absence of detergent) and subsequently refolded by transferring it to pH 4.5 in the presence of detergent, there is a marked inhibition of activity at pH 8.0 and this is only partially (30% at 10 mM C_7PC) recovered over a period of a day (Fig. 2A). The inhibitory effect sets in a little below cmc and is consolidated around 2× cmc. This suggests that detergent monomers and micelles, at concentrations where they do not denature the native state, trap cutinase in an inactive state which folds

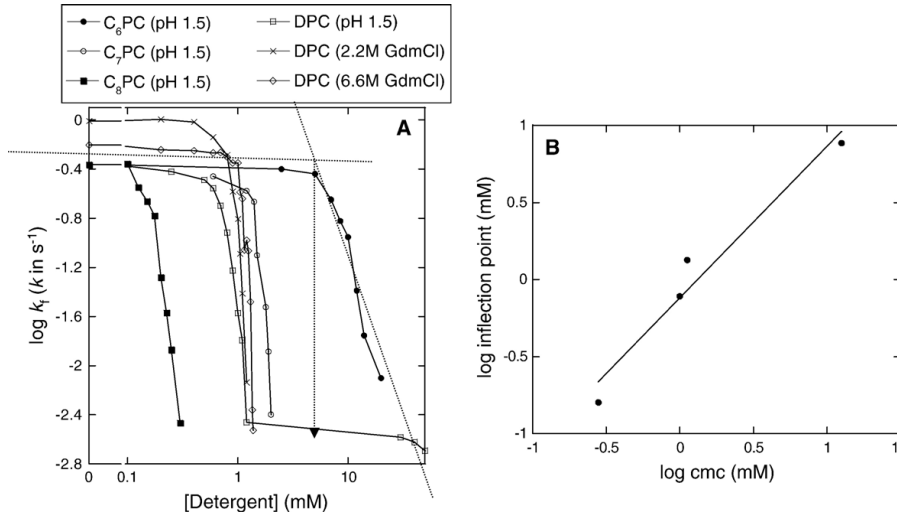

Fig. 1. (A) Cutinase refolding rates at pH 4.5 from different denatured states (indicated in brackets in the graph) into phospholipid detergents of different chain lengths. The estimation of the inflection point for C_6PC is demonstrated. (B) Log inflection point versus log cmc shows a strong linear correlation with a slope of 0.98±0.14 and an intercept of −0.12±0.09.

extremely slowly (hours to days) to the native state. For comparison, the half-life of refolding is never more than ca. 350 s in the presence of urea or GdmCl [29].

We investigated the structure of the activity-reduced state by near- and far-UV CD (Fig. 2C and D). As expected, the pH-denatured state regains a completely native-like near- and far-UV CD spectrum when refolded at pH 4.5; if C_7PC is included in the refolding buffer, the near-UV CD spectrum is also unchanged, but there are minor changes in the far-UV CD spectrum, suggesting a subtle rearrangement.

3.2. Cutinase shows marked decrease in thermal stability in the presence of phospholipids

The investigations in the previous section revealed that phospholipid detergents act as kinetic destabilizers during cutinase refolding, although they do not denature the protein once it is in the native state. To investigate whether these detergents affect the stability of the native state (without denaturing it significantly), we used fluorescence spectroscopy to follow thermal denaturation of cutinase in the presence of different concentrations of DPC. Cutinase undergoes a marked increase in fluorescence upon denaturation (Fig. 3A, insert) which counterbalances the general decline in fluorescence intensity with increasing temperature [16], allowing a reliable determination of the melting temperature t_m (Fig. 3A). Increasing concentrations of DPC lead to a marked decrease in t_m, although the denaturation process remains cooperative and t_m remains sufficiently high to provide an acceptable native-state baseline before denaturation sets in. Between 0 and 2 mM DPC, we observe a steep 16 °C drop in t_m before it stabilizes around 20 °C below the original t_m (Fig. 3B). We do not observe this sensitivity to zwitterionic detergents for other proteins; the thermostability of the water-soluble protein S6, which is destabilized by the ionic detergents SDS and LTAC [11,31], is not affected by DPC, just as the stability of the lipase from *T. lanuginosus* is completely unaffected by short-chain phospholipids [12]. In contrast to refolding kinetics where little retardation occurred below cmc, thermal destabilization sets in well below cmc, suggesting that monomeric species are involved in denaturation, although micelles also may play a role in view of the continued decline above cmc. In order to ascertain whether detergent monomers formed aggregated structures on the cutinase surface, we monitored pyrene fluorescence in the presence of increasing concentrations of detergent with and without cutinase. The ratio of the two emission bands I_3/I_1 is sensitive to environmental polarity and changes significantly when pyrene is transferred from water to a micellar environment [24]. However, cutinase did not affect the way in which pyrene fluorescence was affected by detergent concentration (data not shown), suggesting that the detergent monomers did not form large clustered aggregates on the surface.

We next measured the thermal stability of cutinase in phospholipid detergents of chain length 6–9. In all cases, the decline in t_m starts well below cmc, and the plateau is typically reached at 2–3× cmc (Fig. 4A–D). Nevertheless, the protein remains natively folded throughout, since it unfolds cooperatively, retains enzymatic activity and remains resistant to degradation by as much as 0.1 mg/ml trypsin over 30 min at 37 °C (data not shown). To quantify these destabilization effects, we have fitted the data to a simple empirical model, in which binding of a single detergent species (Det) to cutinase (C) (melting temperature t_m^C, equal to 52.71 °C) leads to a complex with a reduced t_m value ($t_m^{C:Det_2}$). Thus, we only operate with two states of the protein, namely a free and a detergent-bound state,

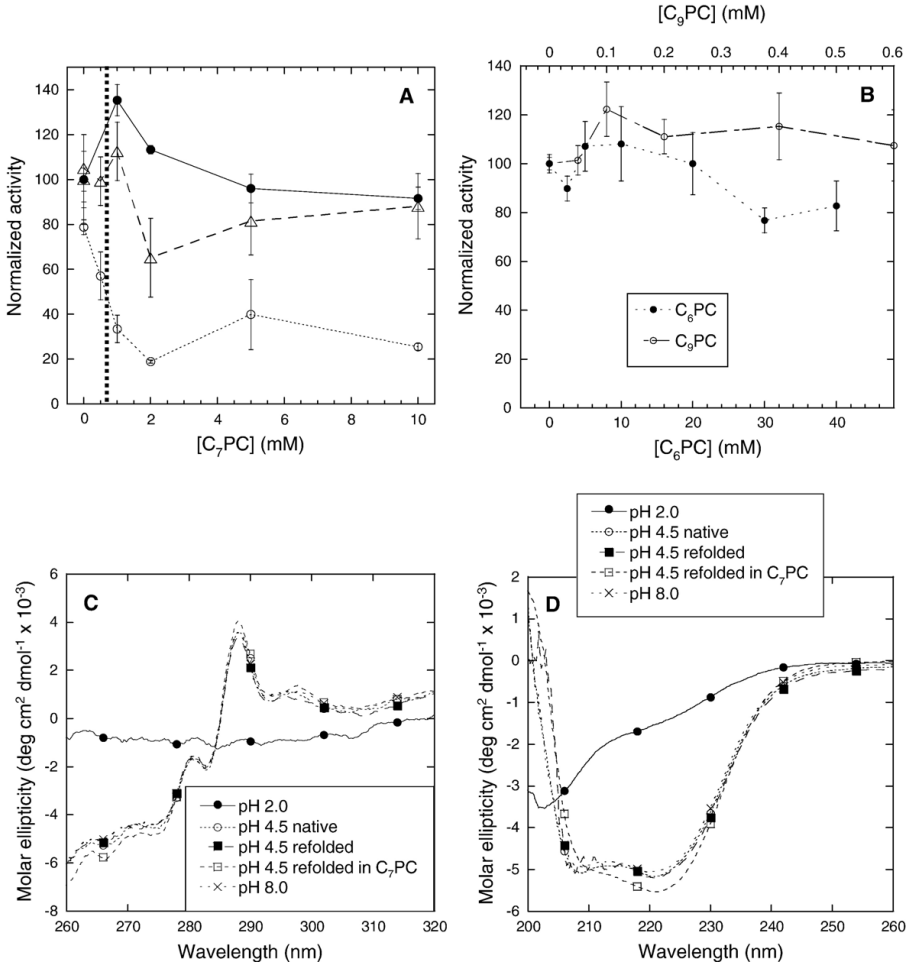

Fig. 2. (A) Activity of cutinase at pH 8.0 as a function of C_7PC concentration under different conditions. (●) Cutinase refolded by transfer from pH 1.5 to pH 8.0, incubated at pH 8.0 for 15 min, and detergent added. (△) Cutinase refolded by transfer from pH 1.5 to pH 4.5, then C_7PC added after 15 min and the solution incubated for 1 day. For activity assays, the protein was transferred to pH 8.0 while retaining the same detergent concentration and the activity was measured straight away. (○) Cutinase refolded by transfer from pH 1.5 to pH 4.5 in the presence of C_7PC and incubated for 1 day. All activities normalized to activity at 0 mM C_7PC. These are respectively 172, 162 and 162 μM hydrolyzed substrate per minute per μM cutinase for the 3 different series of data (the activity in 0 mM C_7PC for Δ and ○ data are based on the same sample). (B) Activity of cutinase at pH 8.0 in the presence of C_6PC and C_9PC. (C) Near- and (D) far-UV CD spectra of cutinase in the pH-denatured state (pH 1.5), the native state at pH 4.5 and 8.0 (not previously unfolded) and refolded from pH 1.5 to pH 4.5 in the absence and presence of 2 mM C_7PC.

ignoring for simplicity the existence of both detergent monomers and micelles. We let two detergent molecules bind to each cutinase molecule to reflect the visibly cooperative decline in T_m:

$$C + 2\mathrm{Det} \overset{K_{\mathrm{Det}}}{\longleftrightarrow} \mathrm{C:Det_2}$$

where

$$K_{\mathrm{Det}} = [C][\mathrm{Det}]^2/[\mathrm{C:Det_2}].$$

This leads to the following equation describing the decline in t_m:

$$t_m^{\mathrm{obs}} = \frac{K_{\mathrm{Det}} t_m^{C} + t_m^{\mathrm{C:Det_2}}[\mathrm{Det}]^2}{K_{\mathrm{Det}} + [\mathrm{Det}]^2} \quad (3)$$

This model fits the data satisfactorily for most of the detergents (except for C_8PC, where a straightforward binding equation based on a simple binding equilibrium between one molecule each of cutinase and detergent is sufficient to fit the data satisfactorily), but we emphasize that the model does not

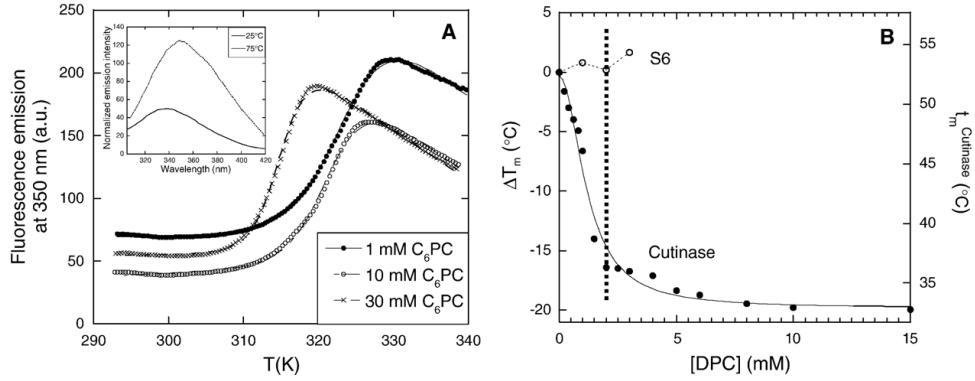

Fig. 3. (A) Thermal denaturation of cutinase at pH 4.5 in different concentrations of DPC. The data are fitted to Eq. (1) to obtain the melting temperature t_m. Spectra of native (25 °C) and thermally denatured (75 °C) cutinase are shown in the insert. (B) t_m for cutinase and S6 versus [DPC]. Cutinase data are fitted to Eq. (3).

necessarily reflect the molecular details of binding. Nevertheless, it allows us to obtain reliable estimates of the two key parameters, namely the efficiency of detergent binding (K_{Det}) and the degree of destabilization ($t_m^{C:Det_2}$) for strictly comparative purposes. We use $\sqrt{K_{Det}}$ (except for C_8PC, where the dissociation constant derived from the simple binding equation

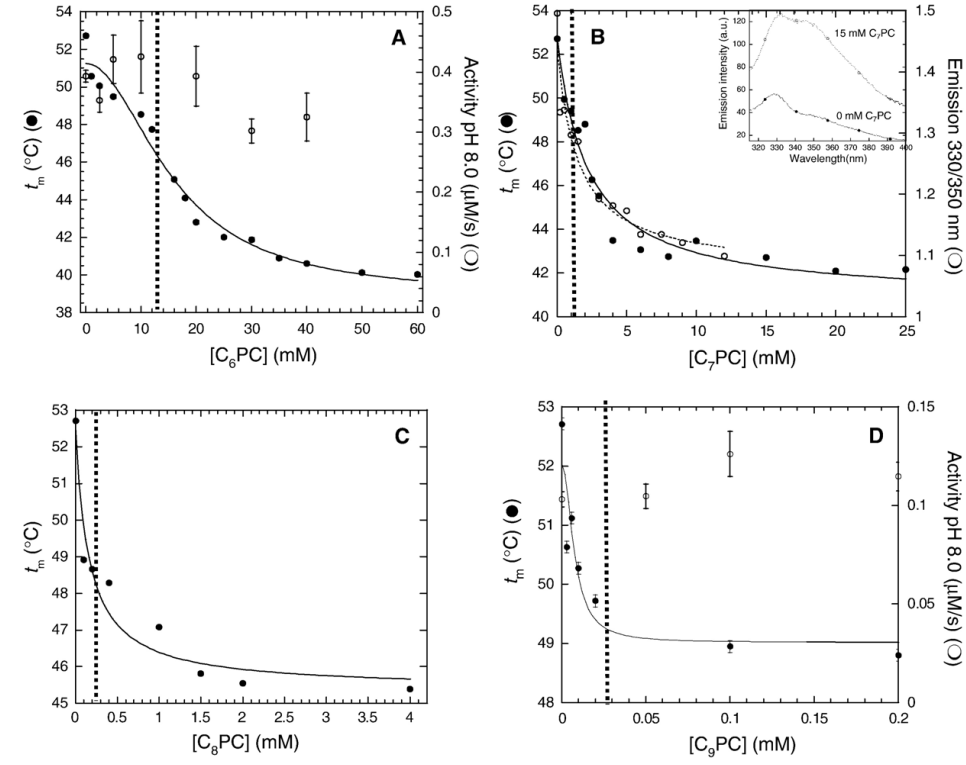

Fig. 4. Changes in t_m for cutinase at pH 4.5 in the presence of phospholipids of chain length 6–9. In addition, effect of C_6PC and C_9PC on activity as well as the effect of C_7PC on cutinase fluorescence are displayed for ease of comparison. All data are fitted to Eq. (3) except for C_8PC which is fitted to a simple binding curve without cooperativity. Insert for C_7PC shows the change in the fluorescence spectrum of cutinase in 0 versus 15 mM C_7PC.

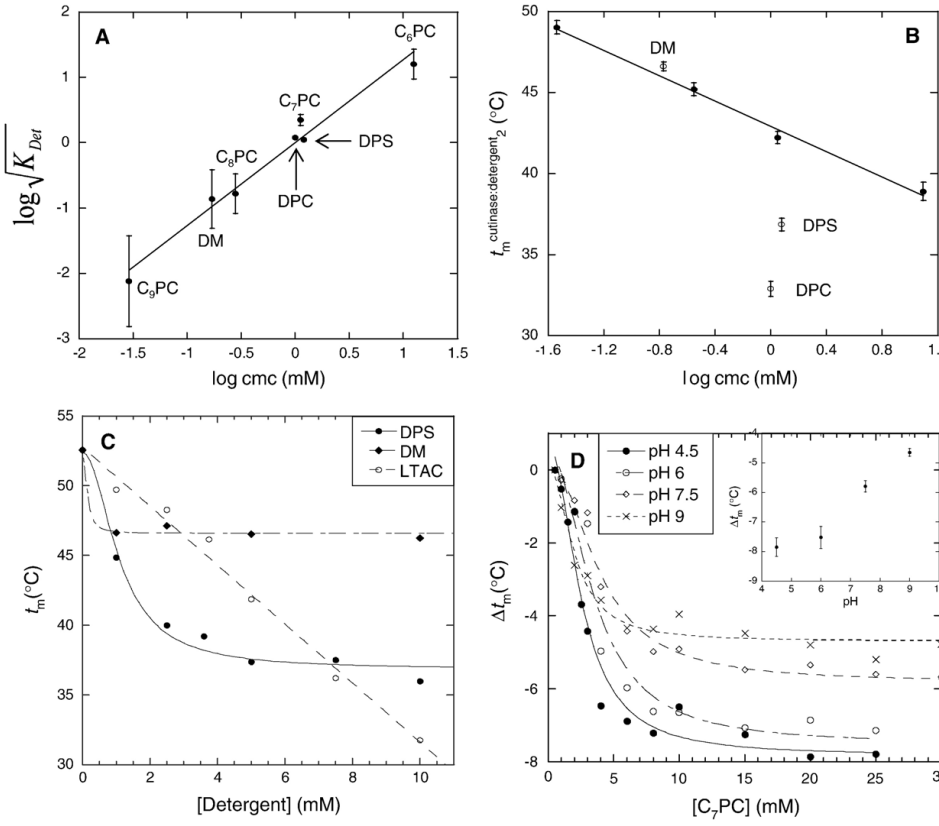

Fig. 5. (A) log $\sqrt{K_{Det}}$ (Eq. (3)) versus log cmc for phospholipids and other detergents (except for C_8PC for which the direct dissociation constant is used). (B) $t_m^{C:Det_2}$, the melting temperature of the cutinase:detergent complex, versus log cmc. The line show the best linear fit to the data for phospholipids of chain length 6–9. DPS and DPC lie well off the line, in contrast to DM. (C) t_m for cutinase in the presence of the non-ionic detergent DM, the zwitterionic detergent DPS and the cationic detergent LTAC. Data for DM and DPS fitted to Eq. (3), data for LTAC fitted to a straight line. (D) Δt_m for cutinase at pH 4.5–9 at different C_7PC concentrations. Data fitted to Eq. (3). Insert: $t_m^{C:Det_2}$ versus pH.

can be used directly) as this corresponds to the detergent concentration where t_m is half way to $t_m^{C:Det_2}$. $\sqrt{K_{Det}}$ is essentially equal to cmc; a log–log plot of $\sqrt{K_{Det}}$ versus cmc gives a slope of 1.23±0.20 and an intercept of 0.12±0.18 (Fig. 5A). Moreover, $t_m^{C:Det_2}$ declines linearly with the log of cmc (Fig. 5B), leading to an intercept of 42.9±0.2 °C (at 1 mM detergent) and a slope of −3.9±0.2 °C/log unit concentration. Extrapolation suggests that a $t_m^{C:Det_2}$ of 25 °C can only be achieved using a detergent with a cmc around 42 M, an unrealistically high cmc that is only (theoretically) achieved by a phospholipid of chain length 2. Thus, all micelle-forming phospholipids only have a destabilizing rather than denaturing effect on cutinase. Furthermore, a $t_m^{C:Det_2}$ of 53 °C (the t_m of cutinase in the absence of detergent) would by the same linear correlation be obtained for a detergent with a cmc of 2.6 μM, corresponding to C_{10}PC. However, it would be illogical to expect the linear extrapolation to be maintained to indefinitely low cmc values, otherwise long-chain vesicles would be highly stabilizing; thus, C_{14}PC (with a monomer concentration of 6 nM in equilibrium with vesicles) could be expected to lead to a $t_m^{C:Det_2}$ of 73.4 °C. In fact, vesicle-forming lipids such as DLPC, DMPC and DOPC (with sub-nM monomer concentrations) have no effect on the cutinase thermal melting profile in the concentration range 1–8 mg/ml (data not shown).

3.3. Other zwitterionic and non-ionic detergents also destabilize cutinase

The zwitterionic detergent dimethyldodecylammoniopropane sulfonate (DPS) has the same type of destabilizing effect on cutinase as short-chain phospholipids, as does the non-ionic detergent dodecyl maltoside (DM) (Fig. 5C). The values of $\sqrt{K_{Det}}$ for DM, DPS and DPC correlate very nicely with their cmc values (Fig. 5A), but the $t_m^{C:Det_2}$ values for DPS and DPC fall well off the $t_m^{C:Det_2}$-log cmc line established for the phospholipids (Fig. 5B). This indicates that although the monomer–micelle transition is central in destabilization regardless of detergent, the degree of destabilization is modulated by the chemical nature

of the headgroup. The importance of the head group is emphasized even more by the behaviour of cutinase in the presence of the cationic detergent lauroyl trimethylammonium chloride (LTAC). There is a linear decline in t_m with [LTAC] (Fig. 5C), which does not level off at a plateau level; above 10 mM LTAC, cutinase is unfolded already at room temperature and no cooperative unfolding transition is seen (data not shown). The linear relationship between $t_m^{C:Det_2}$ and log cmc in Fig. 5B would for LTAC (cmc-value in buffer 7–8 mM [12]) predict a $t_m^{C:Det_2}$-value of ca. 39 °C, but the actual $t_m^{C:Det_2}$ is obviously much lower. Similar strongly destabilizing effects are seen for SDS where no cooperative transition is observed as low as 1 mM SDS, which is only half of SDS' cmc value in buffer [12].

Due to the zwitterionic nature of phosphocholines, we would not *a priori* expect a strong electrostatic factor in the destabilization of cutinase. In fact, C_7PC maintains similar destabilizing tendencies over the pH range 4.5–9, although the effect becomes somewhat attenuated at higher pH values (Fig. 5D).

3.4. Phospholipid detergents lead to local but not global changes in cutinase structure

As mentioned previously, activity of native cutinase is not significantly affected at any concentration for the two phospholipids C_6PC and C_9PC (Figs. 2 and 3). In contrast, the change in fluorescence (measured by the ratio of the emission at 330 and 350 nm) follows the change in t_m closely, indicating that the destabilization is caused by the accumulation of a state where the Trp environment (Fig. 4B), but not the activity, is affected. In addition, there is no change in the secondary structure or aromatic environment of cutinase under these conditions as indicated by near- or far-UV CD spectra in the presence of C_6PC (data not shown) or C_7PC (Fig. 2C and D).

To probe the structural changes wrought by C_6PC in more detail, we analyzed cutinase by NMR at a concentration where the stability is only slightly affected (4.4 mM C_6PC) and at a concentration where t_m has declined by almost 10 °C (30.8 mM C_6PC, well above the cmc of 12 mM). Only insignificant changes in chemical shifts were seen at 4.4 mM C_6PC. Slightly more pronounced shift changes were observed at 30.8 mM C_6PC, but only a small subset of signals changed position upon titration with C_6PC. Therefore we concluded that the overall structure of cutinase was not altered upon titration with C_6PC. Significant changes in chemical shifts were almost exclusively confined to the region surrounding the active site. In particular, residues 170–174 and residues 180–186, located in one of the two flexible loops, showed strong changes. Also residues 80, 82 and 83, located in the onset of the other loop, experienced

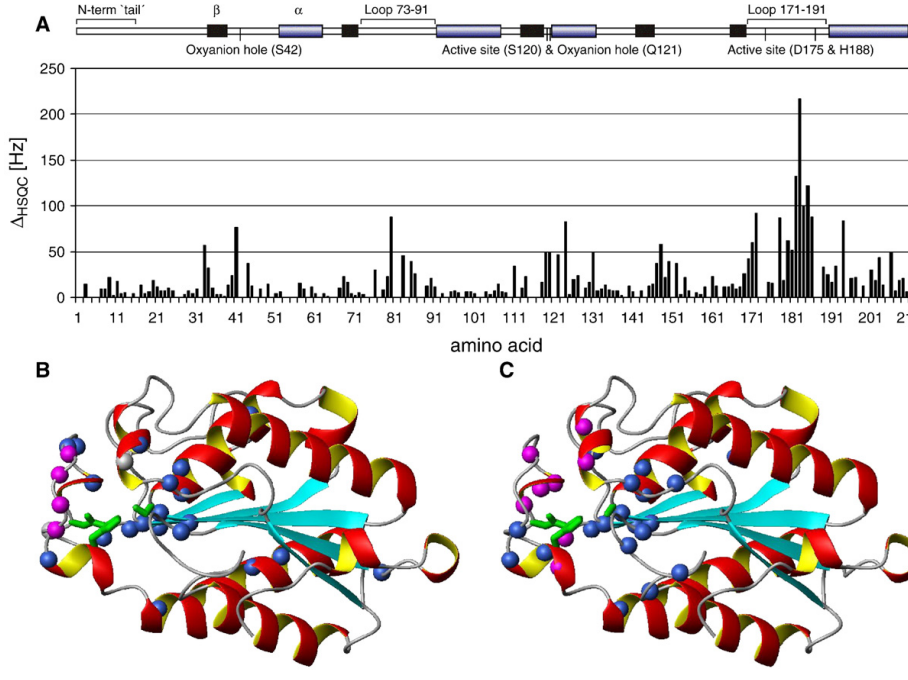

Fig. 6. Δ_{HSQC} as defined in Eq. (2) for cutinase at pH 4.5 upon addition of 30.8 mM C_6PC. (A) Δ_{HSQC} plotted against the sequence of cutinase. The bar on top indicates secondary structure elements and residues of interest. (B) Δ_{HSQC} upon interaction with C_6PC mapped onto the 3D-structure of cutinase (PDB file 1CEX): magenta spheres denote N-atoms of residues, whose $\Delta_{HSQC} > 100$ Hz, blue spheres: 100 Hz $\geq \Delta_{HSQC} > 40$ Hz, grey: signals appearing upon addition of C_6PC. The catalytic triad is shown in green. The figure is prepared with MOLMOL [34]. (C) Δ_{HSQC} upon interaction with 16-DOXYL-stearoylglycerol mapped onto the 3D-structure of cutinase (data from [10]): magenta spheres denote N-atoms of residues, whose $\Delta_{HSQC} > 60$ Hz, blue spheres: 60 Hz $\geq \Delta_{HSQC} > 30$ Hz. The active site is shown in green, however, the S120A mutant was used for this work.

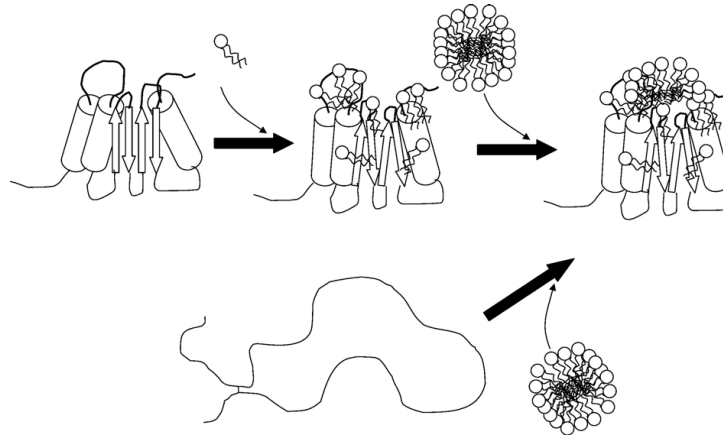

Fig. 7. Proposed model for action of monomeric and micellar detergent on cutinase. Monomers are proposed to sensitize cutinase to subsequent micelle binding. During refolding, monomers do not bind to cutinase as they require contiguous hydrophobic patches to bind.

changes in chemical shifts upon addition of C_6PC. Likewise, residues 122 and 124 situated in the N-terminal end of helix α3, next to the active site, the catalytic residue serine 120, and residues 41, 119, 148 and 170, all situated at the very C-terminal end of a β-strand, forming the bottom of the active site, were affected by the presence of the detergent. Only a few residues distant from the active site were found to show altered chemical shifts, these are amino acids 33, 131, 203 and 206. The results are summarized in Fig. 6.

No significant line broadening was observed in the NMR spectra, which indicates that the majority of the protein is not bound to large micellar particles; however, linewidths are not sensitive enough to detect binding to monomers.

4. Discussion

We have shown that the cutinase from *Fusarium solani pisi* is significantly destabilized in the presence of zwitterionic phospholipids and other detergents. Let us first summarize the observations prior to proposing a model to account for them. The binding of the detergents below and above the cmc manifests itself as a reduction in melting temperature and a subtle modulation of the native state, particularly around the active site loops, although activity is essentially unaffected. This suggests that the change in Trp fluorescence is more likely to be caused by local binding of detergent molecules than by changes in tertiary structure (confirmed by the lack of change in near-UV CD spectrum, Fig. 2C). Secondary structure is not affected either. The relatively low pH-sensitivity of destabilization between pH 4.5 and 9 (Fig. 5D) suggests that binding is predominantly mediated by hydrophobic interactions, coinciding with the presence of contiguous hydrophobic patches around the active site for binding triglyceride substrates.

What are the roles of detergent monomers and micelles, respectively, in this phenomenon? Refolding experiments suggest that micelles are the active species in the strong retardation of protein folding, since no retardation is seen below cmc (Fig. 1). On the other hand, thermal destabilization starts below cmc (although the midpoint is around cmc) and the degree of destabilization scales with the concentration of monomer present in solution (Fig. 5B). Furthermore, no effect is manifested by vesicle-forming phospholipids which have extremely low concentrations of monomer. This suggests that both monomer and micelle play a part. It is possible that the monomer "primes" the micelle for binding to the protein. A simple linkage relationship would predict that binding of detergent monomers to the native state should stabilize it; however, if the monomers induce the formation of an alternative and more flexible state, this would lead to destabilization. We propose a model (Fig. 7) in which monomer molecules attach to various hydrophobic patches on the surface and might, due to their small size and exposure of the hydrophobic chain, also penetrate more easily into the protein interior than the micelle, as indicated by the chemical shift changes around the C-terminal part of the central β-sheet (Fig. 6B), which is located at the bottom of the active site. This could lead to a propagation of subtle structural changes and would induce the formation of a less stable but still native-like state. Subsequently, the micelle can presumably bind to this more flexible state of cutinase. In the case of refolding, it is possible for the micelle to bind to this flexible state at an early stage in the conformational changes associated with folding and thus block refolding. Alternatively, the monomers do not have any strong affinity for non-native states (and thus do not exert an effect on refolding rates), because they bind to contiguous hydrophobic patches which are only found on the native state surface. Unlike conventional denaturants, the detergent micelles affect the activation barriers to refolding much more than the actual equilibrium distribution between native and denatured state. This reveals a remarkable ability to trap a protein in a metastable state.

A caveat with the model in Fig. 7 is that we have only been able to identify a relatively small number of residues with

significant changes in chemical shift and most of these are in the active site region, while only Asp 33 is located at the very end of the β-sheet distant from the active site. We also note that no chemical shift changes can be detected for Trp69, despite the clear change in fluorescence. It is possible that this apparent contradiction reflects the specific environment of Trp69, whose fluorescence is quenched by a vicinal disulfide bridge (Cys31–Cys109). Altering the environment of this disulfide bridge by unfolding [32] or photoreduction [33] markedly enhances its fluorescence and leads to a clear red-shift in the emission spectrum while leaving the near-UV CD spectrum unaltered. A small dislocation of the disulfide bridge caused by the binding of detergent to nearby side-chains could conceivably lead to significant fluorescence changes. Although the changes in the chemical shifts of Cys31 and Cys109 caused by the presence of C_6PC lie under the threshold used in Fig. 6B, it is noteworthy that Asp 33 (close to Cys31) and Asp111 (close to Cys109) both have significantly affected chemical shift changes which may affect the Trp environment.

An alternative possibility could be that the monomers and micelles simply destabilize cutinase by preferentially binding to the denatured state and that micelles by virtue of their larger contact surface can bind the protein sufficiently well to increase the activation barrier for refolding substantially more than the monomer. However, we dismiss this model, because it predicts that the activation barrier for refolding should also be raised in the presence of monomeric detergent (since the monomers obviously destabilize the native state according to thermal scans), leading to a decline in the refolding rate below the cmc. In fact, we see no effect on refolding rates below the cmc.

Due to the many different contact points between monomer and protein, it is to be expected that variations in the head group will modulate the efficiency of binding. Thus, DPC and DPS are in fact more destabilizing than would be predicted from their cmc alone (Fig. 5B), while DM fortuitously places itself on line with the phospholipids. Similar variations caused by different head groups have been observed for the activation of the *T. lanuginosus* lipase [12].

The reason for the particular sensitivity of cutinase to zwitterionic and non-ionic detergents is presumably related to its binding of hydrophobic substrates, which means that it is evolved to respond structurally to amphiphilic substrates. Substrate mimics may then "hitch a ride" to other parts of the protein, aided by the high affinity for the surface. However, it is not a general phenomenon for all enzymes with hydrophobic substrates, cfr. the insensitivity of the *T. lanuginosus* lipase [12].

NMR chemical shift data give an indication of regions of the protein where subtle changes in structure occur. It is interesting to compare the location of chemical shift changes in the structure upon interaction with C_6PC with the changes occurring upon interaction with a monoglyceride substrate reported earlier [10]. This comparison is shown in Fig. 6B. No significant difference can be seen between the interaction site of the monoglyceride substrate and the phospholipid with cutinase (it must be noted, that in the case of the monoglyceride, an inactive cutinase mutant (S120A) was used, while the wild-type enzyme was used in the case of the phospholipid). In both cases, the residues most affected are situated in the loops surrounding the active site as well as in the bottom of the active site. Moreover, a previous study with a covalently bound inhibitor ((*R*)-1,2-dibutyl-carbamoylglycerol-3-*O*-p-nitrophenyl-butylphosphonate) also showed chemical shift changes in this region of the molecule [12]. The data point to an essentially identical mode of interaction of cutinase with monoglycerides and phospholipids. Small differences in binding cannot be inferred from these data.

It is remarkable that this extensive colonization of the region around the active site loop has no significant consequences for enzyme activity, which is usually extremely sensitive to conformational changes around the active site. A reason could be that activity is retained as long as the loops remain attached to the main scaffold of the protein in the same overall architecture while retaining the flexibility needed to provide access to the substrate. Another reason might be that the protein's affinity for the substrate used here is sufficiently higher than for the detergents used in this study, so that the detergent molecules cannot compete for the active site. Furthermore, a geometry of detergent binding to the active site may be envisioned, that does not block for access of substrate to the catalytic residues. In addition, substrate binding may be facilitated by the prior presence of amphiphilic molecules at the active site.

In conclusion, we have shown that seemingly innocuous zwitterionic detergents can significantly destabilize and even trap metastable states of a protein with existing binding sites for amphiphilic molecules. We suggest that this occurs by an interplay between monomeric and micellar states, highlighting how a detergent's simple distribution between different aggregated states can profoundly affect the conformational properties of proteins.

Acknowledgements

We thank Mythily Thavagnanam for production of a ^{15}N labeled cutinase sample. P.S. was supported by a grant to the innovation consortium BIOPRO by the Danish Ministry of Science, Technology and Innovation. D.E.O. is supported by the Danish Research Foundation (inSPIN) and the Villum Kann Rasmussen Foundation (BioNET). R.W. and the NMR Laboratory at Aalborg University are supported by the Obel Foundation.

References

[1] C. Martinez, A. Nicolas, H. van Tilbeurgh, M.P. Egloff, C. Cudrey, R. Verger, C. Cambillau, Cutinase, a lipolytic enzyme with a preformed oxyanion hole, Biochemistry-Us 33 (1994) 83–89.
[2] J.D. Schrag, M. Cygler, Lipases and alpha/beta hydrolase fold, Methods Enzymol. 284 (1997) 85–107.
[3] H. Chahinian, L. Nini, E. Boitard, J.P. Dubes, L.C. Comeau, L. Sarda, Distinction between esterases and lipases: a kinetic study with vinyl esters and TAG, Lipids 37 (2002) 653–662.
[4] S. Longhi, M. Czjzek, V. Lamzin, A. Nicolas, C. Cambillau, Atomic resolution (1.0 A) crystal structure of Fusarium solani cutinase: stereochemical analysis, J. Mol. Biol. 268 (1997) 779–799.
[5] C. Martinez, P. De Geus, M. Lauwereys, G. Matthyssens, C. Cambillau, Fusarium solani cutinase is a lipolytic enzyme with a catalytic serine accessible to solvent, Nature 356 (1992) 615–618.
[6] S. Longhi, A. Nicolas, L. Creveld, M. Egmond, C.T. Verrips, J. de Vlieg, C. Martinez, C. Cambillau, Dynamics of Fusarium solani cutinase

investigated through structural comparison among different crystal forms of its variants, Proteins 26 (1996) 442–458.
[7] S. Longhi, M. Mannesse, H.M. Verheij, G.H. De Haas, M. Egmond, E. Knoops-Mouthuy, C. Cambillau, Crystal structure of cutinase covalently inhibited by a triglyceride analogue, Protein Sci. 6 (1997) 275–286.
[8] J.J. Prompers, A. Groenewegen, C.W. Hilbers, H.A. Pepermans, Backbone dynamics of *Fusarium solani pisi* cutinase probed by nuclear magnetic resonance: the lack of interfacial activation revisited, Biochemistry-Us 38 (1999) 5315–5327.
[9] J.J. Prompers, B. van Noorloos, M.L. Mannesse, A. Groenewegen, M.R. Egmond, H.M. Verheij, C.W. Hilbers, H.A. Pepermans, NMR studies of *Fusarium solani pisi* cutinase in complex with phosphonate inhibitors, Biochemistry-Us 38 (1999) 5982–5994.
[10] K.R. Poulsen, T.K. Sorensen, L. Duroux, E.I. Petersen, S.B. Petersen, R. Wimmer, The interaction of *Fusarium solani pisi* Cutinase with long chain spin label esters, Biochemistry 45 (2006) 9163–9171.
[11] D.E. Otzen, Protein unfolding in detergents: effect of micelle structure, ionic strength, pH, and temperature, Biophys. J. 83 (2002) 2219–2230.
[12] J.E. Mogensen, P. Sehgal, D.E. Otzen, Activation, inhibition and destabilization of *Thermomyces lanuginosus* lipase by detergents, Biochemistry 44 (2005) 1719–1730.
[13] D.J. Pocalyko, M. Tallman, Effects of amphipaths on the activity and stability of *Fusarium solani pisi* cutinase, Enzyme Microb. Technol. 22 (1998) 647–651.
[14] L.D. Creveld, M. Meijberg, H.J. Berendsen, H.A. Pepermans, DSC studies of *Fusarium solani pisi* cutinase: consequences for stability in the presence of surfactants, Biophys. Chemist. 92 (2001) 65–75.
[15] T. Ternström, A. Svendsen, M. Akke, P. Adlercreutz, Unfolding and inactivation of cutinases by AOT and guanidine hydrochloride, Biochim. Biophys. Acta 1748 (2005) 74–83.
[16] S. Pedersen, L.W. Nesgaard, R.P. Baptista, E.P. Melo, S.R. Kristensen, D.E. Otzen, pH-dependent aggregation of cutinase is efficiently suppressed by 1,8-ANS, Biopolymers 83 (2006) 619–629.
[17] S.H. McLaughlin, S.E. Jackson, Folding and stability of the ligand-binding domain of the glucocorticoid receptor, Protein Sci. 11 (2002) 1926–1936.
[18] B. Kierdaszuk, S. Eriksson, Selective inactivation of the deoxyadenosine phosphorylating activity of pure human deoxycytidine kinase: stabilization of different forms of the enzyme by substrates and biological detergents, Biochemistry 29 (1990) 4109–4114.
[19] P. Sehgal, D.E. Otzen, Thermodynamics of unfolding of an integral membrane protein in mixed micelles, Protein Sci. 15 (2006) 890–899.
[20] M. Lauwereys, P. De Geus, J. De Meutter, P. Stanssens, G. Mathyssens, Cloning, expression and characterization of cutinase, a fungal lipolytic enzyme, in: L. Alberhina, R.D. Schmid, R. verger (Eds.), Lipases — structure, function and genetic engineering, VCH, Weinheim, 1991, pp. 243–251.
[21] E.-J. Wang, M. Jaraiedi, T.F. Torries, M.J. Sebastião, J.M.S. Cabral, M.R. Aires-Barros, Improved purification protocol of a *Fusarium solani pisi* recombinant cutinase by phase partitioning in aqueous two-phase systems of polyethylene glycol and phosphate Enz, Microb. Technol. 18 (1996) 251–260.
[22] K.R. Poulsen, T. Snabe, E.I. Petersen, P. Fojan, M.T. Neves-Petersen, R. Wimmer, S.B. Petersen, Quantization of pH: evidence for acidic activity of triglyceride lipases, Biochemistry-Us 44 (2005) 11574–11580.
[23] S. Yadav, F. Ahmad, A new method for the determination of stability parameters of proteins from their heat-induced denaturation curves, Anal. Biochem. 283 (2000) 207–213.
[24] K. Kalyanasundaram, J.K. Thomas, Environmental effects on vibronic band intensities in pyrene monomer fluorescence and their application in studies of micellar systems, J. Am. Chem. Soc. 99 (1977) 2039–2044.
[25] C. Bartels, T.-H. Xia, M. Billeter, P. Günter, K. Wüthrich, The program XEASY for computer-supported NMR spectral analysis of biological macromolecules, J. Biomol. NMR 5 (1995) 1–10.
[26] R. Keller, The Computer Aided Resonance Assignment Tutorial, CANTINA Verlag, Goldau, 2004.
[27] S. Mori, C. Abeygunawardana, M.O. Johnson, P.C. van Zijl, Improved sensitivity of HSQC spectra of exchanging protons at short interscan delays using a new fast HSQC (FHSQC) detection scheme that avoids water saturation, J. Magn. Reson., Ser. B 108 (1995) 94–98.
[28] E.P. Melo, L. Chen, J.M. Cabral, P. Fojan, S.B. Petersen, D.E. Otzen, Trehalose favors a cutinase compact intermediate off-folding pathway, Biochemistry 42 (2003) 7611–7617.
[29] D.E. Otzen, L. Giehm, R.P. Baptista, S.R. Kristensen, E.P. Melo, S. Pedersen, Aggregation as the basis for complex behaviour of cutinase in different denaturants, Biochim. Biophys. Acta 1774 (2007) 323–333.
[30] A.R. Fersht, Structure and mechanism in protein science. A guide to enzyme catalysis and protein folding, Freeman & Co, New York, 1999.
[31] D.E. Otzen, M. Oliveberg, Burst-phase expansion of native protein prior to global unfolding in SDS, J. Mol. Biol. 315 (2002) 1231–1240.
[32] J.M.G. Martinho, A.M. Santos, A. Fedorov, R.P. Baptista, M.A. Taipa, J.M. Cabral, Fluorescence of the single tryptophan of cutinase: temperature and pH effect on protein conformation and dynamics, Photochem. Photobiol. 78 (2003) 15–22.
[33] J.J. Prompers, C.W. Hilbers, H.A. Pepermans, Tryptophan mediated photoreduction of disulfide bond causes unusual fluorescence behaviour of *Fusarium solani pisi* cutinase, FEBS Lett. 456 (1999) 409–416.
[34] R. Koradi, M. Billeter, K. Wüthrich, MOLMOL: a program for display and analysis of macromolecular structures, J. Mol. Graph. 14 (1996) 51–55.

The molecular understanding of the interaction of proteins and peptides with biological membranes requires knowledge on the structure of the membrane bilayer, the location of membrane-bound peptides, their structure and the changes in membrane structure induced by the presence of the protein or peptide. This thesis provides further insights into the structure, location and membrane-perturbing properties of the antimicrobial peptide novicidin and a synthetic pore construct between cyclodextrins and alamethicin and their impact on the structure and integrity of lipid membranes.

Whereas many antimicrobial peptides gain a defined structure only in a lipid environment, water-soluble proteins often possess a well-defined three-dimensional structure and function in aqueous environment devoid of lipids. Using cutinase from F. Solani pisi, the peptide hormone kisspeptin and the cytotoxic complex between equine lysozyme and oleic acid (ELOA) as model systems, this thesis shows that the structure and function of such proteins can potentially be altered in the presence of lipids and lead to decreased stability, modulation of activity, structural rearrangements or even gain on of new functions of potential biological relevance.

A primary aim at the Faculty of Agricultural Sciences is to educate scientists with extensive knowledge within agriculture, food and environment. The Graduate School of Agriculture, Food and Environment (SAFE) ensures that the PhD programmes offered are of high international standard. For more information visit our website at www.agrsci.au.dk